Antarctic Meteorites XXVII

Papers presented to the Twentyseventh Symposium on Antarctic Meteorites

June 11-13, 2002

NATIONAL INSTITUTE OF POLAR RESEARCH
TOKYO

国立極地研究所

Paul Buchanan

Tuesday, June 11, 2002

0900 – 1200 Registration Auditorium (6th Floor)

*Speaker

Chairs: Hiroi T. and Fagan T.J. **Page**

Tuesday, June 11, 2002

1230 – 1330 Lunch Time

Chairs: Nagahara H. and Yada T. **Page**

1515 – 1545 Tea Time

-- Special Talk (I) --

Chair: Buchanan P.

Wednesday, June 12, 2002

Chairs: Mikouchi T. and McKay G. **Page**

1215 – 1315 Lunch Time

Chairs: Misawa K. and Ebihara M.

Special Session: The Yamato nakhlite consortium

Wednesday, June 12, 2002

-- Special Talk (II) --

Chair: Nakamura N.

1730 – 1930 Reception Lounge (6F)

Thursday, June 13, 2002

Chairs: Tomiyama T. and Buchanan P. **Page**

1230 – 1330 Lunch Time

Chairs: Zolensky M. and Burbine T.

Thursday, June 13, 2002

ABSTRACTS

The formation process of compound chondrules inferred from bulk compositions and oxygen isotopic ratios

[1)] Takeshi Akaki, [1)] Tomoki Nakamura, and [2)] Takaaki Noguchi

1) Department of Earth and Planetary Sciences, Faculty of Sciences, Kyushu University, Hakozaki, Fukuoka 812-8581, Japan

2) Materials and Biological Science, Ibaraki University, Bunkyo, Mito 310-8512, Japan

Introduction

Compound chondrules, which consist of two or more chondrules fused together, occur in all classes of chondrites [1]. They have been presumed to form by a collision of totally or partially molten particles in the early solar nebula [1]. This random collision model required either much longer molten period that would lead to the evaporation of large amount of volatile elements or implausibly high mean density of matter in the nebula [2]. Therefore, a recent model [2] suggests that most independent compound chondrules, consisting of chondrules with different texture, were formed by flash melting of a porous dust aggregate containing a chondrule that was not itself melted.

The compositional and isotopic properties of compound chondrules offer crucial information on the physical and chemical state of solid material in the early solar nebula during chondrule formation. For this purpose, we compared individual chondrules in compound chondrules based on the major element concentration and oxygen isotopic composition.

Samples and analytical procedures

Sixty-three polished thin sections having total area of 27 cm^2 were prepared from Allende CV3 (21 cm^2) and Axtell CV3 (6 cm^2) chondrites and examined petrographically using a petrographic microscope. Thirty compound chondrule sets, 28 sets from Allende and 2 sets from Axtell, were found. Back-scattered electron and cathodoluminescence imaging was made so as to identify mineral phases using a scanning electron microscope. Bulk chemical compositions of 28 chondrules from 14 compound chondrules were obtained using an electron probe microanalyzer with 50 μm broad-beam. The number of beam spots, which depends on the size of the chondrule, was about 100 points per one chondrule on average. Measurements of oxygen isotope composition were performed using a CAMECA ims-6f ion microprobe. San Carlos olivine was used as standards for the analysis of olivine in chondrules. The measurements of bulk chemical composition and oxygen isotope composition are now in progress and we report here the results of analysis completed so far.

Results and discussion

Each chondrule consisting compound chondrules were classified to primary chondrule and secondary one according to the criteria given in [2]. Primary chondrules are those that were rigid enough to retain their original shape during the formation of compound chondrules. On the other hand, secondary chondrules are those that had viscosities low enough to allow them to conform to the shape of the boundary to the primary.

It was reported that mafic minerals such as olivine and low-Ca pyroxene in secondaries tend to have slightly higher FeO contents than those in primaries [2]. In this study, we compared primaries and secondaries on the bulk chemical composition, and found that the primaries tend to have higher Al_2O_3, TiO_2, and CaO contents and lower FeO and MnO contents than the secondaries [Fig.1 (a)~(f)]. SiO_2, MgO, Na_2O, NiO, and S contents show no obvious tendency. The results indicate that Al, Ti, Ca-rich and Fe, Mn-poor chondrules were solidified first prior to Fe, Mn-rich chondrules.

Based on the bulk compositional data, we calculated the liquidus temperature of each chondrule in compound chondrules using the MELTS, which is a software for modeling crystallization of magmatic systems [3]. The result showed that, in spite of differences in major element concentrations, liquidus temperature of primaries and secondaries is roughly similar to each other. This suggests that both primaries and secondaries start to solidify at similar temperature. Therefore, the difference of bulk chemical composition between primaries and secondaries are thought to take little effect on the formation of compound chondrules, if the two chondrule precursors have been heated up and cooled down simultaneously.

Oxygen isotope compositions of barred olivines in one compound chondrule were measured. This compound chondrule consists of barred olivine primary and barred olivine secondary. Bulk composition of this chondrule pair was shown as squares in Fig.1. Oxygen isotopic analysis was made on 13 spots and all data lie on or close to carbonaceous chondrite anhydrous mineral line [4]. Seven data obtained from the primary chondrule show $\delta^{17}O$ from –5.0‰ to 0.3‰, and $\delta^{18}O$ from –0.4‰ to 6.0‰. On the other hand, six data obtained from the secondary chondrule show $\delta^{17}O$ from –4.7‰ to 0.2‰, and $\delta^{18}O$ from 0.8‰ to 7.2‰. Both data sets exhibit similar distribution and clearly overlap on the oxygen three isotope plot. This tendency was similar to the result obtained in two previous studies of Allende compound chondrule [5],[6], which have reported that oxygen isotopic composition of olivines in primary chondrule and secondary one are broadly similar. The result suggests that this compound chondrule had been formed from two precursors originated from similar dust reservoirs.

References: [1] Gooding and Keil (1981) *Meteoritics*. **16**, 17-43. [2] Wasson *et al.* (1995) *Geochim. Cosmochim. Acta*. **59**, 1847-1896. [3] Ghiorso and Sack (1995) *Contrib. Mineral. Petrol.* **119**, 197-212. [4] Clayton *et al.* (1977) *Earth Planet. Lett.* **34**, 209-224. [5] Maruyama *et al.* (1998) *Lunar and Planet. Sci.* **XXIX**, #1342. [6] Russel *et al.* (2000) *Lunar and Planet. Sci.* **XXXI**, #1949.

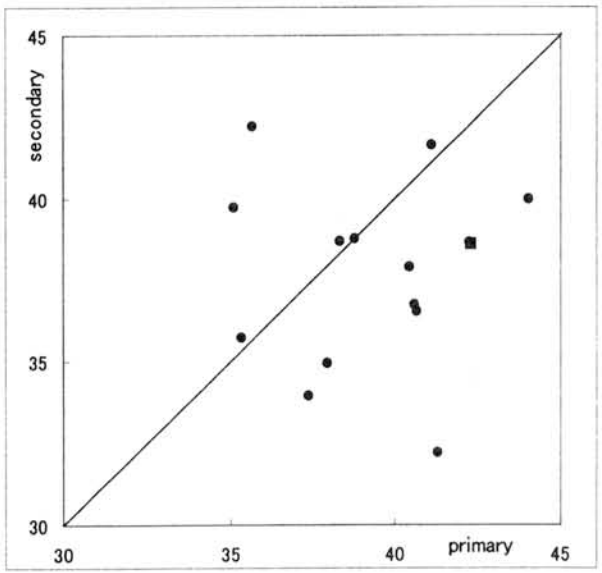

(a) SiO_2 (wt%)

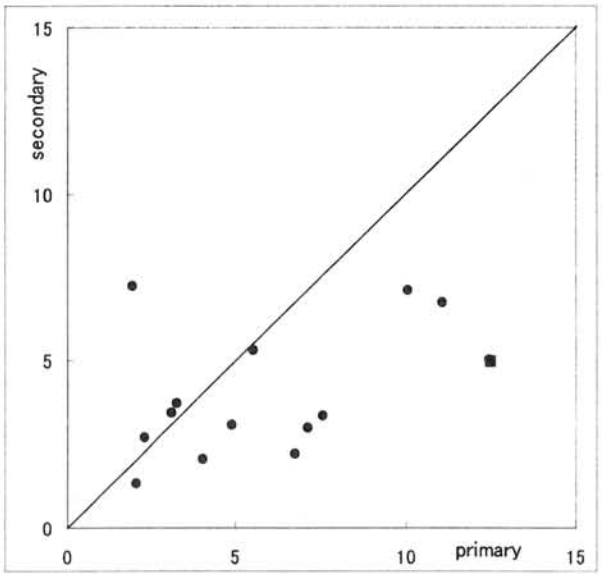

(b) Al_2O_3 (wt%)

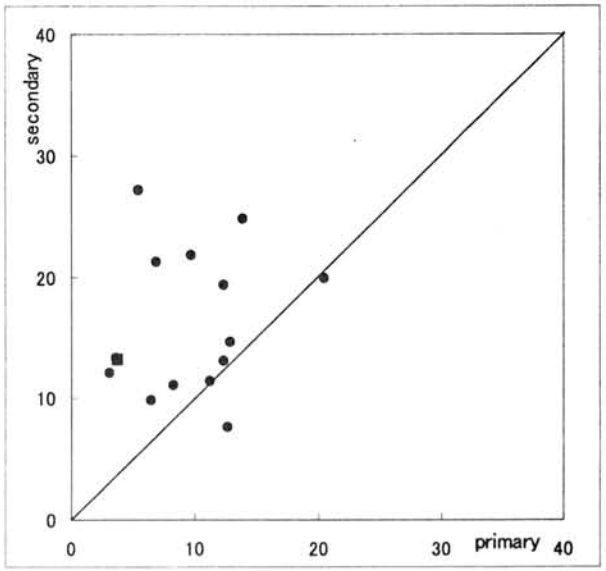

(c) FeO (wt%)

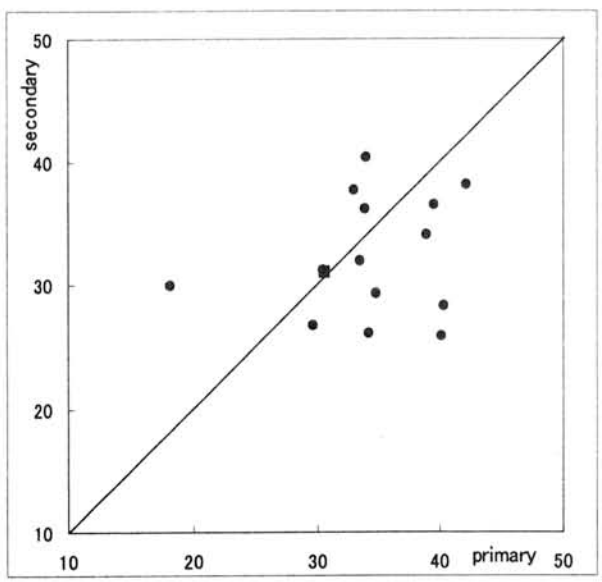

(d) MgO (wt%)

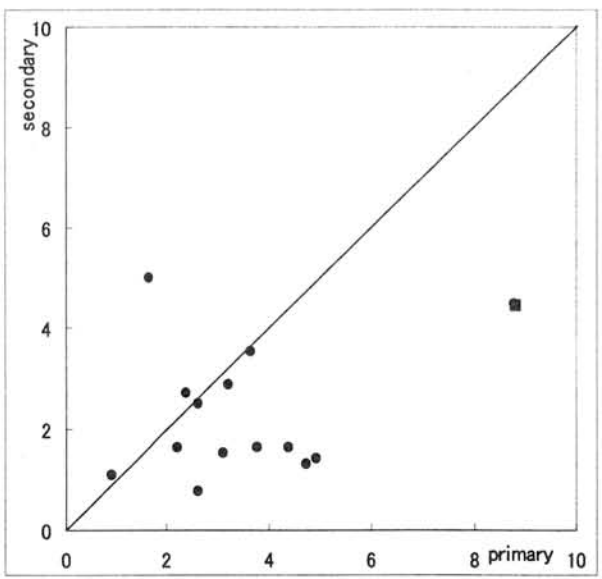

(e) CaO (wt%)

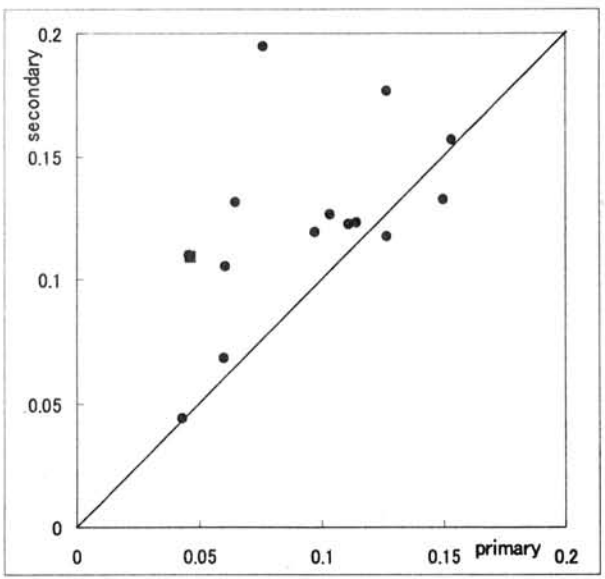

(f) MnO (wt%)

Fig.1 Diagrams showing the bulk chemical compositions of secondaries versus those of primaries. A point plotted in square indicates the bulk data of a compound chondrule that was analyzed by SIMS.

A NEW LUNAR METEORITE YAMATO 981031: A POSSIBLE LINK BETWEEN TWO LUNAR-METEORITE SOURCE CRATERS

T. Arai[1] , T. Ishii[2] and M. Otsuki[2]
[1]Space Station Mission Operations Department, National Space Development Agency of Japan (NASDA), Tsukuba Space Center 2-1-1 Sengen Tsukuba, Ibaraki 305-8505 Japan, arai.tomoko@nasda.go.jp
[2]Ocean Research Institute, University of Tokyo, 1-15-1, Minamidai, Nakano-ku, Tokyo 164-8639 Japan

Introduction: Over 30 years after the Apollo/Lunar missions, continuing studies of lunar samples, including lunar meteorites are expanding our understanding of the lunar interior, regolith, and surface processes. Yamato (Y) 981031 is the 7th Antarctic lunar meteorite of mare origin. Among the six pre-found mare meteorites, Yamato (Y) 793169 and Asuka (A) 881757 are unbrecciated mare basalts with 3.9 Ga age [e.g., 1, 2, 3, 4, 5], while Y793274, QUE94281, EET87521, and EET96008 are brecciated mare basalts with some highland components [e.g., 6, 7, 8]. Y793169 and A881757 (YA basalts) are probably launch-paired and derived from a common basalt suite [e.g., 2, 5]. Y793274 /QUE94281 (YQ meteorites) and EET87521 / EET96008 (EETs meteorites) are launch-paired, namely ejected from a common source crater on the Moon, respectively [e.g., 7, 8]. In this study, mineralogy of Y981031 is investigated to identify its source mare-basalt suite/source crater, and to assess its genetic relationship with other mare lunar meteorites and Apollo/Luna samples.

Sample and Methods: The polished thin section (PTS) 981031, 53-4 is provided by the National Institute of Polar Research. Analyses of mineral compositions and chemical mapping were done by a JEOL 733 electron probe microanalyzer (EPMA) and JEOL EPMA (8900 Super Probe) at the Ocean Research Institute, University of Tokyo.

Results: Y981031 is a polymict, regolith breccia, consisting of diverse mixture of mineral fragments and clasts from various rock types which are embedded in a dark, glassy matrix. Mineral fragments, 100-500 μm in size, are mostly pyroxene, plagioclase and olivine of apparent mare-basalt derivation, with smaller (< 100 μm) fragments of ilmenite, chromite, ulvöspinel, Fe-Ni metal, troilite and silica minerals. A variety of clasts are anorthositic impact-melt clasts, dark melt clasts, mare basalt clasts, and a Mg-rich dunite clast. Anorthositic impact-melt clasts commonly show poikilitic or granulitic fine-grained matrix with various abundances of mineral fragments and rock clasts. A clast-laden impact melt clast, 2 mm across, includes fragments of coarse-grained plagioclase (up to 500 μm) with minor olivine and ilmenite (Fig. 1a). An ovoid-shaped dark melt clast, 4 mm across, includes mostly dendritic plagioclase crystal with minor pyroxene and ilmenite, despite of its dark brown color. This clast demonstrate rapid cooling from anorthositic impact melt spherule.

The Mg-rich dunite clast (DN), 750 μm across, consists of dominantly Mg-rich olivine with minor plagioclase and Mg-rich high-Ca pyroxene (Fig. 1b). Equigranular crystals of olivine cumulate are 30 μm -200 μm in size. The composition and modal abundance (vol. %) of each phase is: olivine (Fo90) = 88, plagioclase (An88-90) = 9, and high-Ca pyroxene (Wo48En48Fs6, Fe/Fe+Mg = 0.1) = 3. The high-Ca pyroxenes are plotted in pyroxene quadrilateral and Fe# (=Fe/(Fe+Mg) molar) vs. Ti# (=Ti/(Ti+Cr) molar) diagram (Fig. 2 and 3). Although the modal abundance and mineral composition are analogous to those of an Apollo 17 brecciated dunite 72415 [9], finer grain size of olivine cumulate, probably produced by crystallization from a smaller scale of locally-trapped melt, suggests closer link with a Mg-gabbronorite clast in 14305, 92, which is reported as the oldest mare basalt clast of 4.23 Ga crystallization age [10]. It is noted that the DN clast has more primitive composition for olivine and pyroxene, compared with the primitive composition of 14305, 92 (pyroxene: Wo37Fs16En47, Fe# = 0.25, olivine: Fo =75, plagioclase: of An =92) (Arai, 1998 [unpublished data]).

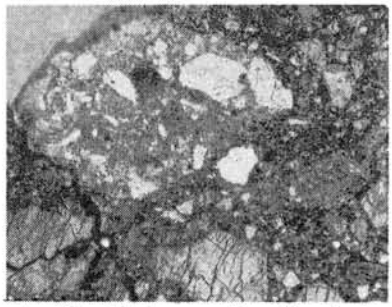

Fig. 1a. Clast-laden anorthositic clast.

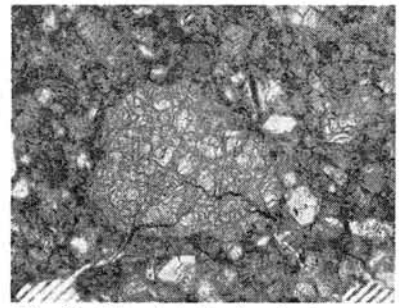

Fig. 1b. Mg-rich dunite clast

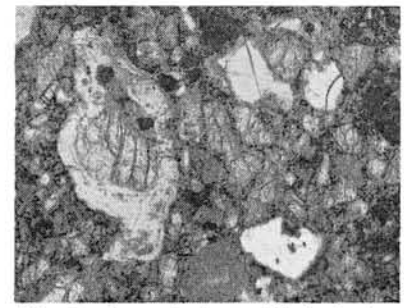

Fig. 1c. Impact glass with inclusion

(Filed of view for the photomicrographs is 3.3 mm for Fig. 1a, and 1.7mm for Fig. 1b, 1c)

The coarse-grained mare basalt clasts (MB1), dominantly consisting of 0.5 - 1 mm-size pyroxenes (Fig. 1d), and associated mare pyroxene fragments are clustered in one corner of the thin section. A basalt clast with coarser-grained pyroxene (up to 2.0 mm across) with symplectite of faylite and silica mineral is also found (MB2) (Fig. 1e). The MB1 clast is composed of zoned pyroxenes with a Ca-rich core (Wo35Fs20), plagioclase (An85-96), with mesostases including fayalite (Fo17-19), ilmenite, chromian ulvöspinel (Chr3Her12Ulvo81-Chr32Her12Ulvo56), and troilite. Mineral assemblage, especially in the mesostasis are remarkably similar to that in A881757 (Fig. 1f), and the composition of the MB1 chromian ulvöspinels is close to that of A881757, which are slightly more Cr-enriched (Chr3Her6Ulvo89-Chr25Her7Ulvo69) [11]. Note that the MB1 chromian ulvöspinels show both zoning within a grain and grain-to-grain compositional variations, like those in A881757 [11]. The pyroxene compositions from the MB clasts and associated fragments are plotted in pyroxene quadrilateral and Fe# vs. Ti# plot (Fig. 2 and Fig. 3). Major composition of the pyroxenes are within same range of that in YQ/EETs meteorites [7, 8] and partly of that in YA basalts [e.g., 2, 4]. These pyroxenes constitute a series of crystallization trend in the Fe# vs. Ti# plot, which is typical of zoned pyroxenes in the Ti-poor mare basalt, and the trend is slightly steeper and Ti-rich than that of YQ/EET meteorites [7, 8]. Although the Fe# in mare pyroxenes in Y981031 is more Mg-rich (Fe# =0.31-0.71) than that of A881757 (Fe# =0.49-0.87), Fe#-Ti# trend of Y980131 and A881757 are almost identical, overlapping in the range of Fe#=0.49-0.71. Based on an empirical correlation between Ti# in pyroxene and bulk-rock TiO_2 abundance [11], a source basalt of MB pyroxenes is estimated to have a bulk-rock $TiO_2 \approx 1.3 - 1.5$ wt % (Fig. 4), which falls between YQ/EETs meteorites ($TiO_2 \approx$ 1.0 wt %) [7, 8] and YA basalts ($TiO_2 \approx 1.5$ - 2.0 wt%) [e.g. 2, 3]. Mare pyroxenes from MB clasts and fragments commonly feature a few micron-wide exsolution. These coarse pyroxene exsolution by mare basalt standard, are also reported in YQ/EETs meteorites [7, 8]. Symplectite in MB2 is also found in A881757 pyroxene [2, 5]. Petrogenesis of the DN clast and genetic relation with the mare basalt components are enigmatic.

The Y981031 contains glass spherules and spherule fragments. Pale-green glasses are larger (100 - 600 μm across) than other colored glasses and one glass has inclusion of fragments of pyroxene and plagioclase (Fig. 1c). Smaller, colorless or brown glass spherules are 50-100 μm in diameter. Among the nineteen glass data collected, eight pyroclastic glasses that is product of a volcanic vent, are screened, based on the Delano's criteria [12], such as intra and inter-sample homogeneity, absence of inclusion/ schlieren and Mg/Al >1.5. The rest of glasses are anorthositic impact glass or mare impact glass [13]. YQ meteorites also include pale-green, brown, and colorless glasses [7]. The population of the pristine glasses per surface area are close to that for YQ meteorites, where eighteen pristine glasses from two thin sections of QUE94281 and 18 from two thin section in Y793274 [7]. The pyroclastic glasses are plotted with those in YQ meteorites (Fig. 5). It is to be noted that composition of these pristine glasses are within the range of lower-Ti group (TiO_2 = 0.37-0.63 wt%) of YQ glasses [7], while the higher-Ti group (TiO_2 = 0.99-1.22 wt%) of YQ glasses [7] are not found in Y981031. A light brown fusion crust (0.2 - 0.3 mm thick) is found with abundant vesicles. The fusion crust shows relatively homogeneous composition and the average composition is almost identical with the bulk-rock analysis reported in Meteorite News [14].

Discussion: Mare basalt components in Y981031 show many common features with A881757 (namely YA basalt), in coarse-grained texture, mineral assemblage, composition of pyroxene and spinel, pyroxene crystallization trend and having symplectite in pyroxenes. Symplectic pyroxenes indicate that mare basalt of Y980131 and A881757 commonly experienced shock metamorphism after the basalt cooled. All these facts imply that mare basalt components in Y981031 have cooled from a common lava flow and have experienced a common shock events with A881757. The Fe#-Ti# trend of pyroxenes in YQ/EETs meteorites is slightly Ti-poor, but their compositional variation falls still within the same range as that of Y981031 and A881757. Thus, it is possible that YQ/EETs meteorites also shares common source basalt (TiO_2 =1.0 - 2.0 wt%) with Y981031 and A881757 (YA basalts).

The overall breccia texture, mineralogy, abundance of mare-highland component, the population/composition of pyroclastic glasses all support that Y981031 with YQ meteorites are likely derived from a common source crater on the Moon. The common coarse pyroxene exsolution by mare standard suggests that mare-basalt remnants (mainly pyroxene) in these lunar mare breccias preserve a common cooling process such that the source basalt experienced relatively slow cooling in a thick lave flow/lave pond, and/or are suffered from thermal annealing during brecciation after the basalt formed.

Conclusion: Y981031 includes mare basalt clasts derived from the low-Ti "YA-basalt suite" with $TiO_2 = 1.0 - 2.0$ wt%, which formed at 3.9 Ga, and the pyroclastic glasses which yield around the source crater of the YQ meteorites. These facts lead to conclusions that Y981031 is a possible link between the two source craters of YA basalts and YQ (and possibly EETs) meteorites, and Y981031/YQ (and possibly EETs) meteorites formed after 3.9 Ga when YA basalts formed.

References: [1] Misawa et al. (1993) *GCA* 57, 4687-4702. [2] Yanai K. & Kojima H. (1991) *Proc. NIPR Ant. Met.* 4, 70-90. [3] Warren P. H. & Kallemeyn G. W. (1993) *Proc. NIPR Ant. Met.* 6, 35-57. [4] Takeda H. et al. (1993) *Proc. NIPR Ant. Met.* 6, 3-13. [5] Yanai K. (1991) *Proc. LPSC* 21, 317-324. [6] Takeda et al. (1992) *Proc. LPSC*, 22, 355-364. [7] Arai T. & Warren P. H. (1999) *MPS*, 34, 209-234. [8] Arai T. (2001) *Antarctic Meteorites XXVI, 2-6.* [9] Taylor G. J. et al. (1991) *Lunar Sourcebook*, pp.183-284, Cambridge U. Press. [10] Taylor L. A. et al. (1983) *EPSL*, 66, 33-47. [11] Arai T et al. (1996) *MPS*, 31, 877-892. [12] Delano J.W. (1986) Proc. *LPSC*, 16, D201-D213. [13] Delano (1988) *Proc. LPSC* , 18, 59-65. [14] Meteorite News , June 2000 published by NIPR.

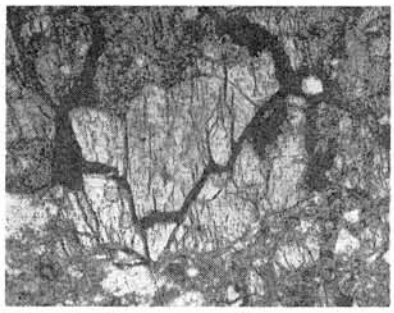

Fig. 1d. MB1 clast with mesostasis

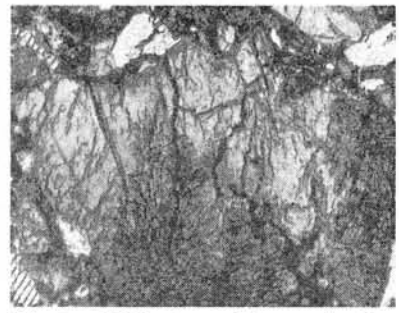

Fig. 1e. MB2 clast with symplectite

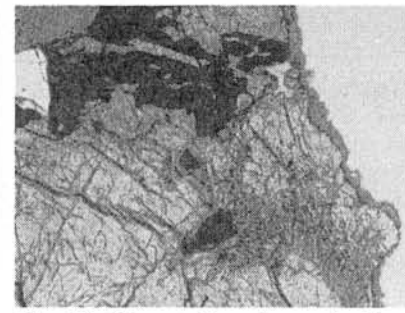

Fig. 1f. Mesostasis and symplectite in A881757

(Filed of view for all the photomicrographs is 1.7mm)

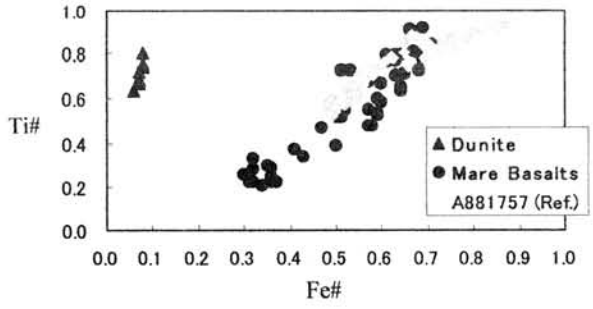

Fig. 2 Fe# vs. Ti# diagram for pyroxene.
A881757 data from Arai (1998)[unpublished data].

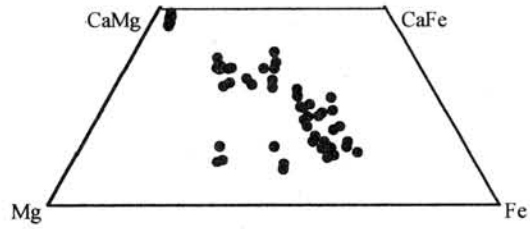

Fig. 3 Pyroxene quadrilateral. Pyroxenes in DN clast are plotted in a cluster of Ca-Mg rich corner

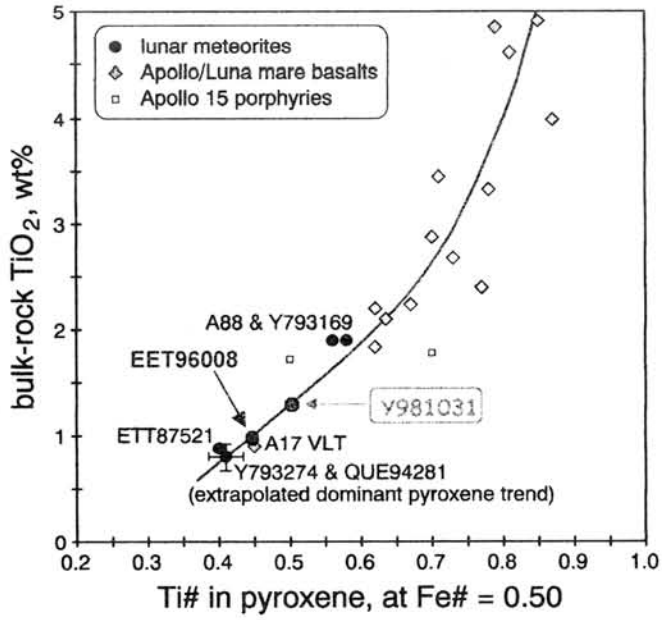

Fig. 4 Bulk-rock TiO_2 of source-basalts for mare breccias, based on Fe#-normalized pyroxene Ti# (intercept at Fe#= 0.5 in Fig. 2).
Data except Y981031 are from [7] and [8].

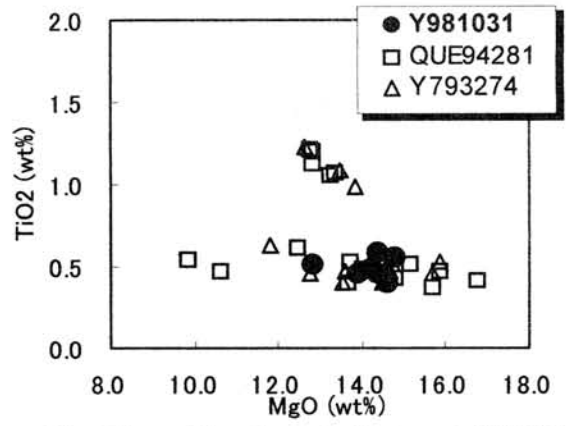

Fig. 5 Composition of pyroclastic glasses in Y981031.
Glass data of YQ meteorites are from [7].

Lithic components in the paired howardites EET 87503 and EET 87513: characterization of the regolith of Vesta

P. C. Buchanan
Antarctic Meteorite Research Center, National Institute of Polar Research, 1-9-10 Kaga Itabashi, Tokyo 173-8515 Japan. e-mail: buchanan@nipr.ac.jp.

Introduction: The howardites EET 87503 (1734.5 g) and EET 87513 (394.5 g) were found on the Texas Bowl Icefield in Antarctica. Hand specimen examination suggests that both meteorites are relatively unaltered (alteration classifications A and A/B, respectively) (Score and Lindstrom, 1990). Both meteorites are regolith breccias with matrix pyroxenes that have a broad range of compositions and they both contain a wide variety of eucritic and diogenitic rock fragments. Based on these data and similarities in bulk compositions, Buchanan et al. (2000) concluded that these meteorites are paired. Hiroi et al. (1994) concluded that the reflectance spectra of 4 Vesta were most similar to that of the finest grain-size fraction of EET 87503. Hence, these paired meteorites may be appropriate as approximate analogues for the surface regolith of the asteroid. The present study is a discussion of the lithic components that are mixed together in these breccias based on an examination of twenty-four clasts and a large number of matrix mineral fragments. Preliminary data for this study were also discussed in Buchanan and Lindstrom (2000).

Data:

When only matrix minerals are considered, the EET 87503/EET 87513 breccia contains 25-35% diogenitic material and 65-75% eucritic material. Hence, these meteorites are howardites. Unfortunately, mineral compositions alone do not provide adequate criteria to discriminate between the different types of eucrites. For example, the pyroxenes in Stannern and Juvinas are similar in Mg#. Hence, it is also necessary to consider the proportions of the various types of clasts in these meteorites to determine the proportions of the various types of eucritic materials. Fortunately, EET 87503 and EET 87513 contain large numbers of clasts.

Three clasts are predominantly composed of magnesian orthopyroxene and have been deformed to varying degrees. Clast D from EET 87503 is mildly deformed with orthopyroxenes displaying undulating extinction and incipient mosaicism. Clasts A/EE and 9 from EET 87513 are diogenites that apparently were brecciated and later recrystallized. Normalized REE abundances of clast A/EE are 1-2 x CI with a slight positive Ce anomaly and are similar to some diogenites.

A variety of eucrite clasts are present in EET 87503 and EET 87513. These eucrite clasts display a variety of degrees of equilibration. Some of these eucrite clasts have ophitic/subophitic volcanic textures, whereas others are coarser-grained and are probably igneous rocks derived from shallow intrusive bodies. Among these fragments of igneous and volcanic rocks there is a broad range of mineral compositions and a great deal of variation in the bulk abundances of trace elements. Clast Y from EET 87513 contains feldspar and relatively magnesian pyroxene and has a normalized REE pattern that is ~1 x CI with a positive Eu anomaly. It possibly represents a fragment of cumulate eucrite.

Clast B is enriched in REE relative to clast E, which has abundances that are typical of "main group" eucrites.

Relatively unshocked eucrite clasts form a continuous series with clasts that have been affected by varying degrees of shock deformation. These shocked eucrite clasts include those with pyroxenes that are blackened and those that are composed of silicate mineral fragments in a black, glassy matrix. There are also clasts that represent fragments of lithified eucrite and howardite clastic breccias.

A carbonaceous chondrite clast (clast N) was previously described in EET 87513 (Buchanan et al., 1993). It was classified as CM2 based on geochemical, mineralogical, and oxygen isotope data. A second carbonaceous chondrite clast (clast 7) from the same meteorite was also analyzed and is apparently also a CM2 fragment.

Conclusions: Based solely on the spectrum of pyroxene compositions in the matrices of these meteorites, EET 87503 and EET 87513 contain 25-35% diogenitic material. This agrees well with the suggestion, which was based on INAA of bulk samples, by Mittlefehldt and Lindstrom (1991) that EET 87503 contains ~20% diogenitic material and EET 87513 contains ~35% diogenitic material. This range in proportions of diogenitic and eucritic materials is reasonable for different locations in the same regolith breccia and for different samples of the same breccia. However, when only clasts are considered, these proportions are somewhat different. Clasts in these breccias include 10-15% diogenites and 75-80% eucrites, including equilibrated eucrites, unequilibrated eucrites, "main group" eucrites, Stannern-trend eucrites, Nuevo Laredo-trend eucrites, and a variety of eucrite breccias, including black matrix breccias. It must not be forgotten that significant proportions of these clasts represent petrogenetically unrelated materials, including carbonaceous chondrites. These clast materials must also be considered when approximating the regolith of Vesta.

Acknowledgments: This study was partially funded by NASA grant NAG9-365 to A. M. Reid and NASA grant RTOP 344-31-00-05 to D. J. Lindstrom.

References:

Buchanan P.C., Zolensky M.E., and Reid A.M. (1993) Carbonaceous chondrite clasts in the howardites Bholghati and EET87513. *Meteoritics* **28**, 659-669.

Buchanan P.C. and Lindstrom D.J. (2000) New clasts from the paired howardites EET87503 and EET87513. *Lunar and Planetary Science XXXI*, #1714.

Buchanan P.C., Lindstrom D.J., and Mittlefehldt D.W. (2000) Pairing among EET87503-group howardites and polymict eucrites. *in* Schultz L., Franchi I., Reid A., and Zolensky M. (eds.) *Workshop on extraterrestrial materials from cold and hot deserts*. LPI Contribution #997, Lunar and Planetary Institute, Houston, 99pp.

Hiroi T., Pieters C.M., and Takeda H. (1994) Grain size of the surface regolith of asteroid 4 Vesta estimated from its reflectance spectrum in comparison with HED meteorites. *Meteoritics, 29,* 394-396.

Mittlefehldt D.W. and Lindstrom M.M. (1991) Geochemistry of 5 Antarctic howardites and their clasts. *Lunar and Planetary Science* **XXII**, 901-902.

Score R. and Lindstrom M. M. (1990) *Ant. Met. Newsletter* **13**, 1.

Deriving Asteroid Mineralogies from Reflectance Spectra: Implications for the Muses-C Target Asteroid

T. H. Burbine[1], T. J. McCoy[1], E. Jarosewich[1], and J. M. Sunshine[2]
[1]Department of Mineral Sciences, National Museum of Natural History, Smithsonian Institution, Washington, DC 20560-0119, USA (burbine.tom@nmnh.si.edu)
[2]Advanced Technology Applications Division, Science Applications International Corporation, 4501 Daly Drive, Chantilly, VA 20151, USA

Introduction:

To determine an upper limit on how much mineralogical information can be derived from an asteroid spectrum, we have initiated a spectral study of over 70 samples with known bulk compositions that are found in the Smithsonian's Analyzed Meteorite Powder collection [1]. We have also measured the spectra of a number of meteorite types (e.g., primitive achondrites, angrites) that are not well represented in the powder collection. We hope to derive better relations for predicting asteroid mineralogies from reflectance spectra. The Muses-C mission to 25143 1998 SF36 will allow any derived mineralogies to be tested with a returned sample.

Data:

Reflectance spectra (Figure 1) were obtained using the bidirectional spectrometer at Brown University's Keck/NASA Reflectance Experiment Laboratory (RELAB). The spectral coverage was 0.32 to 2.55 μm with a sampling interval of 0.01 μm. The meteorite samples from the Smithsonian's Analyzed Meteorite Powder collection were ground in an agate mortar in a hood with positive air pressure. The samples were then sieved to usually pass through a 100 mesh (< 150 μm) nylon sieve. The fine-powdered fraction (< 150 μm) consisted of silicates and sulfides and contained up to 0.4 wt.% of fine-grained metal. The meteoritic fraction larger than 100 mesh (>150 μm) was primarily metal.

Band area ratios and band centers were calculated from the spectra. The band area ratio is the ratio of the area of Band II divided by the area of Band I. The band center is the band minimum after a linear continuum has been divided out of the spectrum. We are currently probing thin sections of each meteorite to obtain olivine and pyroxene compositions. CIPW norms were used to calculate mineralogies from the bulk compositions. We also plan on using this spectral data to test the precision of the Modified Gaussian Model (MGM) [2] for determining modal abundances and mafic mineral chemistries from reflectance spectra.

Results:

As expected [3], the band area ratios (BAR) for the ordinary chondrites (plus the unusual chondrite Burnwell and the primitive achondrite Acapulco) correlate very well with the normative ratio of olivine (ol) to pyroxene (pyx). These meteorites have ol/(ol+pyx) ratios between ~0.50 and ~0.70. The preliminary least-square fit to the currently-assembled data (Figure 2) give an equation of $ol/(ol+pyx) = -0.232*BAR + 0.765$. Average uncertainties for the calculated ol/(ol+pyx) ratios are $\pm$0.03. Our equation does not hold for the olivine-dominated R chondrites and does not predict well the mineralogy of achondrites such as the angrites and eucrites.

Our equation is dramatically different in slope than previously published work ($ol/(ol+pyx) = -0.417*BAR + 0.948$) (Figure 1), which was recalculated from an equation for

determining the pyx/(ol + pyx) ratio [4]. Their equation was derived from the work of Cloutis et al. [3] for weight percent fractions of orthopyroxene to olivine.

For chondritic meteorites, the average fayalite content of the olivine tends to increase with increasing abundance of olivine; however, we are currently determining how well the band area ratio can be used to estimate the average fayalite content of a chondritic asteroid. We found no linear correlation between band area ratio and any of the oxide abundances (e.g., SiO_2, FeO).

Caveats:

There are a number of caveats that need to be noted when deriving compositional information from an asteroid. Meteorite reflectance spectra are measured at room temperature; however, main-belt asteroids tend to have much lower surface temperatures (~150-200 K) [5]. Moroz et al. [6] has shown that there are slight changes in the band area ratio for ordinary chondrite samples with decreasing temperature.

It is unclear how alteration of the surface (usually called "space weathering") affects the band area ratio. Irradiation experiments by Yamada et al. [7] using a pulse laser, which is hoped to duplicate the effects of micrometeorite impacts on the surface of an asteroid, have shown that it is easier to spectrally alter olivine than pyroxene.

Some asteroids with band area ratios consistent with olivine-pyroxene assemblages may have vastly different mineralogies. Sunshine et al. [8] have identified a number of objects with band area ratios that fall within the range of ordinary chondrites, but have spectral features due to low- and high-Ca pyroxenes and appear to contain little olivine.

Muses-C Target Asteroid:

The target asteroid for the Muses-C mission is S-asteroid 25143 1998 SF36. The ground-based spectrum of 1998 SF36 [9] has a band area ratio of 0.40 ± 0.02. This implies an ol/(ol+pyx) ratio of 0.67. This mineralogy is found in both L and LL chondrites; however, the Band I center (0.99 ± 0.01 μm) for this object is consistent [9] with LL chondrites.

Conclusions:

The derived equation for determining the ol/(ol+pyx) ratio from the band area ratio appears valid for mafic mineralogies roughly similar to those found in ordinary chondrites and should be useful for estimating the mineralogies of chondritic and primitive achondritic assemblages. The Muses-C sample return mission will allow us to test how well we can determine asteroid mineralogies from reflectance spectra.

References:

[1] Jarosewich E. (1990) *Meteoritics, 25,* 323-337. [2] Sunshine J. M. and Pieters C. M. (1993) JGR, 98, 9075-9087. [3] Cloutis E. A. et al. (1986) *JGR, 91*, 11641-11653. [4] Gastineau-Lyons H. K. et al. (2002) *Meteorit. Planet. Sci., 37*, 75-89. [5] Hinrichs J. L. et al. (1999) *Geophys. Res. Lett., 26*, 1661-1664. [6] Moroz L. et al. (2000) *Icarus, 147,* 79-93. [7] Yamada M. et al. (1999) *Earth Planets Space, 51*, 1255-1265. [8] Sunshine J. M. et al. (2002) *LPSC XXXIII*, Abstract #1356. [9] Binzel R. P. et al. (2001) *Meteorit. Planet. Sci., 36*, 1167-1172.

Acknowledgments:

Brown University's Keck/NASA Reflectance Experiment Laboratory (RELAB) is a multi-user facility supported by NASA grant NAG5-3871.

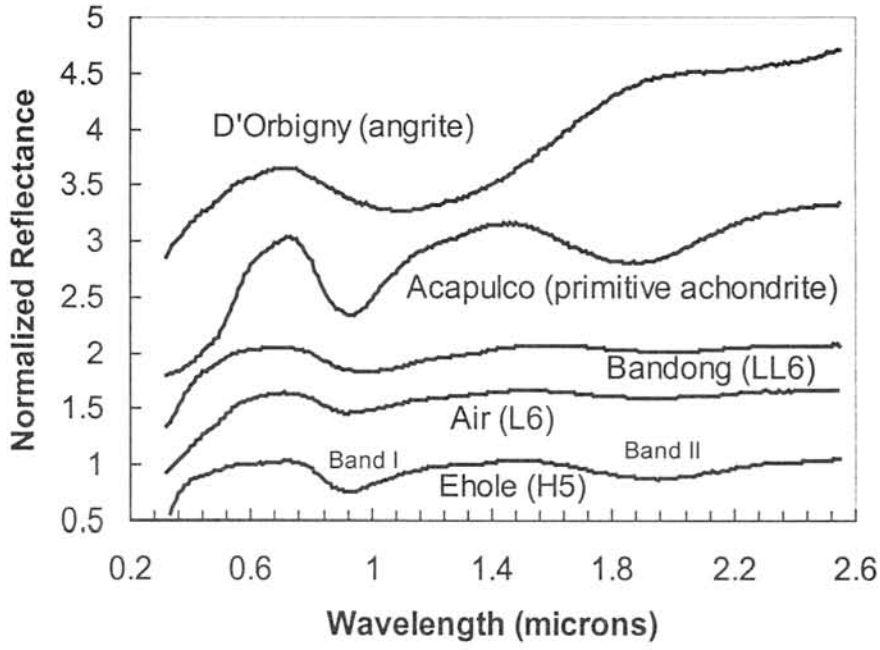

Figure 1. Reflectance spectra of a number of meteorite samples. Grain sizes for Ehole, Air, and Bandong are less than 150 microns. Grain sizes for Acapulco and D'Orbigny are less than 125 microns.

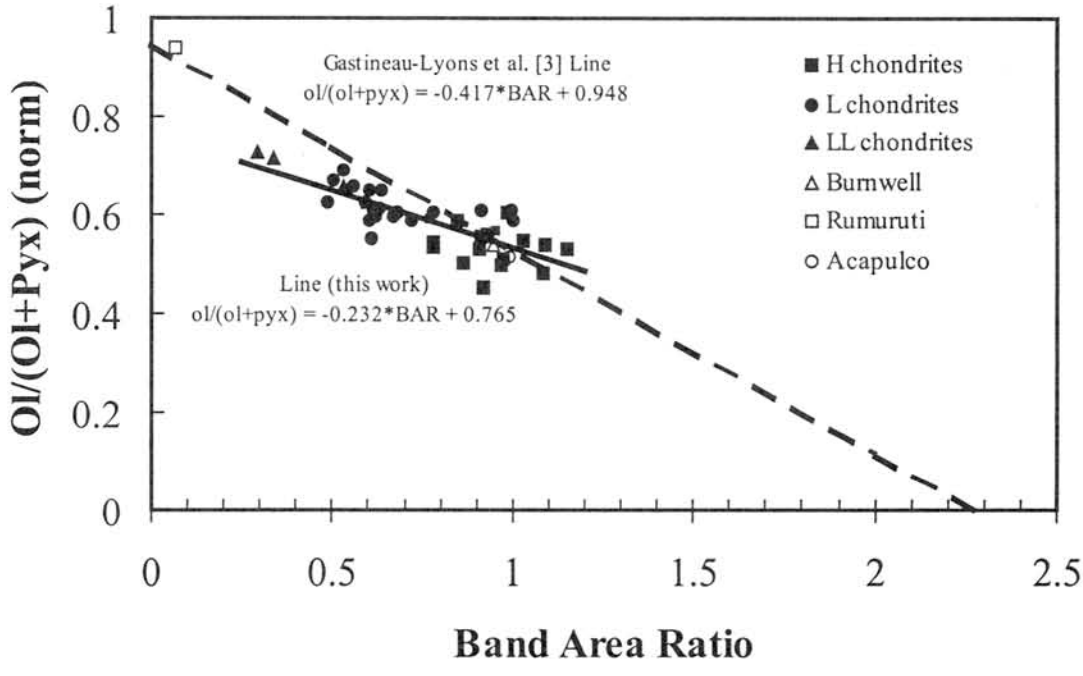

Figure 2. Plot of band area ratio versus normative ol/(ol+pyx) ratio.

CONSTRAINTS ON MARTIAN EVOLUTION FROM SNC METEORITES

G. Dreibus and E. Jagoutz, Max-Planck-Institut f. Chemie, P.O. BOX 3060, D-55020 Mainz, Germany, (dreibus@mpch-mainz.mpg.de).

Introduction:

The entire 27 SNC meteorites are generally believed to represent magmatically differentiated Martian rocks expelled from the Martian surface by large impacts. From their chemical composition it is possible to estimate the composition of the Martian mantle and, using some assumptions, even on the composition of the Martian core [1]. The radiogenic isotopes of the SNCs reveal their initial isotopic reservoirs and the time scale for the chemical evolution of the Martian mantle [2]. The Pb isotopes of the two paired Antarctic nakhlites from the Japanese collection have been measured and will be compared with the existing Pb isotopic systematic of the SNC meteorites (Fig. 4).

Bulk composition of the Martian mantle:

The bulk composition of the Martian mantle (Fig.1) was calculated from element correlations observed in **s**hergottites, **n**akhlites, **C**hassigny, and the orthopyroxenite ALH 84001 (SNC meteorites) and general cosmochemical constraints. The refractory lithophile elements in a planetary body have chondritic abundances, whereas during the planetary accretion and evolution with formation of metallic and silicate phases, the siderophile and volatile elements are more or less depleted in the mantle.

The mean abundance values for moderately volatile elements Na, P, K, F, and Rb and most of the volatile elements like the halogens in the Martian mantle exceed the terrestrial values by about a factor of two. The enrichment of bromine on Mars compared to terrestrial mantle is illustrated in Fig. 2. For the volatile element Br and the refractory lithophile element La we found a good correlation among all analyzed falls and finds of SNC meteorites which were not collected in hot deserts. An unusual enrichment of Br was observed in the desert meteorites DaG 476, SaU 005, Dhofar 019 and in Nakhla. In all SNCs from the Antarctica no depletion or enrichment of Br relative to La were observed. Surprisingly, the new nakhlite Y-000593 from the Antarctica, collected by a Japanese expedition, has a Br content of 78 ppb and plots below the Br-La correlation line in Fig.2. The data point for the Mars' mantle in Fig. 2 is obtained from the Br/La correlation line, assuming a Si normalized CI abundance of La.

The abundances of all chalcophile elements are lower in the Martian mantle compared to the terrestrial mantle (Fig. 1). This observation has been taken as evidence for the extraction of these elements from the Martian mantle by FeS segregation to the core during the accretion process of the growing planet. Core formation must have occurred concurrently with the rapid accretion of Mars, which is inferred from excess ^{182}W in Martian meteorites [3]. Wänke and Dreibus [1] calculated a sulfur-rich Martian core with about 14 % S and a total core mass of 21.7 %. In comparison with the Earth and its large Fe-Ni core of 33 % the FeO content of the Martian mantle is about a factor of 2 higher. In situ measurements on the Martian surface by X-ray spectroscopy of the Viking [4] and the Pathfinder [5] missions confirmed the high FeO contents of about 20 % for soils and rocks.

The X-ray analyses of Viking and Pathfinder revealed also extremely high concentrations of the volatile elements Cl (0.6 %) and S (7 % SO_3) in the Martian soil. Sulfur and Cl both dominate in the soil and were interpreted to originate from an interaction of volcanic gases with the surface material [6]. An extraction of the halogens from the interior into the crust can also be deduced from the observed higher $^{129}Xe/^{132}Xe$ in the Martian atmosphere compared to the interior of Mars [7, 8]. In contrast, the $^{129}Xe/^{132}Xe$ ratio in terrestrial rocks is equal or higher than the atmospheric ratio. The enrichment of $^{129}Xe_{rad}$ in the Martian atmosphere produced by the decay of ^{129}I with a half-life of 15.7 Ma points to a very early extraction of iodine into the crust and its release into the present atmosphere over geological time.

Sm-Nd, Rb-Sr, and U-Pb isotopes in SNC meteorites:

Isotopic data are a powerful tool for the study of planetary evolution. From the Rb-Sr isotopic systematic of 6 SNC meteorites Jagoutz [2] postulated about 10 years ago the existence of 3 isotopically distinct reservoirs on Mars, which remained isolated for a period of 4.3 ± 0.2 Ga. Since then, 21 more SNC meteorites have been found in hot and dry deserts. New isotope data from these recently recovered SNCs confirm the three isotopically distinct reservoirs on their parent body (Fig. 3).

The first group of the basaltic shergottites Shergotty, Zagami and Los Angeles have relatively high abundances of radiogenic Sr, which might originate from a planetary crust. The new shergottite Dhofar 378 recently classified by Ikeda et al [9] with equal parts of coarse grained pyroxene and feldspar seems to be a late magmatic differentiate. There is a good chance that this shergottite will give us the possibility to get insight into intercrustal magmatic differentiation on Mars. U-Pb isotope measurements on ultraclean mineral separates are under way.

A second group, characterized by non-radiogenic Sr, consists of the two mafic cumulates Nakhla and Chassigny, the olivine rich shergottites DaG 476, SaU 005 and Dhofar 019, and the basaltic QUE 94201 and may represent the depleted mantle. This and the first group are chemically complementary, suggesting that crust formation has caused the mantle depletion. The depletion of this reservoir must have taken place during a very early process. This can be derived from the primitive Sr isotopes and the existence of Nd-142, the daughter product of the extinct Sm-146, found in Chassigny, the Nakhlites, SaU 005, DaG476, and QUE 94201 (E42 group). The origin of the E42 group from a common $^{143}Nd/^{144}Nd$ reservoir was also postulated. This premise derived mainly from Nd isotopic systematics measured on minerals of the E42 group. While the acid leach-residue of Sm-Nd isochrons for SaU 005, DaG 476 and QUE 94201 yield ages between 300 and 400 Ma, their separated mafic minerals plot along an isochron of 700 Ma as do hand-picked pyroxene and olivine separates of Nakhla.

A third group with intermediate Sr isotopic composition, represented by the olivine gabbroic LEW 88516, ALHA77005, and Yamato793605, might originate from a primitive, unfractionated mantle. However a mixing process of crust and depleted mantle cannot be excluded [10]. The Sr isotopes of all SNCs plot close to a 4.5 Ga isochron. The requirement to keep three isotopically distinct reservoirs isolated for a period of about 4.5 Ga places severe constraints on the tectonic activity of the planet.

The Pb isotopes of all measured SNCs show a similar pattern as the Sr isotopes and agree with the postulated common reservoir for E42 meteorites. First results of a leach residue experiment of the two Antartic nakhlites from the Japanese collection are very similar to those of Nakhla and made it possible to obtain the first concordant Pb-Pb-ages (Fig. 4). The present study of the Pb isotope systematics might give the strongest indication for an early differentiation of Martian mantle and crust. The initial Pb data from plagioclase separates of Los Angeles, Shergotty, and Zagami from the enriched crustal reservoir and of Nakhla and SaU 005 from the depleted mantle reservoir plot close to the 4.5 Ga Pb-Pb isochron (Fig 3). In contrast to Nakhla, SaU 005 was found in the Oman Desert. Terrestrial weathering has strongly influenced the Sm-Nd as well as the Rb-Sr systems of this meteorite. Thus, there was no expectation of finding a significant internal age relation using the U-Pb isotopes on this heavily altered SNC meteorite. Instead, we concentrated our effort on identifying its initial Pb isotopic composition, for which we used 5 mg of optically pure maskelynite grains. SaU 005 plagioclase Pb is within analytical error identical to Nakhla initial Pb (Fig 3 and 4).

The conformity of the U-Pb and Rb-Sr isotopic systematics reflects similar magmatic fractionation behaviour of Rb and U during crust mantle evolution. We used the correlation of the isotopically related Rb/Sr ratio versus the μ value in all our analysed SNCs to estimate the μ value for the Martian mantle. The Rb/Sr ratio of the Martian mantle of 0.084 yields a μ value of 3.1 corresponding to 366 ppb Pb in the Martian mantle. Compared to the Earth with a $\mu = 8$, Pb on Mars is enriched by at least a factor of 2.5, as was found for all other moderately volatile and volatile elements (Fig.1). Contrary to the Earth, the Martian core is sulfur-rich and all chalcophile elements are depleted in the Martian mantle according to their sulfur/silicate partition coefficients. In iron-meteorites Pb shows a chalcophile tendency. However, the more than twofold enrichment of Pb in the silicate phase of Mars compared to that of Earth might exclude its chalcophile behaviour (Fig. 1). Lead, with a condensation temperature from a solar gas lower than 600°K belongs to the group of volatile elements. Obviously, during planetary formation and evolution Pb behaves like a volatile and not like a chalcophile element.

Summary:

Compared to Earth Mars is a volatile rich planet. The ^{129}I-^{129}Xe ($T_{1/2}$ 16 Ma) and the ^{146}Sm-^{142}Nd ($T_{1/2}$ 103 Ma) isotope systems indicate a rapid accretion and a very early formation of the crust with its enrichment of volatile and highly incompatible lithophile elements. The absence or at most very limited plate tectonic activity on early Mars excludes a crustal recycling back to the mantle and preserves the Rb-Sr and U-Pb isotopes systems derived from the early crustal differentiation. The observed correlation of radiogenic ^{182}W with radiogenic ^{142}Nd by [3] points also to a close relationship between core formation and mantle melting in the first ~30 Ma of the Martian accretion.

References:

[1] Wänke H. and Dreibus G. (1988) *Phil.Trans. R. Soc. Lond. A325*, 545-557. [2] Jagoutz E.(1991) *Space Sci. Rev. 56*, 13-22. [3] Lee D.-C. and Halliday A.N. (1997) *Nature 38*, 854-857. [4] Clark B.C. et al. (1982) *J. Geophys. Res. 87*, 10,059-10,067. [5] Rieder R. et al. (1997) *Science 278*, 1771-1774. [6] Clark B. C. (1993) *GCA 57*, 4575. [7] Swindle T.D. et al. (1986) *GCA 50*, 1001. [8] Ott U. and Begemann F. (1985) *Nature 317*, 509. [9] Ikeda Y. et al. (2002) *LPSC XXXIII*, # 1434. [10] Borg L. E. (2001) *GCA 65*, in press.

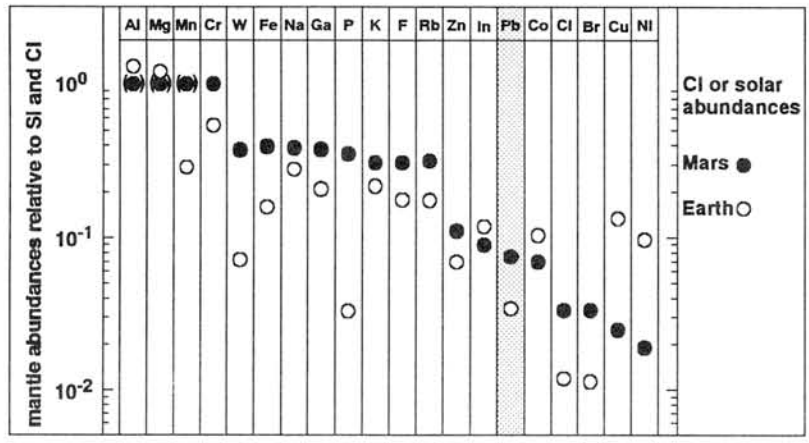

Fig. 1

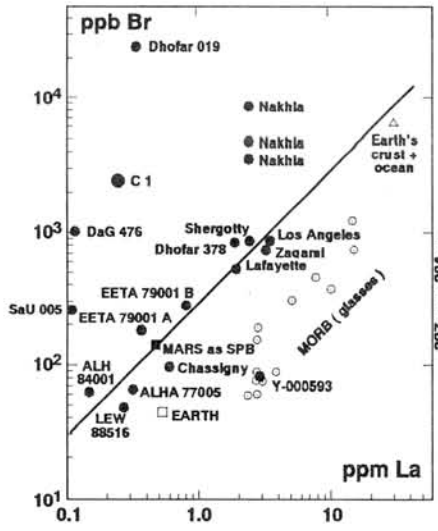

Fig. 2

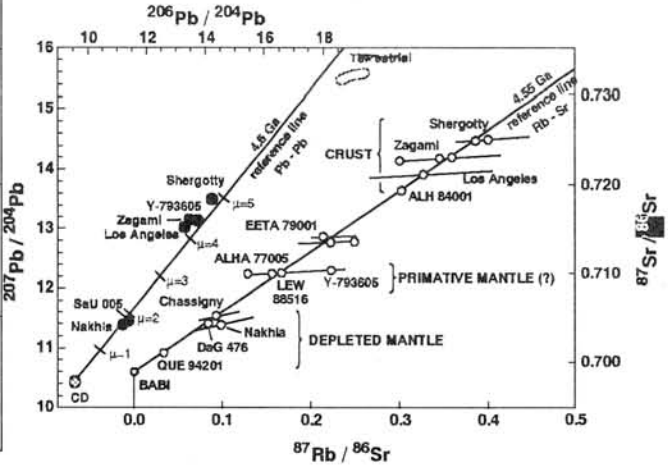

Fig. 3

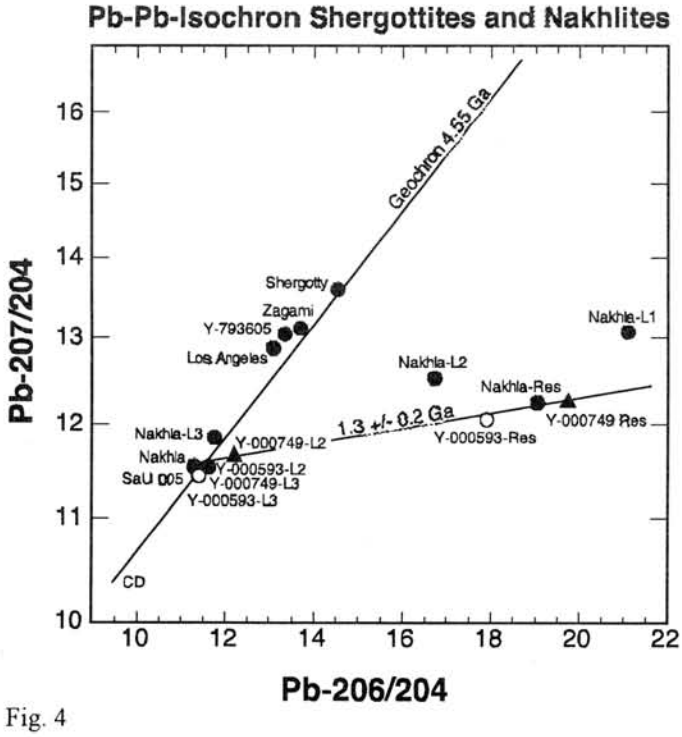

Fig. 4

Contrasting oxygen isotopic evolution of fine and coarse refractory inclusions from the CV3 Efremovka

Timothy J. Fagan*[1], Hisayoshi Yurimoto[1], Alexander N. Krot[2], Klaus Keil[2]

[1]Department of Earth and Planetary Sciences, Tokyo Institute of Technology, 2-12-1 Ookayama, Meguro, Tokyo 152-8551, Japan
[2]Hawai'i Institute of Geophysics and Planetology, University of Hawai'i at Manoa, Honolulu, HI 96822, USA
*fagan@geo.titech.ac.jp

INTRODUCTION and APPROACH

The ^{16}O-isotopic enrichment characteristic of coarse-grained Ca,Al-rich inclusions (CAIs) in CV chondrites suggests that refractory objects in chondritic meteorites formed from a different source of oxygen than less refractory chondrules and matrix (Clayton, 1973; 1993). Recent isotopic analyses of fine-grained CAIs and amoeboid olivine aggregates (AOAs), which are also refractory relative to chondrules, are consistent with this hypothesis for the CV chondrites (Aleon et al., 2002; Fagan et al., 2002). In light of this association of refractory materials in the CVs with ^{16}O-rich compositions, the longstanding controversy over the origin of ^{16}O-poor melilite in coarse-grained CAIs remains puzzling (Clayton, 1993; Young and Russell, 1998; Yurimoto et al., 1998).

In this study, we present a direct comparison of textures, major element compositions, and isotopic compositions of melilite-bearing fine- and coarse-grained CAIs from the reduced CV3 Efremovka. Our main goal is to test whether the coarse-grained melilite attained its ^{16}O-poor composition during parent body alteration, as has been suggested recently for the COs (Wasson et al., 2001).

ANALYTICAL METHODS

Textures, major element compositions and *in situ* oxygen isotopic compositions were collected from melilite-rich domains in one fine-grained and one coarse-grained CAI in the same thin section of the reduced CV3 Efremovka. Textures and elemental compositions were analyzed using a JEOL JSM-5310LV scanning electron microscope and a JEOL JXA-8800 electron microprobe. Oxygen isotopic analyses were determined using the Titech Cameca 1270 ion microprobe under conditions described previously (Yurimoto et al., 1998).

RESULTS and DISCUSSION

Fine-grained CAI (FGI): The FGI is characterized by fine, anhedral, equant crystals of spinel, melilite, Al-diopside, and minor forsterite and perovskite. The FGI is composed of nodules of spinel partially to completely surrounded by melilite (MacPherson et al., 2002), and a diffuse network of Al-diopside connecting the spinel-cored nodules (Fig. 1A,B). Forsterite forms a discontinuous rim around the margins of the FGI. FGI melilite has a nearly constant major elemental composition of $Åk_{\sim 14}$. *In situ* oxygen isotopic analyses are consistent with the ^{16}O-rich compositions associated with refractory objects in CV chondrites. Spinel and forsterite have compositions near –40‰ in both $\delta^{18}O$ and $d^{17}O$ (Fig. 1C); mixed analyses of Al-diopside with adjacent melilite and matrix material yield somewhat heavier isotopic compositions, but this is due, at least in part, to beam overlap with adjacent grains. In contrast, four closely spaced analyses of melilite are ^{16}O-depleted and yield a range of about 20‰ (Fig. 1B,C).

Coarse–grained CAI (CGI): The CGI is dominated by very coarse-grained Al,Ti-diopside and melilite typical of type B1 CAIs (Fig. 1D,E). Anorthite is less abundant and finer grained, and spinel occurs as widespread equant inclusions on the order of 10 to 15 μm across. Melilite occurs along the margin of the CGI, and in the interior as elongate, euhedral prismatic crystals. The major element composition of CGI melilite varies over $Åk_{11-45}$ in the mantle and over $Åk_{40-70}$ in the interior. The Åk-content increases from core to rim in euhedral interior crystals, consistent with fractional crystallization during a single igneous cooling event. Oxygen isotopic compositions are similar, but do not conform exactly, to the generally accepted model for CV CGIs. Spinel, Al,Ti-diopside, and anorthite have ^{16}O-rich compositions near –30 to –40‰ with slightly higher $\delta^{18}O$ than $\delta^{17}O$ (Fig. 1F). Multiple analyses of melilite from the core and margin of the CGI and from domains with widely different Åk-contents all yield similar ^{16}O-depleted compositions.

Discussion: Exchange of oxygen during alteration on the Efremovka parent body cannot account for the contrasts in texture and composition of the CGI and FGI melilite. The FGI melilite is fine-grained, unzoned in major elements, and exhibits variable ^{16}O-depletion, whereas the CGI melilite is very coarse-grained, is zoned in major elements, and has a constant ^{16}O-depleted isotopic composition. Exchange of ^{16}O-poor oxygen from a hydrothermal fluid with ^{16}O-rich oxygen in primary melilite in a parent body setting would reset fine-grained melilite before coarse-grained melilite. Therefore, partial resetting of oxygen could result isotopically zoned CGI melilite and uniform ^{16}O-depleted compositions in FGI melilite. Our results show the opposite pattern, indicating that the ^{16}O-depletion of CGI melilite must have preceded formation of the Efremovka parent body (Yurimoto et al., 2001).

Whatever caused the ^{16}O-depletion of melilite in CV CGIs must have been strong enough to reset oxygen compositions of very coarse melilite crystals separated by 100s of μm. At the same time, the process must have been selective, because other primary minerals have retained their original ^{16}O-rich compositions. Oxygen exchange may have occurred during rapid heating of CGIs and kinetically favored melting of melilite in the presence of a ^{16}O-poor gas (Yurimoto et al., 1998). The presence of ^{16}O-poor anorthite in several CV CGIs indicates that oxygen was exchanged in minerals in addition to melilite in some cases (Clayton, 1993; Yoshitake et al., 2001).

REFERENCES

Aleon J., et al. (2002) LPSC XXXIII #1426.

Clayton R.N. (1993) Annu. Rev. Earth Planet. Sci., v. 21, p. 115-149.

Clayton R.N., et al. (1973) Science 182, 485-488.

Fagan T. J., et al. (2002) LPSC XXXIII #1507.

MacPherson G. J., et al. (2002) LPSC XXXIII #1526.

Wasson, J.T., et al. (2001) Geoch. Cosmochim. Acta, v. 65, p. 4539-4549.

Yoshitake, M., et al. (2001) Metorit. Planet. Sci. 36, A229-A230.

Young E. D. and Russell S. S. (1998) Science 282, 452-455.

Yurimoto H. et al., (1998) Science, v. 282, 1874-1877.

Yurimoto H. et al., (2001) Metorit. Planet. Sci. 36, A230.

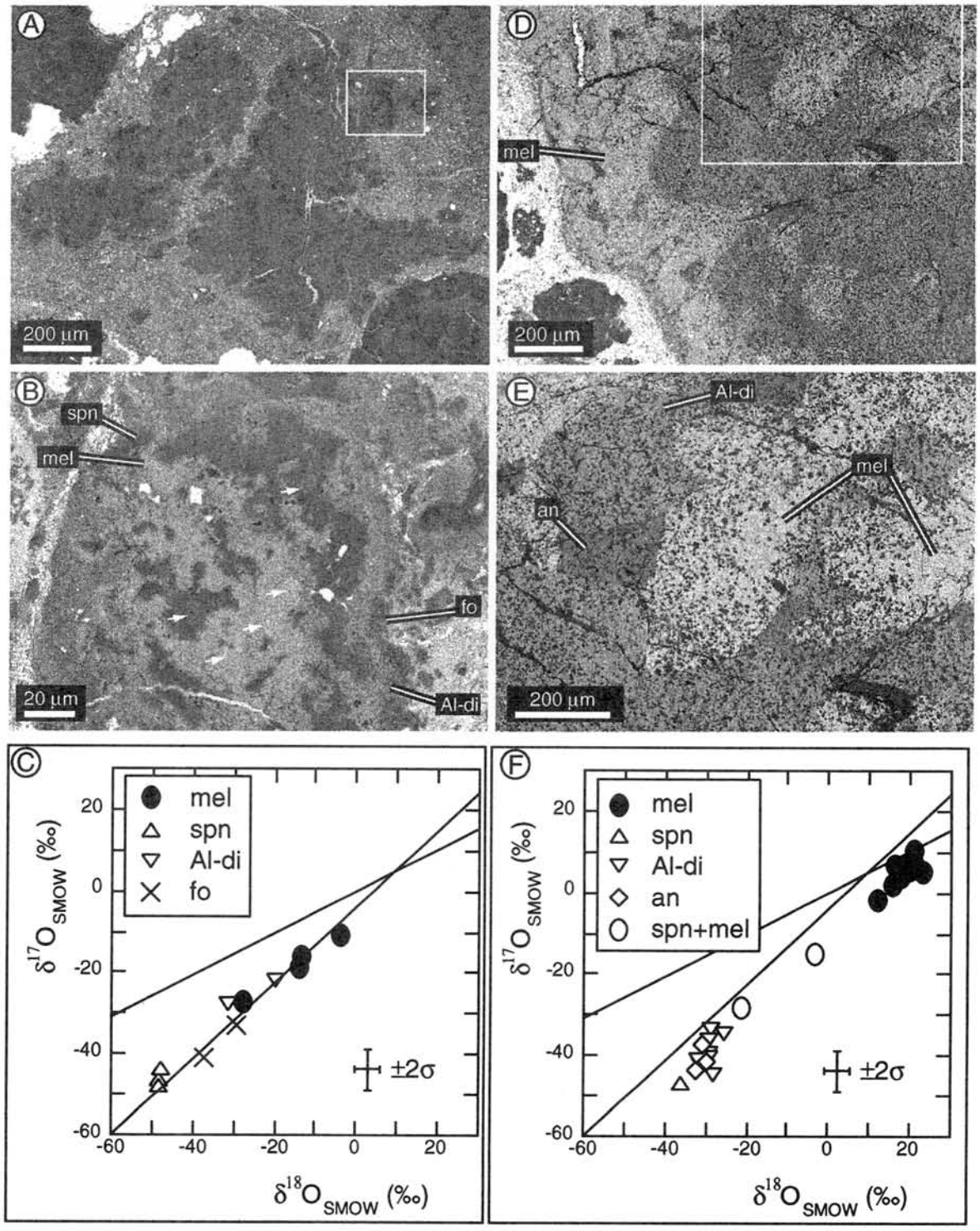

Figure 1. Backscattered electron (BSE) images and oxygen isotopic results from a fine-grained CAI (A, B, C) and coarse-grained CAI (D, E, F). Boxes in A and D highlight areas shown in greater detail in B and E. Arrows in B show pits excavated during SIMS analyses. Mineral abbreviations: Al-di, Al,Ti-diopside;an, anorthite; fo, forsterite; mel, melilite, spn, spinel.

LIGHT ELEMENT GEOCHEMISTRY OF LUNAR METEORITES

I.A. Franchi, A.B. Verchovsky and R.C. Greenwood

Planetary and Space Sciences Research Institute, Open University, Walton Hall, Milton Keynes, MK7 6AA, United Kingdom (i.a.franchi@open.ac.uk).

Introduction Lunar meteorites now constitute a significant source of material which complements that returned by the Apollo and Luna sample return missions approximately 30 years ago. While the differences between the lunar meteorites and the returned samples offer further insight into lunar processes it is critical that we have a clear understanding of the effects of the ejection, atmospheric entry and terrestrial weathering associated with the lunar meteorites. Equally, these effects may help shed new light on existing problems.

The location, origin and isotopic composition of implanted nitrogen, carbon and the noble gases in lunar soils and breccias has been an area of considerable research these past 30 years – however, many issues remain, to a greater or lesser extent, un-resolved. The large variations in nitrogen isotopic composition have yet to be explained, although a number of recent papers have indicated that most of the observed variation is from input of an isotopically variable non-solar wind component [1-3]. De-convolution of the solar and non-solar components has proved elusive, particularly as there appears to be a degree of homogenisation of these components, as can also be seen in the co-release of solar wind ^{36}Ar and re-implanted lunar atmospheric ^{40}Ar (Assonov et al 2002). These authors have considered the effects of regolith processing on the location of the implanted gases within the mineral grains and glassy agglutinates in lunar samples to explain the complex, but regular release profiles observed in many returned lunar samples. Preliminary results by [4] noted that the release profiles of nitrogen and argon from lunar meteorites were quite distinct from any observed from returned samples, and suggested this may be the result of terrestrial weathering preferentially affecting the gas-rich irradiated rims of mineral and rock fragments. This paper reports further analysis of lunar meteorites, including the new anorthoscitic breccia Yamato 981031, using the fully automated Finesse mass spectrometer system which measures the abundance and isotopic composition of carbon, nitrogen, neon, argon and xenon together with the abundance of helium and carbon from high resolution stepped heating experiments (see [5] for details on the method).

Results The samples analysed for this study are the anothoscitic breccia Y82192, anothoscitic regolith breccias Y791197 and Y981031. Previously analysed samples include the anorthoscitic regolith breccias DaG 262, MAC 88105 and ALHA 81005 and the basaltic microbreccia QUE 94281. All samples have relatively low weathering grades, and between 2 and 10 mg of chips of each sample was used for each analysis. The data from the noble gas analyses for Y791197 and Y82192 are consistent with previous results, showing the characteristics of a very gas rich rock and an unusually gas poor one respectively. The Y981031 is somewhat intermediate in its gas content as can be seen in Table 1. The Ne/Ar ratio is also somewhat low for a lunar rock – further analyses are underway to verify this unusual result.

Table 1 Summary of gas content in Y981031 (noble gas content as $x10^{-8}$ cc/g)

	ppm N	$\delta^{15}N$	ppm C	[^{4}He]	[^{20}Ne]	20/22	21/22	[^{36}Ar]	38/36	40/36
Y82192	10.3	10.8	386	191				12.6*		
Y791197	41.5	-32.6	483	329100	67570	12.0	0.0393	36810	0.184	2.86
Y981031	28.8	-3.6	288	93350	18481	11.8	0.0482	19100	0.194	2.11

*^{40}Ar measurement – ^{36}Ar not detected above blank.

The nature of the release profiles of all the gas rich lunar meteorites analysed to date (Y981031, Y791197, ALHA81005, QUE94281 and DaG 262) are strikingly different to those observed from any returned lunar soils. The example of the nitrogen releases from Y981031 and Y791197 are shown in comparison with the breccia components of the 200 to 450 μm fraction of the returned mature regolith Luna 1635 [from 3] in Figure 1. A very similar pattern is displayed by argon. Indeed, Figure 2 shows that the release profiles of the nitrogen and argon are virtually identical (with the exception of low temperature terrestrial contamination) with virtually a constant $^{40}Ar/^{36}Ar$ ratio across the main release. While the somewhat perplexing co-release of solar wind ^{36}Ar and lunar atmospheric ^{40}Ar in returned lunar samples, implanted a grossly different energies, has be discussed previously [3] the similarity in their release is even more striking in the lunar meteorites. If this co-release is a result of regolith processing, either by annealing or immurement then lunar meteorites may represent a more developed example of this process. Interestingly, the xenon release profile is also almost identical to that of the nitrogen and argon indicating that the effects of diffusion are not significantly affecting the release profile, but rather that the onset of melting at around 1050°C is liberating gases well protected within the rock, at least for the heavier gases.

The light gases, helium and neon, have virtually identical release profiles but at much lower temperatures than the heavier gases (Figure 3), with much broader releases indicative of a greater influence of the role of diffusive loss. However, the great difference in release temperature between neon and argon, in contrast to that between helium and neon suggests that there has been extensive mobilisation of all the implanted gases in the rock, possibly during the thermal effects of the shock event associated with the excavation of these rocks from the lunar surface, with the light gases eventually being large located in a distinct site from the heavier gases. Intriguingly, the neon isotopic pattern of all the gas rich lunar meteorites still show a release pattern of decreasing $^{20}Ne/^{22}Ne$, generally interpreted as sequential release of solar wind followed by solar energetic particles, reflecting their differing implantation depths. Clearly such an interpretation is not consistent with extensive mobilisation of the gases and therefore further work is required to resolve these conflicting views.

The carbon release profile from the lunar meteorites is also virtually identical to that of the heavier gases – such that, in contrast to typical returned lunar samples, the indigenous carbon is now well resolved from the large amounts of terrestrial contamination, a problem which has to date hindered investigation of solar wind carbon. The atomic C/N ratio is generally around 2.6 or even lower, in contrast to the solar value of ≈3.25 [6]. Further investigation of this aspect of the lunar meteorites, particularly with carbon isotopic measurements, offers the possibility of helping to constrain the nature of the non-solar nitrogen component and its implantation mechanism as meteoritic or cometary material is one of the more likely sources.

The oxygen isotopic composition of Y981031 has also been determined using a high precision laser fluorination technique [7], giving a $\delta^{18}O$ of +6.00‰ and a $\Delta^{17}O$ of –0.033‰ - clearly consistent with that of other lunar samples (Figure 5). Also shown are the results of other lunar meteorites [8] and lunar rocks [9].

References [1] Wieler et al (1999) *Earth Planet. Sci Lett.* **167**, 47-60. [2] Hashizume et al (2001) *Antarctic Meteorites* **XXVI**, 66-68. [3] Assonov et al (2002) *Met. Planet. Sci.* **37**, 27-48. [4] Franchi et al (1999) *LPI Tech Report* **#997**, 33-35. [5] Verchovsky et al (1998) *Faraday Discuss.* **109**, 403-416. [6] Anders and Grevesse (1989) *GCA* **53**, 197-214. [7]

Miller et al (1999) *Rapid Comm. Mass Spectr.* **13**, 1211-1217. [8] Calyton and Mayeda (1996) *GCA* **60**,1999-2017. [9] Wiechert et al (2001) *Science* **294**, 345-348.

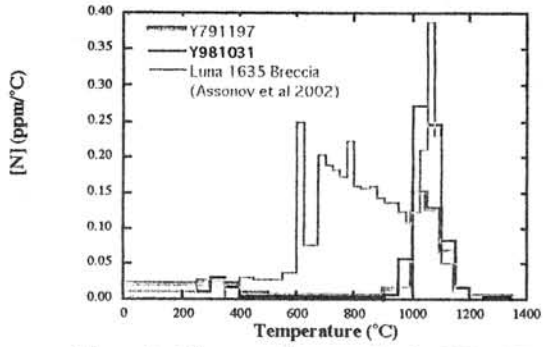

Figure 1 Nitrogen release profile for Y791197, Y981031 and the breccia components of the 200 to 450 μm fraction of Luna 1635

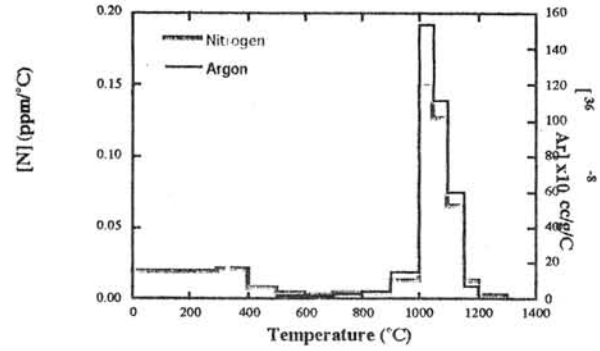

Figure 2 Nitrogen and argon release profiles of Y981031

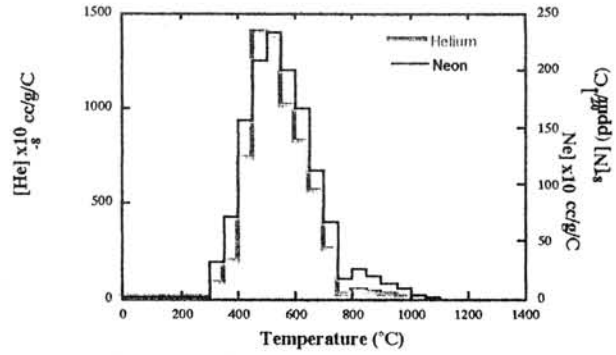

Figure 3 Helium and neon release profiles of Y791197

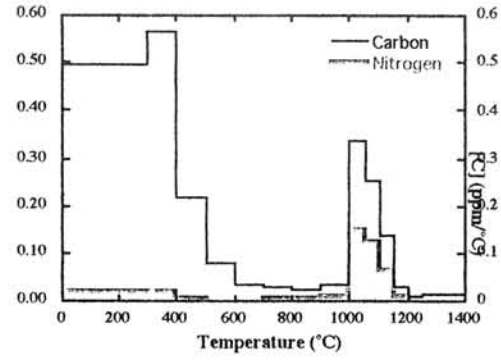

Figure 2 Nitrogen and carbon release profiles of Y981031

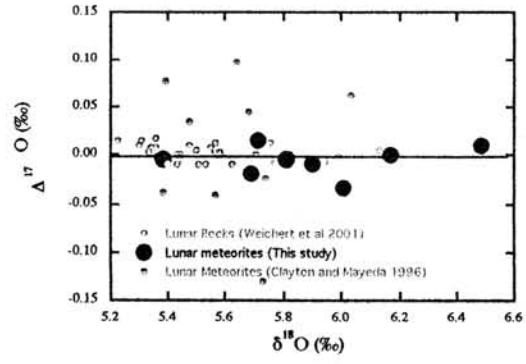

Figure 5 Oxygen isotopic composition of lunar meteorites, with previous results from other studies of lunar meteorites [8] and rocks [9].

The origin of natural remanent magnetization of Kobe (CK4)

M. Funaki[1] and N. Nakamura[2]

1: National Institute of Polar Research, 9-10 Kaga 1 Itabashi Tokyo 173-8515, Japan

2: Department of Earth and Planetary Sciences, Faculty of Science, Kobe University, Nada, Kobe 657-8501, Japan

1. Introduction

Kobe meteorite classified into CK4 based on chemical compositions consists of chondrules, blackened clast and fine-grained white objects in the matrix (Nakamura et al. 2000). According to Tomeoka et al. (2000), magnetite is the most abundant opaque mineral in both chondrule and the matrix. Larger magnetite grains more than 50μm in diameter contain exsolution of ilmenite and spinel lamellae of typically 1-3μm wide. Spherical chlorapatite is also dispersed in magnetite. Fine-grained aggregates of pentlandite are included in the matrix associated with a minor amount of troilite to be on intimate with pentlandite. Usually fine-grained magnetite in terrestrial rocks give significant paleomagnetic information, while sulfide is not due to unstability against the environmental changes. If magnetite in Kobe carries the stable natural remanent magnetization (NRM), we may estimate the existence of the magnetic field in the parent body. This study is carried out to reveal the evidence of magnetic field when Kobe was magnetized.

2. Experiments

We obtained a sample (C-4C, 0.132g) from the interior Kobe for magnetic study. Its NRM was intensity (R)=2.36x10^{-4}Am^2/kg, inclination (I)=31 and declination (D)=159. The sample was divided into 3 pieces (C-a (0.05304g), -b (0.04590g), -c (0.01758g)) with the same coordinate of the sample C-4C for the samples C-a and C-b, while the sample C-c was obtained without orientation due to too small size. The NRM of these samples varied to R=2.28x10^{-4}Am^2/kg, I=17, D=216 for the sample C-a, R=3.33x10^{-4}Am^2/kg, I=34, D=87 for that of C-b and R=4.34x10^{-4}Am^2/kg for the sample C-c. The NRM intensities were similar values but the direction scattered widely. The sample C-c was demagnetized to 100mT in steps 5mT by alternating field (AF demagnetization). The results indicated that the NRM was relatively stable up to 50mT, as shown in Fig. 1, but it was more unstable between 50 and 100mT.

The sample C-c was supplied to measure a magnetic hysteresis loop between -1.0 and 1.0T and thermomagnetic (Js-T) curves at 1.0T in the vacuumed to 10-4 Pa. The Js-T curve showed reversible magnetization with magnetite Curie Point at 580°C in the heating and cooling curve. Therefore, the principal magnetic mineral is concluded to be magnetite, but iron sulfide is nonmagnetic. The hysteresis properties showed the saturation mangetization (Js)=7.76 Am^2/kg, that is equivalent to the mangetization of 8.4wt% of magnetite in the sample, because the Js valeu of magnetite is 92 Am^2/kg. Pseudosingle-domain (PSD) of magnetite is inferred from the hysteresis

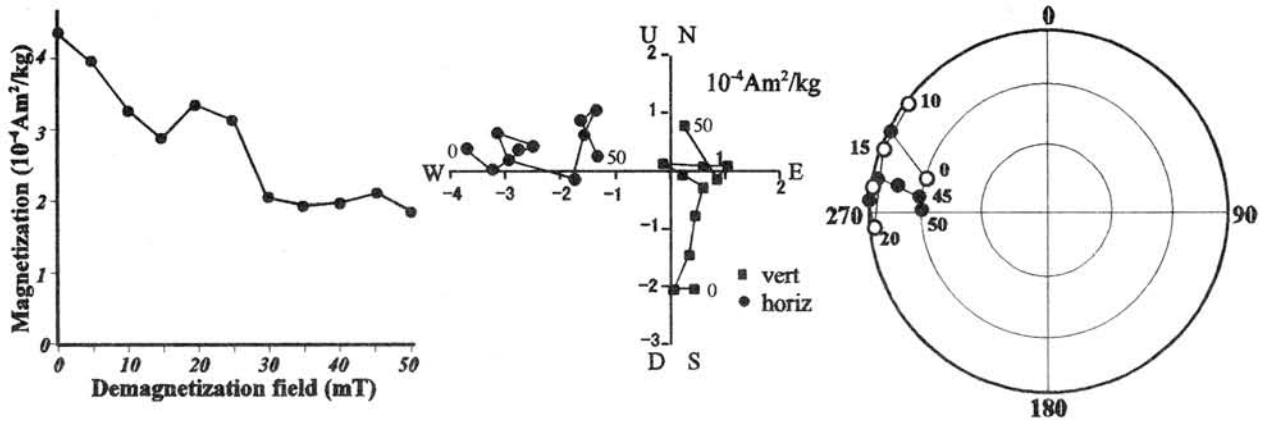

Fig. 1 AF demagnetization of NRM. Left: intensity change, center: component change, right: direction change

parameters.

The sample C-b was polished to identify the magnetic minerals by reflected right microscope. The sample included magnetite and iron sulfide in the matrix and chondrules. Various size of magnetite grains up to 200x130μm in diameter was included in the sample. The larger grains were invaded by the lamellae and vains. When magnetotactic bacteria were applied to the sample, the bacteria made clusters on the magnetite grains, but not sulfide, in NRM state.

3. Discussions

The NRM direction of the divided samples scattered widely. Nevertheless, the NRM was relatively stable against AF demagnetization. Although the number and size of samples are not enough for terrestrial paleomagnetic level, it may be estimated whether the magnetic field existed or not when Kobe was magnetized. The deviated direction of samples C-a and C-b may suggest that the NRM of Kobe was not regulated by external magnetic field, suggesting metamorphosed in the negligibly weak magnetic field. Tomeoka et al. (2001) estimated a shock metamorphism of Kobe under mild shock pressure (<25GPa) and a high temperature as 600°C. If shock metamorphism attacked entire Kobe, the prior magnetization should be remagnetized or demagnetized by the shock heating. The distribution of NRM may also suggest the extremely weak magnetic field during the shock metamorphism.

References

Nakamura, N. et al. (2000), Abstract of Antarctic Meteorites XXV.

Tomeoka, K. et al. (2001), Meteorites & Planetary Science, 36, 1535-1545.

The meaning of unstable natural remanent magnetization of Y000593

M. Funaki[1], V. Hoffmann[2] and K. Fukuma[3]

1: National Institute of Polar Research, Tokyo, Japan: 9-10 Kaga 1 Itabashi, Tokyo 173-8515

2: Institut fur Geologie und Palaontologie, Arbeitsbereich Geophysik, Univ. Tubingen, 72076 Tubingen, Germany

3: Faculty of Science, Kumamoto Univ., 2-39 Kurokami 1 Kumamoto 806-8501

1. Introduction

Antarctic meteorite, Y000593, was classified into Nakhlite from the evidences of petrography and mineralogy by Imae et al., (2002). It consists of coarse-grained clinopyroxene and augite associated with olivine and minor amount of Ti-rich magnetite. We obtained 3 pieces of this Nakhlite, #1 (0.8538 g), #2 (0.5350 g) and #3 (0.1445 g) from the fresh surface of the mass. The orientations of these samples were expected to reappear from a photo taken in the sampling, but it was impossible due to the breakable and featureless disk-like shapes for 2 among 3 samples.

2. Experiments

The intensities of natural remanent magnetization (NRM) of these samples were between 4.02×10^{-5} and 6.07×10^{-5} Am^2/kg. The sample #1 with inclination (I)=40 and declination (D)=215 of the NRM direction was fixed by resin prior to cutting into 3 subsamples (#1-1, -2 and -3) with the orientation. The NRM directions of the subsamples were scattered as (I=-39, D=85) for #1-1, (I=-54, D=87) for #1-2 and (I=-42, D=171) for #1-3. The subsample #1-3 was demagnetized by AF field up to 100 mT in steps of 5 mT. The demagnetization curve showed zigzag decreasing of the intensity change and rapid change direction; it was very unstable NRM throughout the demagnetization. We conclude, therefore, that Y000593 is not magnetized in any significant NRM component, but it has only unstable component as acquired by the viscous remanent magnetization etc.

Thermomagneitc (Is-T) curves under the external magnetic field at 1.0 T in the vacuum 10^{-4} Pa were obtained from the powder samples that were produced during sample treatments. The 1st run curve was irreversible with the Curie point at 530°C in the heating curve and 570°C and about 300°C in the cooling curve. The 2nd run curve was almost reversible with the main Curie point at 600°C and minor one at about 300°C in the heating curve and 600°C in the cooling curve. If Ti-rich magnetite described by Imae et al., (2002) carries magnetization, the Curie point should be more stable and much lower than magnetite Curie point at 580°C. Complicate I_S-T curves suggest us chemical alteration of magnetic minerals during heating, suggesting more unstable magnetic phase thermally than Ti-rich magnetite for main magnetic minerals in Y000593.

The hysteresis properties were obtained from hysteresis loops between +1.0 and -1.0 T at the

room temperature for the samples of pre- and post-heating to 800°C. The saturation magnetization (I_S), saturation remanent magnetization (I_R), coercive force (H_C) and remanent coercive force (H_{RC}), were listed in Table 1 associated with the values of I_R/I_S and H_{RC}/H_C. Relatively high H_C and H_{RC} values of the original sample may be able to have the stable remanent magnetization from the evidence of terrestrial basalt. These increased vales suggest that the fine-grained magnetic minerals newly produced during heating to 800°C. A polished surface was observed by a reflected right microscope. We confirmed larger titanomagnetite grains less than 300μm in diameter and sulfide grains less than 50μm in diameter. We are still under the consideration which mineral is dominant magnetic carrier for Y000593.

3. Conclusions.

We concluded from these viewpoints that Y000593 has only unstable NRM, nevertheless, it may be physically able to carry the stable NRM components. The most plausible explanation of the magnetic properties of this meteorite is no contribution of fine-grained magnetic minerals to the NRM. Namely, Y000593 seems to be magnetized or remagnetized in the negligibly weak magnetic field from the present magnetic analyses.

Table 1. Magnetic hysteresis properties at room temperature.

	I_S	I_R	H_C	H_{RC}	I_R/I_S	H_{RC}/H_C
original	0.640	0.0730	6.8	31.1	0.114	4.574
post heating to 800°C	0.909	0.149	12.2	37.6	0.164	3.082
unit	Am^2/kg	Am^2/kg	mT	mT		

Reference:
Imae et al. (2002): The first Nakhlite from Antarctica. Lunar and Planetary Science XXXIII, 1483.P

The nonmagnetic field in the parent body when magnetite was formed in the Tagish Lake meteorite (CI2)

M. Funaki[1], M. Zolensky[2] and N. Imae[1]

1: National Institute of Polar Research, 9-10 Kaga 1 Itabashi Tokyo 173-8515, Japan

2:Earth Science and Solar System Exploration Division, NASA Johnson Space Center, Houston, TX 77058, USA

1. Introduction

According to Brown et al. (2000), Mikouchi et al. (2001), Zolensky et al. (2001), Tagish Lake (CI2) consists of phyllosiliccate-rich matrix, clasts, sparse chondrules, sparse CAIs, grains of olivine, magnetite, Fe-Ni sulfides, Cr-Ni phosphides and Ca-Mg-Fe carbonates. Magnetite and/or sulfides are common both inside and rimming chondrules. Most chondrules have fine-grained phyllosilicate-rich rims up to 200 μm thick. Magnetite is very abundant in the matrix and also in clast with morphologies of framboids. Most sulfides are pyrrhotite, but pentlandite is much less than common. We report the magnetic properties of Tagish Laka and the meaning of the properties in the parent body.

2. Natural remanent magnetization

Natural remanent magnetization (NRM) of the interior samples (A-1, A-2, A-3) and the surface samples including fusion crust (F-1, F-2, F-3) were demagnetized by alternating field up to 100mT in steps of 5mT to confirm the stability. Unfortunately, the samples were obtained without orientation due to too small samples. The respective NRM intensities 4.53×10^{-4}, 2.24×10^{-4} and 4.29×10^{-4} Am^2/kg of the interior samples were demagnetized gradually to about $8\times10^{-5}Am^2/kg$ at 30 mT, and then they showed zigzag variations to 100 mT. The direction of these samples changed widely within the limited areas throughout the demagnetization. It may be, therefore, that Tagish Lake carries relatively unstable NRM. The NRM intensities of the respective surface samples were1.15×10^{-3}, 4.58×10^{-3} and 10.7×10^{-3} Am^2/kg which are stronger than those of the interior ones. The NRM intensities were quickly demagnetized to about $4.5\times10^{-4}Am^2/k$ at 20 mT, and then they decreased gradually. Their directions were unstable between 0 and 30mT, but very stable between 30 and 100 mT. The stable NRM of surface samples might be acquired due to the atmosphere heating.

3. Hysteresis and thermomagnetic curves

Thermomagnetic curves of the interior sample (A-1) and the surface sample (F-1) were obtained in the vacuumed condition under the steady magnetic field 1.0 T. The interior sample showed irreversible curve with clearly defined Curie Point at 620°C and minor ones at 350° and 500°C in the heating curve and 620° and 220°C in the cooling curve. Two magnetic humps appeared at about 170° and 530°C. These complicate curves are inferred to be unstable magnetic minerals such as Fe sulfide and Fe-Ni sulfide. The thermomagnetic curve of the surface sample showed almost reversible curve with the main Curie point at 580°C in the heating and cooling curves, although a small Curie point at 240°C and a magnetic hump at about 200°C appeared in the heating curve. The main magnetic mineral in the surface sample is estimated to be pure magnetite.

4. Microscopic observation

An interior sample was polished to identify magnetic minerals by magnetotactic bacteria and a reflected right microscope. The bacteria should migrate to the S pole along the mangetic field. In the state of NRM, there are no obvious bacterial clusters on the polished surface, while small and weak clusters appeared on some Fe-Ni sulfide grains and some area on the matrix. The sample acquired the isothermal remanent magnetization at 0.1 T to magnetize the S poles on the polished surface. Consequently, clealy defined strong clusters appeared around rims of clasts and chondrules. Any such strong clusters, however, were not observed on the sulfide grains.

The bacteria were applied to the surface sample having fusion crust in the NRM state. The bacteria make small clusters on the fusion crust which includes numerous magnetite grains of 1μm in diameter.

5. Discussion

The principal magnetic mineral of Tagish Lake is Fe-Ni sulfide estimated by the thermomagnetic curve and microscopic observations. Although magnetite grains in the matrix were not confirmed by the microscopic observation, magnetite is also dominant mangetic mineral, because very abundant of magnetite grains in the matrix and clast were reported (Zolensky et al, 2001). The NRM is not so stable against AF demagnetization suggesting that larger magnetic grains carry NRM. If fine-grained of magnetite in the matrix and clasts has responsible for NRM, the NRM must be much stable. Therefore, the NRM of Tagish Lake may be carried by Fe-Ni sulfide, as pyrrhotite and/or pentlandite, but the contribution of magnetite grains may be minor. Strong clusters of magnetotactic bacteria at the limbs of chondrules and clasts indicate that the fine-grained of magnetite concentrated in phyllosilicate layers around these limbs during hydrothermal alteration. When the grains were formed, the external magnetic field might be absent or negligibly small.

References

Brown et al. (2000), Science, 290, 320-325

Mikouchi et al. (2001), LPSC XXXII

Zolensky et al. (2001), abstract, Antarctic Meteorites XXVI

MEASURING ELECTROSTATIC PROCESSES IN THE DUST: MODELLING THE LUNAR DUST AND SOLAR RADIATION INTERACTION WHICH GENERATES A LEVITATING ELECTRICALLY CHARGED DUST CLOUD ABOVE THE SURFACE OF THE MOON

T. FÖLDI[1], SZ. BÉRCZI[2], R. EZER[3], E. PALÁSTHI[1], S. HEGYI[4]

[1]FOELDIX, H-1117 Budapest, Irinyi J. u. 36/b. Hungary,
[2]Eötvös University, Faculty of Science, Department of General Physics, Cosmic Materials Space Research Group, H-1117 Budapest, Pázmány Péter sétány 1/a, Hungary, (bercziszani@ludens.elte.hu)
[3]Arthur Andresen Ltd. H-1134 Budapest, Váci út 35. Hungary,
[4]Pécs University, Dept. Informatics and G. Technology, H-7625, Pécs, Ifjúság u. 6., Hungary

ABSTRACT

We measured electrostatic processes in a dusty region activated by evenly distributed electrodes. As a paralel process we studied the united effects of UV radiation and solar wind from the Sun on a dusty surface which also can be modelled as a region activated by evenly distributed electrodes (i.e. charged particles). We suggest that this model of the charging/discharging mechanism can generate the charged dusty and ion-cloud above any dusty (i.e. lunar) planetary surface.

INTRODUCTION

A levitating charged lunar dust cloud appears above the lunar surface according to the measurements of Surveyor landers and Apollo 17 LEAM experiments. This levitating dusty ion-cloud form a quasiatmosphere where charged dust particles can take part in various processes. We studied such electrostatic mechanisms of lunar (and planetary) dust in an instrumental experimental arrangement of FOELDIX-1. We consider that our instrumental arrangement gives a good approximation of the lower section of the lunar quasiatmosphere, because of a) the method of electrostatic activation of the dust particles, b) both systems consist of randomly scattered electrodes, and c) as a consequence, the process of the charging-discharging interaction gives essentially the same products. We discuss this results after the experiments.

FOELDIX-2: PROCESSES IN THE INSTRUMENT

The experiments were carried out in a normal pressurized (1 atm) space, on atmospheric temperatures [1]. There were two systems of electrodes, which were arranged in a comb-like mode in the experimental space. One system of electrodes operated on + and - 8,5 kV potentials. The volume of the active space was 400 cubic decimeters. The effective working time was 10 months during the day. (ca. 2000 hours). The sum mass of the dust produced during this experimental interval was 1000 gm. (We used 3 FOELDIX-2 instruments in the experiments: FOELDIX 2A, 2B, and 2C parallel.)

The size distribution of the dust collected and produced by this set of instruments is found to be similar (in 70-80 % correlation) with that of the lunar dust (micrometeorite) estimation of Vanzani [2]. This similarity between the two dust spectra inspired us to build a modell instrument working on the Hunveyor [3].

The next step in our modelling will be that we place this lunar size distribution dust on the ground of the Hunveyor (on the test-field) and we measure the generated levitating could, which can be measured by the Hunveyor's mass spectrometer. Such way we may prove that the effect works (and how it works) on Hunveyor [4]. In these experiments we use an artificial

Sun for triggering UV effects on the dust. This artificial Sun is be a metal-halide light source (Dy type, 2 kW) which was taken out from its glass tube.

DISCUSSION: COMPARISON OF THE LUNAR AND THE INSTRUMENTAL PROCESSES

The main reason of the similarity is that in both systems randomly scattered electrodes represent a characteristic stage of the charging-discharging interaction process. Charging-discharging ratio is in equilibrium. However, the radiation (or the activation in our experimental model) again and again violates and push charging-discharging process towards the dust agglutination stage. When charging activation stops, both the levitating charged dust cloud and the instrumental agglutination process cease to work, and dust cloud disappears, agglutinated dust particles drop out from the systems.

SUMMARY

We studied various effects of the solar radiation (UV, solar wind) on a dusty surface and we modelled the radiation affected region by an experimental arrangement with evenly distributed electrodes. We have found that dust particles can agglutinate by the alternating process of receiving and loosing charge. We found that during a longer interval in this process the electrostatically charged dust particles may produce larger and larger grains. In these studies we concluded that dust particles can agglutinate by the alternating process of receiving and loosing charge. We found that during a longer interval in this process the electrostatically charged dust particles may produce larger and larger grains. Earlier we have found that agglutinating grains also attract and include H_2O molecules.

There is another consequence of the alternating charging-discharging process considering longer time intervals. Then there is a trend on any dusty planetary surface that composite agglutinated particles grow, and they are dragged by the solar radiation pressure toward the poles. In the vicinity of poles larger agglutinated particles are finally discharged, fallen down and accumulated on the surface.

FURTHER PLANS OF THE COAGULATION EXPERIMENT

Because of the consequence our model [5] that H_2O molecules help agglutination and accumulation in the fine dust our next experimental step will be to use water vapor precipitation zone in the experiment.

REFERENCES:

[1] T. Földi, R. Ezer, Sz. Bérczi, Sz. Tóth. (1999): Creating Quasi-Spherules from Molecular Material Using Electric Fields (Inverse EGD Effect). In *Lunar and Planetary Science XXX*, Abstract #1266. Lunar and Planetary Institute, Houston (CD-ROM), [2] Vanzani, V.; Marzari, F.; Dotto, E. (1997): Micrometeoroid impacts on the lunar surface. In *Lunar and Planetary Science XXVIII*, Abstract #1025, Lunar and Planetary Institute, Houston (CD-ROM). [3] Földi T., Bérczi Sz., Koris A., Kovács B., Hegyi S., Kovács Zs. I., Roskó F. (2001): New experiment plans (electrostatic, lunar dust measuring, bio-filtering) to the Hunveyor educational planetary landers of universities and colleges in Hungary. In *Lunar and Planetary Science XXXII*, Abstract #1301, Lunar and Planetary Institute, Houston (CD-ROM). [4] T. Földi, Sz. Bérczi (2001): Measurements on the ion-cloud levitating above the Lunar surface: Experiments and modelling on Hunveyor experimental lander. *Meteoritics & Planetary Science*, vol. **36**, Supplement, p.A59, [5] T. Földi, Sz. Bérczi. (2001): The source of water molecules in the vicinity of the Moon. In *Lunar and Planetary Science XXXII*, Abstract #1148, Lunar and Planetary Institute, Houston (CD-ROM).

PLANETOLOGY GROUP'S COMPLEX EDUCATIONAL ACTIVITY AT EÖTVÖS UNIVERSITY. H. Hargitai[1], A. Kereszturi[1], A. Sik[1], T. Varga[2], Sz. Bérczi[1,3]. [1]Eötvös University, Faculty of Science, Planetology Group, H-1117 Budapest, Pázmány P. sétány. 1/a. Hungary, [2]Aries Plus Kft. H-1111 Budapest, Bertalan L. u. 20. Hungary, [3]Eötvös University, Faculty of Science, Dept. G. Physics, Cosmic Materials Space Research Group, H-1117 Budapest, Pázmány Péter sétány. 1/a. Hungary. (hargitai@emc.elte.hu)

Introduction: We describe the educational activities and the new educational materials made by the Planetology Group at the Eötvös University. Our specialization is in planetary surface geomorphology and cartography. We worked out and distributed various educational units, including Online hypermedia package, Atlas of Planetary Bodies in the Little Atlas Series of the Solar System [1], and On - and offline lecture note series educational video on Petrologic Studies of Solar System Materials.

A web-based hypermedia package: We have prepared an online hypermedia environment for the distant education of planetology in Hungary. Our educational outreach project on our website includes a daily cosmic calendar, a monthly star map, and planetary topographic or photomosaic maps with nomenclature. On the site we present Hungarian space activity and presence (astronauts, space devices, Hungarian names in the planetary nomenclature). Our new project is based on the idea of American radio programs, but is more planetology oriented than those. It contains short interviews with planetologists about actual events, news or a general planetology topic. The "Audio Atlas of the Solar System" is available on our website http://planetologia.elte.hu. We compiled a monthly cosmic calendar with star map in which we also describe planetary features and processes. Every Astronomy Circle and Secondary School can subscribe this publication for free of charge. Our final goal is to make printed, audio and online, quality (and scientifically correct) materials that reach the Hungarian public - especially the younger generation - on a daily basis.

Planetology lectures: We organized an autumn semester course in 2001 named *General Planetology* at the Eötvös Loránd University of Sciences . In this course we kept lectures from a general point of view dealing with certain processes and spheres of planetary bodies. The lessons went through from the internal structures and heat sources, volcanism and tectonism toward the external factors (atmosphere, hydrosphere, winds, weathering, ice, water etc.) influencing the evolution of planetary bodies. The aim was to combine the most basic elementary knowledge with the up-to- date scientific results. In the 2002 spring semester we organize a *Regional Planetology* course which is the next step for the students. In these lectures we take the planetary bodies one by one from a comparative point of view. The bodies organized into two evolutionary sequences, one for the icy bodies (from primitive cometary nuclei to Europa) and another for rocky bodies (from primitive asteroids to Earth). Beside the theme of the certain lessons the framework of the two courses is important too because it draws a global evolutionary picture on the planetary bodies in the Solar System.

Small Atlas of the Solar System: The Atlas of Planetary Bodies: In this - free - printed educational material we collected the most important and typical features of our planetary neighbours - one feature for every body. For example the volcanism on Io, the boulders and grooves on Eros and Phobos, or the greenhouse-effect on Planet Venus, etc. We call it Atlas, because the pages are packed with a lot of maps and figures (not only images) so it is a kind of workbook or an "interactive publication". The main parts are: Rocky Planets, Galilean moons and Small Bodies. Certainly the chapters are connected to the lectures of our special lecture at the university.

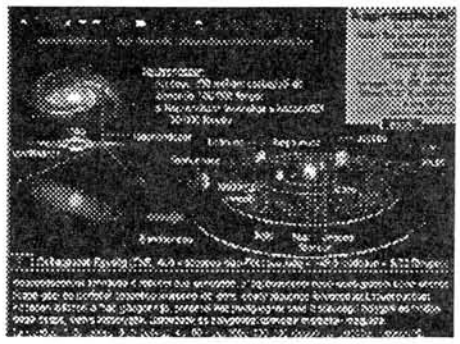

Bodies of the Solar System - Slide Series: Like an assistant or a teaching material we compiled a series of photo slides. (It is an analog way of presentation, but in the schools of Hungary the computer-projector unfortunately not too common yet, so a compact disk is not too practical for this purpose.) The series consist of 20 slides - in a thematical and logical order. First of all our place in the Galaxy and the structure of the Solar System. Then the Sun, the Mercury, Venus, Earth, Moon, two slides for Planet Mars, then the Asteroids, Jupiter, Io, Europa, Ganymedes/Callisto, Saturn, Titan, Uranus, Neptune, Comets/Meteorites and finally one slide about the exoplanets. The layout and style of the slides are "cyber-like" and the screens are divided into different parts: title, images, data, text and serial number. This way it is easy to "navigate" between them - like in the frames of a web-page (but is not interactive). On the basis of this series a normal geography lesson can be hold in a secondary school - 2 minutes for every slide. We hope that lesson will be exciting and interesting for the students - and some of them will choose this topic for university studies.

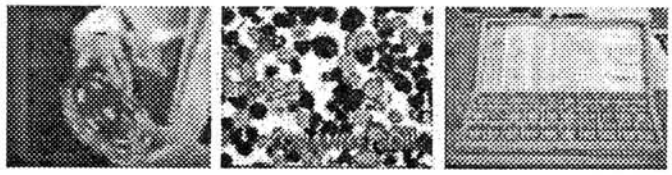

Video Education Online: To make educational materials available in English for foreign students and also in the mother language of Hungarian students, we started a bilingual educational website on the Internet. In this website we put a special emphasis on studies of meteorites. The multimedia form of scientific (higher education level) distant education presented here is not yet common on the internet.
A newly created video series have been made available online for download. The content of the film is related to our textbook (fig. 1., left) on Meteorites and Lunar Samples, where students can make their own drawings and colorings of the textures of thin sections. On the video (fig. 2.). It also follows the structure of our regular university course offered for students of geology and geography. 6-10 minutes blocks lectures enlight problems to study, such as Meterorites; Chondritic Body Evolution; Lunar Stratigraphy, Lunar Samples; Martian Meteorites; and Planetary Body Evolution. (illustration: From left: NASA Lunar Samples, Orange Soil thin section, NIPR Antarctic Meteorite Set.)
The film is especially useful to present the rotating thin sections under the microscope. The video is available in Windows Media format. The video is accompanied by a static (also bilingual) website in which we present the lunar samples that is loaned from NASA; and here students can find additional information related to the Lunar samples and the thin sections appearing on the video or in the classroom. An other video series also downloadable from our website presents the Japanese NIPR Antarctic Meteorites and the NASA Lunar Samples in more detail.

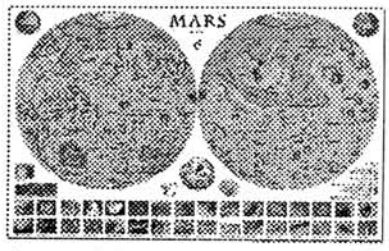

Planetary Cartography: Under support of the Commission on Planetary Cartography of the International Cartographic Association we have prepared a multilingual map of Mars [3] for use in Central European universities, in Coatian, Czech, Hungarian and Polish languages. The map was prepared in cooperation with the following institutions: Observatory and Planetarium Prague, Zagreb Astronomical Observatory, Jagiellonian University Observatory, Krakow, the Department of Geology of Zagreb University and the Tectonics and Geological Cartography Section of Faculty of Geology of Warsaw University. The Shade relief base map [4] was supported by the Moscow State University for Geodesy and Cartography.

The map is designed in the first place for use by middle and university students. It also can be used as a wall map, which is especially useful for astronoly clubs and school classes. Our purpose is that is be a part of middle schools geographic map collection. The map will be distributed in Hungary to all members of the Hungarian Astronomical Association (MCSE) for a very low price, but individuals can also order it. There seem to be a high interest from all age groups, who knows about the map but the advertising is difficult. This map is especially useful in schools where computer projector is not avalaible.

Translation, transcription for local use

We think that translating the planetary names is an important and necessary work, since this makes planetary science understandable for young students and the public - this is the only way of making planetology widely understood. Using only latin names even in popular publications makes this science understandable for only the few members of the scientific community.

We found that in Hungarian there are no appropriate planetary nomeclature for terms like Sulcus or Chasma - or even ejecta - which are often used in planetology but not in geology. Since we make educational materials for elementary and secondary schools, these should not include Latin or English terms, only Hungarians so that the students understand it.

We realized that we should translate the planetary nomenclature in a way that is accepted by all members of the scientific community.

For a multiligual map, we had to publish feature names on the map in a common language. This is naturally the IAU latin nomenclature. However, we found that in maps made for local public, generally students, (in a one language environment) the feature names may appear differently, by translating one or both elements of the geographic name.

Our observation is that even in these 4 countries involved in the making of the map we have translated terms of geologic ages using different methods: one such method is to stick to the original, English / Latin term (Amazonian, as used in Czech), other one is to translate the term (Amazoni or Amazoniszi in Hungarian, Amazonsko in Croatian, Amazoński in Polish). We found that in a later local planetary nomenclature and map making, we can use the experiences from the making of the local nomenclature system of Earth seafloor topography. [5]

The Multilingual Map of Mars has won the Special Price in the Hungarian Map Competition 2001., organized by the Lazar Deak Cartographic Foundation and the Hungarian National Széchenyi Library in the category Scientific Maps and Atlases [6]. The reasons were that "in the publication the hard and popular scientific functions are in a good harmony. Following the traditions of the representation of Earth it depicts the two hemispheres in two parts, indicating the particular topographic elements and their nomenclature.

References: [1] Bérczi Sz. Hargitai H., Kereszturi Á., Sik A. (2001): *Kis Atlasz a Naprendszerről (3): Bolygótestek atlasza. (*Little Atlas of the Solar System Series (3): *Atlas of Planetary Bodies).* (In Hungarian) UNICONSTANT, Püspökladány; [2] Bérczi Sz. (2001): *Kis Atlasz a Naprendszerről (1): Planetáris és anyagtérképek holdkőzetekről, meteoritekről. (Planatary and Material Maps of Lunar Samples and Meteorites.*) (In Hungarian) UNICONSTANT. Püspökladány; [3] Multilingual map of Mars, *in print*. Editors of language sections: Hungarian: H. Hargitai, Czech: A. Rükl, Croatian: D. Roša, Polish: T. Kundera [4] Map of Mars. Cartographers: L. S. Oreshina, L. Yu. Baeva. Editors: B. V. Krasnopevtseva, K. B. Shingareva, Moscow State University for Geodesy and Cartography (MIIGAiK). [5] Márton, Mátyás: A magyar tengerfenék-domborzati nevek megalkotásáról. (On the making of the Hungarian Seefloor Topography Nomenclature) Névtani Értesíto 14: 84–116. 1992.
[6] Szép Magyar Térkép 2001. - 2002. March. 22. - Publication in the Supplement of Térinformatika 2002/2.

Revisiting the Search for the Parent Body of the Tagish Lake Meteorite — Case of a T/D Asteroid 308 Polyxo —

Takahiro Hiroi[1] and Sunao Hasegawa[2]

[1] *Deptartment of Geological Sciences, Brown University, Providence, RI 02912, USA*
[2] *Research Division for Planetary Science, Institute of Space and Astronautical Science, 3-1-1 Yoshinodai, Sagamihara, Kanagawa 229-8510*

Last year, Hiroi *et al.* [1] reported that the Tagsh Lake meteorite was likely from a D asteroid based on comparison of their visible-NIR reflectance spectra. However, because asteroid classification is usually performed based on a limited range of wavelength, the asteroid classes and surface compositions may not necessarily have one-to-one correspondence. In this paper, we show that an asteroid classified either D or T in fact has a similar reflectance spectrum to the Tagish Lake sample we have studied.

An asteroid 308 Polyxo is classified as T type by Tholen [2] and D type by Barucci [3]. Shown in Fig. 1 are reflectance spectra of the Tagish Lake sample and Polyxo [5-9]. Although there are some differences among telescopic spectra of Polyxo, the overall characteritics are very similar to the Tagish Lake spectrum. Especially notable is the presence of the 3-μm band indicating existence of water in the surface materials of Polyxo, which is consistent with mineralogy of the Tagish Lake meteorite.

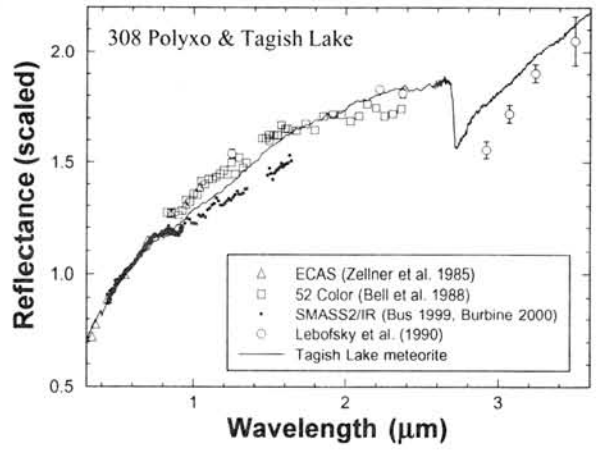

Fig. 1. Comparison of reflectance spectra of the Tagish Lake meteorite sample and a T/D asteroid 308 Polyxo. Reflectance values are normalized to 1 at 0.55 μm.

One significant difference between the Tagish Lake meteorite and Polyxo is brightness. Although the reflectance spectrum of our Tagish Lake powder sample shown in Fig. 1 has reflectance of about 2 % at 0.55 μm, the IRAS albedo of Polyxo [4] is 4.8 ± 0.3 %. In order to investigate whether their difference is due to difference in viewing geometry, reflectance of the Tagish Lake sample has been measured also at 14, 11, and 7° incidence angles and 0° emergence angle, relative to Spectralon as an assumed Lambertian surface. The results are shown in Fig. 2 together with the albedo of Polyxo. Although the exact behavior of neither our standard material Spectralon which is a near-Lambertian surface nor the reflectance of Polyxo near

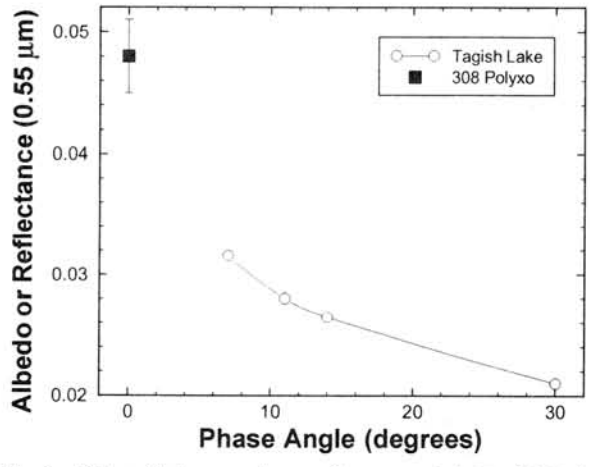

Fig. 2. Effect of phase angle on reflectance of the Tagish Lake meteorite sample at 0.55 μm with 0° emergence angle. Albedo [4] of 308 Polyxo is also plot at 0° phase anlge as a reference.

opposition is well known, the trend that the apparent reflectance of asteroids tend to increase at small phase angle seems true and consistent with our laboratory study of the Tagish Lake meteorite sample.

The last point to check in addressing whether the asteroid Polyxo could be the parent body of the Tagish Lake meteorite is their orbital properties. The fall of the Tagish Lake meteorite was observed by several satellites and its orbit is well estimated: Semimajor axis $a = 2.1 \pm 0.2$ AU, eccentricity $e = 0.57 \pm 0.05$, and inclination $i = 1.4 \pm 0.9°$. Its aphelion distance is 3.3 ± 0.4 AU. This suggests that the Tagish Lake meteorite left its parent body within about 3.3 AU from the Sun if any orbital evolution after it left its parent body can be disregarded. If it is truly the case, the parent body must have an orbit which comes to the distance of about 3.3 AU or less from the Sun during its orbital period. Listed in Table 1 below are albedos, diamters, and orbital elements of the D asteroids whose orbits come within 3.3 AU from the Sun. Asteroid 308 Polyxo has an orbit which stays well within 3.3 AU and is about 0.07 AU away from the nearest Kirkwood Gap which is believed to be a window of delivering meteorites to the Earth caused by the mean motion resonance with Jupiter. If the Tagish Lake meteorite came from Polyxo, in order to take its final orbit, the Tagish Lake meteorite would have had to gain some energy through an impact when it was ejected from Polyxo or gradually after its departure before reaching the Earth by some other mechanism such as the Yarkovsky effect.

All the asteroids listed in Table 1 need to be investigated in detail in order to determine which asteroid the Tagish Lake meteorite possibly came from.

Acknowledgment: Reflectance spectra of the meteorite sample were measured at RELAB, a multiuser facility supported by NASA grant NAGW5-3871.

References: [1] Hiroi T. et al. (2001) *Science* **293**, 2234. [2] Tholen D. J. (1984) Ph.D. thesis, Univ. Arizona. [3] Barucci M. A. et al. (1987) Icarus 72, 304. [4] Tedesco E. F. (1989) in *Asteroids II*, R. P. Binzel *et al.*, Eds. (Univ. Arizona Press), pp. 1090. [5] Zellner B. *et al.* (1985) *Icarus* **61**, 335. [6] Bell J. F. *et al.* (1989) *Lunar Planet. Sci.* **19**, 57. [7] Bus S. J. (1999) Ph.D. thesis, Massachusetts Institute of Technology. [8] Burbine T. H. (2000). Ph.D. thesis, Massachusetts Institute of Technology. [9] Lebofsky L. *et al.* (1990) *Icarus* **83**, 16.

Table 1. Albedos, diameters, and orbital elements of the D-type asteroids whose orbits come within 3.3 AU from the Sun. Kirkwood Gaps are also listed. Asteroid 308 Polyxo is about 0.07 AU from the nearest gap.

Albedo	*D*/km	*a*	*e*	sin(*i*)	No.	Class	Name
0.042	72.0	2.252	0.091	0.110	336	D	Lacadiera
0.058	39.0	2.457	0.068	0.192	732	D	Tjilaki
		2.500					***Gap 3:1***
0.050	33.1	2.716	0.096	0.253	1471	D	Tornio
0.048	140.7	2.750	0.047	0.079	308	T/D	Polyxo
0.049	80.1	2.788	0.277	0.144	415	DP	Palatia
		2.824					***Gap 5:2***
0.033	99.1	2.858	0.047	0.301	773	D	Irmintraud
0.050	36.8	2.858	0.102	0.157	1702	D	Kalahari
	32.0	2.922			3501	D	Olegiya
		2.956					***Gap 7:3***
0.032	74.5	3.070	0.170	0.163	368	D	Haidea
		3.181	0.218	0.252	2375	D	Radek
		3.276					***Gap 2:1***
0.029	53.6	3.384	0.184	0.233	2266	D	Tchaikovsky
0.039	69.0	3.413	0.073	0.114	1167	D	Dubiago
0.050	82.6	3.551	0.083	0.135	721	D	Tabora
0.020	18.7	4.230	0.713	0.512	3552	D	Don Quixote

Rare Earth Element Abundances in the Rims and Cores of Two Type B1 CAIs from CV Chondrites.

Hajime Hiyagon
Department of Earth and Planetary Science, Gradate School of Science,
University of Tokyo, Bunkyo-ku, Tokyo 113-0033, Japan.

Introduction

Refractory inclusions, or CAIs, are generally surrounded by a series of characteristic mineral layers, so called "Wark-Lovering rims" (hereafter W-L rims) [1]. The W-L rims consist of the following layers from interior to exterior: (1) spinel + perovskite layer, (2) melilite (and its alteration products) layer, (3) diopsidic pyroxene layer and (4) olivine $\pm$ hedenburgite $\pm$ andradite layer [1,2]. The total thickness is typically ~50μm. The origin of the W-L rims, however, is still not well understood. It was once proposed that the W-L rims were formed by alteration of melilite (mobilization and transport of Ca to outside) and reaction with the nebular gas [3]. However, the ^{16}O-rich composition of diopside in the W-L rim of an Allende type A CAI [4] strongly suggests that the W-L rim is a primary feature rather than a secondary one. Recently, a more complicated two stage model was proposed by [5]. In the present study, *in situ* micro-analyses of Ba, rare earth elements (REE) and Hf were performed using an ion microprobe to better understand the formation process of the W-L rims.

Samples

Two type B1 CAIs were studied: SH1 from the SAH98044 CV3 chondrite and Allende 002 from the Allende CV3 chondrite. A brief petrographic description of SH1 and oxygen isotopic compositions of minerals in the core and rim of SH1 are given in [6]. Diopside and perovskite in the W-L rim and melilite just inside of the W-L rim of SH1 were analyzed. Diopside shows almost normal oxygen isotopic composition (δ^{18}O ~0‰) [6]. Allende 002 is also a type B1 CAI, but it has unusual rim structures. Outside of the melilite mantle is a layer of spinel + diopside (inner rim), which possibly was the original W-L rim but now spinel and diopside crystals are rather randomly distributed. It is further covered with a thick (up to ~100μm) fassaitic pyroxene layer (outer rim), in which small ($\leq$ a few μm) olivine grains are enclosed. Fassaite in the outer rim, diopside in the inner rim and melilite just inside of the inner rim were analyzed. Oxygen isotope data are not available for this inclusion.

Analytical Conditions

Abundances of rare earth elements (La to Lu), Ba and Hf were determined by the energy filtering method using an ion microprobe (CAMECA, ims-6f) at the University of Tokyo. An O^- primary beam with a 12.5keV energy and 20-25 μm in diameter with a beam intensity of 2.5-4.5 nA was used for the analyses. For melilite, which has low REE concentrations, a larger primary beam of ~40μm in diameter with an intensity of 13-16nA was used. Positive secondary ions were accelerated at 10kV, energy filtered by applying an energy offset of 60V with an energy window of ~30V, mass filtered with a mass resolving power of ~300, and detected using an electron multiplier in the ion counting mode for Ba, REE and Hf, or using a Faraday Cup for ^{24}Mg, ^{27}Al, ^{28}Si and ^{40}Ca. For Ba, REE and Hf, all the peaks from mass 135 to 185 were measured using peak jumping and used for the data reduction. The

method of calculation of Ba-REE-Hf abundances is similar to that described by Fahey (1988) [7] but somewhat modified. Relative sensitivity factors for REE^+/Ca^+, etc., were determined using synthetic glass standards containing various REE species with concentrations of a few x100 ppm as well as the NIST 612 glass standard.

Results and Discussion

The results for SH1 are shown in Fig.1 and those for Allende 002 in Fig.2. The data are normalized to CI abundances. All the phases in SH1 show group II REE patterns (i.e., depletion of HREE, except Tm, relative to LREE). Perovskite in the W-L rim shows very high REE concentrations (100-500 x CI). Diopside in the W-L rim, in contrast, shows the lowest REE abundances (~1 x CI) among the three. The bulk Allende 002 may have relatively flat REE abundance pattern if REE in all the phases are averaged. Fassaite in the outer rim shows significant enrichment in REE (25-70 x CI). Even diopside in the inner rim shows high enrichment in REE (6-25 x CI). This is different from the case for SH1.

Generally CAIs show REE enrichment of 15-20 x CI, which is understandable if CAIs represent the most refractory phases (~5% of the total solid phases) including all REE. The question is the origin of the high REE concentrations of diopside and fassaite in the rims of Allende 002. During the formation of CAIs, essentially all REE would have been incorporated in the solid phases (i.e., cores of CAIs), so that there might not be enough REE left in the gas phase in the CAI formation region. This would result in a lower REE concentration in the W-L rim if it was formed from the rest of the gas. However, this is not the case for Allende 002. Significant amounts of REE must be brought into the rims of Allende 002. Melilite and spinel in the core of this inclusion have heavily fractionated Mg isotopes with Δ^{25}Mg of 7-12 and 3-5‰/amu, respectively, [7] relative to PO chondrules (assuming ~0‰ [8]). This indicates that Allende 002 has experienced significant evaporation. It is questionable even such an evaporation event could concentrate REE to explain the present observation. It is apparent that Allende 002 has experienced rather complex evaporation/ condensation history, and the present REE results may not be applied for other inclusions.

References

[1] Wark D. A. and Lovering J. F. (1977) *Proc. Lunar Sci. Conf.* **8th**, 95-112. [2] MacPherson G. J., Wark D. A. and Armstrong J. T. (1988) In *Meteorites and the Early Solar System* (eds. Kerridge J. F. and Matthews M. S.), pp. 746-807. [3] MacPherson et al. (1981) *Proc. Lunar Planet. Sci. Conf.* **12b**, 1079-1091. [4] Hiyagon H. (1988) *Lunar Planet Sci.* **XXXIII**, Abstr. #1582 (CD ROM). [5] Wark D. and Boynton W. V. (2001) *Meteoritics Planet. Sci.* **36**, 1135-1166. [6] Hirai K., Ushikubo T. and Hiyagon H. (2002) *Lunar Planet Sci.* **XXIV**, Abstr.#1494 (CD ROM). [7] Fahey A. J. (1988) PhD Thesis, Washington University, St. Louis, Missouri, USA. [8] Ushikubo T. et al. (2002) *Abstr. Goldschmidt Conf.* (submitted). [8] Galy A. et al. (2000) *Science* **290**, 1751-1753.

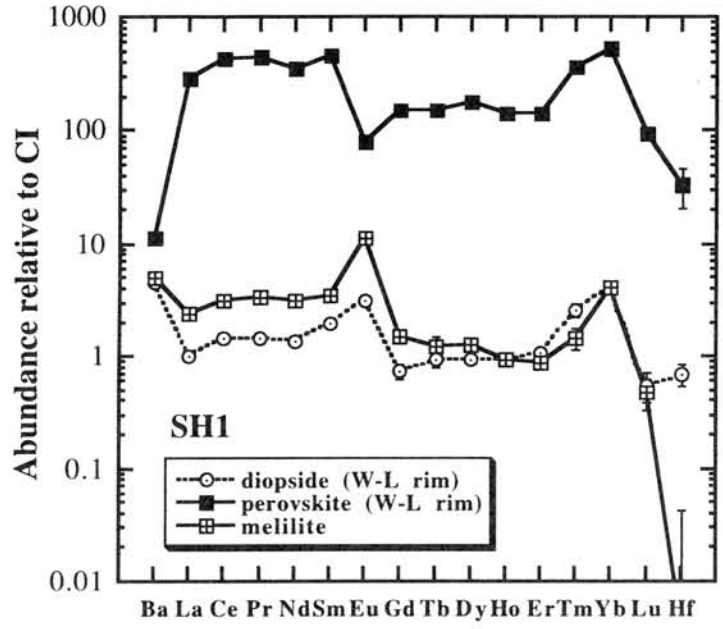

Fig.1 Abundance patterns of Ba, REE and Hf in a type B1 CAI, SH1, from SAH98044 CV3 chondrite.

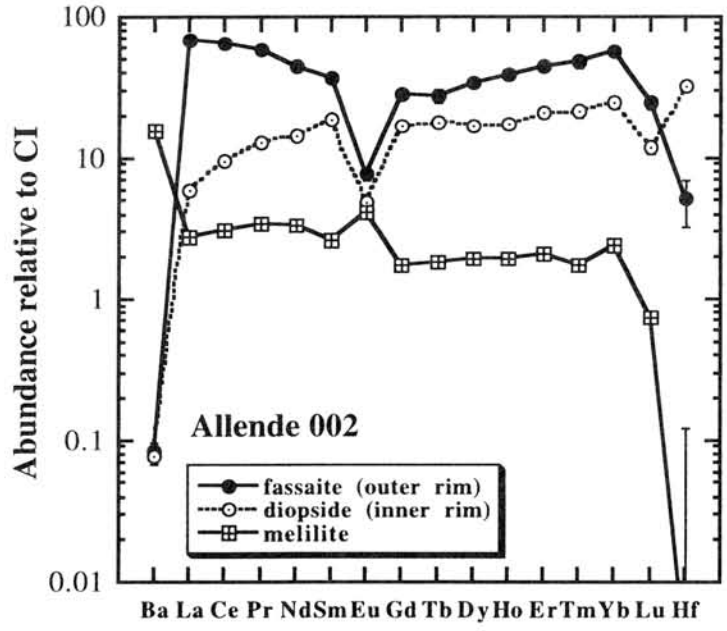

Fig.2 Abundance patterns of Ba, REE and Hf in a type B1 CAI, Allende 002.

"Biogenic" Dark Dune Spots on Mars and Probable Antarctic Analogues

András Horváth[1,2], Tibor Gánti[3], Szaniszló Bérczi[4], Albert Gesztesi[1] and Eörs Szathmáry[3,5]

[1]Konkoly Observatory, H-1525 Budapest Pf. 67, Hungary, [2]Budapest Planetarium, H-1476 Budapest Pf. 47, Hungary (planet@mail.datanet.hu), [3]Collegium Budapest (Institute for Advanced Study), Szentháromság tér 2., H-1014 Budapest, Hungary, [4] Eötvös University, Dept. G. Physics, H-1117 Budapest, Pázmány s. 1/a. Hungary, [5] Eötvös University, Dept. Plant Taxonomy/Ecology, H-1117 Budapest, Pázmány s. 1/a. Hungary

Abstract: Dark Dune Spots (DDSs) are remarkable morphological features, which appear during late winter and spring mainly on intra-crater dark sand sheets in the southern polar regions of Mars. We studied the high-resolution MGS MOC images and the morphological dynamics of the spots suggested that the previously suggested frosting-defrosting mechanism cannot explain solely their formation. We proposed that DDSs are signs of life activity and we suggested a lifecycle of putative Martian photosynthetic surface organisms.

Introduction: The images of Mariner 9 revealed that dark-toned „splotches", inside or outside the craters, could be found in the low latitudes of Mars. Using the Viking images it has been suggested that the dark „splotches" are eolian dunes made up of fine-grained sediments of dark blue in color (**1, 2, 3**). The dark dunes in both polar areas have colors and albedo similar to that of the dunes at low latitudes, but they are dramatically different from the widespread bright dust dunes on Mars (**4**). The dark dunes are composed of low-albedo, sand-sized eolian sediments, mainly dense basaltic sand (**5**).

On the Mars Orbiter Camera (MOC) images of the Mars Global Surveyor (MGS) made between 1998 and 1999 we studied south polar regional dark dune fields, which are the first surfaces to frost in the fall and defrost during late winter/early spring, (still frost may well persist on them until late spring or even early summer. There DDSs and their clusters were observed during late winter and early spring. In earlier analyses Edgett at al. (**6**) and Malin & Edgett (**7**) concluded that a complex process of CO_2 and H_2O sublimation and re-precipitation occurs as defrosting process. This process is function of the seasonal and local temperature controlled by surface and interior physical properties of the dunes.

Observations: We have analyzed 200 MGS MOC pre-processed images (http://www.msss.com/moc_gallery/) published on the net by the Malin Space Science Systems. From the two polar regions of the Mars (different, **8**), the DDSs of the southern one were chosen for morphological analysis. MOC red wide-angle context images (λ=600-630 nm) helped orientation, MOC narrow-angle images (λ=500-900 nm) covering (1-3)X(20-80) km^2 area, with a high resolution of 1,4-5,5 m.) were used for analysis (**Figs. 1, 2, 3, & 5**). The narrow-angle images were taken between June 1999 and June 2001 and cover areas between 48°S–82°S latitudes. On all of these images nearly circular DDS and their clusters can be seen. The DDSs frequently have an inner ring-structure (**6, 7**) which can be seen only on the highest resolution images (**Fig. 1**).

Our interesting new observation was the relationship between the fine-scale topography and the circular shape of the individual DDSs on top of the dune sheets. (**Fig 2** illustrates the general situation.) This circular shape of DDSs indicates that spots are formed not (or not only) by sublimation but rather by some radially spreading process (e.g. water leaking into homogeneous sandy soil). If the defrosting process is only sublimation, then the preferential sites for frost sublimation are those surfaces, which receive the highest radiation flux from the Sun. For this reason spots with sublimation origin ought to have diverse, irregular, rather than circular, shapes.

Another observation is that on slopes the spots are elongated downwards. On slopes the circular spots are replaced by DDSs with ellipsoid or fan shape, indicating that gravitational force does affect spot morphogenesis (**Fig. 1** and **3**), too. There are spots from which extensions start to outflow downward. All these observations suggested us that a fluid phase (most likely water) played a fundamental role in spot morphogenesis.

Fig. 3A shows a spectacular example of elongated dark spots in the crater located near 61°S, 5°W. The presence of liquid phase and surface waters flow is supported by **Fig. 3B**. The image shows DDSs that are not only elongated but are arranged in several hundred meter long, winding stripes, which are most probably tracks of water flows. In other environments Malin and Edgett (**9**), Mangold et al. (**10**) have already found recent groundwater seepage and surface runoff gullies on Mars, but Reiss and Jaumann (**11**) found extremely fresh runoff gullies within the last Martian year.

On a plain surface the spots tend to have circular shape, surrounded by a gray ring (**Fig. 1B, C** and **D**). On slopes they develop into an ellipsoid (**Fig. 3C**), elongated in the direction of the gradient, or they form a fan-shaped region at the lower end (**Fig. 3D**). With time the spots grow and coalesce, and by the end of the summer the whole territory turns dark..

Biological interpretation: In order to interpret the shown sequence of changes of the DDSs phenomenon in our model we involve activity of living organisms, called MSOs (Martians Surface Organisms). In the Edgett *at al.* (**5**) and Malin and Edgett (**6**), models DDS phenomenon was interpreted as sinple defrosting process. However, the systematic variations and repeated appearance of DDSs and their patterns cann't be interpreted only by surface relief and physical defrosting reasons.

In our model two fundamental questions are explained: 1) How can liquid water form at temperatures obviously below freezing, and if formed, why does not it freeze immediately? 2) If some mechanism produces liquid water, how on Mars does not it evaporate immediately in the very thin Martian atmosphere? Our answer to these problems were solved by the suggested existence of Martian Surface Organisms (MSOs) which have adapted to an above the ground, below-ice lifestyle (they have some earthly analogues).

The photoautotrophic MSOs must have evolved pigments with high absorbance. We suggest they conduct the following lifecycle. During the winter the soil below the spots is deep-frozen and some form of ice/frost covers them. MSOs must occupy a layer between the soil surface and the ice sheet. Because ice is transparent to light, MSOs intensely absorb the emerging sunlight (which is continuously available in the polar region) and thus warm up at the end of the winter. From a frozen state they pass to a molten one, which also applies to part of the ice around them. Thus MSOs find themselves in a liquid solute, in contact with the

underlying soil, enabling them to take up the necessary nutrients. The volume and extension of the liquid region increase with the intensity of the insolation. The ice cover above the forming liquid water provides excellent heat insulation and prevents fast evaporation that otherwise would be inescapable due to the low atmospheric pressure. (The fact that the spots mainly appear in the polar region indicates that a long period of sunlight is a necessary condition for their formation, since it prevents night frosting of water around the MSOs.) Thus the most basic living conditions of the MSOs prevail until there is sunlight and until the ice sheet above them does not evaporate. The proposed mechanism of spot formation is shown in **Fig. 4.**

The MSOs "Martian" type life conditions in Antarctica: It is important that life under similar conditions is known on Earth. Priscu *et al.* have found that the 3-6 m thick ice cover of the lakes in the dry valleys of Antarctica contains wind-blown sediments in the middle region. Photosynthetic organisms on the surface of these sediment grains absorb sunlight and melt the ice around them, thus partly creating their own living conditions (**12, 13**). A multi species consortium is found on the grains, able to perform continuous photosynthesis, nitrogen fixation and decomposition, forming a small ecosystem with nutrient cycling.

The Martian ice cover would also protect MSOs from intense UV radiation. (Although atmospheric CO_2 filters out UV below 190 nm, the flux of UVB (280-320 nm) and UVC (200-280 nm) radiation is higher on Mars than on present-day Earth, which must constrain life processes, especially photosynthesis, whether of earthly or endemic origin (**14**).) Aggressive chemical reactivity of the Martian soil at the Viking landing sites is likely to be due to super-oxide ions that form under UV irradiation (**15**). Thus shielding from UV irradiation should also reduce the concentration of harmful super-oxide ions in the habitat of the MSOs, in addition to the fact that the color of the dunes indicates a local depletion of iron, necessary for the formation of superoxide. (the present-day UV exposure of the Martian surface is comparable to that of the Archean Earth, **16, 14**). Martian organisms could easily have adapted to present-day UV conditions through billions of years. Note that even on Earth today one finds organisms such as *Deinococcus radiodurans* (**17**) or *Rubrobacter radiotolerans* (**18**), tolerant of enormous levels of radiation, including UV. *Deinococcus* is able to survive a dose of 1.5 million rads. After cooling and freezing it may survive 3.0 Mrads (**17**). This extreme radio-tolerance may be by-product of extreme desiccation tolerance.

MSO life sequence from late winter: At the end of the winter sunlight start to warm up the MSOs, activate them and melt the bottom of the ice cover above them. (gray spots) With time the ice shield becomes thinner and thinner, until it melts through up to the surface. In the core, immediately a very intense evaporation begins in the unprotected region culminating in the appearance of the dark, underlying soil, featuring as the dark center in the middle of the gray spot (**Fig. 1C, 1D** and **4B**). The evaporation of liquid water in the middle of the spots and the consequent drop in temperature could be ideal for the preservation of viability of MSOs. It is striking that where the black spots appear by late winter, there are lighter, grayish patches on the images of the defrosted, dark soil. It seems obvious that in these cases a different layer covers the Martian regolith. This layer is, following from our mechanism, a layer of dried MSOs, analogous to dried algal mats or lichen-like covers on the Earth. By the end of fall, or the beginning of winter white frost settles in (first just in the dark dune regions) and the whole territory turns white. The long winter (six earthly months) allows the white frost to become dense and to form proper ice at the bottom, sealing the surface from the atmosphere completely. Sunlight appearing by late winter then warms up MSOs and the cycle is ready to start again.

Summary: Our DDSs transformation sequence and many characteristic features of the DDSs were successfully interpreted by our model involving living organisms. Our considerations showed that photoautotrophic organisms could maintain their own living conditions on Mars. One may wonder whether the low atmospheric pressure is compatible with photosynthesis, but this objection is not hard to reject. First, although it is true that total pressure is just 6 mbar, but 95% of the atmosphere is CO_2, thus its *partial pressure* is higher than on Earth. Second, conditions below the ice sheet are expected to be different (in fact, more favorable). The existence of the postulated MSOs should be detectable by orbiting spectroscopic instruments. It is encouraging that Pershin (**19**) has observed a color index value of 763/554, suggestive of photosynthetic pigments, during analysis of the Martian images made by the Hubble Space Telescope..

If one indeed finds life on Mars, the history of its origin becomes very interesting. Given the fact that viable dried organisms or their propagules could travel regularly between Earth and Mars, while preserving their viable state (**20, 21**), it may be possible that Martian and terrestrial organisms share a common ancestry: phylogenetic sequence analysis should be able to tell whether this holds or not.

Acknowledgements: Processed MGS MOC images of Malin Space Science Systems, discussions with J. Maynard Smith, G. v. Kiedrowski, I. Almár, I. Fejes, F. Horváth, E. Illés-Almár, and N. Gontareva, and OTKA fund by E. Sz. and MŰI-TP-154 fund by Sz. B. are highly acknowledged.

References: [1] Thomas, P., et al. (1992) In *Mars*, Eds. Kieffer, H. H., et al.. (Univ. of Arizona Pr ess, Tucson), 767; [2] Thomas, P., et al. (1986) *Icarus* **66**, 39; [3] Howard, A. D. (2000) *Icarus* **144**, 267; [4] Thomas, P. et al. C. (1989). *Icarus* **81**, 185; [5] Edgett, K. S. et al. (1999) *LPS.* **XXX**, #1029; [6] Edgett, K.S., et al. (2000) *Mars Polar Sci. and Explor.* **II**, # 4041; [7]. Malin, M. C. et al. (2000a) *LPS.* **XXXI**, #1052, & also Malin, M. C. et al. (2000b). *LPS.* **XXXI**, #1056; [8] Malin, M. et al. (2000c) *Mars Polar Sci. and Explor.* **II**, # 4042; [9] Malin, M. et al. (2000d) *Science*, **288**, 2330; [10] Mangold et al. (2002): *LPS.* **XXXIII.** #1215; [11] Reiss, D., Jaumann, R. (2002) *LPS.* **XXXII.** #1606.; [12]. Priscu, J. C. *et al.* (1998) *Science* **280**, 2095; [13] Pearl, H. W. et al. (1998) *Microb. Ecol.* **36**, 221; [14] Rothschild, L. J. et al. (1999) *Mut. Res.* **430**, 281; [15] Yen, A. S., et al. (2000) *Science* **289**, 1909; [16]. Cockell, C. S. (1998) *J. Theor. Biol.* **193**, 717; [17] Battista, J. R. (1997) *Annu. Rev. Microbiol.* **51**, 203; [18] Asgarani E. *et al.* (2000) *J. Radiat. Res. (Tokyo)* **41**, 19; [19] Pershin, S. M. (2000) *COSPAR 2000* Abstr. No. B-04-0008. [20] Davies, P. (1998) *The Fifth Miracle* (Orion Productions); [21] Weiss, B. P. *et al.* (2000) *Science* **290**, 791.

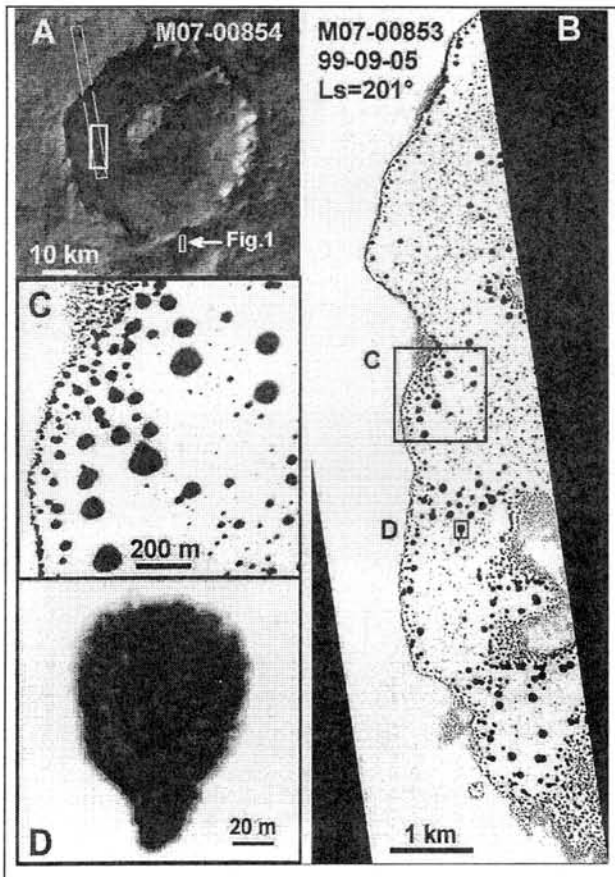

Fig. 1. Characteristic Martian dark dune spots and their clusters. (**A**) A 50-km-wide crater (65°S, 15°W) with intracrater dune field. (**B**) DDSs during early spring along edges and on top of the intracrater dune field, (C) Nearly circular DDSs on the flat dune field. (**D**) Inner ring-structure of one of the DDSs.

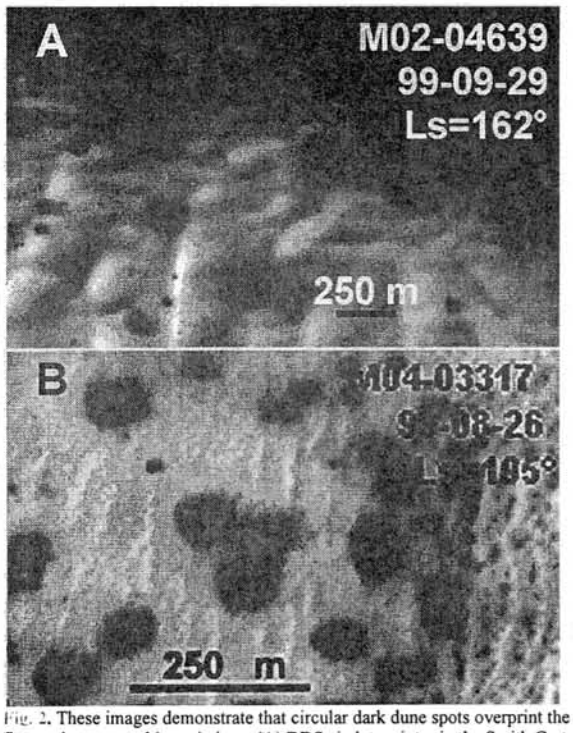

Fig. 2. These images demonstrate that circular dark dune spots overprint the fine-scale topographic variations. (**A**) DDSs in late winter in the Smith Crater. (**B**) DDSs in early spring on the dune field of the Jeans Crater.

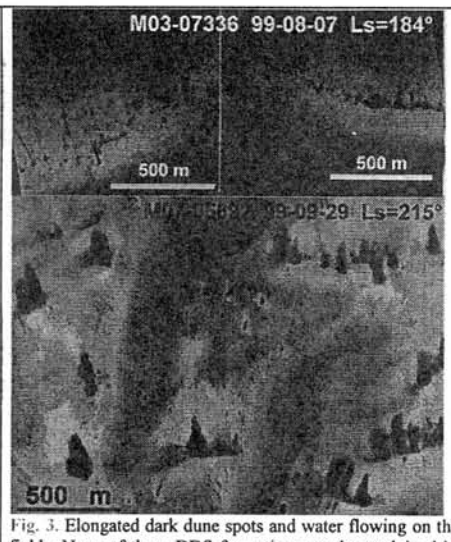

Fig. 3. Elongated dark dune spots and water flowing on the slopes of the dune fields. None of these DDS formations can be explained by a mere defrosting effect, but all of them can be interpreted as showing water seepage and occasional flow. The emergence and continued presence of liquid water are, presumably, due to biological activity.

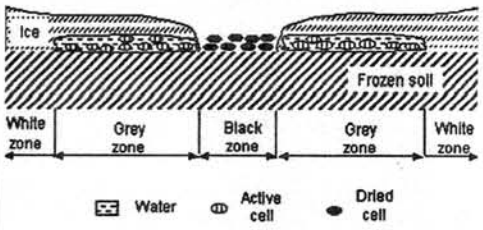

Fig. 4. Dynamics of biogenic spot morphogenesis. (**A**) In the firs phase of spot development organisms on the soil, below the ice warm up by the absorption of sunlight and melt the ice around them. The ice cover provides heat insulation and blocks evaporation. (**B**) The ice cover first disappears in the center, where the melting started. Water evaporates quickly; the organisms desiccate and the dark core of the spots develop.

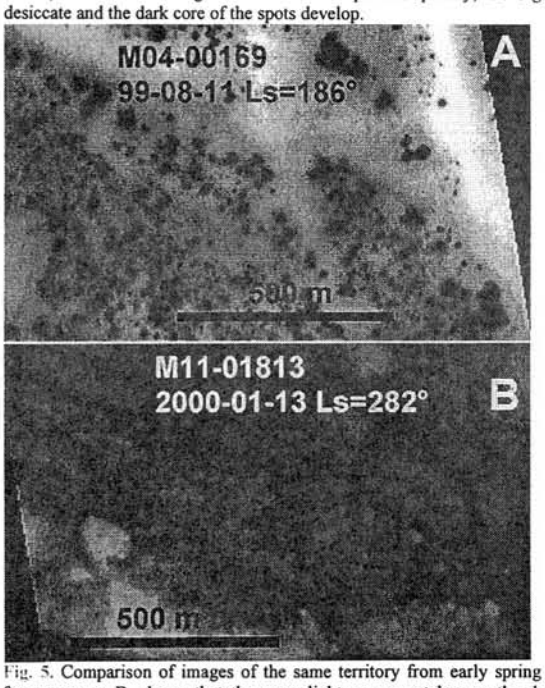

Fig. 5. Comparison of images of the same territory from early spring **A** and from summer **B**, shows that there are lighter gray patches on the dark soil where the dark spots were at the end of the winter. This suggests that a layer with a different albedo covers the dark soil. We interpret this as a layer of desiccated MSOs

A NEW BASALTIC SHERGOTTITE, DHOFAR 378

Yukio Ikeda[1], Hiroshi Takeda[2], Makoto Kimura[1], and Noboru Nakamura[3]
[1]Dept. of Material & Biol. Sci., Ibaraki Univ., [2]Research Inst., Chiba Inst. of Technology, [3]Dept. of Earth & Planet. Sci., Kobe Univ.

[Introduction]

The new basaltic shergottite Dhofar 378 was recently recovered from the Oman desert. The total mass recovered is 15 g with fresh fusion crust. It was approved as a shergottite by the Nomenclature Committee of the Meteoritical Society in December, 2001. It is doleritic with a subophitic texture, and the grain size of the main phases (plagioclase glass and pyroxenes) are 1 mm-a few mm in length.

[Oxygen isotopes]

The oxygen isotopic composition of the stone was obtained by T.K.Mayeda and R.N.Clayton. The result is: delta O^{18} = +4.46 permil, and delta O^{17} = +2.52 permil, indicating that this stone is within the range of previously analyzed Martian meteorites.

[Pairing]

Dhofar 378 was found near the area where the Dhofar 019 basaltic shergottite was recovered. The latter is doleritic, but it may not be a pair with the former, because Dhofar 019 contains olivine grains with Fe/(Mg+Fe) ratios (fe ratios) of 0.4~0.75 [1], although Dhofar 378 does not contain such magnesian olivine. In addition, pyroxenes in Dhofar 019 are more magnesian than those in Dhofar 378. Dhofar 378 is rather similar in lithology to the Northwest Africa 480 shergottite which has no magnesian olivine and a homogeneous maskelynite (An_{46-50}), but the latter has more magnesian pyroxenes than the former [2]. Dhofar 378 resembles the Los Angeles basaltic shergottite: Lithology, texture, grain size, mineral assemblage, and mineral compositions of the latter [3] are nearly identical to those of the former, although the degree of impact shock differs between the two.

[Petrology]

Dhofar 378 consists mainly of ferroan clinopyroxenes (augite and pigeonite) and plagioclase glass with minor minerals of hedenbergite, pyroxferroite, fayalite, silica, rhyolitic glass, titanomagnetite (ulvöspinel) with ilmenite lamellae, sulfide, and phosphates (whitlockite and apatite). The modal composition of the stone is: clinopyroxenes (49vol.%), plagioclase glass (47 vol.%), titanomagnetite (3 vol.%), and phosphates (1 vol.%).

Clinopyroxenes in Dhofar 378 show mosaic extinction under a microscope, indicating their intense impact effects. The fe ratios of clinopyroxenes range from 0.4 to more than 0.9 (Fig. 1). The fe ratios of hedenbergite are from 0.97 to 0.99, and those of fayalite from 0.87 to 0.97. Subcalcic clinopyroxene grains often show an exsolution texture, consisting of augite and pigeonite lamellae, and the width of the lamellae ranges from less than 1 μm up to several μm.

Plagioclase glass has a quenched rim, which consists mainly of fibrous plagioclase. The fibrous plagioclase seems to have grown from the boundaries with pyroxene grains toward the cores of plagioclase glass. The width of the quenched plagioclase rims range from a few tens of μm up to one hundred μm. These rims completely surround the plagioclase glass cores. Anorthite (An) mole contents of the quenched plagioclase rims and plagioclase glass cores are An_{40-56} and An_{33-50}, respectively. The quenched plagioclase rims overlap in An contents to the plagioclase glass cores, although the former are slightly more calcic than the latter. The orthoclase (Or) contents of the former ($Or_{<1.7}$) are lower than the latter ($Or_{1.7-12}$). The K_2O contents of the plagioclase glass which contacts directly with the quenched plagioclase rims tend to be higher than those of plagioclase glass occurring far from the contact. This suggests that this meteorite experienced an intense impact shock, the original plagioclase grains transformed to plagioclase melt, and then the melt crystallized fibrous plagioclase rims at the boundaries between the plagioclase melt and pyroxene to pile up the K_2O content in the plagioclase melt just in front of the growing fibrous plagioclase rims.

Titanomagnetite (or ulvöspinel) in Dhofar 378 is enriched in TiO_2 (23-26 wt%) and includes ilmenite lamellae, about 10 μm wide, which exsolved out in the host titanomagnetite. The averaged Ti/(Ti+Fe) atomic ratios of the host titanomagnetite and the exsolved ilmenite are 0.23 and 0.48, respectively. On an assumption that the titanomagnetite consists mainly of magnetite and ulvöspinel end components and that the ilmenite consists mainly of ilmenite and hematite end components, the coexisting pair of titanomagnetite and ilmenite in Dhofar 378 gives a temperature of about 900 ℃ and oxygen fugacity of 10^{-14} atmosphere, using the iron-titaniferrous oxide system [4]. The oxygen fugacity is consistent with the assemblage of fayalite, quartz, and magnetite.

Phosphates are mainly whitlockite with minor apatite. Whitlockite often occur as large grains up to a few hundred μm across and contains 5-6.5 wt% of FeO and less than 1 wt% of MgO. Chlorine and fluorine contents of apatite are 2-3 wt% and 1.2-1.5 wt%, respectively.

[Fusion crust]

The fusion crust of Dhofar 378 consists mainly of is black glass with many bubbles of 10-100 μm in diameters. As black glass of the fusion crust in the Los Angeles shergottite is similar to the bulk composition of the rock [5], the chemical compositions were obtained by electron-probe micro-analyzer to presume the bulk composition. The average composition of the fusion crust glass in Dhofar 378 is shown in Table 1 with reference of that in the Los Angeles shergottite. The former is similar to the latter, suggesting that the original rock prior to the impact shock was similar to each other.

References

[1] J. N. Grossman 2000) MAPS, The Meteoritical Bull., No. 84, A201. [2] J. N. Grossman (2001) MAPS, The Meteoritical Bull., No. 85, A299. [3] A. E. Rubin et al. (2000) Lunar & Planet. Sci. XXXI, #1963. [4] A. F. Buddington and D. H. Lindsley (1964) Jour. Petr., Vol. 5, 310-357. [5] P. H. Warren et al. (2000) Lunar & Planet. Sci. XXXI,

#2001.

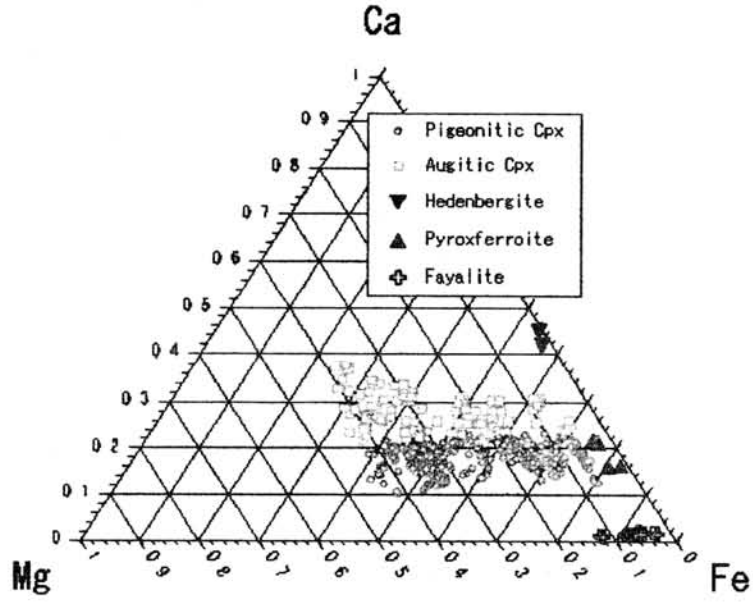

Fig. 1. Clinopyroxene (Cpx), Pyroxferroite and Fayalite in Dhofar 378

Table 1. Average chemical composition of black glass in fusior Dhofar 378

with referece to those in the Los Angeles shergottite (Warren et .

	Fusion Crust Dhofar 378	Fusion Crust Los Angeles	
SiO2	48.08	48.30	47.40
TiO2	1.18	0.92	1.29
Al203	9.50	9.70	9.46
Cr203	0.00	0.05	0.02
FeO	21.11	21.50	24.20
MnO	0.55	0.52	0.57
MgO	5.35	5.11	3.53
CaO	9.76	10.32	9.64
Na20	2.31	1.86	2.02
K20	0.15	0.15	0.19
P205	0.90	1.08	1.26
Total	98.89	99.51	99.88

"Antarctic" meteorites on Mars?

E. Illés-Almár
Konkoly Observatory, H-1525 Budapest Box 67, Hungary
e-mail: illes@konkoly.hu

It is suggested that the boulders on a MOC image are meteorites fallen in ancient times to the surface of Mars. If it will be proven it offers a possibility to guess how much of the regolith layer could have been diminished by sublimation of ground water from the surface, and consequently to estimate the water content of the regolith as a reservoir on Mars.

In [1] there is a report on an investigation carried out by an international student scientist team to find interesting places on Mars using the Mars Orbiter Camera (MOC) onboard Mars Global Surveyor (MGS). One of the specific areas to study in detail was a terrain near 31° N and 290° W, where a group of dark boulders are spread around on the light terrain. Michael Carr of the US Geological Survey commented that the boulders were puzzling and added "There is no indication of any outcrops that could shed such boulders". In my opinion these boulders are meteorites laying on the surface of Mars.

In a letter to Nature [2] Mustard et al. published the results of an analysis on the distribution of fretted terrain found on the surface of Mars. The result is interesting, implying that such collapsed terrain is concentrating between 30 and 60 degrees latitude on both hemispheres. The authors came to the conclusion that as a consequence of an ice age about one hundred thousand years ago on Mars a cold climate made it possible to accumulate – not glaciers, like on Earth – but frost and air-fallen dust cemented together. Later as the climate became warmer up till now, the H_2O sublimated out from the assemblage, leaving the dust behind, and when the soil became unstable, it collapsed.

As a third source of my idea the discovery of antarctic meteorites by Japanese scientists should be mentioned. There the sublimation of H_2O exposed such meteorites to the surface, that had fallen to the icy surface a long time ago, and later were buried together with their impact crater-walls by the precipitating snow.

Such "Antarctic" meteorites are probably visible on the MOC image [3]. They had fallen sometime on the ancient surface of Mars after an explosion caused by air drag, so the incoming body was broken apart. Very likely there were impact craters as well on the surface at that time, but later – as J.F. Mustard et al. stated – the near-surface ground ice sequentially diminished as a consequence of the orbitaly driven variations in Martian climate and a dissected terrain remained. As the major constituent of the soil is probably dust, after the sublimation of the ice, wind could blow the dust away leaving behind the exposed boulders. As the level of the surface lowered, the boulders were also sinking lower and lower. With the lowering of the surface, some day later other boulders, that were penetrated deeper at the time of the impact, were joining the exposed ones. Now we see all the boulders, that were embedded somewhere in the layers that disappeared so far. But it may be that some further part of the incoming body is buried in the deeper layers under the present surface and might be exposed later if the sublimation remains the dominant effect.

I offer this hypothesis to be used to estimate the minimum thickness of the layer that has diminished so far, and this can also help to estimate the water content of the regolith as a water-reservoir on Mars.

REFERENCES
1. Zimmerman, R. Red Rover goes to Mars: student scientists make history. *The Planetary Report* XXI, 16-17 (2001).
2. Mustard, J.F., Cooper, C.D., Rifkin, M.K. Evidence for recent climate change on Mars from the identification of youthful near-surface ground ice. *Nature* 412, 411-414, 2001.
3. Illés, E., Thoughts in connection with the Earth after getting better acquainted with the other members of the Solar System. (In Hungarian) *Természet Világa* Vol.132, No.11, 494-497, 2001.

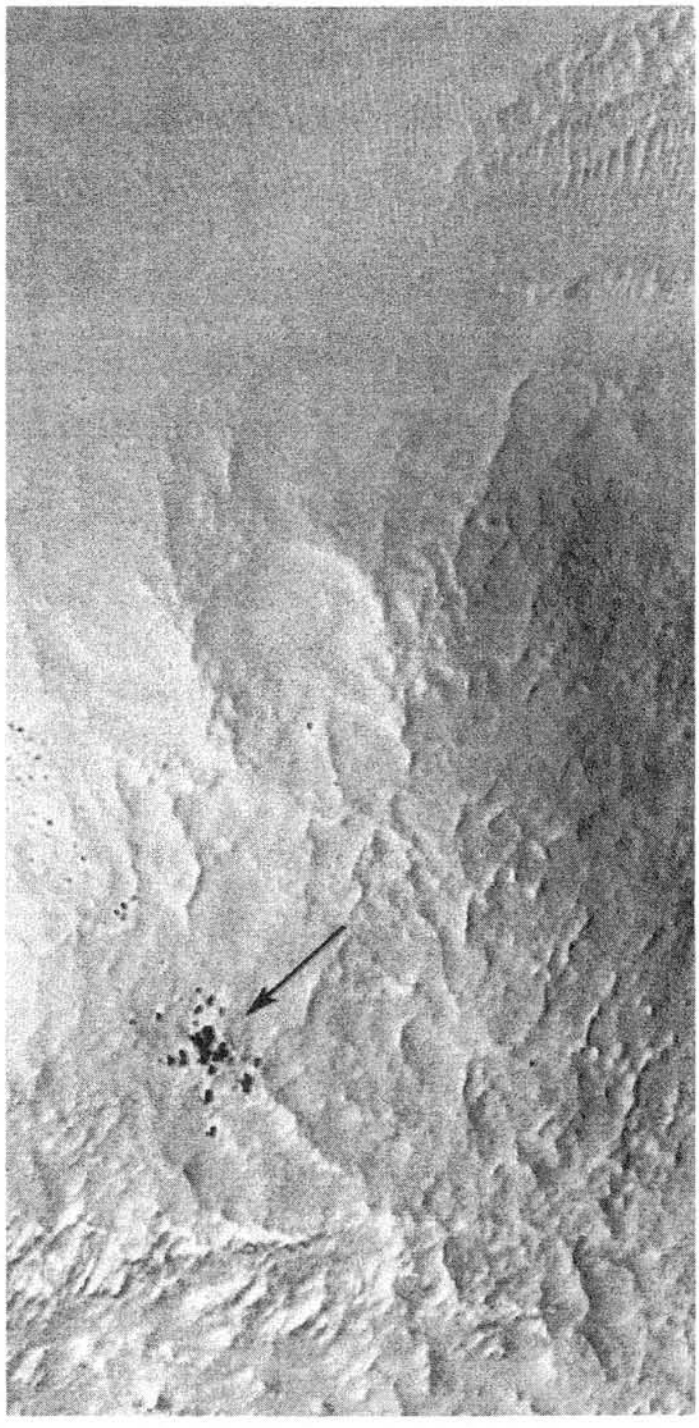

Figure caption
Figure 1 On this high resolution MOC image dark boulders peppering the light colour surface of Mars are interpreted as meteorites. The image covers an area approximately 3 km wide (31° north latitude, 290° west longitude).

Two nakhlites from Antarctica: Y000593 and Y000749

[1]N. Imae, [2]Y. Ikeda, [3]K. Shinoda, [1]H. Kojima, and [4]N. Iwata

[1]*Antarctic Meteorites Research Center, National Institute of Polar Research, 9-10, Kaga 1-chome, Itabashi-ku, Tokyo 173-8515, Japan*

[2]*Department of Material and Biological Sciences, Ibaraki University, Mito 310-8512, Japan*

[3]*Department of Geosciences, Faculty of Science, Osaka City University, 3-3-138 Sugimoto, Sumiyoshi-ku, Osaka 558-8585, Japan*

[4]*Faculty of Sciences, Yamagata University, 1-4-12 Kojirakawa, Yamagata-city, Yamagata, 990-8560, Japan*

1. Introduction

In our previous studies [1], we classified both Y000593 and Y000749 as nakhlites based on mineralogical and/or rare gas studies. In these studies, we clarified the mineralogical features of Y000593, and noted the differences with the other four nakhlites. The variations in the compositions of the augite and olivine phenocrysts (i.e., ferrosilite range and fayalite range, respectively) increase in the sequence of NWA817, Y000593, Nakhla, Governador Valadares and Lafayette (Fig. 1). The core-rim difference in augites is larger compared with that in olivines except for NWA817 (Fig. 1). This implies that the parent rock experienced diffusion controlled heating or annealing at different temperatures, confirming the results of an independent study reported by [2]. Mikouchi and Miyamoto [2] interpreted the cooling history from the analyses of zoning profiles of olivines in nakhlites and suggested that the differences were caused by differences of burial depth. We also found that both the modal abundances of mesostasis and the enstatite components in pyroxenes in mesostasis showed correlations with the olivine heterogeneities in the same sequence.

Y000593 and Y000749 are probably paired judging from the proximity of the paragenesis in the ice field around the Yamato mountains (within 1 km distance). Since Y000593 is the biggest nakhlite as described so far [1], there is the possibility to detect by comparison some chemical differences between paired specimens and/or between different samples of a single specimen (especially for Y000593). If some systematic chemical differences are detected, it may help to elucidate the geological setting in which these cumulate igneous rocks formed.

Thus, in the present study, we describe and compare mineralogical-petrological features of constituent minerals in Y000593 (,61 and ,67-1) and Y000749 (,1-1). Preliminary results (Y000593,61) of the study have been previously reported [1].

2. Experiments

Optical microscope and electron probe microanalysers (JXA-8800 in NIPR and JXA-733 in Ibaraki Univ.) were used for the study. H. Haramura determined bulk concentrations of major elements of Y000593,64 (2.180 g) and Y000749,47 (2.014 g) by wet chemical analyses. The measurement by the Fourier transform infrared microspectrometer (FTIR) was carried out for the weathered parts (especially for iddingsite formed on olivine rims and olivine cracks) of samples of Y000593,57, Y000593,58 and Y000749,49.

3. Results

Both specimens are unbrecciated cumulate igneous rocks consisting almost exclusively of elongated euhedral crystals of augite. Bulk compositions of Y000593 and Y000749 showed similarities with Nakhla. Modal abundances (%) are summarized: Y000593, 61: augite=75.6, olivine=8.0, Ti-magnetite=1.0, mesostasis=15.4. Y000593, 67-1: augite=84.2, olivine=6.9, Ti-magnetite=0.6, mesostasis=8.2. Y000749, 1-1: augite=70.7, olivine=18.4, Ti-magnetite=0.3, mesostasis=10.6.

Cumulate pyroxenes: Core compositions of augite phenocrysts are generally homogeneous ($En_{38}Fs_{22}Wo_{40}$), although inclusions of Ti-magnetite, in some cases, make the compositions somewhat richer in a Fs component. Rims discontinuously become more Fe-rich with a steep slope. The Fe-rich rims on olivine in contact with mesostasis are thicker than those in contact with other minerals.

Olivine phenocrysts: There is a tendency that the cores are more magnesian (Fa 66-70) compared with the rims (74-78). However, compositional zoning profiles of these olivine phenocrysts are not symmetrical. On the other hand, CaO (wt%) zoning profiles indicate that CaO decreases from core (~0.5wt%) to rim (~0.1wt%). Olivine phenocrysts usually have anhedral shapes and often include inclusions of augite that are similar in composition to cores of augite phenocrysts. Rims and cracks in olivines are partially weathered. Exsolution lamellae (or symplectites) are observed in many olivine grains.

Ti-magnetite phenocrysts: Subhedral to anhedral phenocrysts of Ti-magnetite usually include ilmenite lamellae of ≤10 μm in width.

Mesostasis: Mesostasis consists of lath-shaped plagioclase ($An_{28-36}Ab_{60-67}Or_{3.5-4.8}$) and minor minerals of pyrrhotite (nonstoichiometry δ range = 0.09-0.14), Ti-magnetite, Ca-apatite, silica, K-feldspar, and olivine and pigeonite that are more Fe-rich than those in phenocrysts. Olivines in the mesostasis are richer in Fa (~85).

Iddingsite: Weathered phases (iddingsite) abundantly occur in rims and fractures in olivine phenocrysts. FTIR spectra of iddingsite showed a broad absorption peak in the range of 3000-3680 cm^{-1} suggesting the existance of hydrous phases. (Weathered phases in the mesostasis also showed a similar broad absorption peak, but the absorption was larger.)

4. Discussion

Comparison between Y000593 and Y000749

The most striking difference between two nakhlite samples, Y000593 and Y000749 is the variation in abundances of olivine; Y000749 is significantly richer in olivine than Y000593. It may reflect ejection from different parts of the crater.

Iddingsite

Iddingsite in nakhlites consists of mixtures of hydrous minerals [3]. It must have formed on the parent body (Mars surface) [3]. Fusion crust glass just in contact with olivine and filling fractures consisting of alteration phases in olivine (Y000749, 1-1) include bubbles suggesting decomposition caused by heating during atmospheric entry. The texture is very similar to the texture in Nakhla [3]. This is textural evidence indicating that hydrous minerals must have been at least partially dehydrated to form anhydrous minerals. Therefore altered

phases in olivine mostly formed on the parent body by the reaction of water with Fe-rich olivine.

The rare gas studies support the suggestion that weathering products were formed on Mars since Mars atmospheric component (high $^{129}Xe/^{132}Xe$ ratios) is effective and the earth air contamination is very low (low $^{84}Kr/^{132}Xe$). Fall age is very young, 0.02Ma±0.08 [4]. Therefore, we consider that the degree of chemical weathering in Antarctica is very small.

References

[1] Imae et al. (2002) LPSC #1483.
[2] Mikouchi and Miyamoto (2002) LPSC #1343
[3] Gooding et al. (1991) Meteoritics 26, 135-143.
[4] Okazaki et al. (2002) This volume.
[5] Lentz et al. (1999) MAPS 34, 919-932.
[6] Sautter et al. (2002) EPSL 195, 223-238.

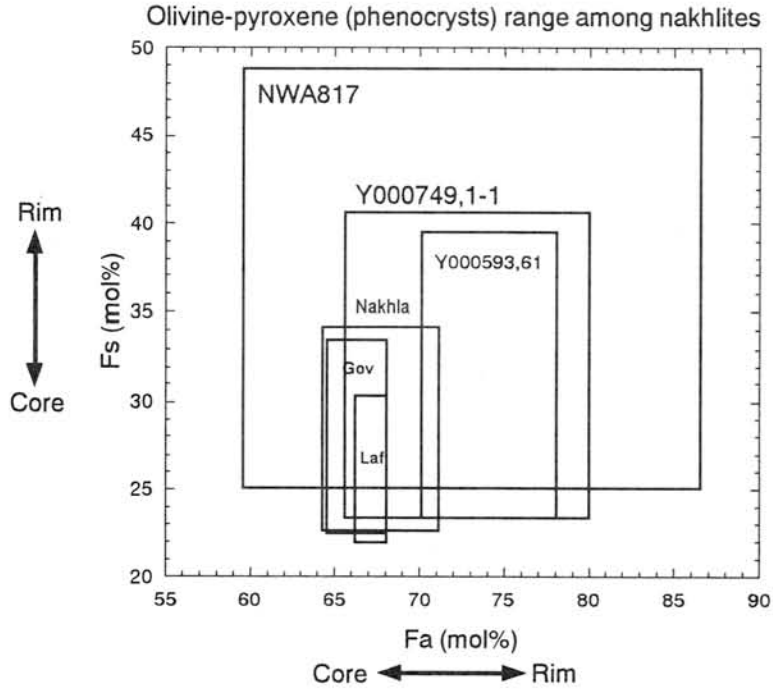

Fig. 1. Comparison of Y000593 and Y000749 with other nakhlites. The data of Lafayette (Laf), Governador Valadares (Gov), and Nakhla were taken from [5]. Data for NWA817 were taken from [6].

NEW U-TH-PB DATING OF METEORITES

JAGOUTZ, E.[1], JOTTER, R.[1],KUBNY A.[1],
VARELA, M. E.[2], ZARTMAN R.1, KURAT, G.[3].
[1]) Max-Planck-Institut für Chemie, Postfach 3060, D-55020 Mainz, Germany (jagoutz@mpch-mainz.mpg.de)
[2])CONICET-UNS, Departamento de Geología, San Juan 670 (8000) Argentina, (evarela@criba.edu.ar)
[3]) Naturhistorisches Museum, Postfach 417, A-1014, Vienna, Austria, (gero.kurat@univie.ac.at)

In order to understand the early evolution of our solar system extreme high resolution dating of formation ages of meteorites is needed. Since most of the meteorite classes were formed in the first 50 Ma (1%) of our solar system's history, high precision dating is necessary. In particular, relative dating using extinct isotopes like the Mn-Cr system hinges on an absolute calibration. Only the Pb-Pb system can serve this purpose, but few such high precisions Pb-Pb ages have been reported (1-3). Some of them have been reported with an age precision of 0,01%, which requires a measurement precision of 0.03% for the $^{206}Pb/^{207}Pb$ ratio -- reached only by using the Faraday collector and a tight control of the mass fractionation.

In the D'Orbigny meteorite for which we have obtained Pb-Pb ages, such a high precision has not yet been achieved because the Pb concentration in the dated pyroxene is extremely low (between 7 and 17 ppb). Four pure mineral separates of clean pyroxenes (of about 15 mg each) yielded only 100 to 250 pg of Pb that was too little to run on the Faraday collector. Instead, measurement was made with an ion counter giving a typical error for the $^{206}Pb/^{207}Pb$ ratio of 0,1 to 0,2 % and translating into an age error of 2 to 4 Ma.
D'Orbigny is the sixth Angrite to be identified and the largest of this rare meteorite class. Until now high-precision Pb-Pb data has existed only for Angra dos Reis and LEW 86010 (1). Two of the D'Orbigny pyroxenes are from the groundmass and the other two are idiomorphic and grew inside druses-like cavities. The latter are considered to be 100% pure while the former may contain some inclusions. Also, we analysed one sample of anorthite, which had a Pb isotopic composition close to that of terrestrial Pb, and may be dominated by terrestrial Pb. The Pb-Pb age of the two matrix pyroxenes are 4549 ± 2 Ma and 4557 ± 2 Ma; however, the U-Pb ages are distinctly discordant for the younger pyroxenes. The druses pyroxenes gave Pb-Pb age of 4555.4 ± 1.9 Ma and 4557 ± 2 Ma, with $^{206}Pb/^{204}Pb$ ratios of 522 and ~2000, respectively. Furthermore, the U-Pb ages for both these pyroxenes are, within the uncertainties of the correction parameters, concordant, as is a Th-Pb age for the second analysis. Unfortunately, the relatively large error of its Pb-Pb age reflects the small amount of Pb on the filament.

The best absolute age of crystallization for D'Orbigny is 4556.3±1.7 Ma this is within the error identical to 4557.8±0.5 Ma as the crystallization age for LEW 86010 and 4557.8±0.4 for Angra dos Reis (1). The ages of Angrites are 10 to 11 Ma younger than the "Allende Inclusions" and about 8 Ma younger than Chondrules. For HED meteorites, however, the crystallization ages are scattered over a considerable time interval. Because HED meteorites belong to a bigger body, which firstly had a considerable cooling time in this early environment, and secondly this bigger body was bombarded intensively which causes that most of the HED meteorites are altered by shock.

Using the Mn-Cr Relative dating method, however, suggest that the "Allende Inclusions are 13.5 Ma and the chondrules are 11 Ma older than the Angrites. From the differentiation isochron in Mn-Cr system it was estimated that HED meteorite differentiation is 7.2 Ma older than the crystallization of the Angrites.(3)

Refereces:

1) Lugmair and Galer (1992) GCA 56, 1673-1694. 2)Göpel et al. (1994) EPSL 121 153. 3) Amelin Y. et al. (2002) LPSC XXXIII 1151. 3)Lugmair and Shukolyukov (1998) GCA 62, 2863-2886

Yamato 983885: A second lunar meteorite from the Yamato 98 collection

Hiroshi KAIDEN and Hideyasu KOJIMA

Antarctic Meteorite Research Center, National Institute of Polar Research
1-9-10 Kaga, Itabashi-ku, Tokyo 173-8515, Japan (kaiden@nipr.ac.jp)

Introduction

More than 4000 meteorites were found around the Yamato and Belgica Mountains, Antarctica by the meteorite search party of the 39th Japanese Antarctic Research Expedition (JARE-39) in the 1998–1999 field season. Among these specimens, two lunar meteorites were distinguished by classification in the field [1], and were officially named Yamato(Y)981031 and Y983885 [2, 3]. One of the meteorites, Y981031, may be paired with the lunar meteorite Y793274 based on texture, mineralogy and bulk chemical composition [1, 4]. Here we report petrographical and mineralogical studies of the other meteorite, Y983885, in order to confirm its lunar origin.

Analytical Methods

A small fragment was chipped from a specimen of Y983385 and made into a polished thin section (PTS). The PTS, Y983885, 71-1, was studied with an optical microscope using transmitted and reflected light. Mineral compositions were determined by quantitative wavelength dispersive X-ray analyses with JEOL JCXA-733 and JXA-8800M electron microprobes at the National Institute of Polar Research, Tokyo, Japan. All electron probe analyses were run at 15 kV and 11 nA. Natural and synthetic standards were used and corrections were made for absorption, fluorescence and atomic number effects using the method of Bence and Albee [5]. The bulk chemical composition of Y983335 was determined by standard wet chemical analysis methods [6].

Results and Discussion

Sample Descriptions

Y983885 was found on the bare ice field around the JARE IV Nunataks (71°33.77′S, 36°00.31′E), Yamato Mountains, Queen Maud Land, East Antarctica on January 11, 1999. The meteorite is a rounded stone with a thin yellowish green fusion crust. The stone weighs 289.71 g and measures 8.4×5.4×5.2 cm. The recovered sample has a smoothly rounded surface, possibly indicating an original face. Macroscopic observation of the sample reveals angular white to gray rock clasts (up to 3 mm in size) and mineral fragments, including white crystalline plagioclases, pyroxenes and dark grains set in a dark fine-grained matrix (Fig. 1).

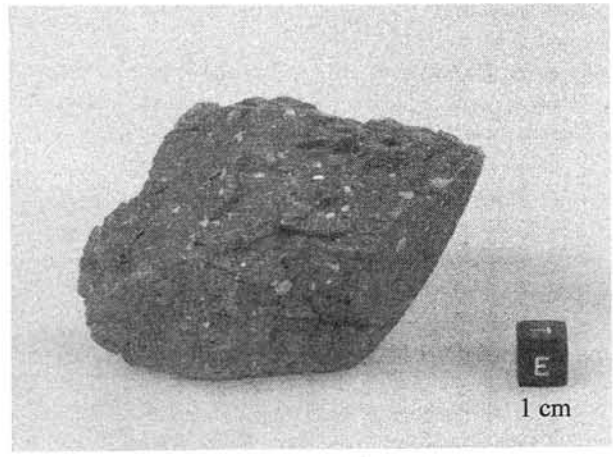

Fig. 1. Photograph of a hand specimen of Y983885.

Examination by optical microscopy of the PTS indicates that the meteorite is a polymict breccia containing abundant rock and mineral clasts set in a dark brown glassy matrix (Fig. 2). Rock clasts include polymineralic, monomineralic and melt clasts (up to 1.2 mm in size). Most large clasts are polymineralic and are composed of Ca-rich plagioclase, pyroxene and olivine. A few large clasts are composed of plagioclase and pyroxene, or only plagioclase. Smaller clasts are commonly mineral fragments of predominant plagioclase, with subordinate proportions of pyroxenes and olivines. Glass spherules, up to 300 μm in diameter, are also observed. Hence, Y983885 is a regolith breccia with abundant clasts, especially feldspathic ones, set in a dark brown glassy matrix. Some clasts are similar to those of eucrites and howardites, but an affinity to basaltic achondrites can be ruled out based on FeO/MnO ratios discussed below.

Mineral Compositions

Electron probe analyses indicate a range of pyroxene composition for the whole meteorite of Wo_{2-40}, Fs_{12-55}, En_{14-85}; a plagioclase range of An_{89-98}; and an olivine range of Fa_{32-36}, except one grain of Fa_{55} (Figs. 3 and 4).

The ratios of FeO/MnO for pyroxenes from Y983885 are plotted in Fig. 5. Pyroxenes of eucrites consistently have FeO/MnO ~33, and pyroxenes of lunar rocks consistently have FeO/MnO ~69 [7]. The pyroxenes of Y983885 have average FeO/MnO = 64, which is distinctly higher than basaltic achondrite pyroxenes. A regression line derived from Y983885 data is consistent with a line for lunar pyroxenes (Fig. 5), providing strong evidence for its lunar origin.

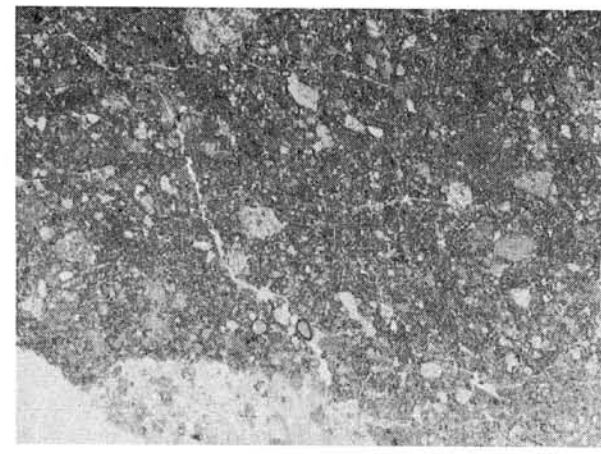

Fig. 2. Photomicrographs of a thin section Y983885, 71-1 (width is 6.0 mm).

Bulk Compositions

The major element compositions of Y983885 determined by standard wet chemical analysis are (in wt%): SiO_2=45.59, TiO_2=0.53, Al_2O_3=21.81, FeO=9.41, MnO=0.15, MgO=7.98, CaO=14.02, Na_2O=0.34, K_2O=0.11, P_2O_5=0.15, Cr_2O_3=0.17, FeS=0.05, Fe=<0.05, Ni=0.005, Co=0.009. Hence, Y983885 is a high-aluminum and -calcium rock with abundant Ca-rich plagioclase (anorthite), indicating it is a lunar highland anorthosite. The bulk chemical composition also has a distinctively lunar FeO/MnO ratio (Fig. 5).

Oxygen Isotopes

The oxygen isotopic composition of a bulk-rock sample of Y983885 was determined [8]; $\delta^{18}O$ = +5.65 ‰, $\delta^{17}O$ = +2.89 ‰ and $\Delta^{17}O$ = –0.05 ‰, where $\Delta^{17}O$ (= $\delta^{17}O - 0.52\ \delta^{18}O$) designates a departure from the terrestrial fractionation (TF) line. Thus, the isotopic composition lies on the TF line, suggesting that Y983885 is lunar [9–11].

Acknowledgments

The authors are very grateful to the other members of the JARE-39 for their cordial assistance. They also thank H. Haramura for the wet chemical analyses.

References

[1] Kojima H. (2000) *Antarct. Meteorites* **XXV**, 55.
[2] Kojima H. and Imae N. (2000) *Meteorite News* **9(1)**, 2.
[3] Kojima H. and Imae N. (2001) *Meteorite Newsletter* **10(2)**, 1.
[4] Kojima H. *et al.* (2000) *Antarct. Meteorite Res.* **13**, 1–8.
[5] Bence A. E. and Albee A. (1968) *J. Geol.* **76**, 382–403.
[6] Haramura H. *et al.* (1983) *Mem. Natl Inst. Polar Res., Spec. Issue* **30**, 109–121.
[7] Warren P. H. and Kallemeyn G. W. (1989) *Geochim. Cosmochim. Acta* **53**, 3323–3300.
[8] Clayton R. N. and Mayeda T. K. (2001) *pers. comm.*
[9] Clayton R. N. *et al.* (1976) *Earth Planet. Sci. Lett.* **30**, 10–18.
[10] Mayeda T. K. *et al.* (1983) *Geophys. Res. Lett.* **10**, 799–800.
[11] Mayeda T. K. *et al.* (1987) *Mem. Natl Inst. Polar Res., Spec. Issue* **46**, 144–150.

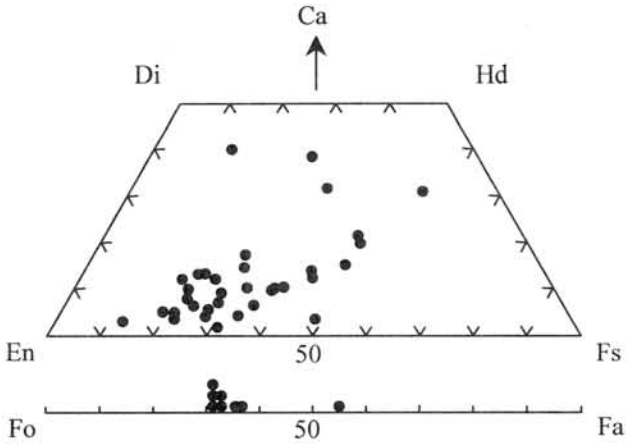

Fig. 3. Pyroxene quadrilateral and olivine compositions in Y983885.

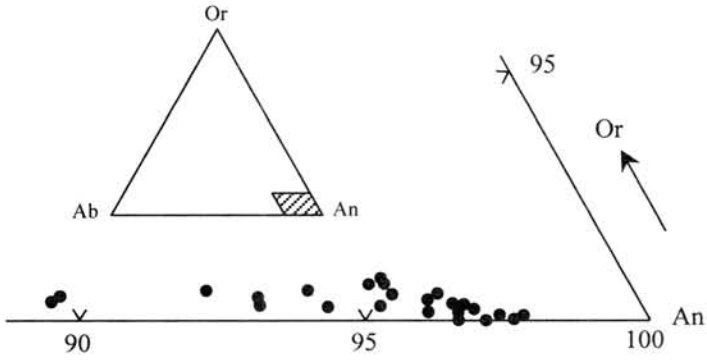

Fig. 4. Chemical compositions of plagioclase in Y983885 plotted in the Ab-An-Or diagram.

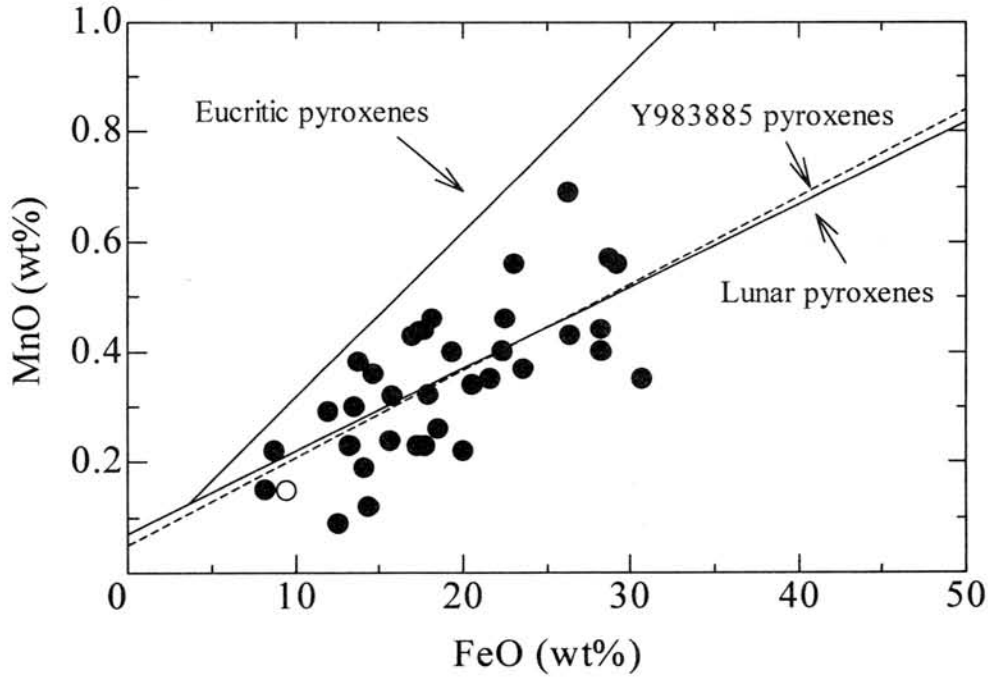

Fig. 5. Pyroxene FeO vs. MnO for Y983885, a eucrite and a lunar rock. Open circle indicates the ratio for a bulk sample of Y983885. The dashed line is based on linear regression for the Y983885 data.

Chemical Composition of lunar meteorites including Yamato 981031

Y. Karouji, Y. Oura and M. Ebihara.

Graduate School of Science, Tokyo Metropolitan University, Hachioji, Tokyo 192-0397, Japan

Yamato (Y) 981031 is the 7th Antarctic lunar meteorite of mare origin, following Y 793169, Y 793274, EET 87521, Asuka (A) 881757, QUE 94281 and EET 96008. Y 981031 was described as a polymict, regolith breccia, having diverse mixture of mineral fragments and clasts from various rock types [1]. Although these seven meteorites are grouped into mare meteorites, there is a large difference in petrographical texture: Y 791031 and A 881757 (hereafter, YA) are unbrecciated mare basalts [e.g. 2] while Y 793274, EET 87521, QUE 94281 and EET 96008 are bracciated mare basalts mixed with highland rocks. Y 981031 is apparently categorized into the latter group. In this study, we determined major, minor and trace element composition of Y 981031 by using several analytical methods and aimed to characterize this meteorites in chemical composition in comparison with those for the pre-found Antarctic mare lunar meteorites.

A total of 0.254 g of powdered specimen was allocated to us for a consortium study of Y 981031. This powder sample was originally prepared for wet chemical analysis using a gram scale of sample, suggesting that the specimen we used is representative of the meteorite in chemical composition. In addition to Y 981031, we also analyzed three lunar meteorites of mare origin; EET 87521, QUE 94281 and EET 96008, which were loaned from Meteorite Working Group, NASA. For these three samples, about 0.3 to 0.5 g of lumps were allocated to us. Samples were first analyzed by neutron-induced prompt gamma-ray analysis (PGA), for which lump samples were used except for Y981031. Following PGA, instrumental neutron activation analysis (INAA) and neutron photon activation analysis (IPAA) were performed. For INAA and IPAA of EET 87521, QUE 94281 and EET 96008, lumps were ground in a clean agate mortar and some aliquants were used.

Table 1 shows chemical composition of four lunar meteorites for major elements determined in this work. Most elements were determined by PGA. Our values for Y981031 are highly consistent with those obtained by wet chemical analysis by Haramura [3]. Lunar mare basalts and highland regoliths are two characteristic petrographical groups and are separable in chemical composition, as demonstrated in Figure 1, where Al_2O_3 is plotted against TiO_2; mare basalts are characterized with relatively high contents in TiO_2 (and FeO) and low contents in Al_2O_3. Apparently, Y 981031 has chemical composition close to those for mare basalts and far from those for highland regoliths. EET 87521 and EET 96008 (hereafter,

EETs), and Y793274 and QUE 94281 (hereafter, YQ) also are contaminated with highland components, having different degrees in admixture; EETs are less contaminated than YQ, to which Y 981031 seems to belong. This is more clearly noticeable in Fig. 2, where Fe0 is plotted against Sc. It is suggested that YQ were launched at the same crater-forming event from moon and touched down on Antarctica separately [4]. Form Fig.1 and Fig. 2, Y 981031 is inferred to have been launched along with YQ.

Figure 3 shows chondrite-normalized REE abundance patterns for lunar meteorites analyzed in this study. It is remarkable that all meteorites have similar patterns except for Eu. These resemble those for lunar highland samples, one of which is shown in Fig. 3 for comparison, although absolute contents are largely different. It is apparent that REE abundances in Y 981031, along with other three meteorites analyzed, are largely characterized by an addition of highland components represented by medium-K Fra Mauro (KREEPy) basalt. Our EET 96008 seems to have less amount of such component than EET 87521.

References: [1] Arai T., Ishii I. and Otsuki M. (2002) *Lunar Planet. Sci.* **XXXIII**, #2064. [2] Takeda et al. (1993) *Proc. NIPR Ant. Met.* **6**, 3-13. [3] Kojima H. (2000) *Antarctic Meteorites* **XXV**, 5 (abstract). [4] Arai T. and Warren P. H. (1999) *Mateor. Planet. Sci.* **34**, 209-234.

Table 1. Chemical composition (in %) of lunar meteorites analyzed in this study.

	SiO_2	TiO_2	Al_2O_3	FeO	MnO	MgO	CaO	Na_2O	K_2O	P_2O_5	Cr_2O_3	total
Y 981031	45.46	0.78	17.31	13.07	0.15	9.30	12.09	0.42	0.07		0.26	98.91
Y 981031*	44.88	0.71	18.44	12.43	0.20	9.42	12.84	0.34	0.04	0.13	0.26	99.70
QUE87521	40.44	0.68	16.96	13.88	0.19	7.94	11.74	0.44	0.08		0.25	92.59
EET87521	46.30	0.69	15.82	16.04	0.21	8.83	12.32	0.43	0.07		0.23	100.9
EET96008	40.70	0.57	14.80	16.02	0.21	11.04	12.05	0.35	0.07		0.33	96.14

*Determined by wet chemical analysis by Haramura [3].

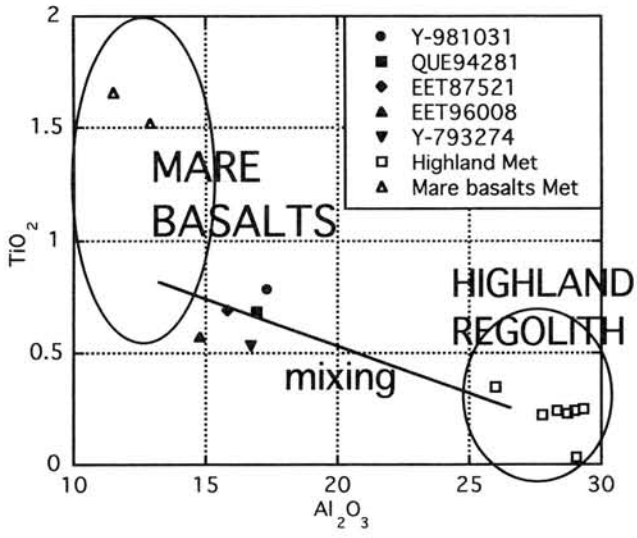

Fig. 1 Al_2O_3 (in %) vs. TiO_2 (in %).

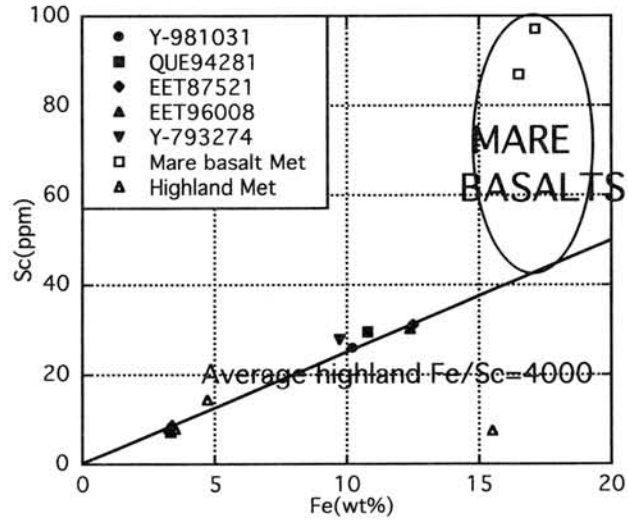

Fig. 2 Fe (in %) vs. Sc (in ppm).

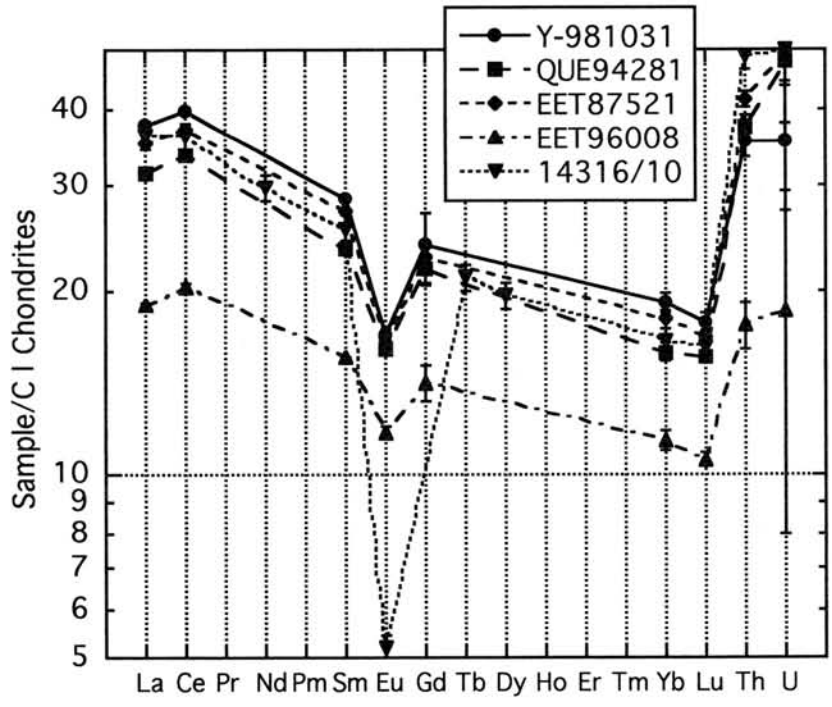

Fig. 3 Chondrite-normalized REE abundance patterns for lunar mare meteorites. REE abundances for a lunar highland rock (14316) are shown for comparison with a scale of 1/10.

The first discovery of back transformation of high-pressure phases in shock veins of ordinary chondrites during atmospheric passage

Kimura M.[1], Chen M.[2], Yoshida T.[1], El Goresy A.[3] and Ohtani E.[4]

[1]Ibaraki University, Mito 310-8512, Japan, [2]Guangzhou Institute of Geochemistry, Chinese Academy of Sciences, Guangzhou 510640, China, [3]Max-Planck-Institut für Chemie, 55128 Mainz, Germany, [4]Faculty of Science, Tohoku University, Sendai 980-8578, Japan.

1. Introduction

Many ordinary chondrites contain shock-induced melt veins. Especially, the shock veins of L6 chondrites are the major hosts for high-pressure phases such as ringwoodite, majorite-pyrope garnet and hollandite-structured plagioclase [e.g., 1-3]. On the other hand, peripheral rims of meteorites experienced reheating for short time during the atmosphere passage. We investigated some ordinary chondrites bearing shock veins and fusion crusts with laser micro Raman spectroscopy, in order to explore the natural effects of transient high-temperatures on the back-transformation of high-pressure phases.

2. Results

Y75267 is a shock vein-bearing H6 chondrite covered by a fusion crust of 60-80 μm in width. On the surface of meteorite, the shock vein is cut by the fusion crust. The fusion crust shows a quench texture consisting of fine laths of olivine (Fa_{25-51}). The shock vein region far from the fusion crust, at distance of more than 280 μm, consists of high-pressure phases, such as wadsleyite, ringwoodite, majorite and hollandite. The vein region near the fusion crust, less than 280 μm, has the same texture, grain size distribution and mineral chemistry as the vein region far from the crust. However, the shock vein near the fusion crust consists entirely of low-pressure phases such as olivine, low-Ca pyroxene and plagioclase glass. The boundary between low- and high-pressure phase regions is very sharp, and it is just parallel to the fusion crust at a distance of 280 μm.

We also studied two L6 chondrites, Y82144 and Y82153. The veins contain wadsleyite and majorite. However, the vein regions near the fusion crusts, less than ~300 μm, completely consist of low-pressure phases.

3. Discussion

Y75267 and two L6 chondrites experienced impact events under high-pressures and temperatures, and silicate phases were transformed to their high-pressure polymorphs. It is undoubtedly that the low-pressure phases in the shock veins near the fusion crusts in Y75267 and others, had primarily been the high-pressure polymorphs. During the atmospheric passage, the peripheral parts of the chondrites were melted and quenched to form the fusion crusts under atmospheric pressures. Simultaneously, the high-pressure phases near the fusion crusts were transformed to low-pressure polymorphs.

Some authors estimated the thermal history of meteorites during the atmospheric passage. Sears [4] calculated that the maximum temperatures of a region of about 300 μm distant from fusion crusts are 600-1500°C. Yabuki [5] estimated that an area of 300 μm inwards distant from fusion crust becomes 1400°C after 5 seconds, assuming that the fusion crust melted at 1600°C. On the other hand, aerodynamic heating was estimated to last for only several seconds [5, 6]. It is, therefore, probable that even at regions near fusion crusts, the high temperature conditions lasted only for a short time, possibly less than several seconds. The distribution of the low-pressure phase assemblage near the fusion crusts studied here shows that high-pressure polymorphs of silicate phases would quickly transform back to their low-pressure phases at high-temperatures, under atmospheric pressures in very short time. The vein regions, more than ~300 μm distant from the fusion crust, should not have been heated up to several hundreds degrees, and high-pressure phases completely survived during the atmospheric passage.

The result obtained here is significant for the estimation of P-T history of shock veins encountered in chondrites. The high-pressure phases in the veins must have crystallized under high-pressures and temperatures [e.g., 1-3]. However, post-shock temperatures were extremely low thus leading to the survival of the high-pressure phases.

References: [1] Chen, M. et al. (1996) Science 271, 1570-1573. [2] Gillet P. et al (2000) Science 287, 1633-1636. [3] Tomioka, N. et al. (1997) Science 277, 1084-1086. [4] Sears D.W. (1975) Modern Geology 5, 155-164. [5] Yabuki H. (1975) J. Fac. Sci. Hokkaido Univ., 18, 85-104. [6] McCrosky R.E. et al. (1971) JGR 76, 4090-4108.

Infrared spectra of pre-solar carbide grains

Yuki Kimura, Chihiro Kaito

Department of Nanophysics in Frontier Project, Ritsumeikan University, Kusatsu-shi, Shiga 525-8577, Japan

Carbide core (SiC, TiC, ZrC etc.)-carbon mantle grains have been produced by noble gas evaporation methods. The size of the carbide core has the same size of pre-solar grains. The infrared spectra of several collected grains were determined. The absorption peak of β-SiC core-carbon mantle grains, TiC core-carbon mantle grains and ZrC grains were 11.3 μm strong feature, 9.5 and 12.5 μm broad feature and 9.4 μm broad feature, respectively.

Metal carbides in meteorites (Si, Ti, Mo and Zr) were identified by transmission electron microscopy (TEM) (Bernatowicz et al., 1991; Bernatowicz et al., 1992; Bernatowicz et al., 1996). Moreover, metal carbides are indeed expected to form in the winds of carbon-rich asymptotic giant branch (AGB) stars (Cherchneff and Cau, 1999; Lodders and Fegley, 1997). Infrared spectra from carbon rich star have several absorption peaks due to metallic carbide grains. The origins of absorption peaks were proposed on the basis of laboratory studies. However, the origins of absorption peaks were not correctly identified with the structure of grains. The origin of 11 μm absorption due to SiC was not clarified with the relation of poly-types. The absorption due to TiC and ZrC grains were hardly seen as the laboratory data. Laboratory production of the grains on these refractory materials was difficult. An important factor for determination of absorption feature is size, shape and structure of the grain.

Metallic, oxide and sulfide grains by the smoke method have been studied on the basis of TEM. The growth mechanism of these particles has been elucidated in a series of experiments (Kaito, 1978; Kaito, 1981; Kaito, 1984; Kaito, 1985). Even with the gas evaporation method, refractory material such as carbide is difficult to obtain. In previous study, we succeeded in the formation of titanium carbide grains of the order of 50 nm by advanced gas evaporation method (AGEM) (Kimura and Kaito, submitted). By this method, several metallic carbide grains can be produced. Therefore, we have started to obtain the characteristic data of carbide grains in laboratory experiments.

The specimens were examined using a Hitachi H-7100R electron microscope.

High-resolution electron microscopy (HREM) images were obtained using a Hitachi H-9000NAR electron microscope. The infrared spectra of the samples embedded in KBr pellets were measured with a Fourier-transform infrared spectrometer (Horiba Inc. FT210). The wavelength resolution was 2 cm^{-1}.

Figure 1 shows a typical electron microscopy (EM) image and corresponding electron diffraction (ED) pattern of the collected specimen obtained by simultaneous evaporation of zirconium and carbon. The ED pattern shows the formation of ZrC particles. The size of ZrC grains determined from an electron microscopy (EM) image is 5 nm. Figure 2 shows the infrared spectrum of the collected ZrC grains embedded in KBr pellets. The absorption peak of spectrum has a broad feature at 9.4 μm.

The correlation of the structure, size and absorption peak of SiC, TiC and ZrC by the same experiment were shown in table 1. 11.3 μm absorption peak of β-SiC was very strong. On the other hand, absorption peaks of TiC and ZrC were weak. This shows the infrared absorption of NaCl-type structure were weaker than any other structure as is discussed on the mixture film of MgO and SiO (N. Suzuki et al., 2000).

Table 1. Correlation of the structure, size and absorption peak

Grain	Structure	Size	Absorption Peak
β-SiC	Zinc-blende	50 nm	11.3 μm
TiC	NaCl-type	50 nm	9.5, 12.5 μm
ZrC	NaCl-type	5 nm	9.4 μm

References

Bernatowicz, T. J., Amari, S., Zinner, E. K., Lewis, R. S., *Astrophys. J.* 373, L73, 1991.

Bernatowicz, T. J., Amari, S., Lewis, R. S., *Lun. Planet. Sci.* 23, 91, 1992.

Bernatowicz, T. J., Cowsik, R., Gibbons, P. C., et. al., *Astrophys. J.* 472, 760, 1996.

Cherchneff, I., Cau, P., In: Le Bertre, T., Lebre, A., Waelkens, C. (Eds.), *IAU Symp.* 191, 251, 1999.

Kaito, C., *Jpn. J. Appl. Phys.* 17, 601, 1978.

Kaito, C., *J. Cryst. Growth* 55, 273, 1981.

Kaito, C., *Jpn. J. Appl. Phys.* 23, 525, 1984.

Kaito, C., *Phys.* 24, 211, 1985.

Kimura, Y., Kaito, C., *Planet. Space Sci.* (submitted).

Lodders, K., Fegley Jr., B., In: Bernatowicz, T. J., Zinner, E. (Eds.), *AIP, New York,* 391, 1997.

Suzuki, N., Kimura, S., Nakada, T., et. al., *Meteorit. Planet. Sci.* 35, 1269, 2000.

Uyeda, R., *in Morphology of Crystal Part B Ed. I*, Sunagawa, 369, (Terra, Tokyo, 1987).

Uyeda, R., *in Progress in Materials Science* 35, 1-96, (Pergamon Press, 1991).

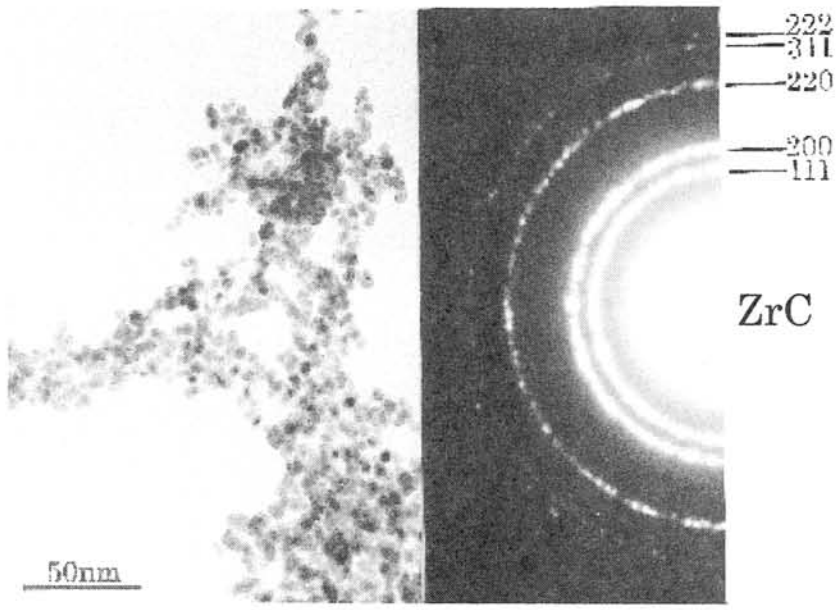

Fig. 1. Typical EM image and ED pattern of the collected ZrC grains.

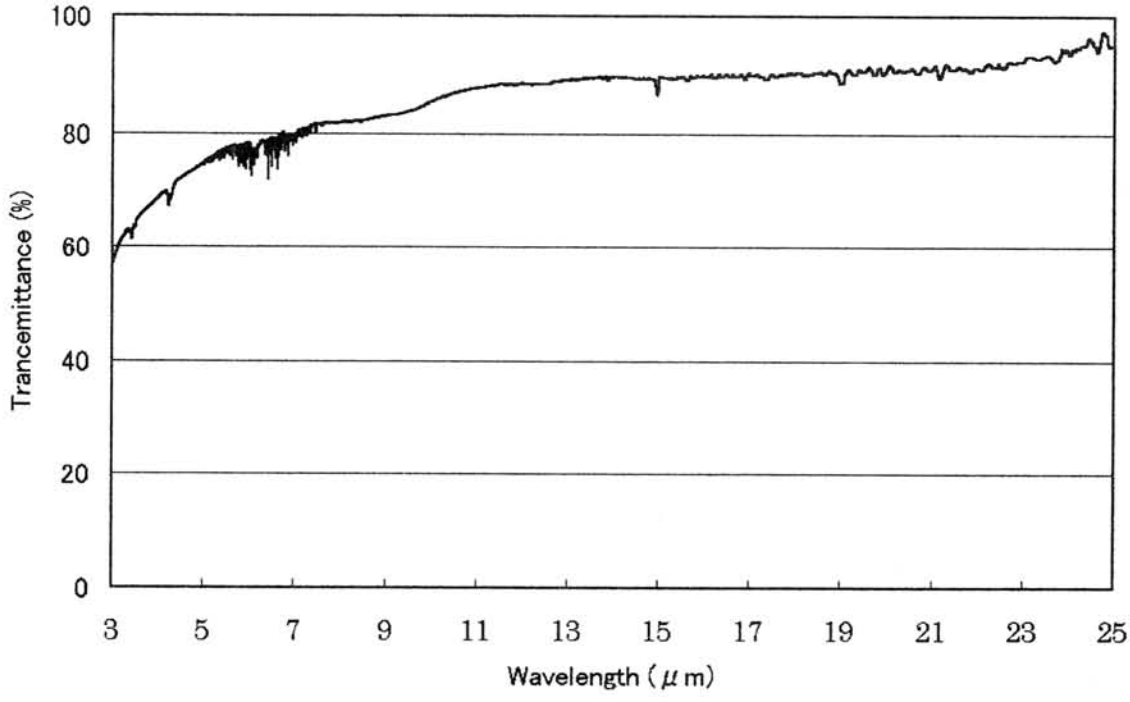

Fig. 2. Infrared Spectrum of corresponding to ZrC grains as shown in Fig. 1.

The SIMS U-Th-Pb measurement of phosphates in shocked ordinary chondrites

N. T. KITA[1], M. KIMURA[2], S.TOGASHI[1] and Y. MORISHITA[1]

[1]Institute of Geoscience, Geological Survey of Japan, AIST, Tsukuba 305-8567, Japan.
[2]Ibaraki University, Mito 310-8512, Japan

Introduction

The secondary ion mass spectrometer (SIMS) has been extensively applied to the zircon U-Pb age determinations for terrestrial and meteoritic samples. Recent attempts were also made to phosphate minerals in terrestrial and meteoritic samples (Kita et al., 1997; Sano et al., 1999). In equilibrated ordinary chondrites, two types of phosphates, apatite [$Ca_5(PO_4)_3(Cl,F)$] and whitlockite [$(Ca,Mg,Na_2)_3(PO_4)_2$], are found as large as 100 μm size. As apatites in equilibrated ordinary chondrites are enriched in U (a few ppm), it is possible to determine a model $^{207}Pb/^{206}Pb$ age of a 4.5 Ga chondritic apatite with the precision better than 20 Ma, by using the 25μm diameter primary ion beam,

In this study, we apply the SIMS U-Th-Pb analysis to phosphate minerals from shock melted chondrites. The young shock metamorphism ages were obtained by using Ar-Ar methods from various chondritic meteorites (Bogard, 1995). The Ar degassing age of L chondrites show the peak at 0.5 Ga, indicating the extensive impact event that could destroy the L chondrite parent body. The Rb-Sr ages of 1.2 Ga are obtained from heavily shocked LL chondrites (Okano et al., 1990). The number of shocked H chondites are much smaller than L and LL and their Ar-Ar ages are variable (0.3 Ga – 4 Ga), possibly because of incomplete degassing of radiogenic Ar (Grier et al., 1997). Therefore, it is interesting to see if there is are differences in U-Th-Pb systems among phosphates from shocked H, L, and LL chondrites, depending on the nature of the shock metamorphism.

Samples

Three Antarctic shock-melted chondrites, Y790746 (H), Y790480 (L), Y790964 (LL), are used for the SIMS analyses. Among them, the 1.2 Ga Rb-Sr age was obtained from Y790964 (LL) (Okano et al., 1990). The Y790746 (H) contains unmelted H6 clast (Kimura et al., 1999). Phosphate grains in the shocked L and LL chondrites are mostly whitlockite with grain sizes 10-30 μm. For the shocked H chondrite, we observed phosphate grains inside of and surrounding the H6 unmelted clasts. They contain both apatite and whitlockite with grain sizes up to 100μm.

SIMS analyses

The IMS-1270 at Geological Survey of Japan was used for the SIMS analyses. The analytical parameters are shown in Table 1. We used the 12μm primary ion, because of small grain sizes. In order to calibrate U/Pb and Th/Pb relative sensitivity, we used the Guarena meteorite (unshocked H6) with known concordant 4.50 Ga U-Pb age. A single measurement was done as a set of 80 cycles of measuring ions [$^{175}Ca_2PO_4^+$(matrix) - $^{204}Pb^+$ - 204.2 (background) - $^{206}Pb^+$ - $^{207}Pb^+$ - $^{208}Pb^+$ - $^{232}Th^+$ - $^{238}U^+$ - $^{248}ThO^+$ - $^{254}UO^+$], which takes 2 hours. Repeated analyses of Guarena apatites showed the constant ^{206}Pb intensity of 20 cps/nA. By assuming the U concentration of Guarena apatite to be 2-3 ppm, (Crozaz et al., 1989; Göpel et al., 1994), the sensitivity of Pb is estimated to be 7-10 cps/nA/ppm, which is similar to the

condition of the zircon analysis using the same instrument. The SIMS results of Guarena apatites on the Pb-Pb isochron diagram well reproduce the literature data obtained for a phosphate separate of the same meteorite by using the conventional TIMS technique (Göpel et al., 1994).

Table 1. Typical condition of Guarena apatite

Primary Ion	0.5-1.0 nA, O_2^-
Mass Resolution	4,500
^{206}Pb Secondary Ions	10-20 cps
^{204}Pb Secondary Ions	$\leq$ 0.02 cps
Detector Background	~0.003 cps (M=204.2)

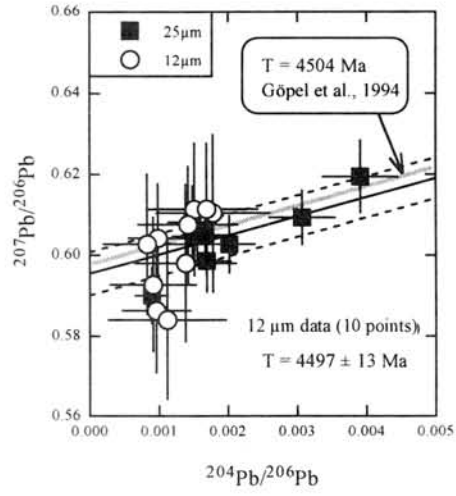

Fig. 1. Pb-Pb age of Guarena apatites. Data obtained using 25μm beam sizes are from Kita unpublished data.

Result and Discussion

The U and Th concentrations of phosphates in shocked chondrites are shown in Fig.2. Apatites and whitlockites in Y790746 (H) showed enrichments of U and Th similar to the Guarena H6 chondrite, while U and Th in whitlockites of shocked L and LL chondrites are not enriched more than 10 times of the bulk concentrations. Both low Th concentrations and low Th/U ratios in shocked L and LL whitlockites might be a result of rapid crystallization after the shock melting, hence the equilibrium trace element distribution was not achieved. Because of the low Th and U concentrations, meaningful U-Th-Pb isotopic data were not obtained for Y790480 (L) and Y790964 (LL).

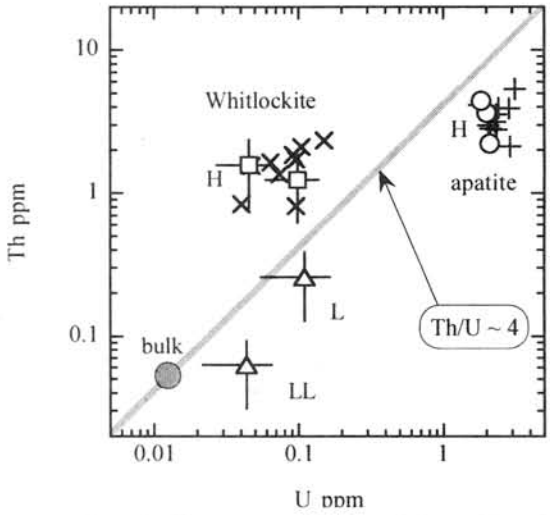

Fig. 2. Concentrations of U and Th in phosphates in shocked chondrites. Crossed symbols are those from the Guarena unshoecked H6 chondrite.

The apatites and whitlockites from Y790746 (H) showed the old 4.5 Ga Pb-Pb age (Fig. 3a, 3b). However, the Tera and Wasserburg U-Pb Concordia diagram of apatites in Fig. 3c indicates a recent radiogenic Pb loss, except for an apatite in the unmelted clast. The upper limit of the lower intercept age is 0.8 Ga. The whitlockite data in Pb-Pb isochron diagram (Fig. 3a) do not show radiogenic Pb isotopic compositions and rather similar to the present bulk chondrite composition, indicating that the Pb isotopes in whitlockites were nearly completely redistributed at the time of shock melting. Because of high Th concentrations in whitlockites, we examined the ^{232}Th-^{208}Pb isotopic system by using the inverse isochron diagram. Assuming the initial $^{208}Pb/^{204}Pb$ ratios between

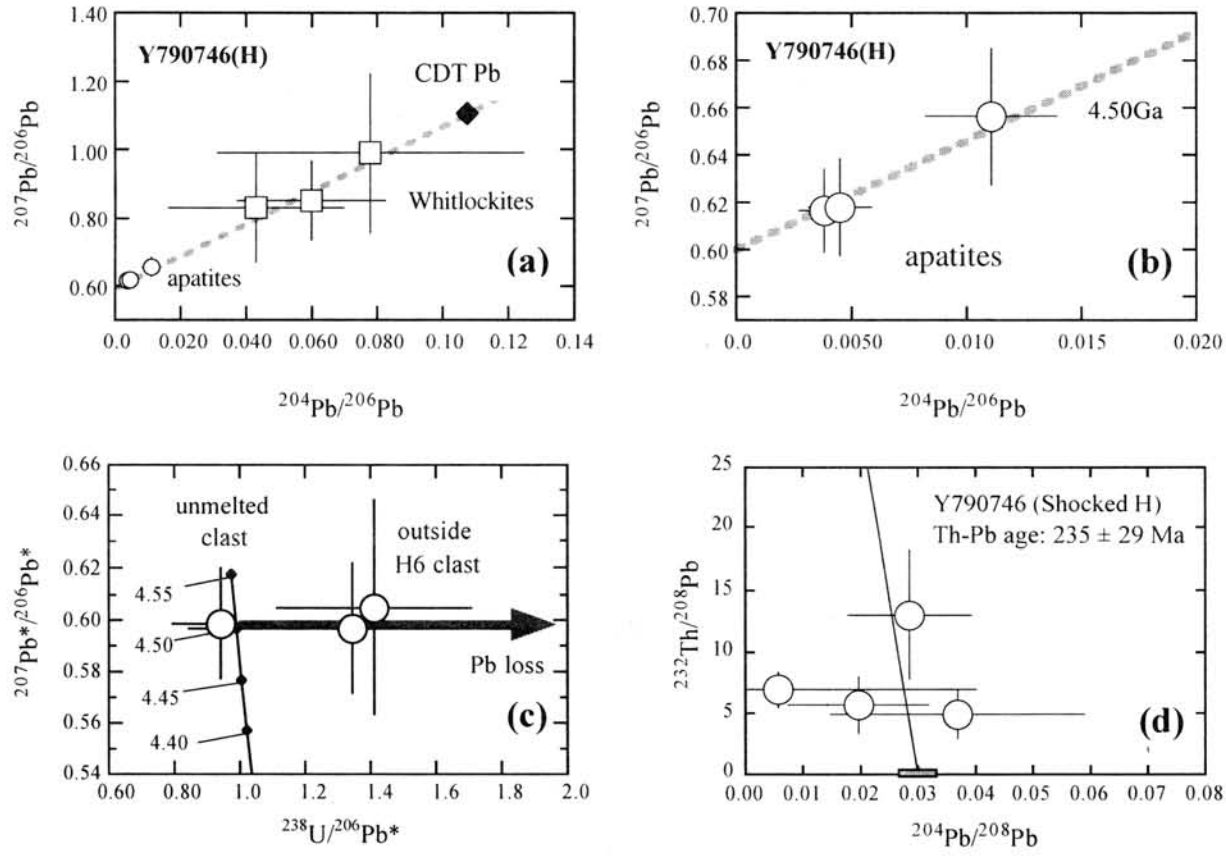

Fig. 3 The U-Th-Pb isotopic systems of phosphates in Y790746 shocked H chondite.

primordial CDT Pb compositions and modern terrestrial compositions, the Th-Pb age of ~0.24 Ga is obtained (Fig. 3d).

The present result indicated that the behaviors of Pb isotopes in two phosphates are different for shock metamorphism; radiogenic Pb in whitlockites are more easily redistributed than apatites. It is not clear if the difference is caused by the crystallization processes of the phosphate minerals, or due to the different self-diffusion rates of Pb in these minerals.

Bogard et al. (1995) noted that there may be multiple impact events on chondrite parent bodies at at 0.3, 0.6, and 1.2 Ga. The present whitlockite Th-Pb age of < 0.3 Ga from Y790746 (H) may correspond to one of the latest major shock event on the H chondrite parent body.

References

D. D. Bogard (1995) Meteoritics **30**, 244-268.
G. Crozaz, P. Pellas, M. Bourot-Denise, S. M. de Chazal, C. Fieni, L. L. Lundberg and E. Zinner (1989) Earth Planet. Sci. Lett. **93**, 157-169.
J. A. Grier, T. D. Swindle and D. A. Kring (1997) Lunar. Planet. Sci. Conf. **28**, 467.
C. Göpel, G. Manhes and C. J. Allegre (1994) Earth Planet. Sci. Lett. 1**21,** 153-171.
M. Kimura, A. E. Goresy, A. Suzuki and E. Ohtani (1999) Symp. 24th Antarct. Meteorite, NIPR 2**4,** 67-68.
N. T. Kita, S. Togashi and Y. Morishita (1997) Meteorit. Planet. Sci. 3**2,** A72-A72.
O. Okano, N. Nakamura and K. Nagao (1990) Geochim. Cosmochim. Acta 5**4,** 3509-3523.
Y. Sano, T. Oyama, K. Terada and H. Hidaka (1999) Chem. Geol. **153,** 249-258.

Effect of cooling rate and oxygen fugacity on the crystallization of the Queen Alexandra Range 94201 martian melt composition

E. Koizumi[1], T. Mikouchi[1], G. McKay[2], L. Le[3], C. Schwandt[3], A. Monkawa[1], and M. Miyamoto[1]
[1]Department of Earth and Planetary Science, University of Tokyo, Hongo, Bunkyo-ku, Tokyo 113-0033, Japan.
[2]Mail Code ST, NASA Johnson Space Center, Houston, TX 77058, USA
[3]Lockheed Martin, 2400 Nasa Road 1, Houston, TX 77058, USA

Introduction: Although many basaltic shergottites have been recently found in north African deserts, QUE94201 basaltic shergottite (QUE) is still important because of its particular mineralogical and petrological features. This meteorite is thought to represent its parent melt composition [1-3] and to crystallize under most reduced condition in this group [1,4]. We performed experimental study by using the synthetic glass that has the same composition as the bulk of QUE. After homogenization for 48 hours at 1300°C, isothermal and cooling experiments were done under various conditions (e.g. temperature, cooling rates, and redox states). Our goals are (1) to verify that QUE really represents its parent melt composition, (2) to estimate a cooling rate of this meteorite, (3) to clarify the crystallization sequences of present minerals, and (4) to verify that this meteorite really crystallized under reduced condition.

Isothermal experiments under IW+1: Fig. 1 shows the pyroxene composition that crystallized at various temperatures. Pyroxene composition shows good agreements with the zoning pattern of pyroxene in natural QUE. Especially, the core compositions of synthetic pyroxenes are close to those of QUE. Furthermore, minor elements (Al and Ti) are similar to QUE, but quite different from Shergotty and Zagami. These results indicate that the bulk composition of QUE is nearly identical to its parent magma composition. Further discussion is seen in the abstract by McKay et al. [5] somewhere in the same volume.

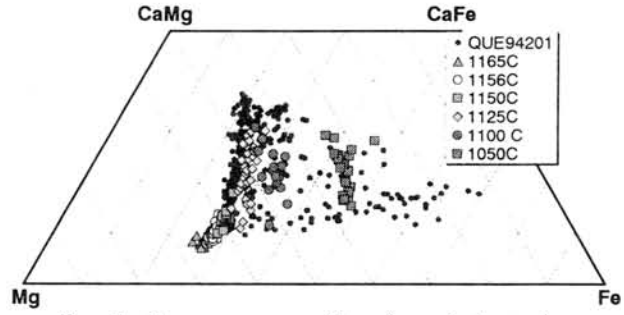

Fig. 1. Pyroxene composition from isothermal experiments under IW+1.

Cooling experiments under IW+1: Cooling experiments were done at cooling rates of 20, 10, 5, 1, 0.7, and 0.5°C/hr from just above the liquidus temperature (1175°C) to 900°C. Fig.2 is the BSE image of pyroxene from the 0.5°C/hr cooling experiment. As this image shows, the simple single-cooling process could reproduce the same zoning pattern that can be seen in natural QUE pyroxene, that is Mg-rich pigeonite core, mantled augite, and Fe-rich pigeonite rim. Fig. 3 shows pyroxene quadrilaterals of pyroxenes from 5 °C /hr and 0.5 °C/hr cooling experiments quenched at 900 °C, along with natural QUE pyroxene composition. Although both experiments have similar zoning sequence to that in natural QUE, the synthetic pyroxene from the 0.5 °C/hr cooling have the better matches with natural QUE in the absence of Ca-Fe-rich pyroxene. Also, Al and Ti contents of pyroxenes become

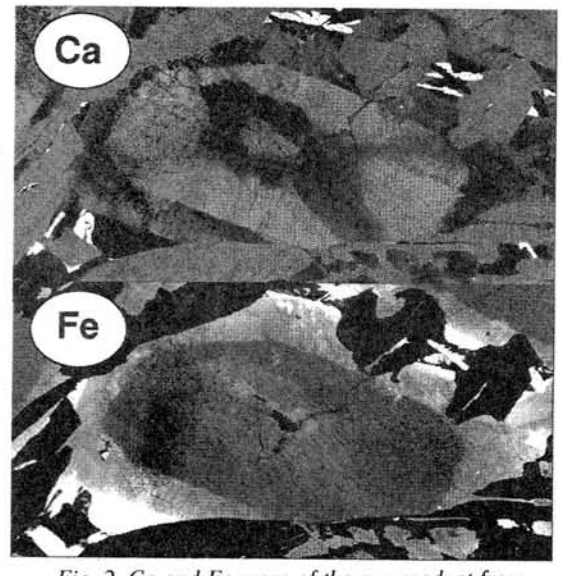

Fig. 2. Ca and Fe maps of the run product from 0.5°C/hr cooling experiment under IW+1.

smaller in slower cooling rate experiments, and both contents in the QUE pyroxene is slightly lower than our slowest cooling rate, 0.5°C/hr. By these reasons, QUE crystallized at the cooling rate between 0.5°C/day [2] and 0.5°C/hr. We also performed 0.5°C/hr and 1°C/hr cooling experiments were quenched at various temperatures. Fig. 4 shows the major elemental composition from 0.5°C/hr cooling runs. It is noted that plagioclase started to crystallize between 1090°C and 1085°C. Run products quenched above 1090°C, which are experiments without plagioclase, have only Mg-rich pigeonite and augite. In contrast, experiments with plagioclase have Fe-rich pyroxenes. Fig 5 is the Al/Ti ratio of these experiments. Experiments with plagioclase have some plots in the area between the lines of 4/1 and 2/1 although all plots derived from experiments without plagioclase stay above the 4/1 line. These results show that the onset of plagioclase crystallization has the relation to the compositional change from Mg-rich to Fe-rich in pyroxenes, and to the abrupt change of Al/Ti ratio. Fig. 6 clearly shows these relations. The Mg/Fe and Al/Ti ratios of pyroxene adjacent to the plagioclase are less or equal to those of the pyroxene core.

Effect of oxygen fugacity: To compare the effects of oxygen fugacity, some isothermal experiments were done under various oxygen fugacities at 1150 °C and 1160 °C. Phase assemblage from these experiments (Table 1) show that olivine crystallized in all runs at QFM-2.0 and above at 1150 °C. Also, under QFM-2.0, pyroxene coexists with olivine, and under IW+1, only pyroxene crystallized at 1150 °C. Therefore QUE seems to have crystallized under IW+1 or more reduced condition because QUE has no olivine except fayalite as late-stage phase and this result is consistent with [1] and [4]. Cooling run was also done under QFM. This run product contains olivine, pyroxene, plagioclase, and opaque minerals. Olivine zoned from Fa_{43} to Fa_{71} and pyroxene is also zoned. Pyroxene compositions from this experiment are quite different from those of QUE and synthetic pyroxene that crystallized under reduced condition (Fig. 8). They are closer

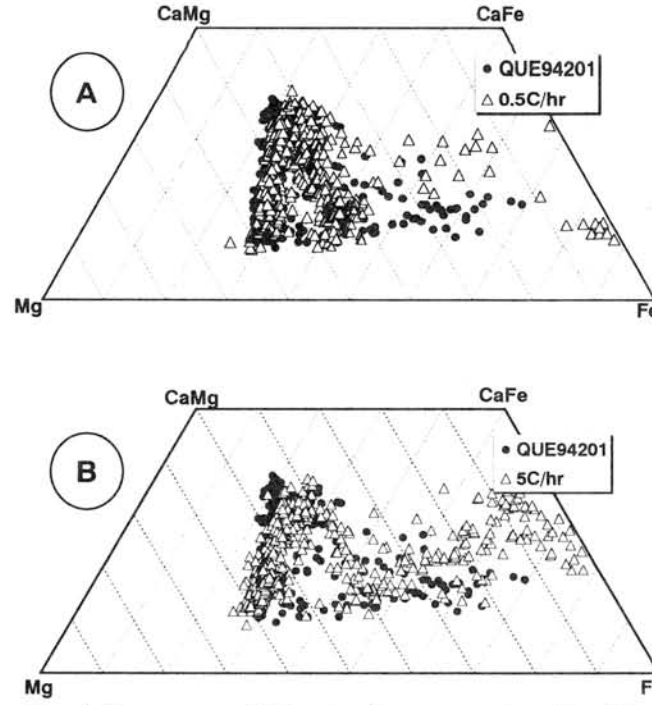

Fig. 3, Pyroxene quadrilaterals of pyroxenes from (A) 0.5 °C/hr and (B) 5 °C/hr cooling experiments quenched at 900 °C with those from QUE94201.

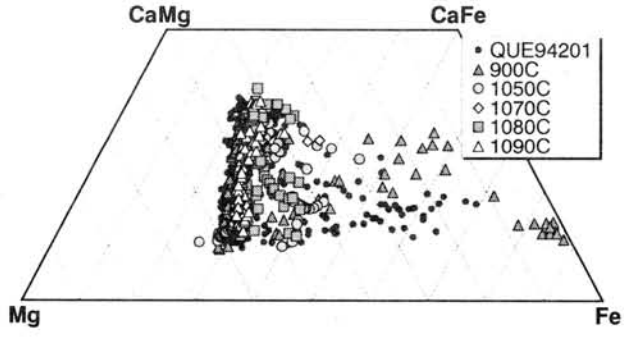

Fig. 4. Pyroxene quadrilateral of pyroxene from 0.5°C/hr cooling experiments quenched at various temperatures.

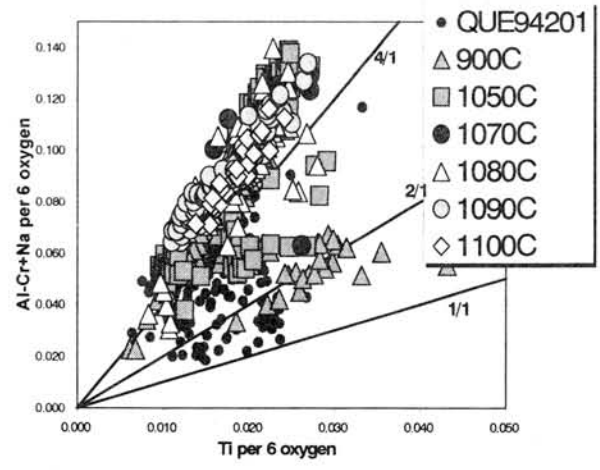

Fig. 5 Al/Ti ratio of pyroxene from 0.5°C/hr cooling experiments quenched at various temperatures.

to those of nakhlites, although the contents of minor elements are different (e.g. Al content of synthetic pyroxene from this cooling experiment is higher than those of nakhlites pyroxene.)

Conclusion: According to these series of crystallization experiments, we have obtained the following conclusions. (1) The bulk composition of QUE is the same or very close to the composition of its parent melt. (2) Simple single-cooling history could reproduce the zoning pattern that is seen in natural QUE. (3) Slower cooling than 0.5°C/hr would produce more similar analogue of QUE in texture and chemical composition. Furthermore, by the contents of minor element of synthetic pyroxene from cooling experiments, QUE is thought to have cooled slower than 0.5°C/hr. (4) Plagioclase began to crystallize after the end of Mg-rich pyroxene crystallization, and at the same time of Fe-rich pigeonite rim crystallization. (5) The abrupt change of Al/Ti ratio of pyroxene can serve as a good marker of the onset of plagioclase crystallization. (6) QUE crystallized under the IW+1 or more reduced condition because olivine crystallized from the bulk composition of QUE under oxidized condition although natural QUE does not contain olivine. (7) Pyroxene from the cooling experiment under QFM is augite that is different from those of QUE, and is similar to nakhlites pyroxene in major element composition.

References: [1] McSween H. Y. et al. (1996) *GCA, 60*,4563-4570. [2] Mikouchi T. et al. (1998) *Meteorit. Planet. Sci., 33*, 181-189. [3] Wadhwa M. et al. (1998) *Meteorit. Planet. Sci., 33*, 321-328. [4] Wadhwa M. (2001) *Science, 291*, 1527-1530. [5] McKay et al. (2002) Antarctic Meteorites, *XXVII*, (in this volume).

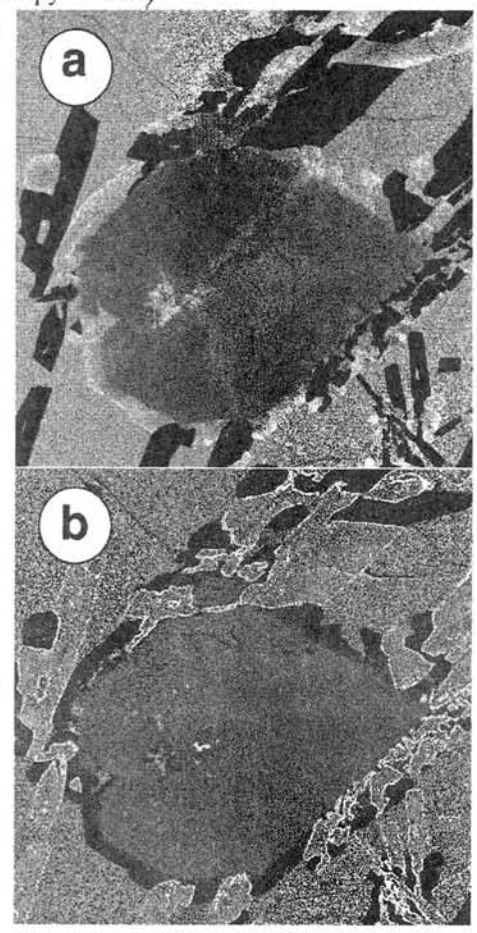

Fig. 6. (a) Fe/Mg and (b) Al/Ti maps of pyroxene grain from 1°C/hr cooling experiment under IW+1 quenched at 1050 °C.

Table 1. Phase assemblages under various fO_2 at 1050°C and 1060 °C.

log fO_2	*1150°C*	*1160°C*
QFM	*Glass, Olivine, Spinel*	*Glass*
QFM-0.5	*Glass, Olivine, Spinel*	*Glass*
QFM-1.0	*Glass, Olivine, Spinel*	*Glass*
QFM-1.5	*Glass, Olivine, Spinel*	*Glass*
QFM-2.0	*Glass, Olivine Pyroxene, Spinel*	*Glass, Pyroxene*
IW+1.0 (QFM-2.5)	*Glass, Pyroxene*	*Glass, Pyroxene*

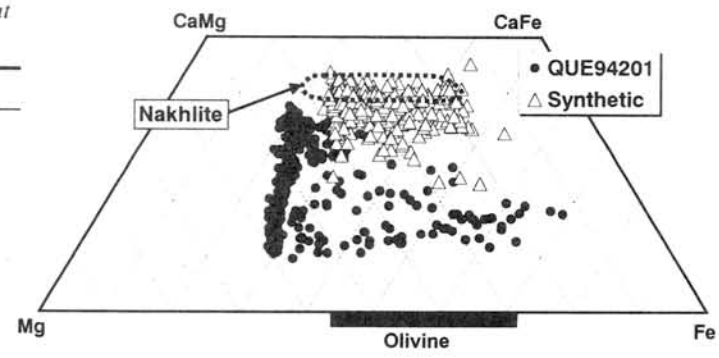

Fig. 7. Pyroxene quadrilateral of pyroxene from 1°C/hr cooling experiments under QFM quenched at 950 °C.

THE YAMATO NAKHLITE CONSORTIUM. Hideyasu Kojima[1], Noboru Nakamura[2], Naoya Imae[1] and Keiji Misawa[1], [1]Antarctic Meteorite Research Center, National Institute of Polar Research, Tokyo 173-8515 (misawa@nipr.ac.jp), [2]Department of Earth & Planetary Sciences, Kobe University, Kobe 657-8501.

Introduction The Wintering Party of the 41st Japanese Antarctic Research Expedition conducted a meteorite search in the bare ice field around the Yamato Mountain area, Antarctica. Among 3550 meteorite samples found, Yamato 000593 (hereafter Y000593) and Y000749 are identified as nakhlites [3,4]. Y000593 is 13.7 kg in weight and the largest achondritic sample recovered in Antarctica. Recently a small 22-gram meteorite Y000802 was identified by one of the authors (H. K.) as the third Yamato nakhlite. About half of the Y000802 surface is covered with fusion crust. These three meteorites were collected in a small area [1], within a few km^2, in the northwest part of the JARE IV Nunataks, suggesting they are paired. Up to the present a total of 7 nakhlites (Nakhla, Lafayette, Governador Valadares, NWA817 [5], and three Yamato) have been identified. The ejection ages of nakhlites, including Y000593 and Y000749, and the dunite Chassigny are ~10 Myr and are the same within experimental errors [4-7], suggesting that the all nakhlites and Chassigny were ejected from Mars in a single impact cratering event [8].

After the announcement of these new nakhlites from Antarctica [3,4], more than twenty sample requests for investigation were received. At a meeting held on 19 March 2002 the Committee of Antarctic Meteorite Research recognized the need for a coordinated consortium study of Yamato nakhlites and approved H. K. and N. N. to lead this consortium.

Curatorial processing of Yamato nakhlites Two 2 gram-sized fragment samples, Y000593,64 (2.180 gram) and Y000749,47 (2.014 gram), were used for wet chemical analysis (H. Haramura, NIPR). Even before the consortium commenced, Y000749,40, a mass of 205 mg, was allocated to R. Okazaki (Univ. Tokyo) for noble gas study that confirmed Y000749 is a nakhlite. In addition to this sample, K. Nagao (Univ. Tokyo) received a 506 mg sample (Y000593,65) for rare gas geochemistry. After the identification of these nakhlites, two 90 mg-sized samples (Y000593,70 and Y000749,70) were allocated to R. Clayton (Univ. Chicago) for measurements of oxygen isotopes.

Initial sample processing for the consortium took place in the Antarctic Meteorite Research Center at NIPR, using stainless steel tools. Most samples were sent to investigators in April 2002. After initial processing, a homogenized powder-sample weighing about 15 gram was prepared by N. I. and K. M. (NIPR) from six of the 2- to 3-gram-sized chips of Y000593,40-45. Using 200 mg-sized aliquots (Y000593,40,1, 41,1, 42,1, 43,1, 44,1, 45,1), M. Ebihara (Tokyo Metropolitan Univ.) is now investigating heterogeneities of the powdered samples by INAA. For bulk analysis we will distribute this sample upon request.

A mass of 4.9 gram (Y000593,54) was allocated to M. Grady's group for a consortium of UK scientists. The samples will be used for mineralogy and petrology (M. Grady, NHM, London), for noble gas chemistry and ^{129}I-^{129}Xe, ^{39}K-^{40}Ar, and ^{39}Ar-^{40}Ar dating (G. Turner, Univ. Manchester), and for light element geochemistry and oxygen isotope compositions (C. Pillinger, Open Univ.). Two large fragments Y000593,66 (1.211 gram) and Y000749,46 (3.663 gram) were allocated to M. Ebihara for nondestructive prompt gamma-ray analysis (PGA). An offcut (Y000593,00-01) was allocated to A. El Goresy (MPI, Mainz) to make polished thin sections (PTS) to estimate the temperature-fO_2 conditions of nakhlites using Fe-Ti partitioning between titanomagnetite and ilmenite. T. Mikouchi (Univ. Tokyo) received a 439-mg sample (Y000593,88) for TEM study of augite and symplectite in olivine. T. Hiroi (Brown Univ.) and M. Miyamoto (Univ. Tokyo) received 62-mg (Y000593,90) and 651-mg (Y000593,86) samples, respectively, for reflectance spectroscopy. N. Imae (NIPR) received Y000593,57 and ,58 (3.171 gram and 0.796 gram, respectively) and Y000749,49 (1.190 gram) to investigate absorbance

spectra of OH using FTIR spectroscopy. A 4.256-gram fragment (Y000592,55) was allocated to N. Nakamura (Kobe Univ.) for the ^{87}Rb-^{86}Sr, ^{147}Sm-^{143}Nd (including ^{142}Nd) and Pb isotope systematics, chlorine isotopic compositions, and lithophile trace elements by TIMS. G. Dreibus (MPI, Mainz) received a 1.371-gram sample (Y000593,81) for the ^{87}Rb-^{86}Sr, ^{147}Sm-^{143}Nd (including ^{142}Nd) and Pb isotope systematics along with for the determination of trace element abundances with INAA. The NASA-JSC group led by L. Nyquist received a 2.265 gram fragment. With JSC personnel D. Bogard and C.-Y. Shi (Lockheed-Martin) he will determine crystallization age by ^{87}Rb-^{86}Sr, ^{147}Sm-^{143}Nd and ^{39}Ar-^{40}Ar, trapped noble gases, mantle differentiated age by ^{146}Sm-^{142}Nd and ^{92}Nb-^{92}Zr systems, neutron capture age by ^{149}Sm-^{150}Sm. Two chips (Y000593,87 and Y000749,52) weighing 487 mg and 616 mg, respectively, were allocated to P. Warren (UCLA) for study of bulk compositions especially siderophile element abundances using INAA and RNAA as clues to Martian core/mantle differentiation. K. Marti (UCSD) received Y000593,85 (685 mg) and Y000749,51 (462 mg) for identification of fission, spallation, and indigenous components of nitrogen, argon, and xenon in the source region of nakhlites. An interior chip, Y000593,84 (796 mg), and six samples of near surface material (Y000593,90-95) of a total weight of 911 mg were allocated to S. Murty (Phys. Res. Lab., Ahmedabad) to investigate cosmic ray exposure ages (CRE) and trapped noble gas and nitrogen components. In order to study in detail the solar cosmic ray effects and pre-atmospheric sizes of Yamato nakhlites using ^{41}Ca, ^{36}Cl, ^{26}Al, ^{10}Be, and ^{53}Mn, K. Nishiizumi (Space Sci. Lab., UCB) was allocated a 1.172 gram-sized interior sample (Y000593,59) and a 1.060 gram-sized exterior sample (Y000593,60) and a 996 mg-sized Y000749,50 chip. He split the allocated samples and sent aliquots of chips to A. Jull (NSF Arizona AMS Lab. Arizona Univ.) for ^{14}C measurement. H. Hidaka (Hiroshima Univ.) will be allocated a 227 mg-sized sample (Y000593,69) to study neutron capture effects on Sm and Gd isotopes by TIMS. G. Herzog (Rutgers Univ.) will receive interior and fusion crust samples of Y000593 and Y000749 to study CRE by measuring nuclides ^{36}Cl, ^{26}Al, ^{10}Be, and ^{53}Mn using AMS. In order to study magnetic properties of nakhlites, M. Funaki (NIPR) received Y000593,71 (871 mg) and Y000593,72 (716 mg).

Apart from the earlier investigation for initial classification, PTS were produced for the Yamato nakhlite consortium, from four separate parent chips (Y000593,62, Y000593,63, Y000593,67, Y000593,68) and from one separate parent chip (Y000749,5) (*see* Table 1). Indeed, we will produce PTS using the samples allocated for PGA (Y000593,66 and Y000749,46). The PTS has not yet been prepared for Y000802. Thus far, PTS have been loaned to C. Goodrich (Univ. Hawaii), Y. Ikeda (Ibaraki Univ.), N. Imae (NIPR), T. McCoy (USNM), T. Mikouchi (Univ. Tokyo), N. Nakamura (Kobe Univ.), K. Terada (Hiroshima Univ.), M. Wadhwa (FMNH), and P. Warren (UCLA) for analysis of mineralogy and petrology. Four PTS, Y000593,62-1, Y000749,5-4 (both loaned to K. Terada), Y000593,63-5, and Y000749,5-5 (both loaned to M. Wadhwa) will be used for ion microprobe analysis.

REFERENCES: [1] Imae, N. *et al.* (2001) *Antarct. Meteorites* **XXVI**, 44-46. [2] Imae, N. & Iwata, N. (2001) *MAPS* **36**, A86. [3] *Meteorite Newsletter* **10**, No. 2. (2001) NIPR. [4] Imae, N. *et al.* (2002) *LPSC* **XXXIIII** #1438 (CD-ROM). [5] Marty, B. *et al.* (2001) *MAPS* **36**, A122-A123. [6] Okazaki, R. *et al.* (2002) this volume. [7] Nyquist, L.E. *et al.* (2001) *Chronology and Evolution of Mars* **96**, 105-164. Kluwer Academic Publishers. [8] Warren, P.H. (1994) *Icarus* **111**, 338-363.

Table 1. Distribution of samples for the Yamato nakhlite consortium, including PTS samples.

Yamato 000593 (13.713 kg) subnumber	weight (gram)	investigator	institution	type of investigation
40	2.447			bulk chemistry (powdered)
41	3.591			bulk chemistry (powdered)
42	2.000			bulk chemistry (powdered)
43	2.591			bulk chemistry (powdered)
44	2.109			bulk chemistry (powdered)
45	2.577			bulk chemistry (powdered)
54	4.922	Grady, M.	NHM, London	UK consortium
55	4.256	Nakamura, N.	Kobe Univ.	chronology & chemistry
56	2.256	Nyquist, L.	NASA-JSC	chronology
57	3.171	Imae, N.	NIPR	FTIR
58	0.796	Imae, N.	NIPR	FTIR
59	1.172	Nishiizumi, K.	Space Sci. Lab., UCB	CRE
60	1.060	Nishiizumi, K.	Space Sci. Lab., UCB	CRE
61	0.607			PTS
62	2.248			PTS
63	1.884			PTS
64	2.180			PTS
65	0.506	Nagao, K.	Univ. Tokyo	rare gas
66	1.212	M. Ebihara	Tokyo Metropolitan Univ.	PGA
67	1.011			PTS
68	2.230			PTS
69	0.227	Hidaka, H.	Hiroshima Univ.	neutron exposure effects
70	0.093	Clayton, R.	Univ. Chicago	oxygen isotope
71	0.871	Funaki, M.	NIPR	rock magnetism
72	0.716	Funaki, M.	NIPR	rock magnetism
81	1.371	Dreibus, G	MPI, Mainz	chemistry & chronology
84	0.796	Murty, S.	Phys. Res. Lab., Ahmedabad	CRE, noble gas & nitrogen isotope
85	0.685	Marti, K.	UCSD	nitrogen, argon & xenon isotopes
86	0.651	Miyamoto, M.	Univ. Tokyo	reflectance spectroscopy
87	0.487	Warren, P.	UCLA	INAA & RNAA
88	0.493	Mikouchi, T.	Univ. Tokyo	TEM
90	0.062	Hiroi, T.	Brown Univ.	reflectance spectroscopy
91	0.086	Murty, S.	Phys. Res. Lab., Ahmedabad	CRE, noble gas & nitrogen isotope
92	0.156	Murty, S.	Phys. Res. Lab., Ahmedabad	CRE, noble gas & nitrogen isotope
93	0.127	Murty, S.	Phys. Res. Lab., Ahmedabad	CRE, noble gas & nitrogen isotope
94	0.258	Murty, S.	Phys. Res. Lab., Ahmedabad	CRE, noble gas & nitrogen isotope
95	0.222	Murty, S.	Phys. Res. Lab., Ahmedabad	CRE, noble gas & nitrogen isotope
00-01	offcut	El Goresy, A.	MPI, Mainz	temperature & oxygen fugacity

PTS; Y000593,61-1 & ,67-1: Imae, N. (NIPR), Y000593,62-1: Terada, K. (Hiroshima Univ.), Y000593,62-2: Goodrich, C. (Univ. Hawaii), Y000593,62-3 ,62-6 & ,68-1: Mikouchi, T. (Univ. Tokyo), Y000593,62-4: McCoy, T. (USNM), Y000593,63-1: Warren, P. (UCLA), Y000593,63-2: Ikeda, Y. (Ibaraki Univ.), Y000593,63-4 & ,63-6: Nakamura, N. (Kobe Univ.), Y000593,63-5: Wadhwa, M. (FMNH).

Yamato 000749 (1.283 kg) Subnumber	weight (gram)	investigator	institution	type of investigation
1	1.415			PTS
5	5.401			PTS
40	0.205	Okazaki, R.	Univ. Tokyo	rare gas
46	3.663	Ebihara, M.	Tokyo Metropolitan Univ.	PGA
47	2.014			PTS
48	1.048	Dreibus, G.	MPI, Mainz	chemistry & chronology
49	1.190	Imae, N.	NIPR	FTIR
50	0.996	Nishiizumi, K.	Space Sci. Lab., UCB	CRE
51	0.462	Marti, K.	UCSD	nitrogen, argon & xenon isotopes
52	0.616	Warren, P.	UCLA	INAA & RNAA
70	0.090	Clayton, R.	Univ. Chicago	oxygen isotope

PTS; Y000749,1-1: Imae, N. (NIPR), Y000749,1-3: Ikeda, Y. (Ibaraki Univ.), Y000749,5-1: Goodrich, C. (Univ. Hawaii), Y000749,5-2: Warren, P. (UCLA), Y000749,5-3: McCoy, T. (USNM), Y000749,5-4: Terada, K. (Hiroshima Univ.), Y000749,5-5: Wadhwa, M. (FMNH).

CRYSTALLIZATION EXPERIMENTS OF OLIVINE AND ANORTHITE MIXTURES: CLUE TO UNDERSTANDING THE TEXTURAL RELATIONSHIPS AMONG OLIVINE, AL-DIOPSIDE AND ANORTHITE IN AMOEBOID OLIVINE AGGREGATES.

Mutsumi Komatsu[1], Masamichi Miyamoto[1], Alexander N. Krot[2], Klaus Keil[2] and Takashi Mikouchi[1].

[1]Dept. of Earth and Planetary Science, Graduate School of Science, University of Tokyo.

[2]Hawai'i Institute of Geophysics and Planetology, University of Hawai'i at Manoa.

(mutsumi@space.eps.s.u-tokyo.ac.jp).

Introduction

Amoeboid olivine aggregates (AOAs) from the CV chondrites Efremovka, Leoville, Vigarano, and Allende are irregularly-shaped objects, up to 5 mm in size, composed of forsteritic olivine and a refractory, Ca, Al-rich component. The AOAs are depleted in moderately volatile elements (Mn, Cr, Na, K), FeNi-metal and sulfides and contain no low-Ca pyroxene. The refractory component consists of fine-grained Ca,Al-rich inclusions (CAIs) composed of Al-diopside, anorthite (An_{100}), and magnesium-rich spinel or fine-grained intergrowths of these minerals; secondary nepheline and sodalite are generally very minor (Allende is the only exception) [1].

The most characteristic feature of the CAIs in AOAs in CV chondrites is that anorthite (and spinel in some CAIs) core is surrounded by Al-diopside; the latter overgrows olivine (Fig.1). Although Al-diopside in AOAs is considered to be a high-temperature condensate [2], no explanation for their variable compositional range in Al_2O_3 and TiO_2 has been proposed yet. Bulk compositions of AOAs from CV chondrites plot along a line extending from forsterite toward anorthite on a ternary diagram $Al_2O_3 - Mg_2SiO_4 - Ca_2SiO_4$, which is consistent with mineralogy of AOAs [3], implying that olivine and anorthite is important component for the origin of AOAs. In order to examine the formation process of Al-diopside in AOAs, and textural and chemical relationships among anorthite, Al-diopside and olivine, we performed heating and crystallization experiments on mineral mixtures of terrestrial olivine+anorthite and synthetic forsterite+anorthite mixtures.

Experiments

A small chip of synthetic forsterite (Fo_{100}), terrestrial olivine (Fo_{91}) and anorthite (An_{96}) were ground to pass through 37μm and 100μm sieve. A pellet of about 80 mg of mixed olivine with anorthite and forsterite with anorthite was placed in Pt-wire and heated to desired temperatures. The samples were held for 3 and 50 hours in a vertical 1-atm H_2/CO_2 gas-mixing furnace at constant oxygen fugacities of $\log fO_2$ = IW (iron-wüstite) buffer, then air-quenched to below red heat in a few seconds by pulling the sample support rod out of the furnace. Crystallization experiments have been performed with cooling rate ranging from10 to 500°C/h. Oxygen fugacity of IW is adopted because carbonaceous chondrites have the intrinsic oxygen fugacity of $\log fO_2$ = IW [4]. The samples were made into thin sections for microscopy and measurements of the chemical compositions using JEOL JXA-8900L and JEOL JSM-733II microprobes.

Results

Heating experiments of olivine-anorthite mixtures

The results of heating experiments on olivine-anorthite mixtures for 3 hours are shown in Fig. 3. Anorthite starts melting at the temperature of 1263°C (Figs.2b, c). At 1288°C, olivine and anorthite show evidence for partial melting to produce a high-Ca pyroxene (Fig.2d). The high-Ca pyroxene like phase appears only between olivine and anorthite; its grain size is 2-10 μm in the <37 μm sample and 5-20 μm in <100 μm sample. At 1301°C, anorthite is completely melted (Fig.2e). At 1438°C, most olivine grains melted extensively, only the relict olivine and the glassy phase are observed (Fig.2f).

High-Ca pyroxene like phase in the sample heated to 1288°C is texturally similar to that in AOAs: it occurs as interstitial phase between olivine and anorthite (Fig. 1). In contrast to the sharp grain boundaries between anorthite and high-Ca pyroxene like phase, the grain boundaries between olivine and high-Ca pyroxene like phase are unclear. Sample heated for 50 hours does not show any difference from the sample heated for 3 hours. It appears that the reaction of olivine and anorthite is completed in less than 3 hours.

Crystallization experiments of olivine and anorthite mixtures

Fig.4 shows the results of the crystallization experiments on forsterite-anorthite (1:1) mixtures heated at 1313°C under the

IW condition. The experiments were performed in the temperature of incomplete melting because our assumption for heating AOAs is not extensive. High-Ca pyroxene like phase (cpx-like phase; brightest color) is observed. They are generally fine-grained, and appear around the anorthite grain boundaries. There is no obvious difference in the cpx-like phase texture in the cooling range of 50°C-500°C/hour.

Chemical composition

Al-diopside in AOAs from the reduced CV chondrites shows a wide range in compositions (40-50 wt% SiO_2, 1-20 wt% Al_2O_3, 0-7 wt% TiO_2, 9-25 wt% MgO, 17-25 wt% CaO); anorthite is compositionally pure; primary olivine is magnesium-rich (ferrous olivine rims observed in AOAs from Efremovka and Allende resulted from late-stage thermal metamorphism). Olivine and anorthite in the experimental charges show no compositional changes after heating experiments. High-Ca pyroxene like phases in heated samples also show a wide range in compositions, 40-45 wt% SiO_2, 10-20 wt% Al_2O_3, 11-30 wt% MgO, 5-16 wt% CaO for the heated and quenched olivine+anorthite sample at 1288°C, 43-48 wt% SiO_2, 15-25 wt% Al_2O_3, 13-14 wt% MgO, 15-17 wt% CaO for the heated and quenched forsterite+anorthite sample at 1288°C, and 43-52 wt% SiO_2, 7-25 wt% Al_2O_3, 10-22 wt% MgO, 16-22 wt% CaO for the heated forsterite+anorthite sample at 1313°C.

Discussion

If the AOAs originate as condensate assemblages, as proposed by [5], their textures pose a problem. The observation that anorthite is rimmed by Al-diopside, which in turn rimmed by olivine (which is originally supposed to be forsterite) grains. This is in direct conflict with equilibrium condensation calculations that consistently predict [6] that forsterite should condense prior to anorthite. If anorthite is not condensation product, but the secondary mineral that replaced primary melilite as suggested by [7], it would also runs counter to the observation that spinel is rimmed by anorthite. Because it implies that spinel formed before melilite in AOA, which is inconsistent with equilibrium condensation calculations that melilite should condense prior to spinel from a gas of solar composition. The core-rim texture of the spinel + anorthite is also observed in the fine-grained spinel-rich inclusions (FGIs). MacPherson et al. [8] suggested that spinel in FGIs was replaced largely by anorthite during open system reactions. The reaction that replacing melilite by Al-rich diopsidic pyroxene and anorthite are also supposed to have took place at the same time. If the FGIs have experienced such late-stage partial melting and evaporation [8], the question occurs how this environment affected AOAs. Because it is suggested that AOAs and CAIs are formed in similar environments [9], AOAs might have experienced the same reaction as FGIs.

Based on the heating experiments of olivine+anorthite and olivine+melilite mixtures and the mineralogical study of AOAs in the reduced CV3 chondrites, it is shown the possibility for the formation of Al-diopside from the olivine+anorthite. The reaction between anorthite and forsterite is consistent with their texture; irregular shape of anorthite and spinel core is not explained by the simple condensation sequence that would have made more concentric texture. We could not reproduce the identical texture with olivine-Al-diopside-anorthite of AOAs in the heating experiments, but the high-Ca pyroxene like phase in the heated samples show the similar texture to that of AOAs; high-Ca pyroxene-phase exists around the anorthite grain boundaries. Compositional analysis showed that high-Ca pyroxene like phase in heated samples is lower in CaO and SiO_2 than Al-diopside in AOAs. Because these experiments were performed in the Ti-free system, the composition would be slightly different in the Ti-bearing system.

Although more studies will be needed to define a formation process of Al-diopside in AOAs, our examination suggests that high-Ca pyroxenes in AOAs could have resulted from small degree of melting of olivine and anorthite. Small degree of melting of AOAs is supported by the presence of rounded FeNi-metal nodules in some of them and their relatively compact textures.

References: [1] Komatsu M. et al. (2001) *Meteoritics & Planet. Sci.* 36, 629-641. [2] Grossman L. and Steele I. M. (1976) *GCA, 40,* 149-155. [3] Komatsu M. et al. (2002) *LPS, XXXIII,* CD-ROM#1258 [4] Brett R. and Sato M. (1984) *GCA, 48,* 111-120. [5] Grossman L. et al. (1979) *GCA, 43,* 817-829. [6] Yoneda S. and Grossman L. (1995) *GCA, 59,* 3413-3444. [7] Hashimoto A. and Grossman L. (1987) *GCA, 51,* 1685-1704. [8] MacPherson G. J. et al. (2002) *LPS, XXXIII,* CD-ROM#1526. [9] Fagan T. et al. (2002) *LPS, XXXIII,* CD-ROM#1507.

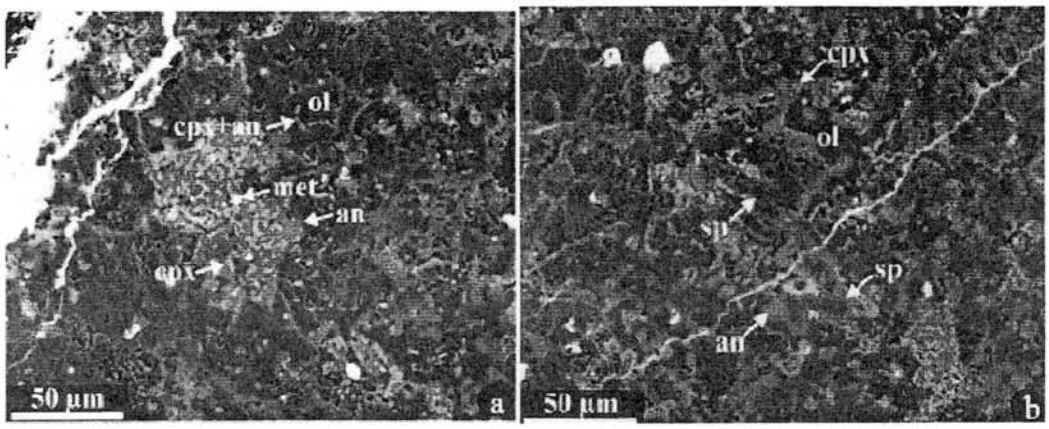

Fig. 1. BSE image of the AOA in Leoville. a,b-Forsteritic olivine is overgrown by Al-diopside. Anorthite fills interstitial regions between these minerals; tiny spinel grains are present only in anorthite.
ol; olivine, cpx;Al-diopside, an; anorthite, sp; Fe-rich spinel.

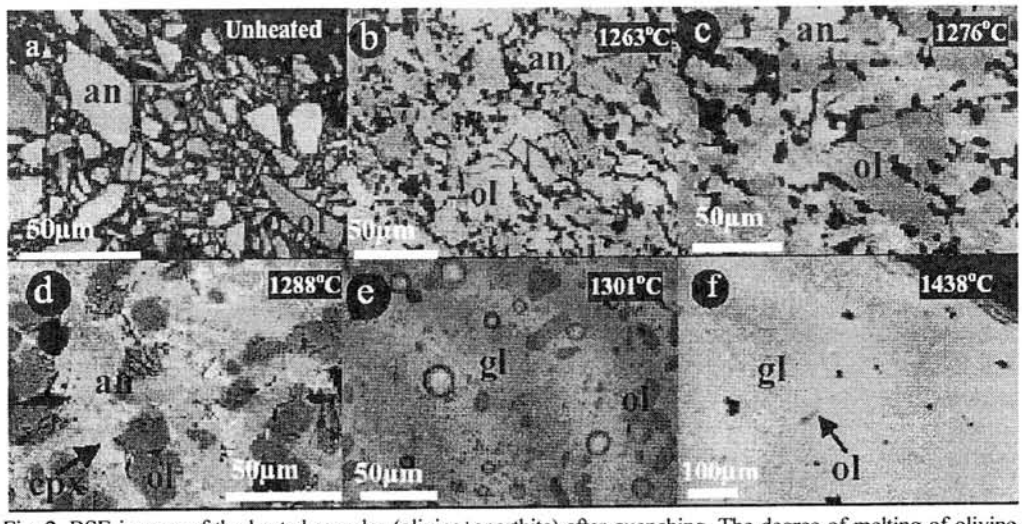

Fig. 2. BSE images of the heated samples (olivine+anorthite) after quenching. The degree of melting of olivine and anorthite increases with increasing heating temperature. ol; olivine, an; anorthite, cpx; high-Ca pyroxene like glass phase.

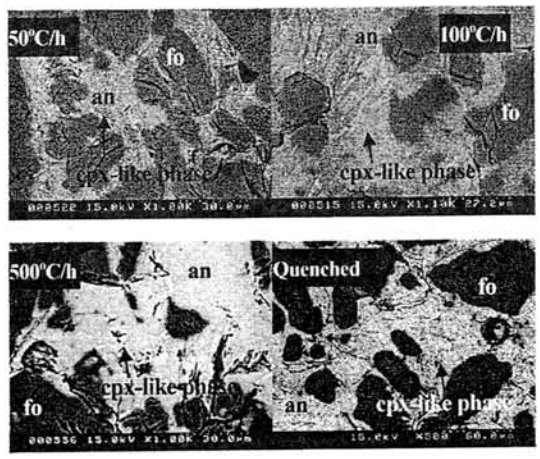

Fig. 3. BSE images of the heated samples (forsterite+anorthite) at 1313°C for 3hours, then cooled with various cooling rates.

LABORATORY SIMULATION OF SPACE WEATHERING: CHANGES OF OPTICAL PROPERTIES AND TEM & ESR CONFIRMATION OF NANOPHASE METALLIC IRON IN LASER-IRRADIATED MATERIALS.

Erika Kurahashi[1], Chihiro Yamanaka[2], Keiko Nakamura[3] and Sho Sasaki[1]

[1]Department of Earth and Planetary Science, Graduate School of Science, University of Tokyo, 7-3-1 Hongo, Bunkyo-ku, Tokyo 113-0033. [2]Department of Earth and Space Science, Graduate School of Science, Osaka University, Toyonaka, Osaka 560-0043. [3]Department of Earth and Planetary Sciences, Graduate School of Science and Technology, Kobe University, Kobe 657-8501.

INTRODUCTION

S-type asteroids, majority in asteroids, are believed to be parent bodies of ordinary chondrites, which are a large majority in meteorites [1]. Both S-type asteroids and ordinary chondrites contain the same mineral assemblage, mainly olivine and pyroxene. However, the steep reddened spectral slopes of S-type asteroids are different from those of ordinary chondrites. Asteroids exhibit more overall depletion (darkening) and reddening of spectra, and more weakening of absorption bands relative to meteorites. This spectral mismatch is explained by space weathering process, where high-velocity dust particle impacts should change the optical properties of the uppermost regolith surface of asteroids.

A recent simulation of space weathering showed that nanosecond pulse laser irradiation, which is comparable with a real dust impact, altered olivine and pyroxene spectra to be darker and redder, and their absorption bands became weaker relative to their untreated samples [2]. In the rims of olivine grains, nanophase metallic iron particles, which were theoretically predicted [3], were observed by a transmission electron microscopy [4]. Recently, nanophase metallic iron particles are considered as the most essential cause of space weathering. Although S-type asteroids and ordinary chondrites should contain much olivine and pyroxene, the space weathering simulation on mixtures of olivine and pyroxene has not performed yet, except for the theoretical modeling [5].

In this study, we describe the spectral changes of olivine and pyroxene mixtures using nanosecond pulse laser irradiation and discuss the optical effects of space weathering with theoretical fitting method. In addition, we also describe the effects of nanophase metallic iron particles of laser-irradiated materials by transmission electron microscopy (TEM) and electron spin resonance (ESR).

EXPERIMENTAL METHOD

In order to simulate space weathering, we use a solid-state Nd-YAG pulse laser beam with pulse duration of 6-8 nanoseconds, which is comparable with real dust impacts [2]. We irradiate pellet samples of olivine and pyroxene mixtures, which are formed of pulverized particles smaller than 75 micrometers in a vacuum chamber. After laser-irradiation, bi-directional reflectance spectra of samples were measured; spectrum range 250-2500nm was recorded at every 5nm [6]. Finally, the irradiated samples were observed by TEM, and

ESR signals of the surface of the laser-irradiated samples were measured by the microwave cavity method where the spins in the surface depth of 100 micron can be detected nondestructively [7].

FITTING BY END-MEMBER SPECTRA FOR OLIVINE AND PYROXENE MIXTURES

In this study, we treated several olivine - pyroxene mixtures; Ol (75wt%) + Px (25wt%), Ol (50wt%) + Px (50wt%), Ol (25wt%) + Px (75wt%). After laser-irradiation, all samples showed the overall reduction and significant reddening of the spectra, and more weakening of absorption bands. To confirm whether the space-weathered spectra can be reproduced theoretically, we fitted the irradiated spectra of the olivine-pyroxene mixtures using the end-member spectra of them by the least-squares method. As a result, we found that the irradiated spectra of mixtures can be reproduced by the end-member spectra (Fig. 1), and the fitting ratios are not consistent with the real mixing ratio. Although the real mixing ratio of olivine and pyroxene is 3:1, 1:1, and 1:3 respectively, the calculated fitting ratio of pyroxene is larger than that of olivine. For example, as for the mixture of Ol (50wt%) + Py (50wt%), the fitting ratio is 30% for olivine and 70% for pyroxene. In addition, the fitting ratios hardly change at any space weathering degree. Fig. 2 shows the relation between the real mixing ratio and the fitting ratio with olivine-pyroxene mixtures. In conclusion, we may estimate real mineral mixing ratio and weathering degree of asteroids with the calculated mixing ratio using end-member spectra.

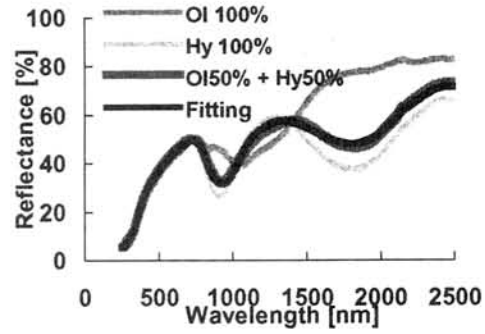

Fig. 1 Results of spectral fitting calculations for olivine (50wt%) + pyroxene (hypersthene) (50wt%) mixtures. All samples were irradiated one time at 30mJ.

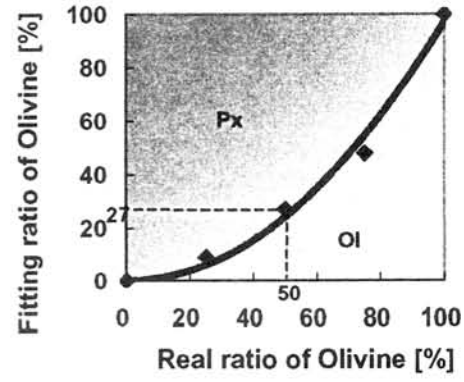

Fig. 2 Relation between the real mixing ratio and the fitting mixing ratio with olivine + pyroxene (hypersthene) mixtures.

ESR CONFIRMATION OF NANOPHASE METALLIC IRON PARTICLES

After laser-irradiations, we also observed the samples by transmission electron microscopy (TEM) to discuss the changes of the physical properties of the space-weathered materials. Nanophase metallic iron particles were found not only in laser-irradiated olivine samples, but also in laser-irradiated pyroxene (enstatite) samples (Fig. 3). This is the new occurrence of nanophase metallic iron in pyroxene.

Moreover, we used an electron spin resonance (ESR) to perform quantitative analysis of nanophase metallic iron particles. Strong ESR signals, which derive from nanophase iron particles, are observed both in irradiated olivine and pyroxene samples (Fig. 4). In addition, ESR intensities increase with the space weathering degree simulated as laser irradiation time.

CONCLUSIONS

In order to simulate space weathering by impact heating of dust particles, we irradiated Ol+Px mixtures using a nanosecond pulse laser. The irradiated spectra of the mixtures can be predicted using the end-member spectra of them. The fitting ratios are not consistent with the real mixing ratios. Nanophase metallic iron particles were found not only in irradiated olivine samples, but also found in irradiated enstatite samples by a TEM. We reported the first description that the quantities of nanophase metallic iron particles in the irradiated samples increase at higher space weathering degree.

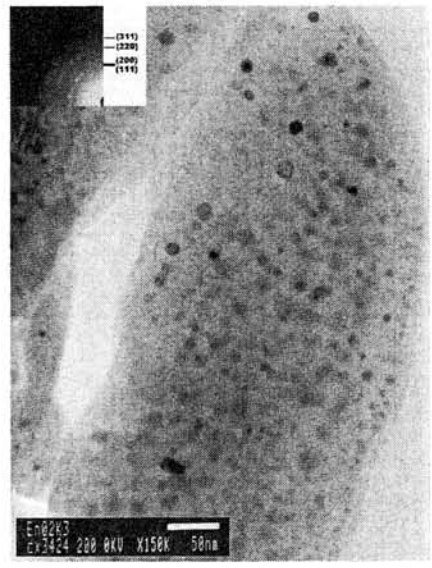

Fig. 3 TEM image of nanophase metallic iron particles of enstatite grains irradiated by ten-times at 30mJ. Numerous iron nanoparticles are included in an amorphous grain.

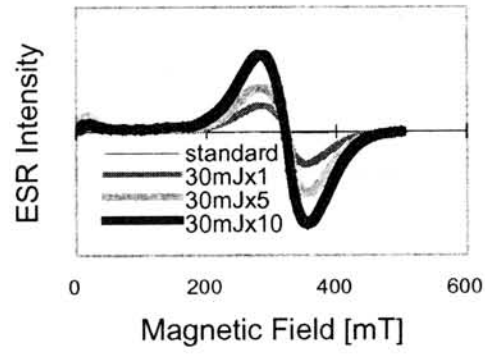

Fig. 4 ESR spectra of olivine samples, which were irradiated by 1, 5, 10 times at 30mJ with non-irradiated.

REFERENCES

[1] Chapman C. R. (1996) *Meteoritics & Planet. Sci.*, 31, 699-725.

[2] Yamada M. et al. (1999) *Earth Planets Space*, 51, 1255-1265.

[3] Hapke B. (2001) *JGR*, 106, 10039-10073.

[4] Sasaki S. et al. (2001) *Nature*, 410, 555-557.

[5] Hiroi T. and Sasaki S. (2001) *Meteoritics & Planet. Sci.*, 36, 1587-1596.

[6] Kurahashi E. and Sasaki S. (2002) *LPSC*, #1479.

[7] Ikeya M. et al. (1994) *Rev. Sci. Instrum.*, 65, 3670-3672.

Noble gas characteristics of lunar meteorite Yamato-981031 paired with basaltic-anorthositic breccia Yamato-793274

S. Lorenzetti and O. Eugster

Physikalisches Institut, University of Bern, Sidlerstrasse 5, 3012 Bern, Switzerland
(eugster@phim.unibe.ch)

Introduction

Meteorite Yamato-981031 (185.8 g) was collected close to the Minami-Yamato Nunataks and was classified as a lunar anorthositic breccia. Y-793274 was recovered with high possibility also in this area [1]. This meteorite is a basaltic-anorthositic breccia and chemically very similar to Y-981031 [c. f. 2]. In this work we studied the noble gas isotopic composition in order to determine the cosmic-ray produced and the implanted solar components of Y-981031. These data are compared with those obtained earlier for Y-793274 [3].

Experimental procedure and results

Two bulk samples of Y-981031 of 5.05 mg and 5.10 mg were heated in vacuum in the extraction system at 90°C for several days to remove adsorbed atmospheric gases. He, Ne, and Ar were extracted by radiofrequency heating in a single step at 1700°C and then analyzed in the mass spectrometer system B. All details concerning the instrument, analytical procedure, background and blank corrections are described by [4]. The results are given in Table 1. The analytical errors correspond to 2σ mean.

Partitioning of the components

The trapped solar (tr) component and the cosmogenic (c) component were derived using the following isotopic ratios: $(^{20}Ne/^{22}Ne)_c = 0.8$, $(^{20}Ne/^{21}Ne)_c = 0.9$, $(^{20}Ne/^{21}Ne)_{tr} = 400$, $(^{36}Ar/^{38}Ar)_c = 0.65$, and $(^{36}Ar/^{38}Ar)_{tr} = 5.32$. The resulting concentrations and isotopic ratios for the cosmogenic and trapped components are given in Table 2.

Cosmic-ray exposure ages and solar gases

The duration of cosmic-ray exposure (CRE) was calculated based on $^{21}Ne_c$, $^{38}Ar_c$, and appropriate production rates. We used the method proposed by Hohenberg et al. [5] for the calculation of the production rates for lunar surface material at an average shielding depth of 40 g/cm^2. We inserted the chemical abundances given by Kojima [1], analyzed by H. Haramura, and obtained a production rate for ^{21}Ne (P_{21}) of 0.115 and a production rate for ^{38}Ar (P_{38}) of 0.110 (units of 10^{-8}cm^{3}STP/g, Ma). The resulting CRE ages are given in Table 2.

A typical feature of lunar surface material is the fact that the ^{21}Ne CRE age (T_{21}) is lower than the ^{38}Ar CRE age (T_{38}) [3]. We obtain a T_{21} of 378 Ma and a T_{38} of about 682 Ma. Obviously a large fraction of cosmogenic ^{21}Ne was lost by diffusion out of the meteoritical material, most probably on the Moon. This $^{21}Ne_c$ loss could be demonstrated to have occurred also for rocks collected at the Apollo missions [c. f. 5]. Therefore, the more reliable CRE age of Y-981031 is that obtained from ^{38}Ar. The CRE age of 682 ± 100 Ma is much longer than the typical Moon-Earth transit time for lunar meteorites of < 10 Ma. (c. f. review of [6]). Thus, the material of Y-981031 must have been exposed to cosmic irradiation as part of the lunar regolith. This conclusion is supported by the relatively high concentration of trapped solar noble gases. The ratio $^{20}Ne/^{36}Ar$ of the trapped noble gas component is 2.43 ± 0.10, a characteristic value for lunar meteorites that yield ratios < 9. Solar gas-rich non-lunar meteorites show $(^{20}Ne/^{36}Ar)_{tr}$ ratios of > 12. This abundance ratio of the solar gases confirms the lunar origin of Y-981031.

Fall-pairing of Y-981031 and Y-793274

Table 2 also gives data for lunar meteorite Y-793274. The concentrations of $^{20}Ne_{tr}$ and the ratio $(^{20}Ne/^{36}Ar)_{tr}$ of Y-981031 and Y-793274 are the same within about 20 %. The CRE ages and $(^{20}Ne/^{22}Ne)_{tr}$ agree within experimental errors. These agreements, together with the observations on mineralogy and chemistry of the two lunar meteorites, lead to the conclusion that the two stones are pieces of the same meteorite fall.

Acknowledgements: We thank the National Institute of Polar Research, Tokyo for the Y-981031 sample. The technical support by H. E. Jenni and A. Chaoui is acknowledged. This work was supported by the Swiss National Science Foundation.

References: [1] Kojima H. (2000) Antarctic Meteorites XXV, 55. [2] Takeda H. et al. (1990) Papers presented to the 15th NIPR Symposium on Antarctic Meteorites, 110. [3] Eugster O. et al. (1992) Proc. NIPR Symp. Antarct. Meteorites **5**, 23. [4] Eugster O. et al. (1993) Geochim. Cosmochim. Acta **57**, 1115. [5] Hohenberg C. et al. (1978) Proc. Lun. Planet. Sci. Conf. **9**, 2311. [6] Warren P. (1994) Icarus **111**, 338.

Table 1. Results of He, Ne, and Ar measurements of lunar meteorite Y-981031.

	^{4}He	^{20}Ne	^{40}Ar	$\frac{^4\text{He}}{^3\text{He}}$	$\frac{^{20}\text{Ne}}{^{22}\text{Ne}}$	$\frac{^{22}\text{Ne}}{^{21}\text{Ne}}$	$\frac{^{36}\text{Ar}}{^{38}\text{Ar}}$	$\frac{^{40}\text{Ar}}{^{36}\text{Ar}}$
	10^{-8} cm^{3}STP/g							
Bulk 1	100'600	30'900	30'500	1941	12.63	20.47	5.17	2.36
(0.00505 g)	± 4'500	± 1'000	± 900	± 60	± 0.15	± 0.20	± 0.05	± 0.03
Bulk 2	146'200	41'100	39'200	2045	12.63	22.08	5.22	2.34
(0.00510 g)	± 5'500	± 2'000	± 1'400	± 20	± 0.13	± 0.20	± 0.05	± 0.05

Table 2. Cosmogenic and trapped noble gases as well as cosmic-ray exposure ages from ^{21}Ne and ^{38}Ar of lunar meteorites Y-981031 and Y-793274.

	Cosmogenic		Trapped			CRE age	
	^{21}Ne	^{38}Ar	^{20}Ne	$\frac{^{20}\text{Ne}}{^{36}\text{Ar}}$	$\frac{^{20}\text{Ne}}{^{22}\text{Ne}}$	T_{21}	T_{38}
	10^{-8} cm^{3}STP/g					Ma	
Y-981031	42.4	81	30'900	2.40	12.86	(369)	736
Bulk 1	± 2.5	± 16	± 1'000	± 0.15	± 0.60		± 140
Y-981031	44.6	69	41'100	2.45	12.81	(388)	627
bulk 2	± 3.0	± 14	± 2'000	± 0.15	± 0.90		± 130
Y-981031	43.5	75	36'000	2.43	12.84	(378)	682
bulk average	± 1.5	± 8	± 6'000	± 0.10	± 0.60		± 100
Y-793274	39.3	57.6	28'700	2.05	12.7	(340)[2]	740[2]
bulk[1]	± 2.5	± 18.0	± 1'300	± 0.15	± 0.2		± 250

1) Ref. [3]; 2) Average values, see Table 6 in [3].

Nitrogen, Ar, and Xe in Martian meteorites: clues to the evolution of interior gas components.

K. J. Mathew and K. Marti, Department of Chemistry and Biochemistry, University of California, San Diego, La Jolla, CA 92093-0317, USA.

The nitrogen and noble gas signatures of SNC meteorites provide insights into the Martian evolution of volatiles (Bogard et al. 2001). Since the chronologies of nakhlites differ from those of shergottites and ALH84001 (Nyquist et al. 2001) distinct atmospheric gases may have been acquired providing clues to the evolution of the Martian atmosphere.

Noble gases in Nakhla apparently suffered elemental fractionation during the formation of weathering products (Drake et al. 1994), alteration by liquid water on Mars. On the other and, ALH84001 shows no evidence for alteration by water, but similar elemental fractionation are observed, which differ from modern Martian atmospheric gases observed in shergottites. Gilmour et al. (1999, 2001) suggested gas adsorption followed by shock implantation as the mechanism of incorporating atmospheric gases into Nakhla and into ALH84001, with distinct shock levels in these two meteorites. The shock levels are low in Nakhla and high in ALH84001, as also reflected by the temperature release patterns of the atmospheric gases. Mathew and Marti (2002) identified Martian atmospheric Xe and nitrogen component in Nakhla that are consistent with those in impact-melt glasses of shergottites. These authors also identified an indigenous Xe component, consistent with the solar Xe signature observed in Chassigny (Chass-S), but modified by a fission Xe component due to ^{244}Pu, documenting the early differentiation of Mars and formation of source region of nakhlites. First results of a new Nakhlite NW817 were earlier presented (Marty et al. 2001) and since no Martian atmospheric component is observed, the N, Ar, and Xe inventories are revealing signatures of indigenous Martian gases. A spallation $^{15}N_C$ and fission Xe components are observed in the high temperature (>1000°C) steps in both Nakhla and Nakhlite NWA817. The inferred cosmic ray exposure ages are consistent and agree with that of Chassigny.

In Figure 1 we show the measured $^{129}Xe/^{132}Xe$ vs. $^{136}Xe/^{132}Xe$ ratios in Nakhla and NWA817. Since mixtures of a Martian atmospheric component and a Chass-S type interior component (dashed line in Figure 1) cannot explain the data, they demonstrate the fission component. Fission excesses ~20 times larger than that produced in situ from ^{238}U are required. Figure 2 compares the release systematics of ^{36}Ar, ^{40}Ar, and ^{132}Xe in Nakhla and NWA817 and shows that the release systematics of the spallation component differs not only from the radiogenic, but also from that of the indigenous component, which allows the calculation of the spallation Xe component by the subtraction method.

We have completed the study of nakhlite NW817 and work on nakhlite Y000749,51 is in progress. We expect that results of this analysis will be available at the meeting.

References: [1] Bogard D. D., Clayton R. N., Marti K., Owen T., and Turner G. (2001) Space Sci. Rev. 96, 425-458. [2] Nyquist L. E., Bogard D. D., Shih C. –Y., Greshake A., Stöffler D., and Eugster O. (2001) Space Sci. Rev. 96, 105-164. [3] Drake M. J., Swindle T. D., Owen T. and Musselwhite D. S. (1994) Meteoritics 29, 854-859. [3] Mathew K. J. and Marti K. (2001) J. Geophys. Res. (Planets) 106, 1401-1422. [4] Mathew K. J. and Marti K. (2002) Earth Planet. Sci. Lett. 199, 7-20. [5] Marty B. Marti K. and the Théodore Monod Consortium (2001) Meteorit. and Planet. Sci. A122. [6] Gilmour J. D., Whitby J. A. and Turner G. (2001) Geochim. Cosmochim. Acta. 65, 343-354. [7] Gilmour J. D., Whitby J. A. and Turner G. (1999) Earth Planet. Sci. Lett. 166, 139-147.

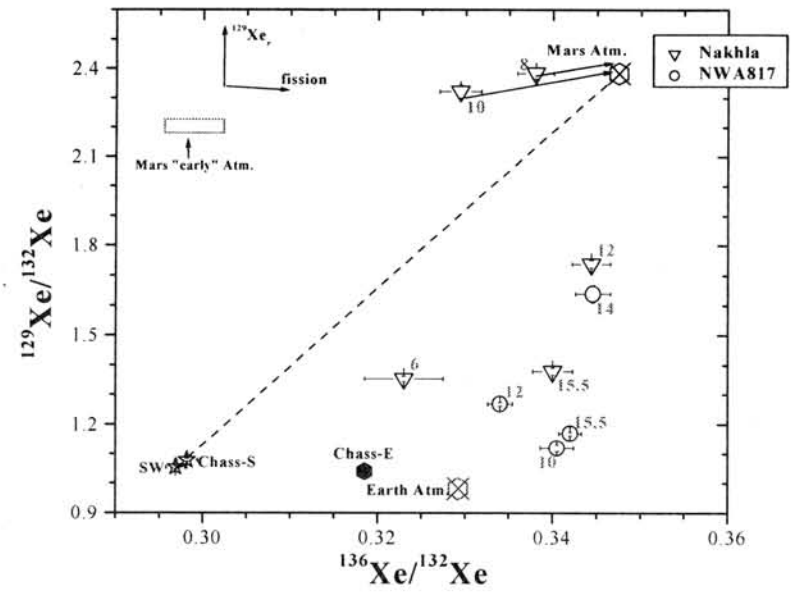

Figure 1. Measured Xe isotopic ratios in Nakhla and nakhlite NWA817. Expected shifts due to spallation Xe component are indicated by arrow. The numbers indicate the extraction temperature (in 100°C). Spallation corrected data of the 800° and 1000°C steps are consistent with Martian atmospheric Xe.

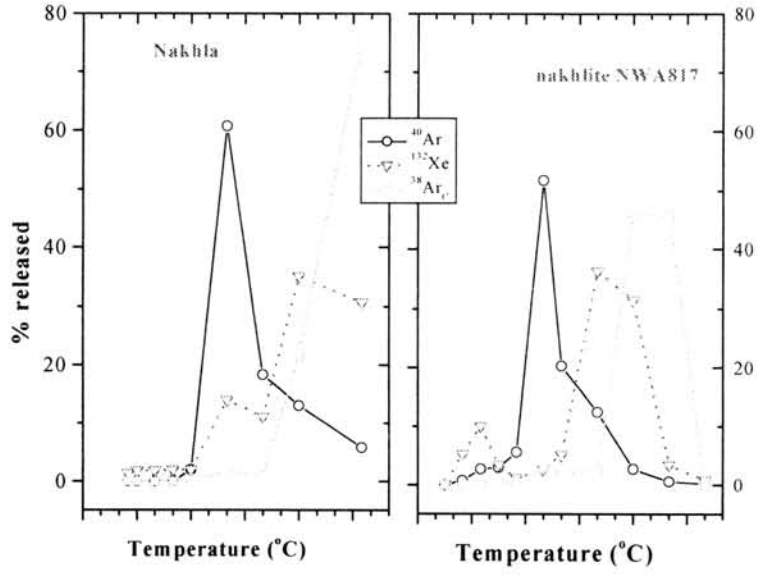

Figure 2. Release systematics of ^{40}Ar, ^{132}Xe, and $^{38}Ar_C$ in Nakhla and nakhlite NWA817. Note the offset in the release of spallation and trapped components which allows an estimation of the spallation spectra.

MARS METEORITES PROVIDE EVIDENCE FOR A HABITABLE SUBSURFACE ENVIRONMENT THROUGHOUT MUCH OF MARS HISTORY

David McKay[1], Kathie Thomas-Keprta[2], Susan Wentworth[2], Simon Clemett[2], and Everett Gibson[1].
[1]NASA Johnson Space Center, Code SA, Houston TX 77058 ; [2]Lockheed-Martin,. Houston TX 77058

Interpretations of Mars Viking and Surveyor orbital images have built a strong case that Mars had surface water during its past geological history. New neutron spectrometer data from Mars Odyssey show that poleward of 60 degrees North and 60 degrees South, significant hydrogen, likely as ice or permafrost, is present in the upper meter or so of the martian regolith. Here we present a summary of independent data from the Mars meteorites showing that liquid water was likely present in the upper few meters or tens of meters as early as 3.9GY and continuing throughout most of Mars history. Conclusions from studies of terrestrial environments are that microbes can live and thrive on earth wherever liquid water and an energy source exist. The evidence from the Mars meteorites shows that the subsurface environment of Mars was favorable (by earth microbial standards) for life throughout much or all of the past nearly 4GY.

Currently, 25 martian meteorites are available in collections on Earth. These meteorites have formation ages ranging from 4.5GY to 165MY. Many if not most of these meteorites also show evidence for aqueous alteration on Mars. Estimates of rock formation depths and residence depths before ejection from Mars range from the upper meter to 500 meters or so. All of the meteorites recovered so far are igneous rocks and would not be expected to contain information on sedimentary or low temperature processes. Yet, most of these meteorites (including ALH84001)contain cracks and pores that contain evidence of secondary alteration, weathering, and precipitation from a water phase. This alteration and precipitation occurred on Mars, but after the original igneous rocks cooled and became fractured. Within these meteorites the evidence for aqueous alteration includes: abundant weathering and corrosion textures, and the production of secondary water-precipitated minerals including smectite, carbonate, magnetite, hematite, Fe-sulfides, halite, Mg and Ca-sulfate, and very thin clay-rich layers deposited in cracks and pores. Many of these secondary minerals likely formed at relatively low temperatures; all apparently formed from liquid water. Redox disequilibrium between the primary igneous minerals and the secondary minerals is common. In general, the secondary minerals are more highly oxidized compared to the primary igneous minerals. Examples of meteorites showing extensive secondary alteration by water include ALH84001, Nakhla, and Lafayette. The nakhlite NWA 817 also contains a hydrous ferrous silicate phase likely to have formed on Mars (Wadhwa et al., 2001, MAPS V36, 9, pA217). New detailed microstratigraphy shows that water corrosion of ALH84001 started before the carbonates were precipitated (3.9GY) and continued after they were formed. Indigenous organic carbon is also present in many Mars meteorites. Nakhla, for example, has at least 40ppm organic carbon, 75% of which lacks terrestrial ^{14}C signature and is therefore from Mars. (Jull et. al., 2000,GCA64, p3763). The carbon isotopic composition of the indigenous reduced organic component is between –15 and –18‰.

Furthermore, some of these meteorites contain features that can be interpreted as biosignatures. While some of these potential biosignatures may be derived from terrestrial processes, most are demonstrably martian. Such potential biosignatures include minerals such as magnetite and carbonate which may have been formed by bioassisted precipitation. Other potential biosignatures include micrometer-size ovoid biomorphs of various composition, ovoid molds, and possibly fossilized biofilms.

Taken together, Mars meteorites are a rich treasure trove of environmental markers from Mars subsurface regions left by water, chemical reactions, and possibly martian microbial life. All of the requirements for life were present: liquid water, organic compounds, and a chemical energy source consisting of redox gradients. It appears that at least some of the martian subsurface has been a hospitable place for life throughout much of Mars history.

EXPERIMENTAL CRYSTALLIZATION OF SHERGOTTITE QUE 94201: A MARTIAN MAGMA.

G. McKay[1], E. Koizumi[2], T. Mikouchi[2], L. Le[3] , and C. Schwandt[3], [1]Mail Code SR, NASA Johnson Space Center, Houston, TX 77058, USA, Gordon.McKay@jsc.nasa.gov, [2]Dept. of Earth and Planetary Science, Univ. of Tokyo, 7-3-1 Hongo, Bunkyo-ku, Tokyo 113-0033, Japan, [3]Lockheed Martin, 2400 Nasa Road 1, Houston, TX 77058, USA

Introduction: QUE 94201 (QUE) is a basaltic shergottite containing subequal amounts of pyroxene and plagioclase, the latter having been converted to maskelynite by shock (Fig. 1) [e.g., 1-3]. Pyroxene occurs as elongate subhedral to euhedral grains up to several mm in length. It has extensive and complex zoning (Fig 2). Typical grains have Mg-rich pigeonite cores mantled by Mg-rich augite, which is in turn rimmed by Fe-rich pigeonite that is sometimes rimmed by a thin discontinuous layer of hedenbergite. Grains often display sector zoning and complex interlayering of augite and pigeonite. This zoning provides a rich record of the crystallization of this meteorite.

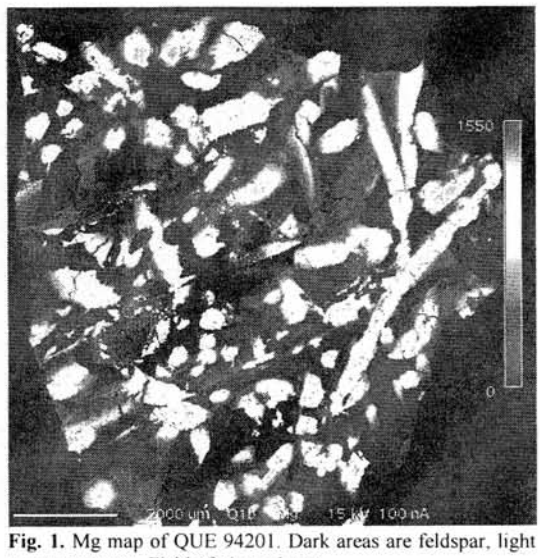

Fig. 1. Mg map of QUE 94201. Dark areas are feldspar, light areas pyroxene. Field of view ~1 cm.

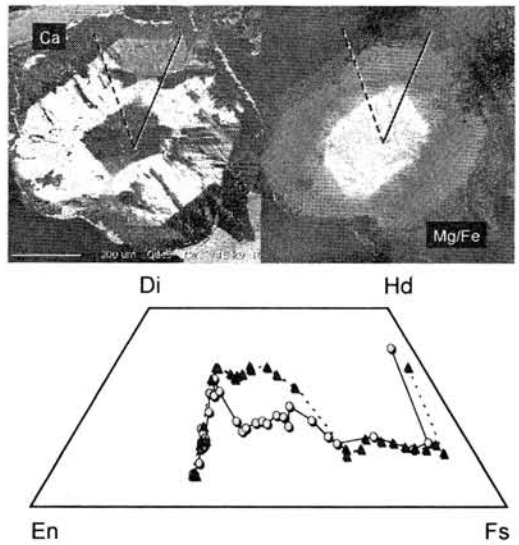

Fig. 2. Ca and Mg/Fe maps of pyroxene grain from QUE94201, and pyroxene compositions along two traverses indicated in maps.

QUE is particularly important among Martian meteorites. Based on the absence of obvious cumulate textures and on the subequal amounts of pyroxene and plagioclase, QUE has been interpreted as a crystallized melt, whereas most other Martian meteorites are enriched in cumulus pyroxene [e.g., 1]. If QUE indeed represents a crystallized magma, it can provide valuable clues to magma petrogenesis on Mars. One petrographic feature bearing on this issue is the abrupt change from pyroxene cores of nearly constant Mg/Fe to rims with strongly zoned Mg/Fe (Fig 1b). Does this transition record a change in crystallization environment (e.g., migration from a magma chamber to a shallow depth or eruption into a lava flow, as suggested for Zagami pyroxenes by [4]), in which case one might consider the pyroxene cores to be cumulus? Alternatively, is it a natural consequence of regular, continuous cooling?

Another important feature of QUE is that it may be more reduced than other Martian meteorites. Fe-Ti oxide compositions and the magnitude of Eu anomalies in QUE plagioclase and pyroxene led [1] and [5] to propose that QUE formed under lower oxygen fugacities than other Martian meteorites [e.g., 1,5]. Variation in oxidation state among the martian meteorites, combined with isotopic systematic isotopic variations, may have important implications for the redox state of the martian crust and mantle. Thus it is important to use multiple means to corroborate the evidence that QUE is reduced.

We are conducting an experimental study of the crystallization of a synthetic QUE analog composition. The goal of this study is to provide information bearing on the above important issues regarding this sample, namely (1) did the sample experience a multi-stage cooling history? (2) did the sample form under more reducing conditions than other martian meteorites? and (3) does the sample represent a crystallized melt. This abstract reports progress in this study since our earlier reports [6,7,8].

Experiments: We performed several sets of experiments, each with its own purpose. In one set of isothermal crystal growth experiments, pre-homogenized beads of synthetic starting glass were placed in gas mixing furnaces at desired T and fO_2, held for 48 hours, then quenched. Most of these experiments were performed at QFM or IW+1 to determine equilibrium phase relations. In a set of reversal experiments, beads

were held at 1100° to grow pigeonite, augite, and plagioclase, then heated to the desired T and fO_2 to allow minerals to dissolve, then quenched. These experiments generally confirmed the phase relations obtained from the isothermal experiments except for plagioclase. They will be discussed in detail elsewhere. A third set of experiments was performed at ½ log unit fO_2 steps from QFM to IW+1 at 1150° and 1160°, to determine the effect of oxygen fugacity on phase relations. Finally, in a set of cooling experiments, beads were placed in the furnace at 1175°C, cooled at various rates, and quenched at various temperatures to "dissect" the crystallization sequence for each cooling rate. These experiments were designed to mimic the natural crystallization of QUE to shed light on the issues of whether it is a melt composition and whether it had a simple single-stage cooling history.

Results and discussion: ***Isothermal experiments.*** BSE images of quenched isothermal runs are shown in Fig. 3. The major result from these experiments is at IW+1, pigeonite is the liquidus phase, as it appears to be in natural QUE. Augite is the second phase to crystallize, and is followed by plagioclase. The composition of the liquidus pigeonites closely matches the composition of the Mg-rich core pigeonite in natural QUE (Fig. 3). This close match strongly supports the idea that QUE represents a magma composition rather than a cumulate like most other basaltic shergottites.

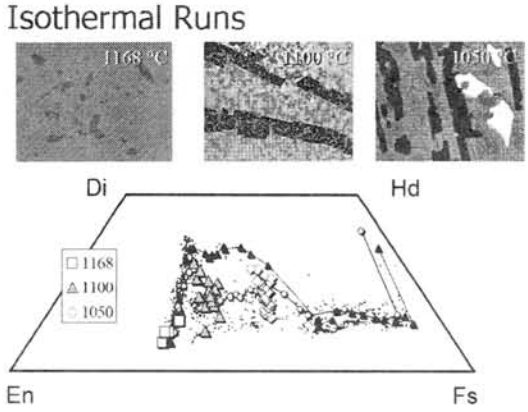

Fig. 3. BSE images from isothermal runs at 1168°C (pigeonite and glass), 1100°C (pigeonite, augite, plagioclase, and glass), and 1050°C (pigeonite, augite, plagioclase glass, and Fe-Ti oxides). Compositions of pyroxenes from these runs are shown in quadrilateral, compared with pyroxenes from natural QUE.

As experimental conditions become more oxidizing, olivine becomes the liquidus phase. The presence of liquidus olivine in oxidizing experiments and its absence in reduced experiments, combined with the lack of olivine in natural QUE, support the proposition that QUE crystallized under redox conditions near IW+1. This topic is discussed in much more detail in a companion abstract by Koizumi *et al.* [9].

Cooling Experiments. Charges from experiments cooled at 0.5°C/hr at IW+1 and quenched at various temperatures are shown in Fig. 4. The systematic decrease in the proportion of glass with falling quench temperature is readily apparent. The porphyritic texture of the 900° charges closely resembles the texture of natural QUE (Fig. 1).

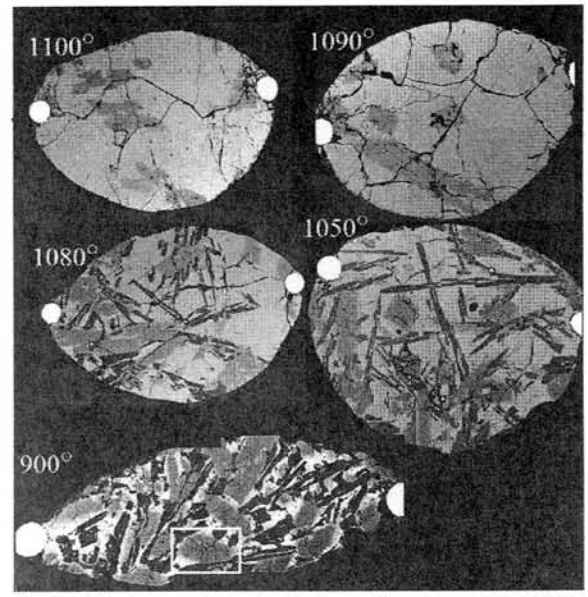

Fig. 4. BSE images of quenched charges from runs with 0.5°C/hr linear cooling at IW+1. 1100° and 1090° charges contain only glass and pyroxene. 1080° and 1050° runs contain glass, pyroxene, and plagioclase. 900° run is nearly completely crystallized, and contains pyroxene, plagioclase, silica, Fe-Ti oxides, and mesostasis glass.

Fig. 5 compares zoning patterns of the pyroxene grain outlined by the white rectangle in the 900° charge of Fig. 4 with zoning patterns from natural QUE. One small difference is that the center of the synthetic pyroxene appears to be augite that is slightly Fe-enriched. We have observed similar grains in natural QUE, and believe that they were initially hollow or "hopper" shaped, and that the hollow portion subsequently filled in with slightly more evolved pyroxene. Despite this minor difference, the synthetic and natural pyroxenes

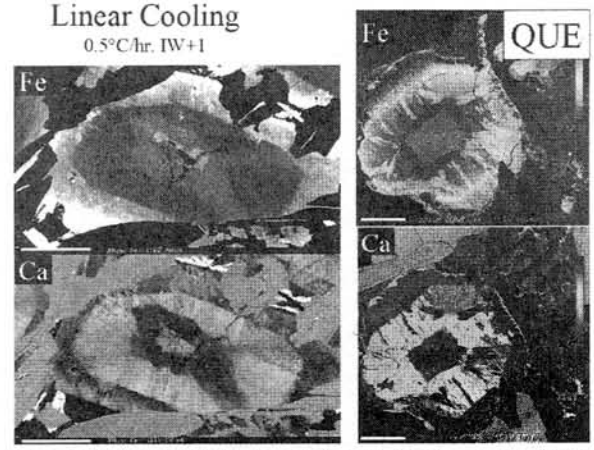

Fig. 5. Fe and Ca maps of pyroxene from 900° isothermal run (white rectangle in Fig. 4) and natural QUE pyroxenes. Scale bars are 20 μm.

show remarkably similar zoning patterns.

Both synthetic and natural pyroxenes have cores with nearly constant Mg/Fe. The outer margin of these cores appears to mark the onset of plagioclase crystallization [8,9]. Apparently, plagioclase nucleation initiates a period of fairly rapid growth, with a change in the growth regime. Before the onset of plagioclase crystallization, the regime appears to be one in which the crystals are exposed to large amounts of liquid and are growing slowly enough that their Mg/Fe ratios do not change significantly. After plagioclase begins to crystallize, growth appears to be sufficiently rapid and/or the amount of liquid available to the growing pyroxene is small enough so that Fe enrichment begins. At this point, the Al/Ti ratio in pyroxene also drops markedly [8,9]. Thus, the onset of plagioclase crystallization appears to have a profound effect on the composition of co-crystallizing pyroxene.

Fig. 6 compares the compositions of a large number of pyroxenes from the 0.5°/hr cooling runs with natural QUE pyroxenes. This plot illustrates one of the most important results of our study, namely the remarkable agreement in composition between the liquidus synthetic pyroxenes and the cores of the natural QUE pyroxenes. This correspondence constitutes strong evidence that our starting composition (i.e., the QUE bulk composition) is that of the melt from which the liquidus pyroxenes in QUE crystallized, without the excess pyroxenes that are present in almost all other basaltic shergottites.

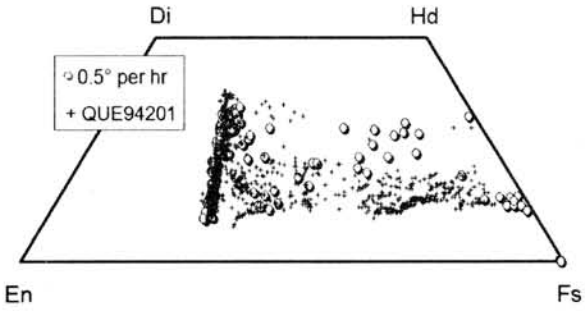

Fig. 6. Compositions of synthetic pyroxenes from cooling run compared with natural pyroxenes from QUE. Agreement for Mg-rich pyroxenes is remarkable.

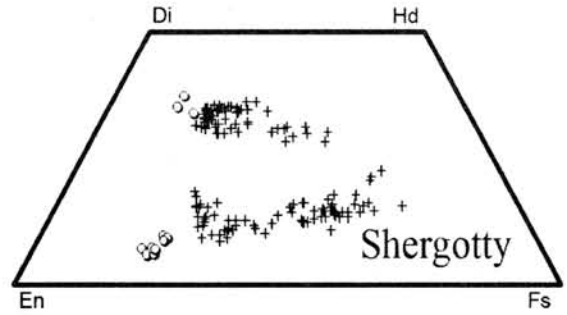

Fig. 7. Compositions of synthetic liquidus pyroxenes from Shergotty crystallization experiments of Stolper & McSween [10] (circles) compared with pyroxenes from the natural sample (+).

In contrast, synthetic pyroxenes from crystallization of a completely molten cumulate sample like Shergotty plot at much higher Mg/Fe than the cores of the cumulus pyroxenes in the sample (Fig. 7). Thus, this result strongly supports the idea that QUE represents a melt.

Conclusions: (1) The presence of olivine in our more oxidized runs, together with its absence in the natural sample, supports the proposition that QUE crystallized under reducing conditions near IW+1. **(2)** The similarity of synthetic and natural samples in textures and zoning patterns supports a simple single-staged cooling history for QUE. In particular, the abrupt change from homogeneous pyroxene cores to strong Fe/Mg zoning appears to be a natural consequence of plagioclase crystallization rather than the result of a change in crystallization environment. **(3)** The remarkable agreement between synthetic liquidus pyroxene compositions and natural QUE core compositions constitutes strong evidence that QUE represents a magma composition without accumulated pyroxene. **QUE was a magma.** Thus this unusual sample holds important clues to basalt petrogenesis on Mars.

References: [1] McSween *et al.*, 1996, GCA 60, 4563. [2] McKay *et al.*, 1996, LPSC XXVII, 851-852. [3] Mikouchi et *al.*, 1998, MAPS 33, 181 [4] McCoy *et al.* 1992. GCA 56, 3571. [5] Wadhwa 2002, GCA, in press. [6] McKay *et al.*, 2001, Antarctic Meteorites XXVI, 77-79. [7] McKay *et al.* 2002, LPSC XXXIII, #2051. [8] Koizumi *et al.*, 2002, LPSC XXXIII, #1442. [9] Koizumi *et al.*, 2002, This volume. [10] Stolper & McSween, 1979, GCA 43, 1475.

Comparative mineralogy of the new nakhlite Yamato-000593 with other nakhlite Martian meteorites

T. Mikouchi, E. Koizumi, A. Monkawa, Y. Ueda and M. Miyamoto

Department of Earth and Planetary Science, Graduate School of Science, University of Tokyo
7-3-1 Hongo, Bunkyo-ku, Tokyo 113-0033, Japan
E-mail: mikouchi@eps.s.u-tokyo.ac.jp

1. Introduction

Nakhlites form an interesting group of Martian meteorites because of their unique mineralogy and chemistry [*e.g.*, 1-5]. Nakhlites are cumulus clinopyroxenites with minor olivine and mesostasis [*e.g.*, 2-4]. Only three samples (Nakhla, Governador Valadares, and Lafayette) had been known belonging to this group until recently, but the fourth sample (NWA817) was found from the African desert in 2001 [6-7]. Furthermore, the fifth sample (paired samples of Y-000593 and Y-000794) was found in Antarctica by the Japanese Antarctic expedition [8] and these two discoveries could offer important informations to better understand the formation condition of this Martian meteorite group. In this abstract, we report preliminary mineralogy and petrology of Y-000593 and compare the results with other nakhlites.

2. Petrography of Y-000593

We studied two thin sections of Y-000593 (Y-000593,62-3 and Y-000593,62-6). Y-000593 is roughly composed of ~85 % augite, 10% olivine, and 5 % mesostasis (Fig. 1). Augite is a euhedral to subhedral elongated grain whose longer dimension is up to 1.5 mm long. Polysynthetic twinning is commonly observed. It is likely that augite is a cumulus phase like other nakhlites. Olivine grains are mostly anhedral and interstitial to augite. It sometimes shows subhedral crystal termination adjacent to the mesostasis. Small grains of olivines (~200 μm in size) are also found and they are all interstitial to augite. Some olivines poikilitically enclose rounded augite grains. Dark lamellar inclusions are commonly observed in large olivine grains. Their distributions within olivine grains are irregular. Olivines are usually altered into brown colors along fractures. The mesostasis is composed of radiating spray of plagioclase intergrown with silica. Plagioclase length reaches up to 200-300 μm although the width is ~20 μm. Scattering lath grains of olivine and augite are also observed. The minor phases in the mesostasis include Ti-magnetite, Ca phosphate and Fe sulfide (pyrite?). Ti-magnetite is up to 300 μm in size. The mesostasis also shows secondary alteration due to the presence of brown rusty products like olivine.

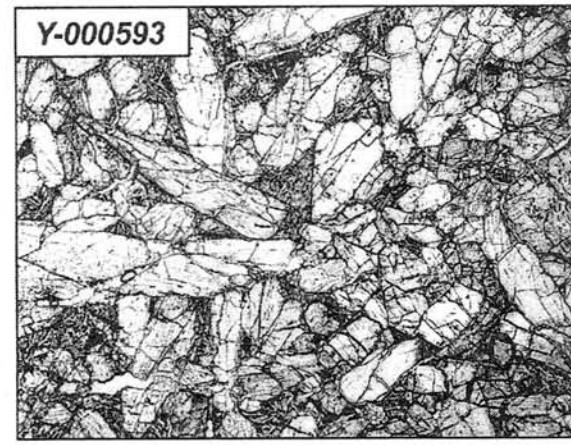

Fig. 1. Optical photomicrograph of the Y-000593 thin section. The field of view is ca. 5 mm. Y-000593 shows a cumulate texture mainly composed of augite with minor olivine and mesostasis.

3. Mineral Compositions of Y-000593

Augite: Augite has a large homogeneous core of $En_{39}Fs_{22}Wo_{39}$ (Fig. 2). The rims adjacent to the mesostasis show enrichment of Fe, but the Wo content is almost uniform except for the 10-20 μm edge. At the boundary with the mesostasis, Fe-rich augite displays a finger-like texture intruding into the mesostasis. Al_2O_3 is 0.4-0.9 wt% in the core, increases to 2 wt% at the rim, and then suddenly drops down to 0.6-1 wt% at the edge. TiO_2 shows a similar behavior, 0.1-0.3 wt% in the core and slightly enriched at the rim (0.5 wt%). At the edge, TiO_2 is 0.3-0.4 wt%. We have not yet done the FEG-SEM analysis of the pyroxene rims to observe microstructures, but the constant En content with variable Wo content suggests the presence of fine exsolution lamellae. Low-Ca pyroxene (pigeonite) is also present. It is uniform in composition ($En_{28}Fs_{64}Wo_8$).

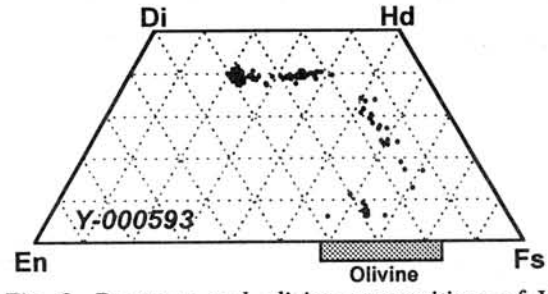

Fig. 2. Pyroxene and olivine compositions of Y-000593. Augite composition is nearly homogeneous ($En_{39}Fs_{22}Wo_{39}$) except for the Fe-rich rims. In contrast, olivine shows extensive chemical zoning.

Olivine: Large olivines show extensive chemical zoning unlike pyroxenes. The most magnesian olivine in the sections studied is Fa_{58}, which is more magnesian than the reported composition (Fa_{65}) [8]. Chemical zoning is more remarkable in larger grains, but small grains (less than ~200 μm) are usually homogeneous. The zoning feature is most extensive at the rim having contact with the mesostasis as augite shows, suggesting that chemical zoning attributed to cation exchange with mesostasis. Olivine composition is Fa_{81-82} at such rims, which is identical to the small grains with homogeneous composition. In some cases, olivines are intergrown with the mesostasis plagioclase. The CaO content of olivine is 0.5 wt% at the core and drops down to 0.2 wt% at the rim. The symplectic inclusions (usually parallel to one direction) consist of magnetite and augite [5] (Fig. 3).

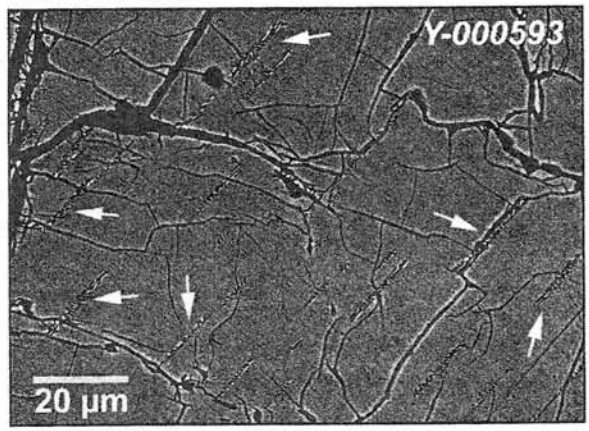

Fig. 3. Backscattered electron (BSE) image of the Y-000593 olivine. Note abundant symplectic inclusions (indicated arrows) composed of fine, dendlitic intergrowth of augite and magnetite.

Mesostasis: The radiating plagioclase intergrown with silica in the mesostasis (Fig. 4) is $An_{35-21}Or_{3-10}$. These plagioclase grains show clear birefringence under optical microscope, ruling out that they transformed into "maskelynite" by shock. Optical microscope analysis shows the presence of abundant rusty brown products in the mesostasis similar to "iddingsite" in the other nakhlites [9]. Because our observation and microprobe analysis of the mesostasis area is far from complete, we have not yet obtained the chemical composition of the brown product. Further analysis is required to confirm the mineral species of the product. The phosphate in the mesostasis is probably an apatite. The EDS analysis shows the presence of abundant Cl. The chemical compositions of pyroxene and olivine in the mesostasis are the same those at the rims of cumulus augite and olivine adjacent to the mesostasis.

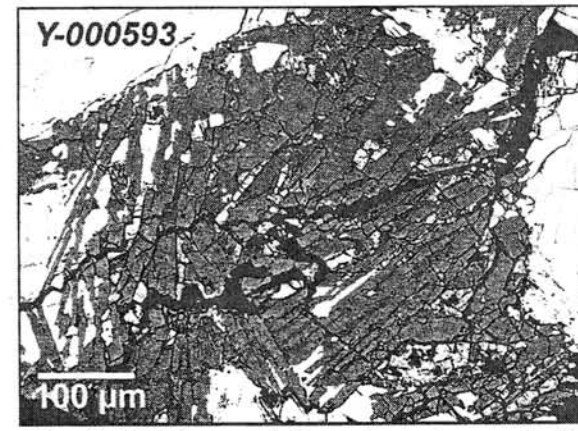

Fig. 4. BSE image of the mesostasis area in Y-000593. The mesostasis is mainly composed of the radiating plagioclase (bright gray) intergrown with silica (dark gray).

Opaques: Ti-magnetite (ulvospinel) is the most common opaque phase in Y-000593. It has 1-3 wt% Al_2O_3, 13-18 wt% TiO_2, and 71-76 wt% FeO. Because the total is 93-96 wt%, significant amount of Fe^{3+} would be present.

4. Comparisons with other Nakhlites

Petrography: The texture of 000000Y-000593 is generally similar to all other nakhlites. The most notable petrography of Y-000593 is the abundance of mesostasis. NWA817 has similar abundance of mesostasis, but the radiating plagioclase is rare (or very thin) in NWA817. NWA817 is rather composed of Si-rich feldspathic glass with skeletal Ti-magnetite, suggesting a faster cooling of the mesostasis. The mesostasis mineralogy of Y-000593 is also similar to Nakhla and Governador Valadares in the presence of radiating plagioclase. However, the plagioclase in Y-000593 is thinner (~20 μm wide) compared to those in Nakhla and Governador Valadares (~50 μm). Therefore, crystallization of the mesostasis was more completed for Nakhla and Governador Valadares than Y-000593. This is probably because Y-000593 cooled faster.

Augite mineralogy: The chemical composition of the augite core in Y-000593 is nearly identical to those of other nakhlites (Figs. 2, 5). The Fe-rich rims adjacent to the mesostasis have slightly more ferroan

compositions than those of Nakhla and Governador Valadares do. The most ferroan augite of Y-000593 is similar to that of NWA817, but NWA817 does not contain Fe-rich augite with variable Wo content (due to the absence of fine exsolution?). Lafayette is quite different from both Y-000593 and other nakhlites in its homogeneous composition due to slower cooling.

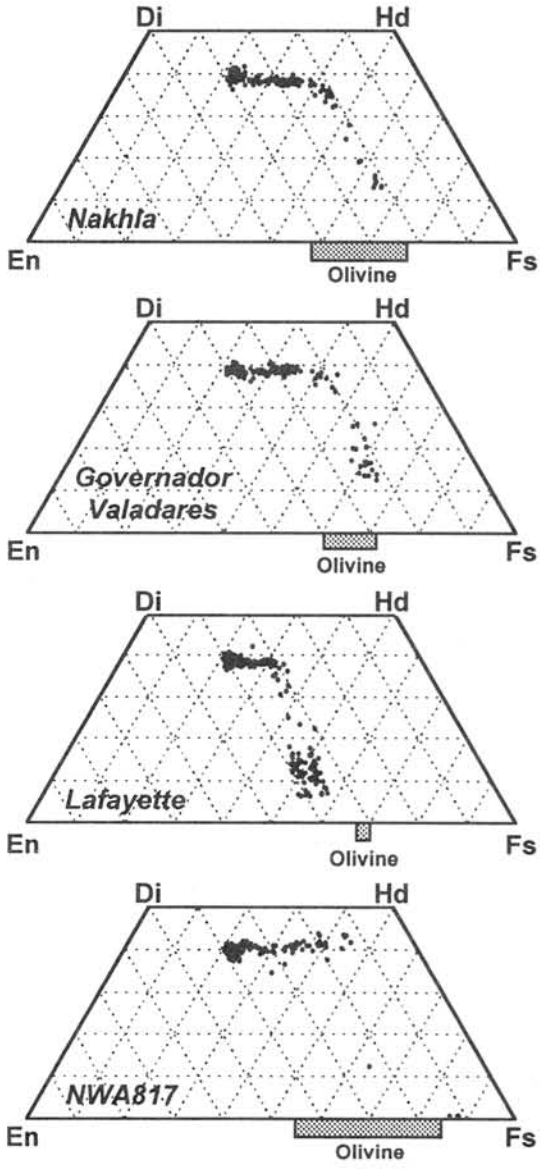

Fig. 5. Pyroxene and olivine compositions of Nakhla, Governador Valadares, Lafayette and NWA817 nakhlites.

Olivine mineralogy: All the nakhlites including Y-000593 have unique olivine compositions (Figs. 2, 5). This is probably because olivine has a fast atomic diffusion rate (compared to pyroxene) and its composition is sensitive to minor difference in thermal history. The most magnesian composition of Y-000593 olivine is identical to that of Nakhla, but Y-000593 olivine extends to more ferroan compositions than Nakhla. NWA817 olivine also has Fe-rich compositions, but the most magnesian olivine is more Mg-rich. Y-000593 and Nakhla olivines may have initially crystallized under the same conditions, but later mesostasis crystallization condition was different (Nakhla cooled slightly slower). The presence of symplectic inclusions in olivine has been observed only in Nakhla and Governador Valadares [5]. This is consistent with the similarity in chemical compositions between Y-000593 and Nakhla.

Opaque mineralogy: The chemical composition of Ti-magnetite in Y-000593 is generally similar to those of other nakhlites, suggesting that all nakhlites formed under similar redox conditions near the QFM buffer [10].

5. Conclusions

There is no doubt that Y-000593 is a new nakhlite as it was found in Antarctica, thousands of kilometers away from other nakhlites. These rocks share similar mineralogy and ages, suggesting that they came from the same igneous unit on Mars and were ejected by the same impact event [*e.g.*, 2-4, 11-12]. In other words, it is very interesting that we have nakhlite samples that show slightly different mineralogy from each other all over the world. The difference would be resulted in different thermal history according to different locations (burial depths) in common cooling cumulate piles. Y-000593 is most similar to Nakhla and the formation of cumulus phases would occur under the same condition. The similarity between Y-000593 and Nakhla is also found in reflectance spectra [13]. Later mesostasis crystallization of Y-000593 was more rapid than Nakhla probably due to faster cooling rate, and produced minor difference between them. We previously estimated that the burial depths of Nakhla and NWA817 were 4-5 m and 0.5 m, respectively, according to the Fa zoning of olivine [12]. This study suggests that Y-000593 would be located between NWA817 and Nakhla. The abundance of the mesostasis or the degree of "packing" of cumulus phases may be related to the burial depths of nakhlites.

References

[1] McSween H. Y. Jr. (1994) *Meteoritics* **29**, 757-779. [2] Harvey R. P. and McSween H. Y. Jr. (1992) *GCA* **56**, 1655-1663. [3] Wadhwa M. *et al.* (1995) *GCA* **59**, 3629-3645. [4] Lentz R. C. F. *et al.* (1999) *MAPS* **34**, 919-932. [5] Mikouchi T. *et al.* (2000) *MAPS* **35**, 937-942. [6] Mikouchi T. and Miyamoto M. (2001) *MAPS* **36**, A134. [7] Sautter V. *et al.* (2002) *EPSL* **195**, 223-238. [8] Imae N. *et al.* (2002) *LPSC* **XXXIII**, #1483. [9] Treiman A. H. *et al.* (1993) *Meteoritics* **28**, 86-97. [10] Reid A. M. and Bunch T. E. (1975) *Meteoritics* **10**, 317-324. [11] Eugster O. *et al.* (1997) *GCA* **61**, 2749-2757. [12] Mikouchi T. and Miyamoto M. (2002) *LPSC* **XXXIII**, #1343. [13] Ueda Y. *et al.* (2002) *Antarct. Meteorites* **XXVII** (this volume).

Carbon-14 terrestrial ages of meteorites

Masayo Minami[1)] and Toshio Nakamura[2)]

1) Division of Earth and Environmental Sciences, Graduate School of Environmental Studies, Nagoya University, Chikusa, Nagoya 464-8602, Japan

2) Center for Chronological Research, Nagoya University, Chikusa, Nagoya 464-8602, Japan

1. Introduction

The terrestrial age of a meteorite is an important time marker that reflects the history of the meteorite. Carbon-14 ($t_{1/2}$=5730 yr) is very useful in determination of relatively young terrestrial ages up to 30kyr. We have constructed a system to extract carbon from meteorites using a vacuum-tight RF furnace melting method, which is a similar method used by the Arizona (Jull et al., 1989a, 1993). The extraction system was examined using iron standards of known carbon content (Minami and Nakamura, 2001). The carbon extraction efficiencies and ^{14}C ages of the iron standards by this method were compared with the results obtained by our old melting system (Nakamura et al., 1995) and a wet oxidation method, which consists of dissolution of iron with a Cu^{2+} solution and dissolution of deposited Cu in HCl (Oda et al., 1999). Higher collection efficiencies of about 90% for the iron samples of relatively high carbon content were achieved by the new system. The efficiency of extracting a small amount of carbon is higher up to near 90% by improving the extraction procedure. The ^{14}C ages of the iron standards were compared to the ages by the wet method, and the results indicate that contamination by modern carbon is negligible in the system. In this paper, we compare the results of ^{14}C activities of two Antarctic meteorites, Y-75102 and ALH-77294, with the already reported ^{14}C terrestrial ages of them by Fireman and Norris (1981), Fireman (1983), Jull et al. (1984) and Jull et al. (1989). We also report the terrestrial ages of Y-74190, Y-75097 and Y-75108, which are thought to have fallen at the same time as Y-75102.

2. Samples and Experiments

Antarctic meteorites of Y-75102 (L6), Y-74190 (L6), Y-75097 (L6), Y-75108 (L6) and ALH-77294 (H5) were examined to measure ^{14}C concentrations using our vacuum-tight RF melting method. The terrestrial ages of Y-75102 were reported to be 4.2±0.8 kyr by counting (Fireman, 1983) and 1.7±0.3 kyr by accelerator mass spectrometry (Jull et al., 1984). Y-74190, Y-75097 and Y-75108 are thought to have fallen at the same time as Y-75102 from $^{3}He/^{21}Ne$ and ^{53}Mn data (Takaoka, 1987). The results of ALH-77294 were 30±0.8 kyr by counting (Fireman and Norris, 1981) and 9.5±1.0 kyr by accelerator mass spectrometry (Jull et al., 1989).

A sample mixed with about 2g combustion accelerator (high purity Fe, LECO corp., part No. 502-231) is combusted in a RF induction furnace (LECO HF-10) in the presence of purified carbon-free O_2 in a closed vacuum-tight glass line system. The meteorite samples were preheated prior to the combustion in the RF furnace in muffle furnace at 500℃ to remove organic contamination and low-temperature weathering products. The sample gases evolved are passed through MnO_2 and Pt/CuO traps, and then the CO_2 is separated in a liq.N_2 trap, by pumping out O_2 completely. The amount of $^{14}CO_2$ is determined by a pressure transducer in a certain volume and diluted with a known amount of ^{14}C-free CO_2. The total CO_2 is graphitized by reducing with hydrogen in a Fe-powder catalyst and the produced graphite is measured of its ^{14}C concentration with a Tandetron accelerator mass spectrometer at the Center for Chronological Research, Nagoya University.

3. Results and Discussion

Table 1 shows the ^{14}C concentrations and the resulting ^{14}C terrestrial ages of two Antarctic meteorites of Y-75102 and ALH-77294. The fourth column gives the $^{14}C/^{12}C$ ratio for the sample divided by the $^{14}C/^{12}C$ ratio for the NBS oxalic acid standard (RM-49). The measurement error is given as one standard deviation. The fifth column gives the disintegration rate of cosmogenic ^{14}C of the meteorites. The saturated activities used are 53 dpm/kg and 43 dpm/kg for Y-75102 and ALH-77294, respectively. The errors of terrestrial ages are determined only by the experimental errors in the ^{14}C determinations.

To measure the background on ^{14}C measurements of meteorites, blank samples of crucibles with 2g high purity iron chips were studied. The blank gives 0.27 ± 0.03 dpm/kg. In Table 1, the data of

Table 1 Terrestrial ^{14}C ages of Y-75102 and ALH-77294

	Weight (g)	CO_2 (cm^3 STP)	$(^{14}C/^{12}C)sam / (^{14}C/^{12}C)std$	^{14}C (dpm/kg)	Terrestrial age (kyr)	Reference
Y-75102						
1	0.982	0.015	74.6±0.8	35.3±1.1	3.4±0.7	This work
2	0.680	0.014	44.9±0.3	30.1±1.5	4.7±0.7	This work
3	------	------	--------	34.1±2.7	4.3±1.0	Fireman (1983)
4	5.0	7.6	--------	46.3±1.4	1.7±0.3	Jull et al. (1984)
ALH-77294						
1	0.832	0.147	2.0±0.1	4.2±0.2	19.2±0.8	This work
2	0.831	0.048	4.1±0.2	3.9±0.2	19.8±0.9	This work
3	10.5	1.32	--------	1.6±0.3	30±2	Fireman and Norris (1981)
4	0.42	------	--------	13.9±0.3	9.5±1.0	Jull et al. (1989)
5	------	------	--------	6.8±0.2	16.5±1.3	Jull et al. (1998)

meteorites are shown with correction for this blank value. Our terrestrial ages of Y-75102 almost agree with the value of Fireman (1983), though a little older than the age of Jull et al. (1984). The ^{14}C terrestrial ages of ALH-77294 are between the value of Fireman and Norris (1981) and the value of Jull et al. (1989). In experimental procedure for ^{14}C determinations, Fireman and Norris (1981) and Fireman (1983) use stepwise heating and small-counter technique, and Jull et al. (1984, 1989) use RF melting and AMS technique. We used the latter technique. The result of the small-counter method tends to be oldest, the result of the AMS method by Jull et al. is youngest, and our result is intermediate.

Y-74190, Y-75097, Y-75108 and Y-75102 gave similar ages of ~4kyr, though Y-74190 gave a slightly younger age of 2.8 kyr (Table 2). These four chondrites might have fallen at the same time.

Further studies are needed to improve analytical technique: reducing back-ground value of the extraction system and complete combustion of meteorites by such as longer heating time in RF furnace and use of much more combustion accelerator. It is indispensable to measure saturated ^{14}C activities of recently fallen meteorites with our extraction system. Furthermore, shielding or depth corrections are needed for ^{14}C terrestrial age determination of a meteorite sample if the meteoroid was very large or very small. We intend to obtain the other radioisotope data such as ^{10}Be to estimate the shielding effect. By normalizing the saturated activity of ^{14}C to that of ^{10}Be in a meteorite, more correct terrestrial age for the meteorite could be obtained.

Table 2 Pairing of Y-75102 -series chondrites

Sample	Weight (g)	CO_2 (cm^3 STP)	^{14}C (dpm/kg)	Terrestrial age (kyr)	$^{3}He/^{21}Ne$	^{53}Mn (dpm/kg Fe)
Y-74190	0.982	0.015	40.8±1.2	2.8±0.7	2.2	441
Y-75097	0.680	0.014	37.5±1.2	3.5±0.6	4.6	424
Y-75108	0.800	0.087	34.7±1.0	4.1±0.5	4.0	407
Y-75102				4.1±0.7[a]	4.8	452

a. The average of our data for Y-75102 in Table 1

b. $^{3}He/^{21}Ne$ and ^{53}Mn values are from Takaoka (1987).

c. The saturated activity used for the chondrites is 43 dpm/kg.

References: Fireman, E.L. (1983) *Lunar Planet. Sci.* **14**, 195-196.; Fireman, E.L. and Norris, T. (1981) *Proc. Lunar Planet. Sci.* **12B**, 1019-1025.; Jull, A. J. T., Donahue, D. J., Zabel, T. H. and Fireman, E. L. (1984) *Proc. Lunar. Planet. Sci Conf. 15th, J. Geophys. Res.* **89**, C329-335.; Jull, A. J. T., Donahue, D. J. and Linick, T. W. (1989a) *Geochim. Cosmochim. Acta* **53**, 2095-2100.; Jull, A. J. T., Donahue, D. J. and Linick, T. W. (1989b) *Lunar. Planet. Sci.* **XX**, 488-489.; Jull, A. J. T., Donahue, D. J., Cielaszyk, E. and Wlotzka, F. (1993) *Meteoritics* **28**, 188-195.; Minami, M. and Nakamura, T. (2001) *Radiocarbon.***43**, 2A, 263-269.; Nakamura, T., Hirasawa, M. and Igaki, K. (1995) *Radiocarbon* **37**, 629-636.; Oda, H, Nakamura, T. and Furukawa, M. (1999) *J.Radioanalytical and Nuclear Chemistry* **239**, 561-564.; Takaoka, N. (1987) In *Science of Antarctic* (ed. National Institute of polar Reseach) **6**, 228-242.

Genesis of Oxidized Chondrules in Carbonaceous Chondrites of the CO3 Type

Olga B. Mitreikina, Nina G. Zinovieva, and Lev B. Granovsky

Department of Petrology, Faculty of Geology, Moscow State University, Lenin Gory, Moscow 119992, Russia
Correspondence author's e-mail address: zinov@geol.msu.ru

In the C1-C2-C3 succession of carbonaceous chondrites, chondrites of the C3 type are the richest in the chondrule material and can be subdivided into C3(V) and C3(O) groups in accordance with the oxidation degrees of this material. They have taxitic structures, which are determined by various chondrules and their fragments imbedded in a Fe-rich matrix and by unsystematically distributed patches with small magnesian chondrules and their fragments. Along with small magnesian chondrules, there are larger Ca-Al chondrules and their fragments (so-called refractory CAL inclusions), whose amounts and sizes are much greater in CV3 chondrites, in spite of the compositional identity between CO and CV chondrites, for example, in terms of alumina and alkali concentrations.

Like other chondrite types, carbonaceous chondrites provide obvious evidence of two successive evolutionary stages, reduced and oxidized, the transition between which in the course of differentiation determines the oxidation degree of the meteorite as a whole. The reduced stage of chondritic material is represented by Mg-rich olivine and Mg-rich olivine-pyroxene material of detrital and chondrulic types and fragments of high-Al inclusions. The genesis of chondrules was related to the initial differentiation of the fluid chondritic melts, a process that involved the onset of liquid immiscibility in the melts and their exsolution into chemically contrasting compositions: the chondrules have a silicate composition and are sharply depleted in Fe, Ni, S, and chalcophile metals relative to the ambient matrix [1]. In the process of the exsolution of chondritic melts, fluids, first of all hydrogen, were preferably concentrated in the Fe-rich matrix phase, as is evident from gas bubbles in chondrules, for example, in the Allende chondrite, in which trails of bubbles accentuate the concentrically zoned inner structures of chondrules [2]. The process of iron-silicate liquid unmixing during the segregation of chondrules can be clearly visualized by considering droplets rich in native Fe or sulfides in their marginal parts. The origin of chondrules as a result of liquid immiscibility finds further support in their crystallization direction, which obvious started from the margins, and, consequently, the development of monomineralic (olivine or pyroxene) rims, while the inner parts of the chondrules often preserve volcanic glass [3].

Evidently, strongly reduced mineral assemblages were the first to crystallize from the matrix. These assemblages were analogous to those in chondrules, which occurred in equilibrium with the matrix melt. This follows from the low Fe# of the olivine (forsterite) that initially crystallized on the chondrule surfaces (together with troilite) and the occurrence of relict kamacite (native Ni-Fe) in fine-grained matrix. The reduced state of the chondrite melts predetermined the early crystallization of olivine and pyroxenes of very magnesian composition (0.6-2.0 mol % fayalite in the olivine). However, these conditions did not persist until the end of crystallization because of selective hydrogen migration and an increase in the water concentration in the fluids, as is evident from the strongly elevated Fe# of the crystallizing silicates. According to the character of matrix crystallization coupled with a rapid increase in the Fe# of the olivine, CO3 chondrites compose the most oxidized type of carbonaceous chondrites, whose Fe# span (0.1-68.3) is wider than that of CV3 chondrites (0.1-44.7).

A change in the redox state of the environment triggered exchange reactions between the matrix melt and crystalline chondrules, with these reactions proceeding the more actively,

the sharper the gradient in the redox potential was and the more conspicuous the compositional differences were. In the Kainsaz (CO3) chondrite, CAL inclusions were the first to be assimilated in the matrix. In this meteorite, their relics occur as "shadows" that are pulled apart along the fluidal matrix textures and merge with the matrix (Fig. 1).

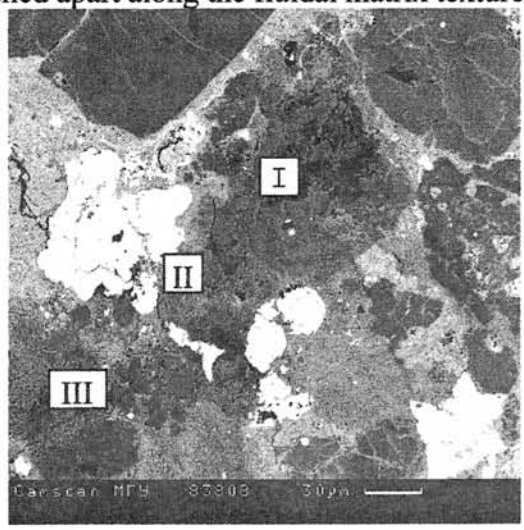

Fig.1. Replacement zones in a CAL inclusion.

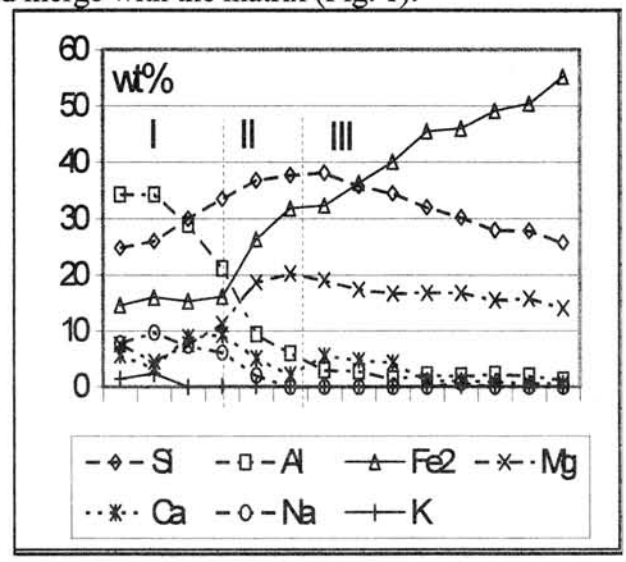

Fig. 2. Petrochemistry of the replacement of CAL inclusions by the matrix melt.

Even the central zones of the inclusions were affected by replacement, which is reflected in an increase in the spinel Fe# compared to the magnesian spinel ($Mg_{0.98}Fe_{0.02}Al_2O_4$) of Efremovka (CV3), whose CAL inclusions are significantly resorbed but, nevertheless, are replaced by the matrix melt only in the margins. The changes in the CAL bulk compositions show a strong depletion, firths and foremost, in alumina and alkalis, coupled with an enrichment of the marginal zones in silica, magnesia, and lime (Fig. 2: *I* - initial compositions, *II* - zone strongly depleted in Al). Therewith, nepheline and clinopyroxene occur in places in association with olivine, whose Mg# somewhat decreases toward grain margins (*Fo* 90 - 78). Patches of strong recycling are notably enriched in Fe at a gradual depletion in Si and Mg, a process that gives rise to the olivine-pyroxene assemblage with small amounts of nepheline. These fragments are penetrated by the matrix material and differ from it by elevated concentrations of Si (36-38 wt %), Al, Ca, and alkalis (Fig. 2, left-hand part of field III). The occurrence of nepheline and perovskite grains confirms their genetic links with CAL inclusions. A further increase in the Fe concentration is associated with the full dissolution of CAL fragments in the chondrite matrix (Fig. 2, right-hand part of field III) and, correspondingly, characterizes the enrichment of the residual melt in elements typical of aluminous inclusions.

The Fe-rich matrix is heterogeneous both texturally and compositionally [4]. According to the crystallinity degree, there are two clearly distinct types of the matrix: M1 is highly crystalline, with typical features of melt textures, composes individualized patches (oxidized chondrules) or zones of eutectoid texture; and M2, which is cryptocrystalline or fine-grained, composes crystalline matrix patches and fills in all interstices between magnesian chondrules, actively penetrates and disintegrates the latter. The petrochemical alterations in the chondrite matrix (Fig. 3: *I*--oxidized chondrules, *II* - eutectoid zones, *III*—residual melt—solution) are readily comparable with the zones of active magmatic replacement of CAL inclusions by the matrix melt (Fig. 2: zone 3). Analysis of the changes in major-component concentrations during the magmatic replacement of CAL inclusions by the matrix melt and during the development of silicate chondrules in the oxidizing stage of the

melt evolution demonstrates clearly pronounced cause-and-effect relations in the specifics of differentiation of the matrix melt of oxidized carbonaceous chondrites. On the one hand, silicate assemblages can segregate from the matrix melt only if the latter is enriched in alumina and alkalis, which were provided, judging from the character of the magmatic replacement, by CAL inclusions (their relict and shadow textures are ubiquitously discernible in the chondrite). On the other hand, the segregation of oxidized chondrules results in a more significant depletion of the residual melt in Si and Mg and, correspondingly, a more notable Fe enrichment as compared to the matrix material of less oxidized CV chondrites.

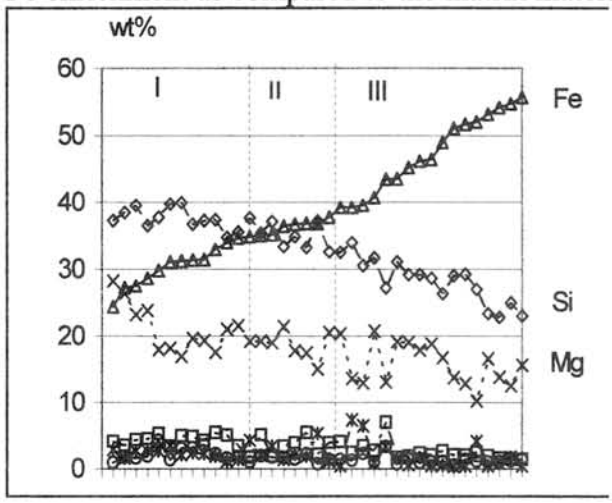

Fig. 3. Petrochemistry of elements in matrix crystallization zones.

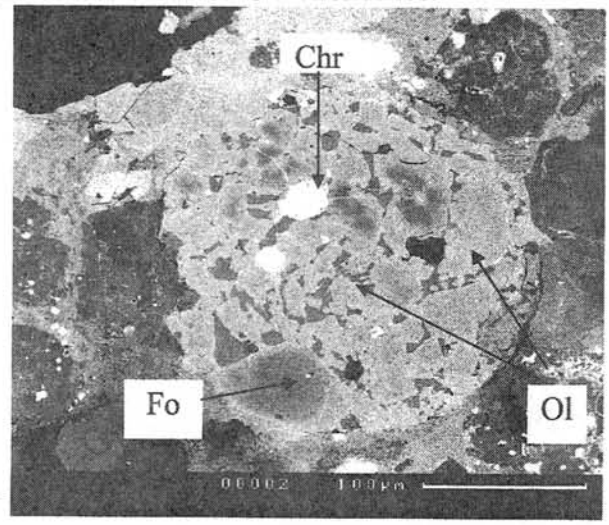

Fig. 4. Oxidized chondrule with a porphyritic texture, zonal olivine, and pyroxene-plagioclase glass.

The discrete character of changes in the compositions of the segregating silicate mineral assemblages, which is, in turn, highlighted by the discreteness in the olivine compositions, strongly suggests that they segregated from the melt because of liquid immiscibility in the latter.

The presence of so-called "oxidized" chondrules of the matrix type in the Kainsaz meteorite indicates that the redox potential of the environment changed here earlier than it did in chondrites of the CV3 type, in which an analogous change in the redox potential either is characterized by a much smaller magnitude or occurred at lower temperatures, which were insufficient for a similarly active interaction with the refractory constituents, which provided alumina and alkalis for the melt when replaced by it and caused a subsequent shift of the differentiation trend toward the acid region and the origin of high-Fe associations. It seems to be the activity of the magmatic replacement processes that can account for the relatively low (as compared to carbonaceous chondrites of the CV type) concentrations of refractory constituents in CO chondrites at similar bulk concentrations of alumina and alkalis.

Acknowledgments: This work was supported by Russian Foundation for Basic Research, grant 00-05-64607 and Program "Universities of Russia - Basic Researches".

References: [1] Marakushev&Bezmen (1983) *Evolutsiya meteoritnogo veschestva planet i magmanicheskich seriy*, Moscow: Nauka-press, p.184; [2] King (1976) *Space geolodgy*, New York-London-Sydney-Toronto, Willey&sons, p.378; [3] Marakushev et al. (1992) Kosmicheskaya petrologiya, Moscow, p.325; [4] Mitreikina&Zinovieva (1999) Abstr. of 24 Symp. Antarct. Meteor., Tokyo, 1999, 105-107.

Impact Crater Investigated from Surface and Drilled Samples of Takamatsu MKT Crater in Japan

Yasunori MIURA, and Atsushi Hirota

Department of Earth Sciences, Faculty of Science, Yamaguchi University, Yoshida, Yamaguchi 753-8512, Japan. yasmiura@po.cc.yamaguchi-u.ac.jp

Abstract

From collected samples of surfaces and borehole at Takamatsu MKT crater in Japan, the crater is considered to be buried and broken impact crater at active islands. Quartz grains with the PDFs (abbreviated from plane deformation features) have been found in granitic rocks and breccias. The PDFs in the quartz mineral grains (measured on a Universal-Stage) occur in the the (10$\bar{1}$2), (10$\bar{1}$3) and (10$\bar{1}$1) crystallographic directions. New drilled samples from surface to 1,600m in depth are similar rocks with surface samples located at south rim of the present crater where there are small andesitic intrusions to transport it to the surface. The original size of the crater is considered to be ca.8km which is modified by small volcanic intrusions at the south rim of the present crater finally to ca.4km in size.

1. Introduction: Crater "MKT" used in this paper is a crater located in Takamatsu, Kagawa Prefecture, Shikoku, Japan is a buried ellipsoidal feature defined by ca. 4-km diameter [1,2] with negative gravity anomaly and by ca. 8km semi-circular structure in an area of Late Cretaceous (ca.90 Ma) Rhyoke granitic rocks [3-9]. Main purpose of the present paper is to propose definition of impact-related event on volcanic and tectonic regions by using bulk compositions, aging, shocked materials of shocked quartz minerals with linear and cross-lamellae, and Ni-rich particles [9].

2. Definition of impact-related events on volcanic and tectonic islands: Almost all impact craters with shocked materials are defined on stable continents which basement are not moved or changed through long terrestrial surface history by plate-tectonics or continental drift. We requires more detailed data of impact craters if we propose new impact crater in tectonic regions as the following proposed indicator and evidence of impact crater in volcanic islands.

1) Obvious difference of aging data connected to impact and volcanic event with older impact age. On the Takamatsu MKT crater, U-Pb zircon dating data of related rocks in the crater are "granitic rocks" of basements (80-97Ma) or "spherule" formation event formed by impact ejecta (15.3Ma) [3-9]. There are no fragments and brecciated rock with the same aging data of Setouchi volcanic event (14 to 12 Ma [2]) in such zircon data of the MKT crater. Therefore, K-Ar dating of related rocks in the crater reported by Japanese volcanologists [2] as possible large volcanic event (ca.14Ma) to form large rhyolitic rocks is considered to be followed volcanic and hydrothermal activities on the active islands of Japan [8,9]. The formation of "the Sea of Japan" and "the Seto-Inland Sea" covers the original crater resulting in "buried or broken semi-circular crater" [3-9].

2) Minor and clear evidence of impact event in bulk chemical compositions and shocked minerals. Impact-related data and materials on the severe tectonic regions, are considered to be minor and small mainly because of strong crushing process followed by volcanic intrusions, earthquakes and land-slides [3-9]. The following five indicators are strong evidences to define impact-related crater in active islands or continental margins.

a) Gravity anomaly: There is negative gravity anomaly on ca.4km [1], though there is larger ca.

8km semi-circluar structure from satellite-image and topological data without clear gravity anomaly [3-9]. The large semi-circular structure is considered to be broken by later tectonics (Fig.1).

b) Clear difference of impact age with later volcanic event: Although K-Ar dating of crater rocks and sediments shows age of the Setouchi volcanic event (14 to 12 Ma) which is considered to be "metamorphic" event (not large volcanic event), but the stable age of zircon data in the MKT crater is U-Pb dated at 15.3 (±0.3) Ma inferred to be the age of the crater structure which is determined by zircon fragment included in glassy spherule shown in Fig.2 [3-9]. The glassy spherule with granitic composition indicates that impact event might be produced on the granitic target rocks near the of the old continents before forming the Sea of Japan, where large crater structure was considered to be broken at the formation of the Seto-Inland Sea.

c) Different bulk compositional data of impact-related rocks and volcanic rocks: All rock types of buried crater with covered sediment and small intrusions can be checked by the XRF bulk data. In fact, there are clearly basement rock of granites and rhyolitic rocks on the MKT crater [9]. From XRF data, there are three types of granites. (1) Granitic rock-1, (2) granitic rock-2, and (3) shocked granite block. There are clearly two zeolite-rich crater sediments: (1) Whitish mordenite-rich sediments, and (2) reddish zeolite-rich sediments. Four types of suevite-type breccias with high Y contents which suggests that it comes direct from granitic basements. Glassy rock which cannot be explained by large volcanic event. On the outer ring of 8km we found two types of breccia-3 (in the sample TK-22 of suevite type rocks), which is close to Mien type rhyolite (i.e. impact glass). Bulk composition of shocked granitic rock of sample TK23 is plotted in the area of the breccia-4. Such various variation of brecciated and granitic rocks are considered to be impact-related process followed by tectonic process of the Japan islands [8,9].

d) Shocked quartz minerals with linear and crossed lamellae: Shocked quartz with clear linear and crossed lamellae is found in the granitic breccia and red breccia in the MKT crater. As quartz mineral has no cleavage or crossed texture in general, such complex lamellar texture is caused by impact shocked process same as in the continental crater (Fig.3) [3-9].

e) Fe-Ni rich grains in glassy spherules: These glassy breccias were found to contain small Ni-rich grains (1 to 94% Ni) in glassy spherules, which cannot be found at volcanic and granitic regions so far, as shown in Fig.5.

3. Shocked minerals: A few quartz grains with planar deformation features (PDFs) have been found in clasts in granitic rocks and breccia outcrops within and around the crater. The PDFs in the quartz grains (measured on a U-Stage) occur in the ($10\bar{1}2$), ($10\bar{1}3$) and ($10\bar{1}1$) crystallographic directions indicative of intermediate shock pressures (Figs.3,4). Feldspar grains showing deformation lamellae and diaplectic glass have been found in granitic clasts with glassy clasts and in the matrix of suevite melt breccias outside the gravity anomaly rim [7-10]. Although quartz with planar and crossed features and possible diaplectic glass are found so far, though further tectonic and volcanic process including buried metamorphism destroys the original Impact texture and minerals in the present MKT crater.

4. Formation Process of the crater: Crater depth starting the similar granite in the bottom is the 1,140m in depth in this borehole analysis. Such deep crater can be well explained by wider diameter of ca. 8km observed by satellite and topographic images. Crater size of ca.4km found by gravity

anomaly is secondary modified crater after small andesitic intrusion at the south side of the crater. In fact, very sharp slope of water at the south side on Jissouji-yama which was one main reason for cauldron volcanic theory of the crater can be well explained by secondary intrusion of andesite from bottom of the original impact crater. From these drilled samples, non-volcanic formation of the original crater is obtained by the following reason:

1) There are no active volcanic rocks of andesite or basalt samples at drilled samples under 230m.
2) We found basement rock of hard granitic rock below 1,140m without any volcanic rocks.
3) This structure is no case of volcanic depression (cauldron) structure because of no volcanic rock to fill it.

After formation of impact crater by meteoritic impact which is proved by shocked quartz on the granitic rocks, the melted breccias of brownish and black mixed layers are deposited for ca.760m in thickness in the crater. Zeolitic layer are formed followed by the Mitoyo group layer. These drilled samples show typical sedimentary layer process with vertical change (compared 2with vetitcal change of magmatic evolution) after the crater formation. Original crater size of *ca.*8km in size with 1,140m in depth (Named MTK crater[7,8,9,10]) was broken by uplift of small andesitic intrusions (with ca.14Ma age) to form smaller size of *ca.*4km in present gravity anomaly reported by Kono (originally called as Takamatsu crater[1]). From at least two steps formation impact and volcano in the same crater, it should be called as joint name of "Takamatsu MKT" crater.

The Takamatsu MKT impact event occurred in target rocks of Late Cretaceous Rhyoke granite on the proto-Japanese islands located near the continental margin at *ca.*15.3 Ma followed by developing an southward opening of the Sea of Japan. The crater was filled and eventually buried during formation of the Japanese Islands to the present location. Original MKT crater structure with 8km in diameter and 1,140m in depth is broken during the northward formation of the Seto-Inland Sea, followed by small basaltic andesite volcanism around and inside the MKT structure at about 14.2 Ma to break original crater structure to form present crater of *ca.*4km in size.

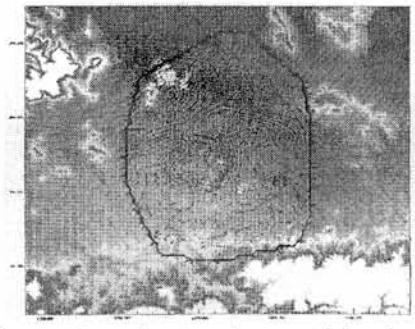

Fig.1. Gravity anomaly to show clear inner ring and broken ellipsoidal structure of Takamatsu MTK crater in Japan [7-9].

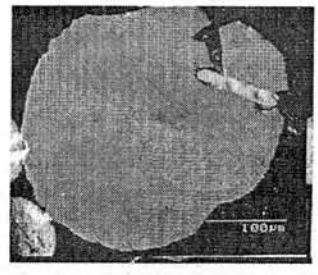

Fig.2. Electron micrograph with the BEI of glassy spherule with zircon mineral [8,9].

Fig.3. Multiple PDFs of shocked quartz in the Takamatsu MKT crater in Japan [7-9]..

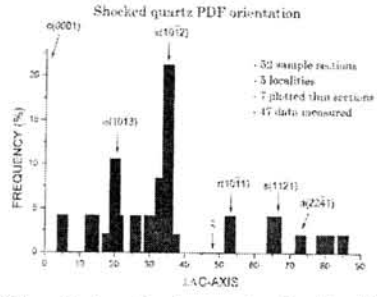

Fig.4. Orientation plot of the PDFs of shocked quartz in the Takamatsu MKT crater in Japan [7-9].

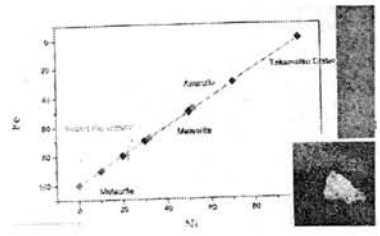

Fig.5. Fe-Ni Contents of metallic fragments in breccias of the Takamatsu MTK crater in Japan [3-9].

5. Summary: The following is summary of the present study.

1) New type of impact-related event can be defined at active tectonic regions by using semi-ellipsoidal structure, and shocked quartz with single and crossed lamellae.

2) Quartz grains with the PDFs have been found in granitic rocks and breccias, with the $(10\bar{1}2)$, $(10\bar{1}3)$ and $(10\bar{1}1)$ crystallographic directions.

3) Preliminary borehole samples indicate the typical sedimentary process in the crater is observed at horizontal change between silica-rich layer and breccias until basement of granitic rock.

4) Original crater size of *ca.*8km in size with 1,130m in depth (Named MTK crater[7,8,9,10]) was broken by uplift of small andesitic intrusions (with *ca.*14Ma age) to form smaller size of *ca.*4km in present gravity anomaly reported by Kono *et al.* [1](originally called as Takamatsu crater).

References: [1] Furumoto M., Kono Y. and Miura Y.(1996): Proc. Int. Symp. Obs. Cont. Crust through Drilling, 8, 172-177. **[2]** Yamada R. and Sato H. (1998): GANKO (in Japanese). 93, 279-290. **[3]**Miura Y. (1999): Materials Proc.Tech. (Elsevier), 85, 192-193. [4] Miura Y. and M. Kedves (2000): Invest. Earth, Ed.by Miura Y. (Japan), 1, 6-7. 8-13. [5] Miura Y. et al. (2000): LPS XXXI(LPI,CD) 2096.1519.1645. [6] Miura Y. et al. (2000): Adv.Space Res.(Pergamon), 25, 285-288. [7] Miura Y., Y.Uedo and M.Rampino (2001): LPS XXXII ,1981. [8] Miura Y. (2001): Meteoritics and Planetary Sciences, 36(9), 136-137. [9] Miura Y. and Maeda T. (2001): Proc. 34th ISAS LPS, 33, 183-186.[10] Miura et al. (2002): LPS XXXIII (LPI, Houston), 33, 1231-1232.

Noble gases in ordinary chondrites : A study on "Ar-rich" component.

Yayoi N. Miura[1], Naoji Sugiura[2], Kaoru Kiyota[1] and Keisuke Nagao[3]

[1] Earthquake Research Institute, University of Tokyo, Yayoi, Bunkyo-ku, Tokyo 113-0032, Japan.
[2] Department of Earth and Planetary Science, University of Tokyo, Hongo, Bunkyo-ku, Tokyo 113-0033, Japan.
[3] Laboratory for Earthquake Chemistry, Graduate School of Science, University of Tokyo, Hongo, Bunkyo-ku, Tokyo 113-0033, Japan.

Introduction

Some unequilibrated ordinary chondrites (UOCs) and CO3 chondrites show more abundant Ar and Ar/Xe ratios higher than "Q"-gas. This component (hereafter Ar-rich gas) seems to be related to isotopically light nitrogen, because both Ar and isotopically light nitrogen are released at the same temperatures under stepped combustion experiments [1,2]. In the previous study [1], 8 out of the measured 24 UOCs have been assigned as a group characterized by the isotopically light nitrogen (hereafter ALH-77214-type based on the name of the representative sample). Most ALH-77214-type UOCs which include H, L, LL chondrites show abundant Ar than other UOCs. Similar characteristics have been observed in CO3 chondrites [2, 3]. Our recent studies on noble gases for some ALH-77214-type UOCs and CO3 chondrites confirmed that Ar is mostly released around 1100 °C under vacuum pyrolysis and the observed $^{36}Ar/^{132}Xe$ ratios are up to ~400, clearly higher than that of "Q"-gas [4, 5]. In order to characterize Ar-rich gas in further detail and clear the origin, we have performed additional noble gas measurements.

Samples and experimental methods

ALH-77167 (L3.4) and ALH-77278 (LL3.7), classified into ALH-77214-type based on nitrogen isotopes [1], are studied in this work. Because it has been reported that HCl-etching or HF/HCl-etching removed large fractions of light nitrogen [1] or Ar [6], whole rock samples and samples applied for HCl-etching have been prepared for noble gas analyses. Small pieces of each sample have been crushed to fine-grained. About 5 mg without chemical treatment (designate WR) and HCl-treated fraction (designate HCl) were analyzed using a mass spectrometer (modified VG5400) at Laboratory for Earthquake Chemistry, University of Tokyo. Conditions of HCl treatment were 3M-HCl 3 hours (ALH-77167 HCl-a) and 1M-HCl 3 hours (ALH-77167 HCl-b and ALH-77278 HCl) at the room temperature. Noble gases were extracted by heating samples stepwisely at temperatures 700, 900, 1000, 1100, 1200, 1300, 1500 and 1700 °C.

Results and discussion

The concentrations of ^{36}Ar, ^{40}Ar, ^{84}Kr and ^{132}Xe are summarized in Table 1. Gases released from 700 °C step are excluded in discussion about trapped component below, because majority

of Ar, Kr and Xe except radiogenic ^{40}Ar seems to be of adsorbed terrestrial atmosphere on the basis of elemental and isotopic compositions. The whole rock samples contain large amounts of trapped Ar and show higher Ar/Xe ratios ($^{36}Ar/^{132}Xe$ is 285 and 185 for ALH-77168 and ALH-77278, respectively). The HCl-treatments left about 40-60 % of their masses, and removed about 90 % of trapped ^{36}Ar, 70–80 % of ^{84}Kr and 60–70 % of ^{132}Xe (Table 1 and Fig. 1). After HCl-treatment the $^{36}Ar/^{132}Xe$ ratios around 1100 °C steps and sum of the ratio from all temperatures became lower and close to that of "Q" (Fig. 2). This indicates that Ar-rich gas is removed by HCl-treatment, that is, it is contained in an HCl-soluble phase or possibly in very fine grains which have been recovered insufficiently during chemical treatment. From difference in measured concentrations between the whole rock and HCl-treated samples, $^{36}Ar/^{132}Xe$ ratio in the HCl-soluble phase is estimated to be ~350 for ALH-77167 and ~250 for ALH77278, respectively.

In spite of distinct Ar/Xe and Kr/Xe ratios from "Q", the isotopic compositions of Ar, Kr and Xe for Ar-rich gas in the whole rock samples are similar to those of "Q". The $^{38}Ar/^{36}Ar$ ratio at 1100 °C of ALH-77167, where cosmogenic contribution may be negligible, is obtained to be 0.1884 +/- 0.0003, which is close to the ratio reported for "Q"-Ar. The Xe isotopic ratios are also similar to those of "Q"-Xe within experimental errors except for terrestrial Xe at 700 °C and Xe-HL around 900 °C.

In order to clarify the degassing characteristics, diffusion parameters are calculated based on the amounts of released gases from each temperature. The obtained values of D/a^2 plot against temperatures (=Arrhenius plot; D is the diffusion coefficient and a is a characteristic size of a sample), which could be helpful for considering host phase(s) of gases. The data for ^{36}Ar and ^{84}Kr of the whole rock samples do not lie on a straight; change of slops is seen at 1100 °C. On the other hand, the data of ^{36}Ar, ^{84}Kr and ^{132}Xe for HCl-treated samples show a better straight line excepting the data of the lowest and highest temperatures. Similar plots are examined for other chondrites without Ar-rich gas, ALH-90411 (L3.7) and Y-82094 (CO3). These chondrites do not contain (or less contain) Ar-rich gas and releases of Ar are appeared at higher temperatures. Their data of each chondrite make a straight line on the Arrhenius plot. The current observations indicate that trapped Ar of the whole rock samples of ALH-77167 and ALH-77278 is in two different phases: one is HCl-soluble phase from where Ar-rich gas is released around 1100 °C, and the other is HCl-insoluble phase (including phase "Q") from where "Q"-gas is released at higher temperatures.

References

[1] Sugiura N., Kiyota K. and Hashizume K. (1998) *Meteoritics Planet. Sci.* 33, 463-482. [2] Kiyota K., Sugiura N. and Zashu S. (2000) *Antarctic Meteorites* XXV, 48-49. [3] Taniguchi Y. and Hashizume K. (1997) *Antarctic Meteorites* XXII, 188-190. [4] Miura Y.N., Sugiura N., Kiyota K. and Nagao K. (2001) *Antarctic Meteorites* XXVI, 85-87. [5] Miura Y.N. (2001) *Meteoritics Planet. Sci.* 36, A137. [6] Schelhaas N., Ott U. and Begemann F. (1990) *Geochim. Cosmochim. Acta* 54, 2869-2882. [7] Busemann H., Baur H. and Wieler R. (2000) *Meteoritics Planet. Sci.* 35, 949-973. [8] Huss G.R., Lewis R.S. and Hemkin S. (1996) *Geochim. Cosmochim. Acta 60*, 3311-3340.

Table 1. The concentrations of Ar, Kr and Xe.

Samples		$^{36}Ar^{\#}$	^{40}Ar	$^{84}Kr^{\#}$	$^{132}Xe^{\#}$
ALH-77167	WR	72.9	2480	34.6	25.6
	HCl-a	4.20	2770	5.60	6.68
	HCl-b	6.92	2870	6.39	6.75
ALH-77278	WR	17.0	6320	11.3	9.36
	HCl	2.97	5160	3.01	3.41

^{36}Ar and ^{40}Ar are given in unit of 10^{-8} cm^3STP/g, and ^{84}Kr and ^{132}Xe are of 10^{-10} cm^3STP/g.
Gas from 700 °C is excluded because we assume it the terrestrial atmospheric origin.

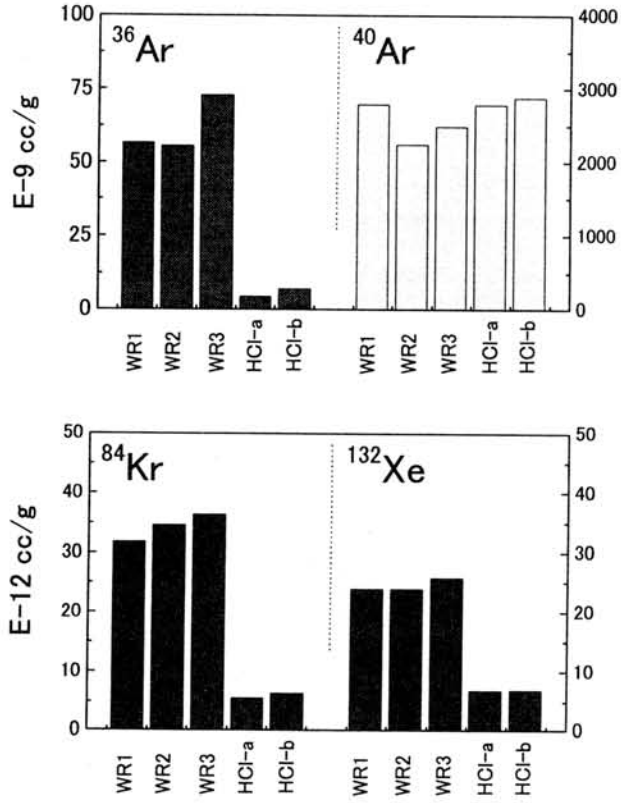

Fig. 1. The concentrations of ^{36}Ar, ^{40}Ar, ^{84}Kr and ^{132}Xe for ALH-77167. WR-3 is the sample studied here, and WR-1 and WR-2 are also whole samples we measured before [4, 5]. Trapped Ar, Kr and Xe are largely removed by HCl-etching.

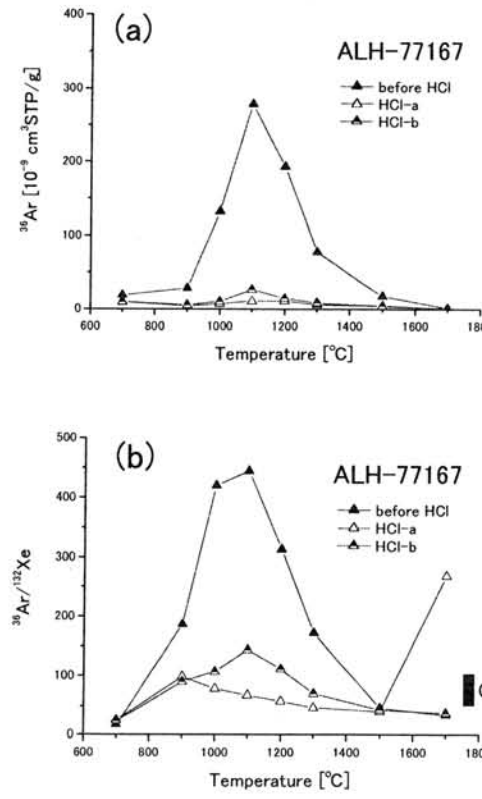

Fig. 2. Release profiles: (a) ^{36}Ar vs. extraction temperatures and (b) $^{36}Ar/^{132}Xe$ vs. extraction temperatures for ALH-77167. The $^{36}Ar/^{132}Xe$ ratios are higher than that of "Q" around 1100 ℃ for the whole rock sample, whereas the ratios become lower after HCl-treatment. Reference data for "Q" are from [7, 8].

Measurement of Si isotopic compositions by SIMS

T.Mizuno, N.Sugiura, T.Ushikubo and H.Hiyagon

Department of Earth and Planetary Science, University of Tokyo

Si is the major element in planetary materials in the solar system. It has three isotopes. Hence presolar isotopic signature can be detected based on the isotopic composition. Also, mass-dependent fractionation of Si can be used for detecting cosmochemical processes such as evaporation. Since the diffusion rate in silicates is known to be slow, it may preserve isotopic compositions more effectively than other elements and hence may be particularly useful for such cosmochemical purposes.

In spite of such potential usefulness, its use has been mostly limited to detecting isotope anomalies in presolar silicon carbide. This is partly because presolar silicates had not been found until this year. Also, with respect to isotope fractionation effects, it has been hampered by the difficulty in measuring the fractionation precisely by SIMS. (Hua, et al.,2001)

Here, we report our up-to-date method of the Si isotope measurements. In the SIMS measurements, the primary ion beam (O-) of 0.3 nA is focused to an area of 30 micrometers in diameter. The secondary ion Si is measured as Si+ ions. All three isotopes are measured by EM in the pulse-counting mode. The Si isotope measurement is difficult because distribution of the secondary ion energy is much broader than that of other ions such as Mg. This makes the secondary ion beam broader, which in turn makes the instrumental mass fractionation more variable depending on the measurement conditions. Therefore, the most important factor for precise Si isotope measurements is to make the measurement condition exactly reproducible. Depending on the set-up conditions of the ion probe, the mass fractionation could easily change by more than 10 permil. Under our experimental condition, the deviation (2 sigma) of ^{30}Si for a standard sample is about 2 permil, which is not much larger than the error expected from counting statistics.

In addition, there are large differences in the instrumental mass fractionation among various minerals. We examined Quartz, Anorthite, Enstatite, Diopside, Akermanite, Gehlenite, Forsterite, Fayalite and San Carlos Olivine. These terrestrial samples can be considered to have normal Si isotopic compositions. The fractionations of ^{30}Si relative to normal Si isotopic composition are shown in Fig.1. The fractionations range from –38 to –69 permil. With such large fractionations among minerals, it is essential to compare the fractionation in target samples with that in appropriate standard samples.

The degree of instrumental mass fractionation is related to the efficiency of ionization, which is in turn related to the chemical composition of the minerals. The mass fractionation of ^{30}Si appears to be correlated with the Si concentration in minerals (Fig.2). Si is rather inefficiently ionized compared with the other cations (Ca,Al,Mg,Fe etc). Therefore, a possible explanation for the correlation in

Fig.2 is as follows. There is a competition between Si and the other cations for ionization. In the presence of the other cations which ionize efficiently, Si cannot be efficiently ionized, which results in a larger Si mass fractionation. Admittedly, the correlation in Fig.2 is not very strong, which suggests that there must be some other factors that control Si mass fractionation measured by SIMS. In particular, in the case of olivine solid solution, San Carlos olivine that has an intermediate composition shows smaller mass fractionation than end-member olivine samples. A similar observation has been made by Hua et al.(2001) and the cause is yet to be clarified.

Preliminary measurements of Si fractionation in CAIs have been made. At present, we still have slight problems in making precise measurements on CAIs. In these measurements, CAI samples and standard samples are set in different holders and hence the measurement conditions could be somewhat different, possibly causing large uncertainties in the mass fractionation measurements. At the symposium we will present up-to-date results of Si isotopic fractionation on CAIs.

References

Hua.X et al.(2001) MAPS 36, A85.

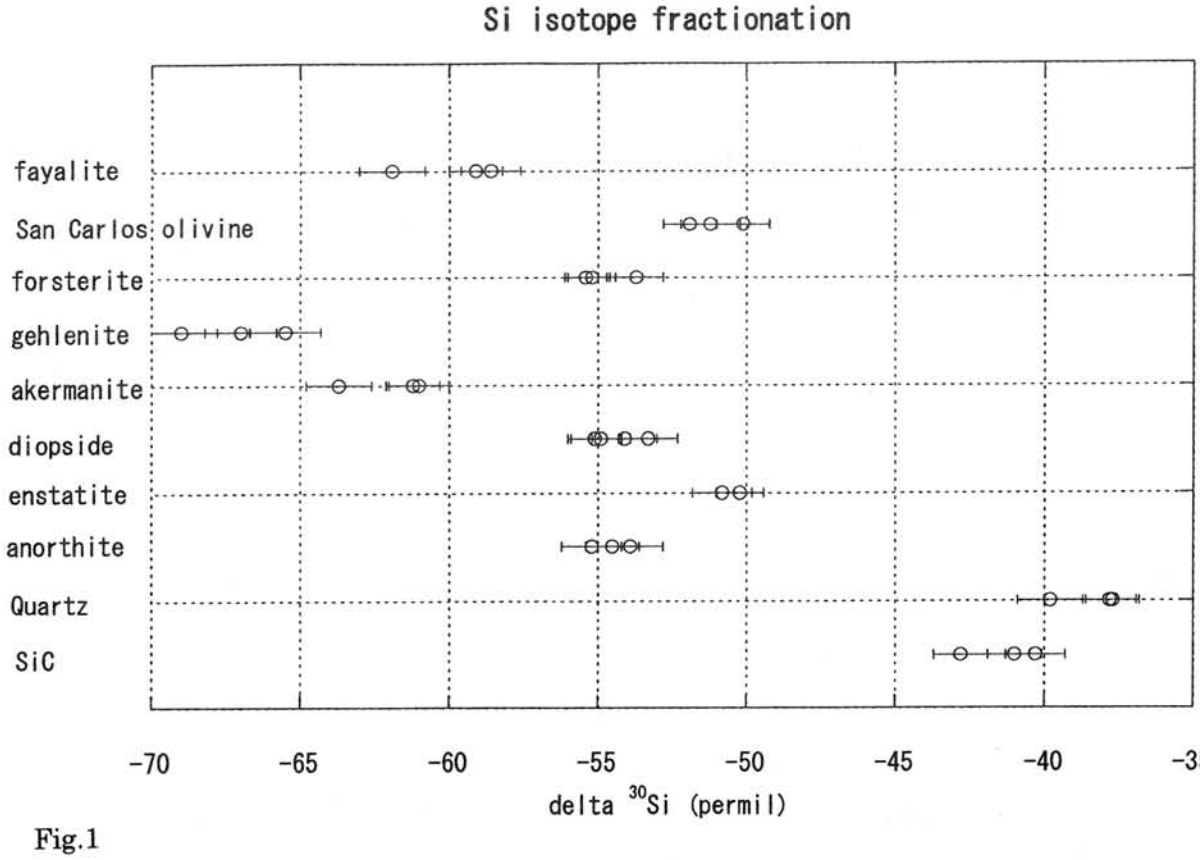

Fig.1

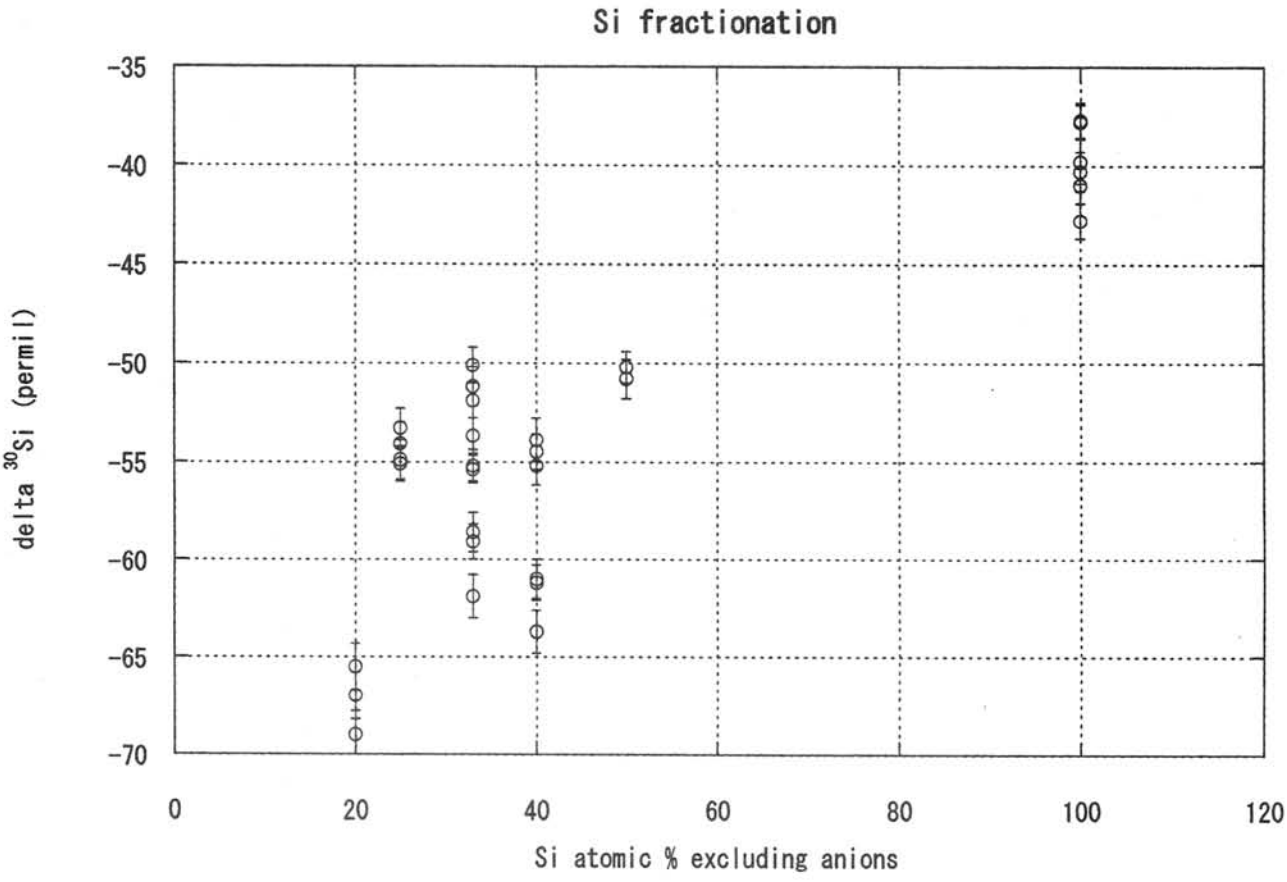
Si fractionation
delta ^{30}Si (permil)
-35
-40
-45
-50
-55
-60
-65
-70
0
20
40
60
80
100
120
Si atomic % excluding anions

Fig.2

On the formation of Ti-rich kaersutite amphiboles in Martian meteorites

A. Monkawa[1], T. Mikouchi[1], M. Miyamoto[1], E. Koizumi[1], Y. Miyata[2], and K. Ohsumi[2]

[1]*Department of Earth and Planetary Science, Graduate School of Science, University of Tokyo 7-3-1 Hongo, Bunkyo-ku, Tokyo 113-0033, Japan*

[2]*Institute of Materials Structure Science, High Energy Accelerator Research Organization 1-1 Oho, Tsukuba, Ibaraki 305-0801, Japan*

1. Introduction

Kaersutite is a member of the amphibole mineral group and is characterized by its Ti-rich (*pfu* of Ti > 0.5) content. Kaersutite has been widely recognized in mantle xenoliths that are entrained in both alkali basalts and kimberlites. Although kaersutites are extremely rare in extraterrestrial samples because of anhydrous environment during their formations, kaersutites occur in magmatic inclusion in some Martian meteorites (*e.g.*, Treiman 1985). The presence of kaersutite in the Martian meteorites has been important in understanding water contents in Martian magmas and mantle. In fact, several attempts have been performed to estimate water contents in Martian magmas and mantle (*e.g.*, Johnson et al., 1991). However, Martian kaersutites are unique in their water-poor and Ti-rich nature compared with terrestrial kaersutites. In this abstract, we discuss a formation process of Ti-rich kaersutites in Martian meteorites according to textural observation and chemical analysis of magmatic inclusions and compared with terrestrial Ti-rich kaersutite (Amami-Oshima, Japan).

2. Results

We observed kaersutite-bearing magmatic inclusions in Zagami (Fig. 1), NWA 856 and LEW 88516 (Fig. 2) Martian meteorites. The size of magmatic inclusions is usually 100-200 μm long and their shapes are irregular. Kaersutite-bearing magmatic inclusions occur only within pyroxene, although olivine (in the case of LEW 88516) also contains similar magmatic inclusions in constituting phases. Kaersutites often coexist with Al-Ti-rich augite, Si-rich glass, magnetite, and hercynite spinel. The important observation is that kaersutites almost always have contact with Al-Ti-rich augite and Si-rich glass. The size of kaersutites is up to 20 μm long. Minor Ca phosphate (merrillite), pyrrhotite, and ilmenite are also present in some cases.

The TiO_2 contents in Martian kaersutites are 8.8 wt% (Zagami), 8.8 wt% (NWA 856), and 10.3 wt% (LEW 88516), respectively (Table 1). We observed significant amounts of Fe^{3+} contents in theses kaersutites estimated by electron microprobe (Monkawa *et al.*, 2002). Unfortunately, we have not analyzed the OH contents of these kaersutites, but Watson *et al.* (1994) reported the OH content of 0.1-0.2 wt%. We also analyzed Martian kaersutites by micro-area synchrotron X-ray diffraction technique (Laue method) developed at BL-4B$_1$ of Photon Factory, High Energy Accelerator Research Organization in Tsukuba, Japan (Ohsumi *et al.*, 1991). We could not obtain diffraction spots, suggesting that they are poorly crystalline or amorphous. Mikouchi and Miyamoto (2000) analyzed kaersutites in Zagami and LEW 88516 by micro Raman spectroscopy and detected Raman peaks characteristic of kaersutites. Therefore, Martian kaersutites would be poorly crystalline.

3. Discussion and Conclusion

So far several studies have been performed to explain the formation of Ti-rich kaersutites observed in Martian meteorites (*e.g.*, Johnson *et al.*, 1991; Minitti and Mysen, 2001). The parent magma that crystallizes Ti-rich kaersutite would be an alkaline and Ti-rich magma. However, it is likely that Fe-Ti oxides would co-crystallize under such a condition. In fact, the crystallization experiments produced coexistence of kaersutite and Fe-Ti oxides (*e.g.*, Johnson *et al.*, 1991). In these cases, kaersutites are always Ti-poor because of the preceding crystallization of Fe-Ti oxides prior to the kaersutite crystallization (Johnson *et al.*, 1991). In kaersutite-bearing magmatic inclusions in Martian meteorites, Fe-Ti oxides (ilmenite or ulvöspinel) are rarely present. Therefore, we need to consider some unusual formation condition to produce Ti-rich kaersutites without Fe-Ti oxides.

Tiepolo *et al.* (1999) pointed out that Ti-rich kaersutites (*pfu* of Ti > 0.8) are not stable due to structural constraint of amphibole. Nevertheless, some terrestrial camptonite rocks (e.g., Amami-Oshima, Japan) contains Ti-rich kaersutites (*pfu* of Ti > 0.9) (Kanisawa *et al.*, 1983) and their Ti-rich contents are comparable to those of Martian kaersutites (Table 1). Probably, these camptonitic kaersutites are most Ti-rich among terrestrial samples. However, the formation of camptonitic kaersutites is quite different from that of Martian kaersutites because camptonite is believed to have formed by hydrothermal metamorphism.

One possible explanation for the formation of Martian Ti-rich kaersutites is a shock origin. When the magmatic inclusion originally contained Fe-Ti oxides, the Ti-rich kaersutites might have been formed by reaction of Al-Ti-rich augite and Si-rich glass plus Fe-Ti oxides during shock. The textural observation of kaersutite-bearing magmatic inclusion is consistent with this assumption. If Fe-Ti oxides were consumed to form Ti-rich kaersutites, we could explain the absence of Fe-Ti oxides in kaersutites-bearing magmatic inclusions. This hypothesis could also explain that only shergottites contain kaersutites, although nakhlites contain similar magmatic inclusions. The degree of shock for nakhlites (~20 Ga) (Greshake, 1998) would not be enough to form kaersutites. If this is the case, the Ti-rich (*pfu* of Ti > 1.0) and water-free nature of Martian kaersutites could be explained.

However, it is not clear for Chassigny whether kaersutites were really formed by shock because biotite coexists with kaersutites in Chassigny (Johnson *et al.*, 1991). The estimated shock degree for Chassigny (~35 Ga) is higher than that for nakhlites (Langenhorst and Greshake, 1999). Detailed observation of Chassigny kaersutites is necessary. We are planning to perform shock experiments of mixtures of Ti-augite, Si-glass, and Fe-Ti oxide to further explore this possibility.

Large incorporation of Fe^{3+} and Ti^{4+} would be necessary to keep charge balance because of the water-poor nature of Martian kaersutites. Although Ti is a ubiquitous minor component in amphiboles in general, it is important in Martian amphiboles. The behavior of Ti in amphiboles is not very well characterized. Further research on Ti in amphibole would be necessary to understand Martian interior condition and formation of Ti-rich kaersutites.

4. References

Greshake A. (1998) *Meteorit. Planet. Sci.*, **33**, Suppl. A63. Johnson M. C. *et al.* (1991) *Geochim. Cosmochim. Acta.*, **57**, 4769-4783. Kanisawa S *et al.* (1983) *J. Mineral. Petrol.*, **78**, 394-404. Langenhorst F. and Greshake A. (1999) *Meteorit. Planet. Sci.*, **34**, 43-48. Mikouchi T. and Miyamoto M. (2000) *Meteorit. Planet. Sci.*, **35**, 155-159. Minitti M. E. and Mysen B. O. (2001) *11th V. M. Goldschmidt Conf.*, Abst. #3419. Monkawa A. *et al.* (2001) *Lunar Planet. Sci.* **XXXII**, Abst. #1620 (CD-ROM). Ohsumi K. *et al.* (1991) *J. Appl. Cryst.*, **24**, 340-348. Tiepolo M. *et al.* (1999) *Eur. J. Mineral.*, **11**, 345-354. Treiman H. (1985) *Meteoritics*, **20**, 227-242. Watson L.L. *et al.* (1994) *Science*, **265**, 86-90.

Table 1. Chemical compositions of kaersutites in Amami-Oshima, Japan (amami) and Martian meteorites

	amami	LEW88516	Zagami	NWA856
SiO_2	37.17	36.98	37.76	36.97
TiO_2	8.04	10.31	8.84	8.83
Al_2O_3	13.83	15.61	14.49	14.18
Cr_2O_3	0.00	0.38	0.03	0.44
Fe_2O_3†	2.17	4.25	3.50	3.39
FeO	8.97	9.93	15.96	14.89
MnO	0.07	0.30	0.84	0.29
MgO	11.33	8.93	5.44	6.58
CaO	12.39	11.04	11.02	10.71
Na_2O	2.60	1.36	2.45	2.39
K_2O	1.10	0.47	0.09	0.12
H_2O*	1.44	0.20	0.20	0.20
Total	99.09	99.74	100.61	98.99

* amami=manometry analysis; three meteorites from Watson et al. (1994).
† determination of Fe_2O_3 content by EPMA analysis

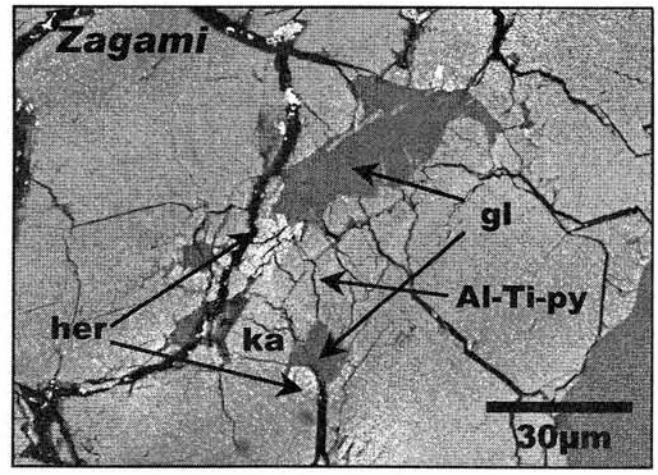

Fig. 1. Backscattered electron image of melt inclusion in Zagami. Kaersutite: ka. Al-Ti-rich pyroxene: Al-Ti-py. Si-rich glass: gl. Hercynite: her.

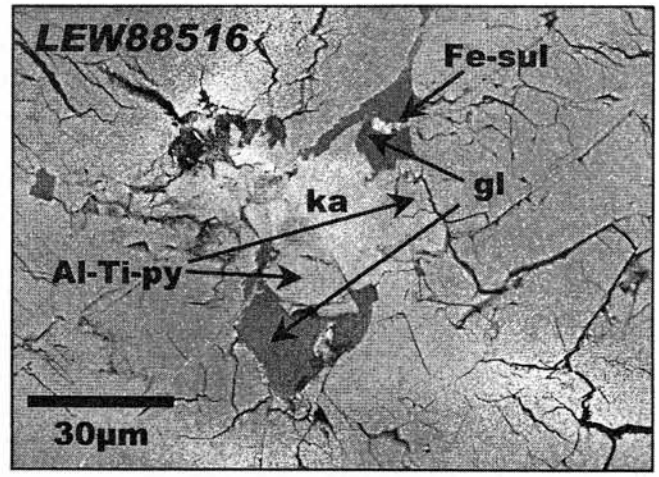

Fig. 2. Backscattered electron image of melt inclusion in LEW 88516. Kaersutite: ka. Al-Ti-rich pyroxene: Al-Ti-py. Si-rich glass: gl. Hercynite: her. Iron sulfide: Fe sul.

INCONGRUENT EVAPORATION OF OLIVINE AT LOW TEMPERATURE

Hiroko Nagahara and Kazuhito Ozawa
Department of Earth and Planetary Science, University of Tokyo
Hongo, Tokyo 113-0033, Japan
(hiroko@eps.s.u-tokyo.ac.jp, ozawa@eps.s.u-tokyo.ac.jp)

Introduction

Partial evaporation of pre-existing minerals is one of important processes that caused chemical and isotopic fractionation in the primitive solar nebula. Olivine, most abundant anhydrous mineral, was shown to evaporate stoichiometrically to magnesian olivine and gas with iron-rich olivine composition in both equilibrium and kinetic conditions (Nagahara et al., 1994; Ozawa and Nagahara, 2001), with large Mg-Fe fractionation. This causes not only Mg/Fe fractionation but also Mg/Si fractionation, and thus played an important role in chemical evolution of the solar system. We, however, experimentally found that olivine evaporates incongruently to form Mg-rich pyroxene at low temperatures.

Experimental

San Carlos olivine (Fo91-92) was cut into slab parallel to three major axes, which was heated in vacuum at temperatures of 1300, 1400, and 1500°C for 3 to 240hours. Each experimental run was carried out for a set of three slabs with larger surface area of (100), (010), and (001). The weight loss and the surface microstructures were observed with an EDS and analyzed with an EPMA after the run, and the compositional zoning from surface to interior in a vertical section was measured. The anisotropy of evaporation rate, chemical fractionation factor, and diffusion rate was simultaneously optimized for a set of experiment.

Results

The olivine evaporated keeping stoichiometry at 1500 and 1400°C regardless of experimental duration and crystallographic orientation, and the residue remained to be olivine. It has become magnesian at the surface with compositional zoning toward interior, and the surface composition and the width of the zoning vary with temperature and duration of experiments. On the contrary, it appears to evaporate incongruently at 1300°C on the (010) surface. The residue has small crystals with lower Mg/Si ratio on the surface, and the composition is very close to Mg/Si=1, which is indicative of being pyroxene. A small amount of Fe was detected in the "pyroxene", of which amount lowers with increasing duration. The phase appears to be enstatite on the basis of X-ray intensity with EPMA, but we have not yet confirmed it with the X-ray diffraction method. The surfaces of (100) and (001) have a stoichiometry of olivine as well as higher temperature experiments.

Discussion

The possible surface composition of enstatite on the surface of (010) shows incongruent evaporation of olivine to magnesian pyroxene, which further indicates the selective evaporation of FeO and formation of pyroxene at the surface. This may be due to much higher volatility of FeO than SiO2 from olivine. The higher volatility of FeO than SiO2 has been experimentally shown for evaporation of silicate melt (Hashimoto, 1983), and the present results are consistent with the behavior of silicate melt.

The presence of enstatite only on the (010) surface is thought to be due to the difference in the bonding energy of Si-O in the three crystallographic orientations. The (010) surface is the only plane of cleavage of olivine, which means the bonding energy of Si-O within this surface is strong compared to other surfaces. Due to stronger Si-O bonding, Fe evaporates with oxygen keeping the charge balance from the (010) surface.

The present results predict that evaporation of olivine and Mg/Fe fractionation between solid and gas are highly suppressed once the surface of olivine is coated by enstatite, which prolongs the lifetime of Fe-bearing olivine. Once enstatite covers the surface, evaporation of olivine is controlled by the decomposition of olivine to enstatite and FeO and the transportation of the FeO component through the boundary layer (enstatite) by diffusion. Enstatite, on the other hand, is shown to evaporate incongruently to forsterite and Si-rich gas (Tachibana et al., 2002) at a very small rate, thus remains long. Fe-bearing olivine thus remains long at temperatures as low as 1300°C and chemical fractionation is suppressed. Whether the growth of enstatite due to preferential evaporation of FeO from olivine is more rapid than the incongruent evaporation enstatite to forsterite or vice versa would depend on temperature and ambient PH2.

References

Hashimoto, A. (1983) *Geochem. Jour.* **17**, 111-145.
Nagahara, H., Kushiro, I., and Mysen, B. O. (1994) *Geochim. Cosmochim. Acta* **58**, 1951-1963.
Ozawa, K. and Nagahara, H. (2000) *Geochim. Cosmochim. Acta* **64**, 173-189.
Tachibana, S., Tsuchiyama, A., and Nagahara, H. (2002) *Geochim. Cosmochim. Acta* **66**, 713-728.

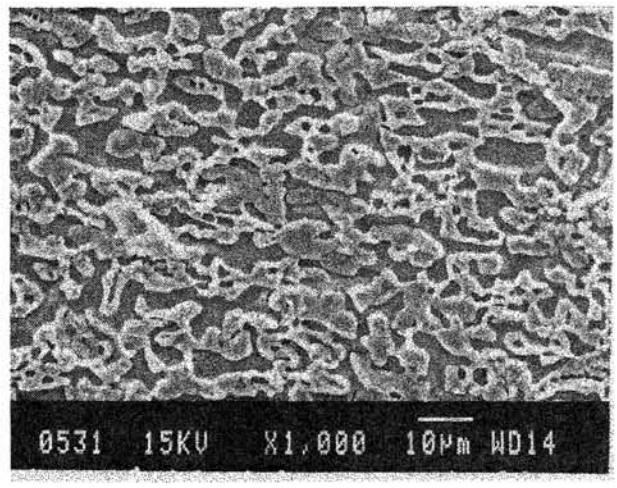

Fig. 1 SEM photograph of the surface of (010) surface of San Carlos olivine heated at 1300°C for 60 hours in vacuum. The bright portion has enstatite composition and the dark portion remains to be olivine composition.

Noble gases of Yamato 981031 lunar meteorite

K. Nagao and R. Okazaki

Laboratory for Earthquake Chemistry, Graduate School of Science, University of Tokyo, Bunkyo-ku, Tokyo 113-0033, Japan. (nagao@eqchem.s.u-tokyo.ac.jp)

Introduction

Yamato (Y) 981031 lunar meteorite has been collected by the meteorite search party of the 39th Japanese Antarctic Research Expedition, and is expected to be paired with Y793274 lunar meteorite based on the texture, mineralogy and bulk composition (Kaiden and Kojima, 2002). Mineralogical study on the Y981031 suggests source-crater paring of Y981031, Y793274 and QUE94281, which are brecciated mare basalts with some highland components (e.g., Arai et al., 2002). However, disagreement between the ejection ages of QUE94281 and Y793274 exclude the source-crater pairing (e.g., Nishiizumi and Caffee, 1996; Polnau and Eugster, 1998). We measured noble gases of Y981031 to confirm the predicted paring with Y793274 and to obtain noble gas signatures characteristic for materials derived from the lunar surface.

Experimental procedure

Noble gases were extracted from two chips weighing 0.1851g and 0.0579g by stepwise heating, and then measured on a modified-VG5400 (MS-II). The temperatures were 400, 600, 800, 900, 1000, 1100, 1200, 1300, 1400, 1600 and 1800°C, though the experiment was accidentally stopped at 1300°C on the sample 0.1851g due to leakage of vacuum of purification line.

Results and discussion

Isotopic ratios of He, Ne and Ar and concentrations of all noble gases are listed in Table 1. Noble gas elemental and isotopic compositions for 0.0579g specimen are characterized by solar composition with small contributions of cosmogenic gases. Huge amounts of He (1.0×10^{-3}cm^{3}STP ^{4}He), Ne (2.3×10^{-4}cm^{3}STP ^{20}Ne) and Ar(1.1×10^{-4} cm^{3}STP ^{36}Ar) were released. The noble gas concentrations and those of cosmogenic ^{21}Ne and ^{38}Ar, 314 and 520 $\times10^{-9}$cm^{3}STP/g respectively, agree well with the reported values for Y793274, indicating long duration (ca. 500Ma) of irradiation by galactic cosmic-rays as well as solar wind particles on the lunar surface as described for Y793274 by Eugster et al. (1991) and Takaoka and Yoshida (1992). Trapped ^{40}Ar/^{36}Ar=2.4, which is an antiquity indicator of regolith breccia, is also

similar to 2.3 for Y793274 (Eugster et al., 1991). Based on the ratio, breccia compaction age of Y981031 is estimated to be about 900Ma using the calibration curve proposed by Eugster and Polnau (1997). All the noble gas signatures determined for Y981031 support the paring with Y793274 lunar meteorite.

Noble gas release patterns show that He and Ne are released in the temperature range of 800-1000°C, while heavier noble gases Ar, Kr and Xe released at higher temperatures of 1100-1300°C, with sharp increases at the extraction temperatures of 800°C for He and Ne and 1200°C for Ar, Kr and Xe. $^{20}Ne/^{22}Ne$ ratio was as high as 12.5 at the lower temperatures (400-900°C), and then decreased approaching to a mixing line between cosmogenic and SEP-like Ne components (Fig. 1). $^{3}He/^{4}He$ ratios are similar to that of solar wind at low temperatures (400-900°C), and approach to SEP He at about 1100°C. In higher temperature fractions (>1100°C), the $^{3}He/^{4}He$ ratios increase due to cosmogenic He. Contrary to He and Ne, $^{38}Ar/^{36}Ar$ ratios at the temperatures lower than 1400°C are 0.190-0.198, which are much lower than the value of SEP-Ar (0.205: Benkert et al., 1993). High energy solar gas is minor component in the total Ar trapped in this meteorite. This may indicate a presence of low energy solar particles firmly trapped in some phases of this meteorite. These data indicate that most of low energy particles have been lost before arrival to the earth, probably due to gas loss by shock heating on the lunar surface

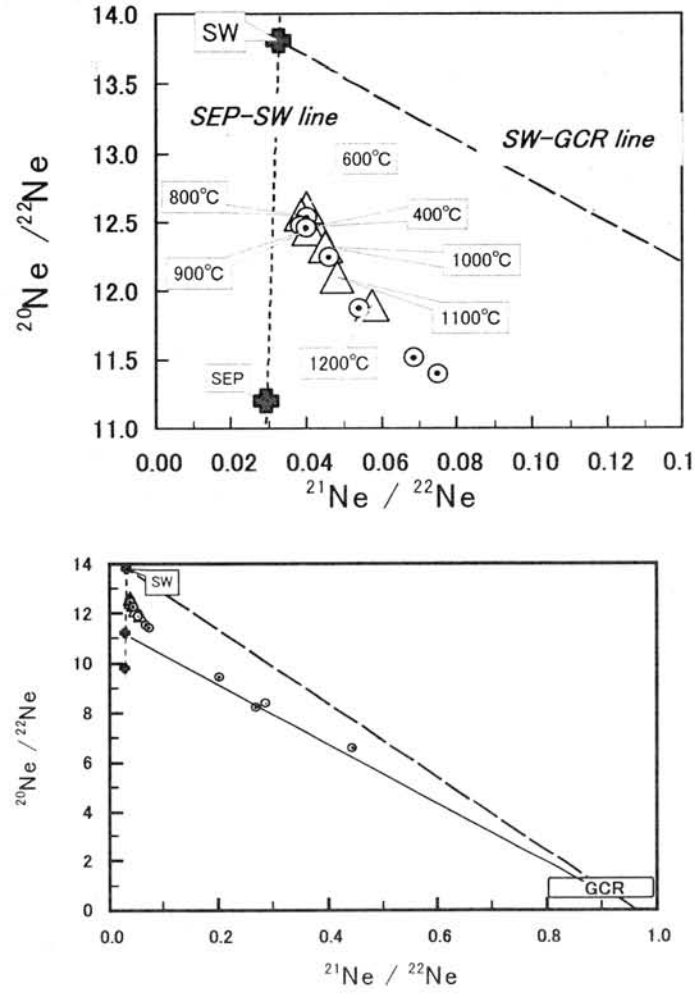

Fig. 1. Ne three isotope plot

Fig.2 shows elemental ratios of heavy noble gases Ar, Kr and Xe. The $^{36}Ar/^{132}Xe$ ratios higher than that for lunar soil (10,000-17,000) are observed at the most temperature steps, and

the values of 185,000 (800°C for 0.0579g specimen) and 172,000 (900°C for 0.1851g specimen) are much higher than the ratio (=67,000) for solar abundance. This may be due to larger diffusion coefficient for Ar compared with those for heavier gases Kr and Xe.

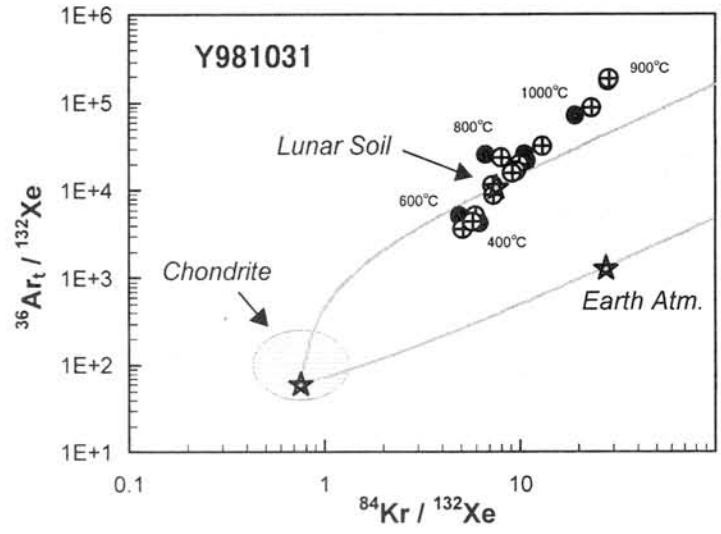

Fig. 2 Elemental ratios of heavy noble gases

References

Kaiden H. and Kojima H. (2002) *LPS* **33**, abstract #1958; Arai T. et al. (2002) *LPS* **33**, abstract #2064; Eugster O. et al. (1991) *GCA* **55**, 3139-3148; Takaoka N. and Yoshida Y. (1992) *Proc. NIPR Symp. Antarct. Meteorites* **5**, 36-48; Nishiizumi K. and Caffee M.W. (1996) *LPS* **27**, 959-960; Polnau E. and Eugster O. (1998) *MAPS* **33**, 313-319; Eugster O. and Polnau E. (1997) *LPS* **28**, 341-342; Benkert J.-P. (1993) *JGR* **98** (13), 147-162.

Table 1. Concentrations and isotope ratios of Y981031 lunar meteorite.

Temp.	^{4}He	$^{3}He/^{4}He$	^{22}Ne	$^{20}Ne/^{22}Ne$	$^{21}Ne/^{22}Ne$	^{36}Ar	$^{38}Ar/^{36}Ar$	$^{40}Ar/^{36}Ar$	^{84}Kr	^{132}Xe
400 °C	5790	0.000550 ± 0.000008	81.3	12.539 ± 0.021	0.0403 ± 0.0004	44.8	0.1898 ± 0.0005	6.108 ± 0.014	28.8	3.92
600 °C	16800	0.000522 ± 0.000002	330	12.479 ± 0.022	0.0386 ± 0.0004	51.6	0.1922 ± 0.0005	7.614 ± 0.016	17.6	2.17
800 °C	718000	0.000615 ± 0.000002	9550	12.462 ± 0.026	0.0401 ± 0.0004	2740	0.1982 ± 0.0004	4.460 ± 0.009	423	14.7
900 °C	207000	0.000492 ± 0.000002	3540	12.246 ± 0.019	0.0461 ± 0.0005	4170	0.1947 ± 0.0005	2.777 ± 0.006	1110	47.3
1000 °C	59600	0.000407 ± 0.000002	2070	11.876 ± 0.028	0.0541 ± 0.0005	2100	0.1974 ± 0.0004	2.731 ± 0.006	855	65.0
1100 °C	26700	0.000344 ± 0.000001	1540	11.517 ± 0.024	0.0686 ± 0.0007	9380	0.1926 ± 0.0005	2.484 ± 0.005	4750	474
1200 °C	2410	0.000628 ± 0.000003	1240	11.398 ± 0.018	0.0750 ± 0.0007	83400	0.1909 ± 0.0005	2.405 ± 0.006	48200	4990
1300 °C	155	0.002407 ± 0.000017	157	9.430 ± 0.017	0.2032 ± 0.0020	7760	0.1958 ± 0.0005	2.727 ± 0.006	6480	875
1400 °C	40.9	0.003753 ± 0.000048	16.9	6.574 ± 0.018	0.4455 ± 0.0044	1690	0.2024 ± 0.0005	2.937 ± 0.007	1940	325
1600 °C	69.7	0.007803 ± 0.000041	5.19	8.377 ± 0.022	0.2877 ± 0.0029	880	0.2034 ± 0.0005	3.117 ± 0.006	1240	240
1800 °C	10.3	0.000283 ± 0.000021	0.865	8.219 ± 0.038	0.2696 ± 0.0029	151	0.1979 ± 0.0004	3.155 ± 0.007	197	34.1
Total	1036576	0.000571	18531	12.174	0.0493	112367	0.1921	2.522	65241	7071

Sample weight: 0.0579g; Concentrations of He, Ne and Ar in unit of 10^{-8}cc/g and of Kr and Xe in 10^{-12}cc/g.

In Situ Observation of Carbonaceous Globules in the Tagish Lake Meteorite: Possible Products of Primitive Organic Reactions

Keiko Nakamura[1], Michael E. Zolensky[2], Satoshi Tomita[3,4], Kazushige Tomeoka[1]

[1] *Department of Earth and Planetary Sciences, Faculty of Science, Kobe University, Japan.*
[2] *Office of Astromaterials Research and Exploration Science, NASA Johnson Space Center, Houston, USA.*
[3] *Department of Electrical and Electronics Engineering, Faculty of Engineering, Kobe University, Japan.*
[4] *Nanomaterial Processing Laboratory, Institute of Physical and Chemical Research(RIKEN), Saitama, Japan*

Correspondence author's e-mail address: keiko@nc.scitec.kobe-u.ac.jp

Introduction: Tagish Lake is a unique carbonaceous chondrite with ~1.3 wt. % carbon that mostly occurs as organic components including interstellar SiC and graphite [1]. Over the last decade, workers have succeeded in characterizing extracts of refractory organics and interstellar materials from meteorites [2], however work on acid soluble organics has not proceeded at the same pace; especially lacking are studies of organic phases *in situ* to elucidate their original morphologies and mineralogical context. Here we report *in situ* observation of carbonaceous grains in Tagish Lake with a novel hollow spherical morphology. These globules may have formed from hydrophobic hydrocarbons during aqueous alteration on the asteroid.

Sample preparation: Multiple fragments were picked from matrix of a Tagish Lake sample and ultramicrotomed for TEM investigation, complemented by EDX and EELS. Our TEM observations, originally made using epoxy-impregnated samples, were duplicated using a pure sulfur filler in place of epoxy, which precludes the possibility that carbonaceous phases in the specimens are simply epoxy embedding resin and indicates that they are indigenous meteoritic material.

Results: Numerous hollow, bubble-like "globules" have been observed from the phyllosilicate-rich matrix, with a distribution of one for every of 100 μm^2 (Fig.1). The globules have apparent diameters of 140-1700 nm; and wall thicknesses of 30-200 nm. Cylindrical or tapered forms have not been observed. These globules often display a layered structure. Some globules contain saponite flakes between layers (Fig.1). The EDX spectra of the globules show that they consist predominantly of C, associated with minor amounts of O, Si, S, Fe and Cl. The presence of these latter elements is probably due to analytical contamination from the surrounding matrix and included saponite flakes. Hydrogen is undoubtedly also present, but not detectable by this analytical technique. An EELS spectrum shows that the globules consist of amorphous carbon, indicating that this material has never been significantly heated, otherwise the carbon would have crystallized to poorly graphitized carbon.

Discussion and conclusion: Direct observation of such amorphous carbon globules has not been previously reported from meteorites, although organics extracted from Murchison form similar structures when

dispersed in alkaline-buffered water [3]. The carbon globules in Tagish Lake are also similar to the vesicle-forming compounds produced by the simulation of some interstellar ice mixture photolytic products [4]. Authors in [4] suggested that they could have formed naturally if such interstellar ice mixture photolyzation products fell into weakly alkaline aqueous environments on the early Earth, and serve as one of the organic precursors to life. The carbon globules in Tagish Lake may have formed in a similar manner, but did so on a primitive asteroid rather than on Earth. The survival of the structures, as well as the large amount of associated interstellar material, indicates that the parent asteroid for Tagish Lake was unusually cold for its entire history.

References: [1] P.G. Brown et al., *Science*, 290, 320 (2000) [2] T.J. Bernatowicz and E. Zinner., *in AIP Conf. Proc. Astrophysical Implications of the Laboratory Study of Presolar Materials*, p402 (1997) [3] D.W. Deamer, *Nature*, 317, 792 (1985) [4] J.P. Dworkin, et al., *Proc. The National Academy of Science* 98, 815 (2001)

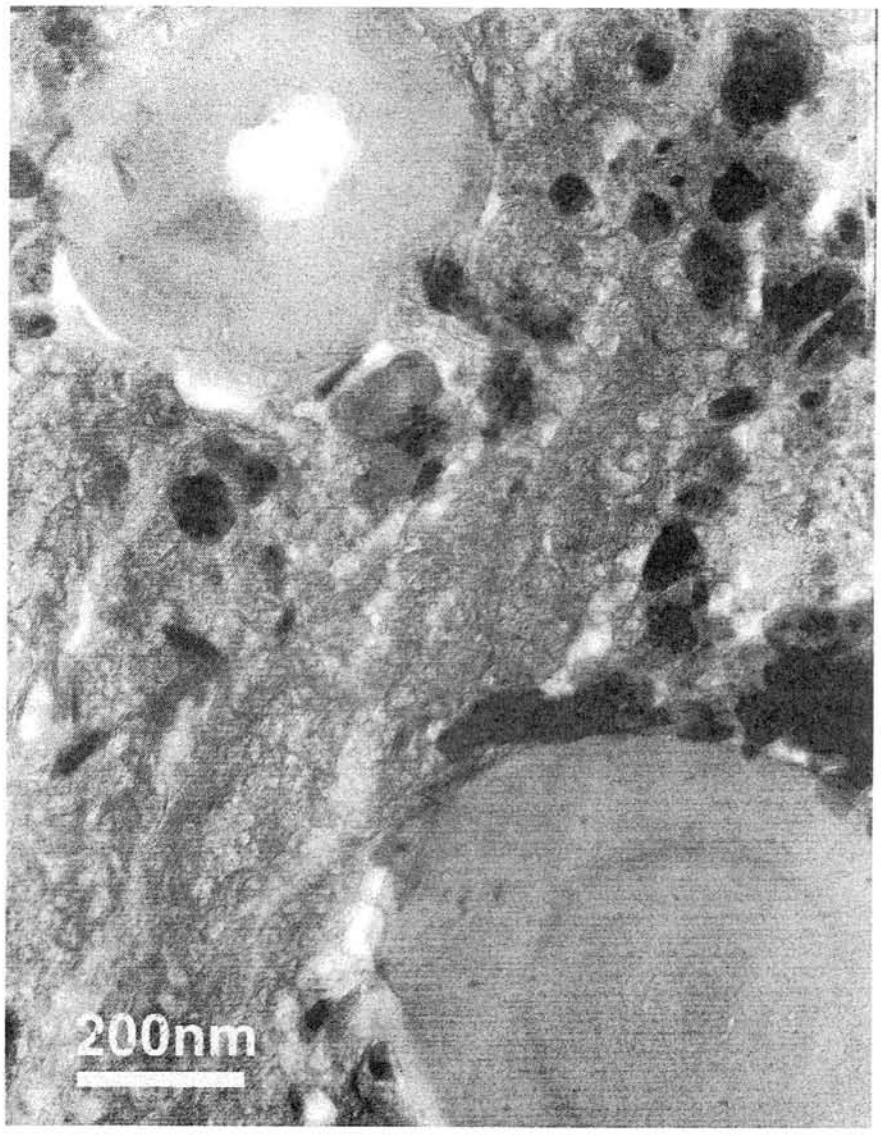

Figure 1: The amorphous carbon globule at lower right has a concentric form, and tiny bubbles (~5nm) between each spherical layer. There is an empty core in the carbon globule at upper left, and saponite flakes are situated between the layers of this sphere, as well as bubbles. The matrix consists of fine grained crystals of saponite with an entangled ribbon-like structure. The grains in dark contrast are sulfides.

REE ABUNDANCES AND Rb-Sr AGE OF A NEW ANTARCTIC NAKHLITE YAMATO 000593.

Noboru Nakamura[1,2], Akane Yamakawa[1], Katsuyuki Yamashita[1], Toshinori Kobayashi[1], Naoya Imae[3], Keiji Misawa[3] and Hideyasu Kojima[3]

[1]Department of Earth and Planetary Sciences, Faculty of Science, and also at [2]Graduate School of Science and Technology, Kobe University, Nada, Kobe 657-8501, Japan. (noboru@kobe-u.ac.jp)

[3]Antarctic Meteorite Research Center, National Institute of Polar Research, Tokyo 173-8515, Japan.

As part of consortium study on a new Antaractic nakhlite, Yamato 000593 (hereafter Y000593) and Y000749 [1], we have undertaken a high precision REE and Rb-Sr, Sm-Nd and U-Pb isotopic analyses. Here present preliminary results of lithophile trace elements and Rb-Sr systematics for Y000593. The preliminary results of Pb isotopes will be presented elsewhere [2].

As shown in Fig. 1, Y000593 exhibits a highly fractionated lithophile trace element (including REE) pattern quite similar to that of Nakhla [3]. The REE abundances in Y000593 are systematically higher than those in Nakhla and the fractionation feature of light-REE-Ba-Sr-Rb is even more pronounced compared to Nakhla. This is consistent with the fact that the new nakhlite contains more abundant mesostasis (mesostasis content; 15% for Y000593 and 8.5% for Nakhla) [1]. It is pointed out that Y000593 has a minor negative Eu anomaly. The lithophile element abundance features as pointed out here appears to be common for Nakhla and Y000593, suggesting that Y000593 was derived by a series of fractionation process from a common (or similar) magma source.

The results of Rb-Sr isotopic analyses for Y000593 is presented in Fig. 2. At present, we have analyzed one whole rock and two hand-picked mineral samples. The green mineral phase constitute major part of the meteorite, representing clinopyroxene. The brown mineral fraction, on the other hand, probably represents a fraction dominated by olivine. In a Rb-Sr isotopic evolution diagram, the green mineral phase exhibits the lowest $^{87}Rb/^{86}Sr$ ratio and the brown phase exhibits the highest. All three data points show a linear array, which define a regression line corresponding to an age of 1269 ± 240Ma and an initial $^{87}Sr/^{86}Sr$ ratio of 0.70251 ± 0.00038. Because of limited samples analyzed here, a larger spread in $^{87}Rb/^{86}Sr$ ratio has not been obtained and thus the age and the initial $^{87}Sr/^{86}Sr$ ratio include large errors. Therefore, further analyses of other phases such as plagioclase and mesostasis are required to confirm this preliminary result.

From our preliminary trace element and isotopic analyses, it is unlikely that the meteorite suffered significant terrestrial contamination or weathering. Our results clearly indecate that the major mineral phases of the meteorite experienced a young event at about 1.3 Ga. It is also pointed out that the Rb-Sr age and the initial $^{87}Sr/^{86}Sr$ ratio of Y000593 are in complete agreement with those of Nakhla [4,5]. It is possible that the meteorite was derived from a magma source with same or similar chemical and isotopic characteristics, as also suggested

from the REE abundances mentioned above.

References: [1] Imae, N. et al. (2002) LPS XXXIII # 1483 (CD-ROM). [2] Yamashita, K. et al. (2002) Antarctic Meteorites XXVII, (this volume). [3] Nakamura, N. et al. (1982) GCA 46, 1555-1573. [4] Gale, N. H. et al.(1975) EPSL 26, 195-206. [5] Papanastassiou D.A.and Wasserburg, G. J. (1974) GRL 1, 23-26.

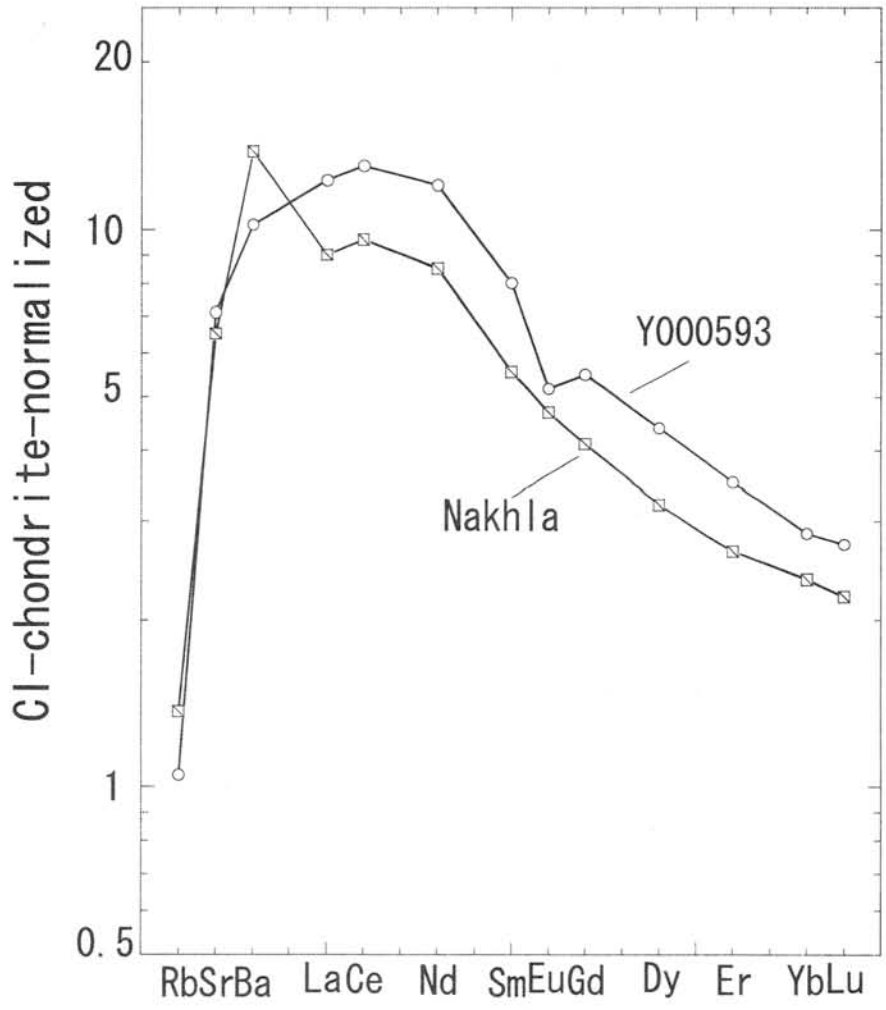

Fig. 1.

CI-chondrite normalized lithophile eement abundance pattern for Y000593 compared with that of Nakhla.

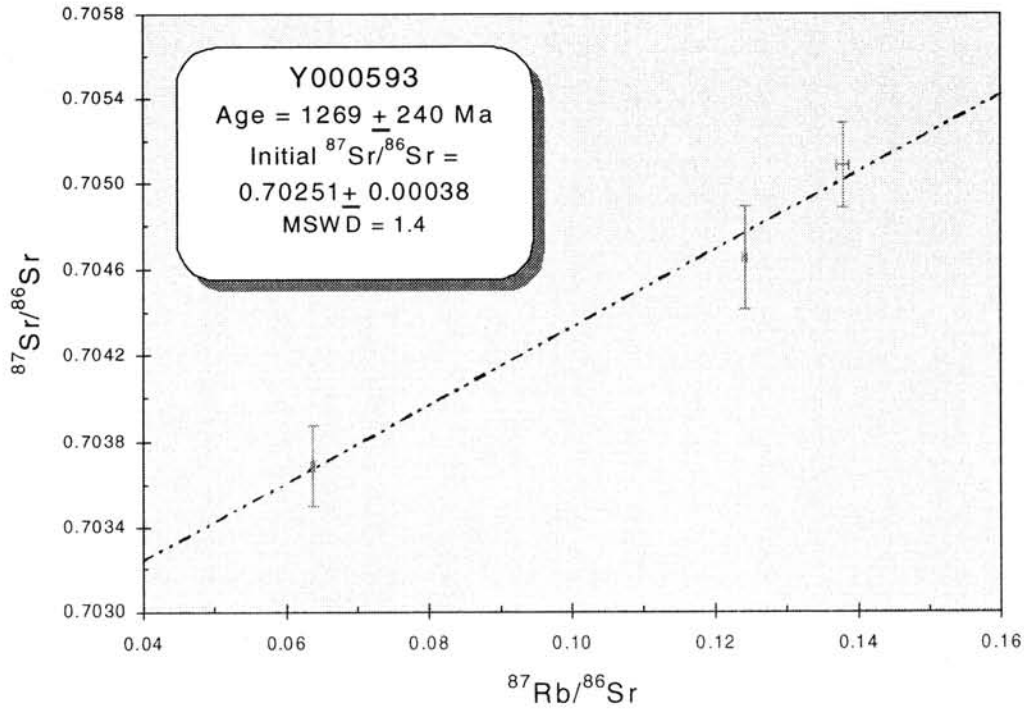

Fig. 2.

Rb-Sr isotopic evolution diagram for the Y000593 meteorite. The lowest data point represent the green colored mineral phase (clinopyroxene), the middle data point represents whole rock, and the highest data point represents the brown colored phase represents probably olivine.

Heterogeneous oxygen isotope ratios of olivine in chondrules in the Allende CV3 chondrite

Nakamura T[1]., Akaki T[1]., Watanabe H[1]., Yada T[2]., and Noguchi T[3].

[1]*Department of Earth and Planetary Sciences, Kyushu University, Hakozaki, Fukuoka 812-8581, Japan*

[2]*Department of Earth and Planetary Sciences, University of Tokyo, Bunkyo, Tokyo 113-0033, Japan*

[3]*Department of Materials and Biological Science, Ibaraki University, Bunkyo 2-1-1, Mito 310-8512, Japan*

Olivine is the most common mineral in chondrules and in certain types of inclusions. It is present in chondrules and inclusions as a result of crystallization from a melt and as a relic mineral that survived melting. Olivines in a totally melted chondrules like barred olivine types are expected to have constant isotopic ratios of oxygen due to homogenization in a melting chondrule [1], while those in amoeboid olivine inclusions, which are believed to be condensation products from hot nebula and escaped high degrees of melting [2], show heterogeneous oxygen isotopic ratios in the ^{16}O-rich regions in the three isotope diagram [2-3].

Chondrules were formed via various degrees of melting of preexisting solid materials and thus crystallized- and relic-olivines coexist in a single chondrule. The relic olivines may retain olivine isotopic ratios of chondrule precursors, although the isotopic exchange reactions at subsolidus temperature may modify the ratios toward the average value of the chondrule. In the present investigation, we have petrologically characterized 17 chondrules by back-scattered and CL imaging and electron-microprobe analysis, and then measured oxygen isotopic ratios of olivines in the chondrules using CAMACA ims 6f SIMS at Kyushu University. San Carlos olivine and pure forsterite crystals, both of which were measured for oxygen isotopic composition using a conventional mass spectrometer, were used as standard minerals. After correction of the instrumental mass fractionation by measurements of standard minerals in between sample analyses, the obtained isotopic ratios have average 1σ error approximately 2 ‰ both for δ^{17}O and δ^{18}O.

Out of 17 chondrules analyzed, four are barred olivine chondrules and the rest 14 are porphyritic chondrules. Three to twenty olivine grains in individual chondrules were measured for oxygen composition. Olivines in all barred olivine chondrules showed constant isotopic ratios within a chondrules, but the average compositions differ between the chondrules ranging δ^{18}O from 0 to 15 ‰ relative to SMOW. This indicates that oxygen isotope exchange in a single chondrule have prevailed during total melting.

Eleven out of 13 porphyritic chondrules have relatively constant oxygen isotopic ratios within single chondrules, but the average ratios differ among chondrules. Most chondrules have δ^{18}O between -8 to 10 ‰, thus isotopically lighter than barred olivine chondrules. The range of compositions is consistent with that of other workers [4]. Electron microscopy indicates that the diameters and fine textures, such as average grain sizes and modal ratios of olivine, pyroxene, and mesostasis, are different among the eleven chondrules. But there are no obvious correlations between the petrologic properties and oxygen isotopic ratios. CL imaging showed that some chondrules contain CL-bright olivine. Such olivine is usually coarse with sizes greater than 100 μm and locates outer portions of chondrules. Comparison between CL-bright and -dark olivines by electron-microprobe analysis showed that CL-bright olivines have consistently low FeO content less than 1.5 wt% and seem no apparent differences in concentrations

in other minor elements, suggesting that CL contrast may be due to differences in FeO concentrations. The CL-bright olivines show oxygen isotopic ratios similar to the CL-dark ones in chondrules analyzed, which is consistent with [5]. But there is one exception found in one chondrule as discussed below.

Two (chondrule A and B) out of 14 porphyritic chondrules show heterogeneous oxygen isotopic composition of olivine. They also show largest ^{16}O enrichment among chondrules analyzed in the present study. The $\delta^{18}O$ distribution is similar between the two chondrules and the range is approximately from -20 to 5 ‰. The range is similar to that of Al-rich chondrules in ordinary chondrites [6]. All data obtained fall on or close to carbonaceous chondrite anhydrous mineral line [1].

The two chondrules have many mineralogical features in common. They consist of two mineralogically different regions. First region consists of olivine and low-Ca pyroxene. The olivines are poikilitically enclosed by low-Ca pyroxene. Both olivine and low-Ca pyroxene have homogeneous chemical compositions whose averages are Fa5 and Fs1Wo1, respectively. The texture and composition suggest that they are crystallized from a melt. On the other hand, second region consists mainly of olivine, low- and high-Ca pyroxene, and anorthite. Contrast to the first region, olivine and pyroxene are compositionally variable with Fa3-10 and Fs1-2Wo1-43, respectively. Low-Ca pyroxene in the second region is richer in Al_2O_3 (up to 2.5 wt%), and Ti_2O (up to 1 wt%) than that in the first region (up to 1 and 0.3 wt%, respectively). Anorthite is An78-89Or0.1 and is partly replaced by nepheline, suggesting that the second regions suffered secondary alteration. The mineral assemblage of the two chondrules is basically similar to those of plagioclase-rich chondrules in carbonaceous chondrites defined by [7-9]. Compared with Al-rich chondrules in ordinary chondrites [6], the two chondrules found in Allende are absent from Al-rich spinel and Al-rich diopside.

Oxygen composition of olivine in the two chondrules seems to have no clear correlation to Fa# and grain sizes. But the most ^{16}O-rich olivines (down to -20‰) in both chondrules are located in the second region, have compositions approximately Fa5, and are dark in CL images. CL-bright coarse forsteritic olivine (Fa3) in the first region has ^{16}O-poor composition. The explanation for the ^{16}O enrichment and the wide range of isotope distribution for the two chondrules can be outlined in the same way as that proposed for Al-rich chondrules in ordinary chondrites [6]. Precursors of the chondrules were enriched in ^{16}O with intermediate isotopic ratios between CAIs and ferromagnesian chondrules and partial exchange of oxygen between ^{16}O-rich chondrules and ^{16}O-poor gaseous reservoirs during chondrule formation resulted in heterogeneous oxygen composition within chondrules. The secondary alteration might have some effects on the heterogeneity of oxygen composition, but the alteration seems not the main reason. Because olivines surrounded by nepheline show ^{16}O-rich composition. Although the two chondrules seem to form via complex processes, it must be emphasized that they are similar in mineralogy, show widest range of oxygen composition, and contain ^{16}O-richest olivines.

Acknowledgments: We thank Dr. Kusakabe for oxygen isotope analysis of standard minerals, Dr. Yamaguchi for CL analysis, Dr. Ninagawa for discussion on the CL imaging, and Mr. Shimada for electronprobe analysis.

References: [1] Clayton (1993) Ann. Rev. Earth Planet. Sci. 21, 115. [2] Krot et al. (2002), Science 295, 1051. [3] Hiyagon and Hashimoto (1999), Science 283, 828. [4] Leshin et al. (2001) LPSC XXXI, 1918 (CD-ROM). [5] Jones et al. (2002) LPSC XXXIII, 1604 (CD-ROM). [6] Russel et al. (2000) EPSL 184, 57. [7] Sheng et al. (1991) GCA 55, 581. [8] Krot (2000) MAPS 35, A93. [9] Krot et al. (2002) MAPS 37, 155.

Classification of ureilites based on characteristics of carbon minerals

NAKAMUTA Yoshihiro[1]*, AOKI Yoshikazu[2], and KOJIMA Hideyasu[3]

[1] *The Kyushu University Museum, Kyushu University, Fukuoka 812-8581, Japan;* [2] *Dept. Earth and Planetary Sciences, Faculty of Science, Kyushu University, Fukuoka 812-8581, Japan;* [3] *National Institute of Polar Research, 1-9-10, Kaga, Itabashi-ku, Tokyo 173-8515, Japan*

*Corresponding author's e-mail address: nakamuta@museum.kyushu-u.ac.jp

Introduction: Ureilites are unique in containing relatively large amounts of C occurring as graphite or diamond [1]. The mode of occurrence of carbon minerals and the presence of the compressed graphite in ureilites show that diamond in ureilites formed by high-pressure conversion of graphite that crystallized during igneous or metamorphic processes [2]. Coexistence of kamacite with diamond in all diamond-bearing ureilites strongly suggests that graphite was converted to diamond with iron as a catalyst [3]. In this study, mineralogical properties of graphite and diamond in ten Antarctic ureilites reserved at the NIPR in Tokyo were investigated by an X-ray line broadening analysis and these ureilites were classified based on the properties. Formation conditions of each ureilites were also discussed.

Experiments: Polished thin sections of ten ureilites listed in Table 1 were observed with reflected light through an optical microscope. Carbon-rich grains of 50-200 μm in size, 6-19 grains for each ureilite as shown in Table 1, were selected from crashed samples of each ureilite and were X-rayed by using a Gandolfi camera. Carbon minerals in ureilites are composed of graphite and diamond that show similar X-ray powder diffraction patterns among ureilites from which carbon-rich grains were obtained except for widths of each X-ray reflection line of them. The line broadening of the 004 and 110 reflections of graphite and the 110 reflection of diamond was evaluated in terms of the integral breadth, the value of a peak area divided by a peak height, which was determined precisely by using a profile-fitting technique.

Results and discussion: Reflected light views of carbon minerals in polished thin sections suggest that carbon minerals occur as well-crystallized graphite having a blade-like or an amoeboid shape and diamond formed by the conversion of such graphite crystals [2,3]. Mineral compositions of each carbon-rich grain are shown in Table 1. ALH 78019 and Y-82100 contain only graphite, Y-8448 and Y-74659 contain both graphite crystals and grains composed of graphite and diamond, and other six ureilites, ALH 77257, ALH 78262, Asuka 881931, MET 78008, Y-74123 and Y-74130 contain only grains composed of graphite and diamond. It is noteworthy that kamacite coexists with diamond in all samples, whereas kamacite can not be observed in graphite grains not containing diamond. Kamacite in Y-74123 shows X-ray diffraction lines shifted a little toward the higher angle side in X-ray patterns and suggests that it has a little smaller unit cell dimensions than the normal one maybe due to Si in the structure.

Integral breadths of 110 and 004 reflections of graphite in graphite-rich grains are plotted in Fig. 1. Fig. 1 shows that the integral breadths of 110 reflections of graphites have a positive linear correlation with those of 004 reflections, suggesting that the graphite crystals were strained equidirectionally. With experimentally shocked olivine crystals, Uchizono et al. showed that integral maximum breadths of olivine have a linear relation to the shock pressures [4]. Referred to their results, the integral breadths of graphites as shown in Fig. 1 are thought to be used as an index of the shock pressure loaded on them. Fig. 1 shows that ALH 78019 and Y-82100, containing only graphite, were less shocked than Y-8448 and Y-74659 that contain both graphite and diamond. In Y-8448, diamond-free graphites were also less shocked than diamond-bearing ones. X-ray reflection lines of diamond-bearing graphites are broadened much more and show that the shock pressures loaded on them were much higher than those on diamond-free ones. In Y-74659, the same relations between integral breadths of diamond-free and diamond-bearing graphites are observed as in Y-8448, although the integral breadths of the diamond-free graphite are wider than those in Y-8448, suggesting that the pressure for the conversion of graphite to diamond was higher in Y-74659 than that in Y-8448. The difference of the pressure for the conversion may suggest that the formation mechanism of diamond differed in Y-74659 from that in Y-8448, for which a catalytic mechanism was proposed [5].

Fig. 2 shows the relations between the integral breadths of graphite 110 and diamond 220 reflections. In Fig. 2, each ureilite is plotted in relatively narrow respective areas. Y-74123 and ALH 77257 show relatively sharp reflections of diamonds having constant integral breadths, whereas the integral breadths of graphite are variable. In Y-8448, ALH 78262, Asuka 881931 and MET 78008, integral breadths of diamond 220 reflections have a linear relation to those of graphite 110 reflections. Y-8448 and ALH 78262 are plotted around the same line and ALH 78262 shows a little wider integral breadths of graphite and diamond than Y-8448. Asuka 881931 and MET 78008 are also plotted around the same line which has a little smaller slope than that of former two ureilites and their integral breadths of diamonds and graphites are wider than those of ALH 78262. Y-74659 and Y-74130 show relatively constant integral breadths of graphites whereas those of diamonds are variable and take the largest values among ureilites.

On the basis of the characteristics of the integral breadths as described above diamond-bearing ureilites are classified into 3 types as summarized in Table 2. Type I is a group of ureilites not containing diamond. It is suggested that diamond in ureilites may have formed by the catalytic conversion of graphite [3]. It is well known that well-crystallized diamond forms by the catalytic conversion of graphite and non-catalytic one bears many stacking faults and shows broadened X-ray lines. By reference to these results, the genesis of diamond for each type was estimated as shown in Table 2.

References: [1] Goodrich C. A. (1992) *Meteoritics*, **27**, 327-352. [2] Nakamuta Y. and Aoki Y. (2000) *Meteoritics and Planetary Sci.*, **35**, 487-493. [3] Nakamuta Y. and Aoki Y. (2001) *Meteoritics and Planetary Sci.*, **36**, A146. [4] Uchizono A. et al. (1999) *Mineral. Jour.*, **21**, 15-23. [5] Nakamuta Y. and Aoki A. (2000) *25th NIPR symposium* abstract, 108-110, Tokyo.

Table 1. Mineral compositions of carbon-rich grains in each ureilite.

Sample	Gr	Di	Kam	Tae	Tr	Sch	Mag	Goe	Jar	Number of grains
ALH 78019	+									10
Y-82100	+									6
Y-8448	+									8
	+	+	+		-		+			10
Y-74659	+		+			-	-			1
	+	+	+		-	-	-		-	7
ALH 77257	+	+	+				-		-	9
ALH 78262	+	+	+		-		+		-	6
Asuka 881931	+	+	-		-		+	-		15
MET 78008	+	+	+	-		-	-			17
Y-74123	+	+	+		-	-	-	-		16
Y-74130	+	+	+	-	-	-	-			19

Gr: graphite, Di: diamond, Kam: kamacite, Tae: taenite, Tr: troilite, Sch: schreibersite, Mag: maghemite, Goe: goethite, Jar: jarosite. +: dominant or subdominant, -: trace amounts.

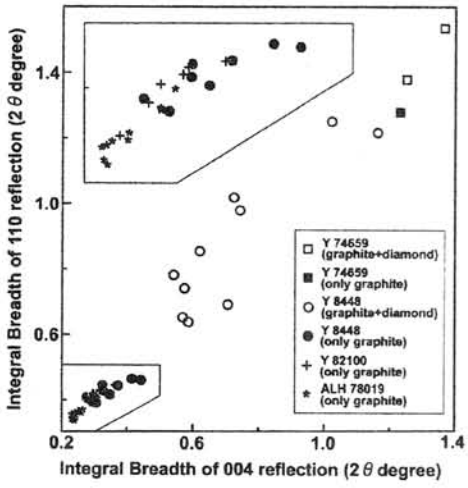

Fig. 1 Relations between integral breadths of 004 and 110 reflections of graphite.

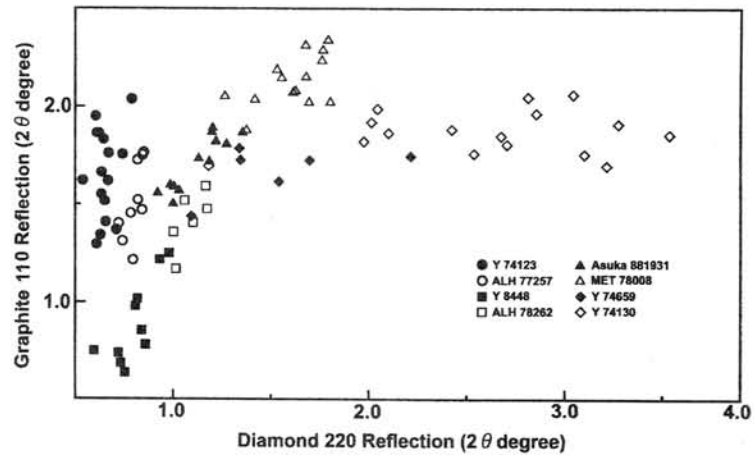

Fig. 2 Relations between integral breadths of diamond 220 and graphite 110 reflections.

Table 2. Classification of ureilites based on carbon minerals.

Type	Sample	Carbon minerals	Genesis of diamond
I	ALH 78019 Y 82100	graphite	no
II	Y 74123 ALH 77257	graphite + diamond	catalytic (high temperature)
III	Y 8448 ALH 78262 Asuka 881931 MET 78008	graphite + diamond	catalytic (low temperature)
IV	Y 74659 Y 74130	graphite + diamond	non-catalytic

CI-LIKE PHYLLOSILICATE-RICH CLASTS IN THE TSUKUBA METEORITE

Daisuke Nakashima[1], Tomoki Nakamura[1], and Takaaki Noguchi[2]

[1]Department of Earth Planet. Sci., Kyushu University, Hakozaki, Fukuoka 812-8581
[2]Department of Materials and Biological Sci., Ibaraki University, Bunkyo, Mito 310-8512

Introduction

The black fine-grained clasts were found in the dark-light structure in the Tsukuba meteorite (H5-6), which is meteoritic "fall" [1]. The clasts are much darker than the dark portion in Tsukuba host. The purpose of this study is to know the origin of the black clasts.

Mineralogical and chemical analyses of the clasts

The black clasts, up to 800μm across, are characterized by the presence of pyrrohtite plates, pentlandites, plaquette, spherulitic and framboidal magnetites, which are typical of CI chondrites [2] (Fig. 1). Synchrotron radiation X-ray diffraction analyses showed that the clasts consist mainly of serpentine and saponite, which are common in CI chondrites [e.g. 3]. The relative abundance of serpentine and saponite is comparable with that of Orgueil. The crystallinity of magnetite is lower than that of Orgueil. There appears to be small amounts of olivine and ferrihydrite. It is not clear that the olivine is indigenous to the clasts or contaminant from the host. If the olivine is indigenous, the degree of aqueous alteration of the clasts was not so high to replace olivine entirely. Major-element concentrations of the clasts, as measured with a broad beam of electron microprobe, have a low total (avg. 83wt.%) and show compositional variations in the Si+Al-Fe-Mg ternary diagram that are similar to those in Orgueil [3]. TEM observation shows that there are euhedral crystals (<200nm) of pentlandite and pyrrohtite. TEM-EDS analysis indicates that the phyllosilicates show compositional variations in Si+Al-Fe-Mg ternary diagram that are similar to those in Orgueil [3] (Fig. 2). Mineralogically and chemically the clasts resemble CI chondrites and quite differ from Tsukuba host [4].

The saponite (001) basal spacing is 13.2Å, consistent with that of intact or weakly heated Orgueil (<500°C) [5]. This and the presence of serpentine suggest that the clasts have never experienced heating above 500°C after accretion to the Tsukuba parent body. The boundary between CI clast and Tsukuba host is measured with a focused beam (2μm) of electron microprobe and has a low total (avg. 85wt.%), suggesting that the boundary is not dehydrated.

Discussion

Based on the results of a series of analyses, formation history of the CI clasts can be evaluated as follows: the clasts were formed as a part of CI parent body. After the ejection from the parent body, the CI meteoroid accreted to the Tsukuba parent body at a certain period after early thermal metamorphism whose temperature was supposed to be 700-1000°C for H5-6 [6]. The clasts were located in the active regolith, because they are found in the dark-light structure of the meteorite. Impact on the regolith have crushed the clasts into smaller pieces and induced lithification of the regolith material, but the temperature of the clasts has never exceeded 500°C during lithification. The lithification class of Tsukuba host is determined from the concentrations of solar noble gases, using the criteria of [8]. Tsukuba host is assigned to a class A breccia that has been subjected to low shock pressures (1-5GPa). Finally, Tsukuba meteoroid including the CI clasts was ejected from the parent body of Tsukuba and fell onto the earth after the transit time 8.1Ma [7].

Acknowledgement

We thank Dr. Watanabe, the Center of Advanced Instrumental Analysis, Kyushu University for the SEM observation and Mr. Shimada for technical support in the EPMA analysis and Drs. Tanaka, Nozaki, and Mori for technical support during X-ray diffraction analysis at KEK.

Reference: [1] Yoneda S. et al. (1996) *Meteorit. Planet. Sci., 31,* A157-A158. [2] Kerridge J. F. (1970) *EPSL, 29,* 299-306. [3] Tomeoka K. and Buseck P. R. (1988) *GCA, 52,* 1627-1640. [4] Okuyama Y. K. et al. (1997) *Chishitsu News, 509,* 35-42. [5] Nozaki W. *personal communication.* [6] McSween H. Y. et al. (1988) *in Meteorites and Early Solar System,* pp. 102-113. [7] Nakashima D. et al. (2002) *Antarct. Meteorit. Res., 15,* in press. [8] Bischoff A. et al. (1983) *EPSL, 66,* 1-10.

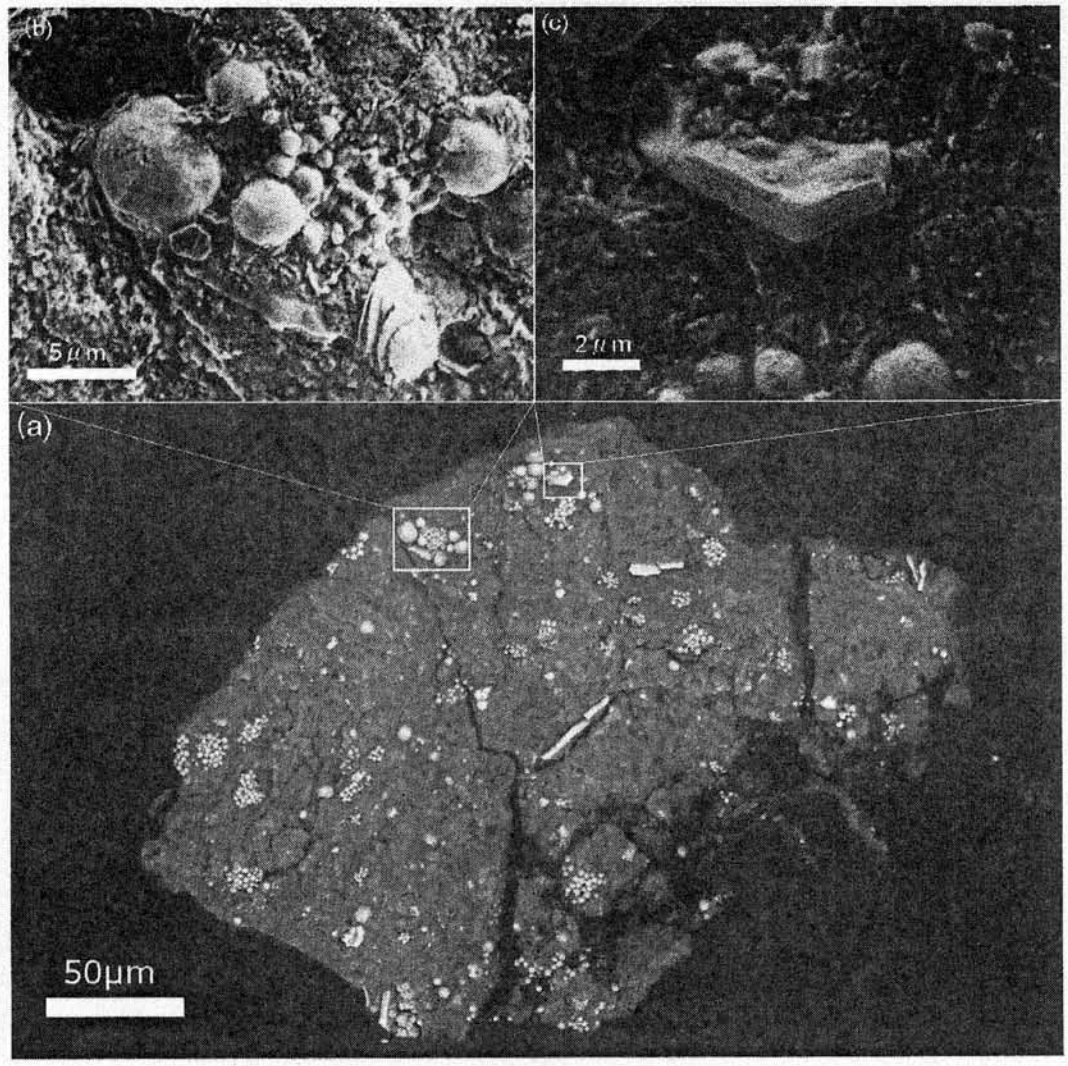

Fig. 1. (a) Backscattered electron (BSE) image of the clast, (b) BSE image of plaquette, spherulitic, and framboidal magnetites, (c) BSE image of a hexagonal pyrrohtite plate.

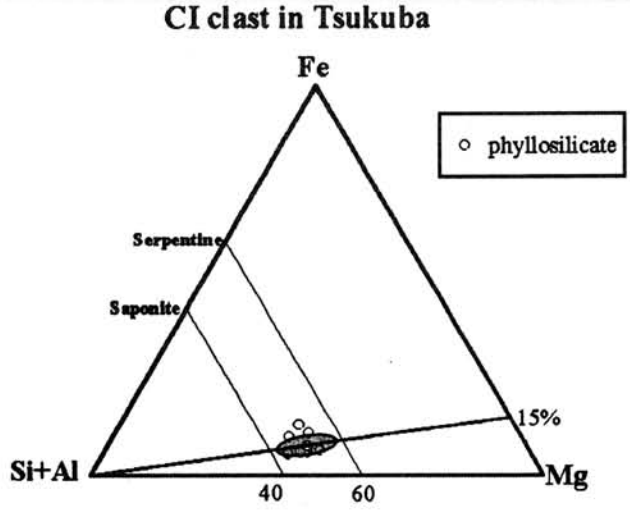

Fig. 2. Si+Al-Fe-Mg ternary diagram (atomic %) of phyllosilicates in the clast. Also shown are the ideal solid solution lines of serpentine and saponite and the line defined by Fe/(Mg+Fe) = 15 atomic % of phyllosilicates in Orgueil [3]. The filled area shows composition of coarse phyllosilicates in Orgueil [3].

Chemical and isotopic compositions of solvent-insoluble organic matter from the Sayama meteorite

H. Naraoka[1)], H. Mita[2)], M. Komiya[3)], A. Shimoyama[2)] and S. Yoneda[4)]

[1)]Dept. of Chemistry, Tokyo Metropolitan Univ., Hachioji, Tokyo 192-0397 Japan.
[2)]Dept of Chemistry, Univ. of Tsukuba, Tsukuba, Ibaraki 305-8571 Japan.
[3)]Natl. Inst. Adv. Indust.l Sci. Tech., Tsukuba, Ibaraki 305-8567 Japan.
[4)]National Science Museum, Shinjuku, Tokyo 169-0073 Japan

Introduction

The Sayama meteorite is a new CM chondrite fell at Sayama-city, Japan in 1986 [1], which has been reported to receive highly aqueous alteration based on microscopic studies [2]. The Sayama contains 1.99wt% bulk carbon with the bulk carbon isotopic composition of +2.9‰ and +6.1‰ (relative to PDB) for two measurements [1], being relatively enriched in ^{13}C compared to average CM chondrites. The high bulk $\delta^{13}C$ value may be due to high abundance of isotopically heavy carbonate, which is a similar isotope signature as a highly-hydrated CM chondrite such as Y-82042 (+9.8‰) [3]. The thermal history, however, has not been considered yet. In this study, we determined C-H-N concentrations and $\delta^{13}C$ value of solvent-insoluble and amorphous organic matter extracted from the Sayama meteorite to apply the relative thermal alteration and metamorphic degree, and to characterize the organic matter of this chondrite.

Using the H/C-N/C ratio of solvent-insoluble and amorphous organic matter extracted from several CM2 chondrites, we have recently proposed an organic parameter to evaluate the relative extent of weak thermal alteration and metamorphism [4]. In brief, the H/C atomic ratio of the purified amorphous matter vary widely from 0.72 to 0.11 with increasing thermal alterarion (Fig. 1). This is because hydrogen is preferentially removed from carbon skeleton of amorphous organic matter. During the H/C change of ~0.7 to ~0.3, the N/C atomic ratio remains ~0.04. However, the N/C ratio decreases from ~0.040 to ~0.017 at the H/C ratio fo ~0.2 for intense thermal alteration of chondrites such as B-7904 and Y-86720. Therefore, the H/C-N/C curve implies different degrees of thermal event among these chondrites, most of which are consistent with the previous mineralogical and chemical studies. The H/C-N/C index is a sensitive and quantitative means to evaluate weak metamorphic degree of carbonaceous chondrites. Furthermore, only in a chondrite with the H/C ratio of >~0.5, bituminous organic compounds such as amino acids and polycyclic aromatic hydrocarbons (PAHs) were appropriately present. The H/C ratio of amorphous organic matter is also a probable means to evaluate indigenous bituminous organic compounds against terrestrial contamination in carbonaceous chondrites.

Experimental

Powdered sample of the Sayama chondrite was extracted with water and organic solvents to analyze solvent-extractable (bituminous) organic compounds such as amino acids and PAHs. The detailed molecular distributions should be reported elsewhere. After the solvent extractions, the residue was treated with 6M HCl and HF/HCl (1/1 by volume) in a Teflon™ bottle by shaking at ~70°C. The acidified residue was washed with H_2O several times to neutral pH, and subquently washed with organic solvents. After drying, the resulting amorphous organic matter was subjected to an elemental analyzer and isotope ratio mass spectrometer coupled with an elemental analyzer to determine its C-H-N concentrations and the $\delta^{13}C$ values, respectively.

Results and discussion

The extracted amorphous organic matter contains 68.3wt% carbon with 3.91wt% hydrogen and 2.76wt% nitrogen, which is highly purified to be the same as carbon content of insoluble organic matter of various CM2 chondrites reported by other studies [4-6]. The H/C and N/C atomic ratios of the purified amorphous matter from the Sayama meteorite are calculated to be 0.68 and 0.035, respectively. As shown in Fig. 1, the H/C

atomic ratio of the Sayama is similar to that of the Murchison (0.70), Y-791198 (0.67) and A-881458 (0.72), which suggest that the Sayama has not been thermally altered. In addition, because these three CM2 chondrites yielded indigenous organic compounds such as amino and carboxylic acids, sugars and hydrocarbons, this thermally unaltered signature of the Sayama may be consistent with the existence of bituminous organic compounds such as amino acids and PAHs.

The $\delta^{13}C$ value of the amorphous organic matter is –15.3‰, which is similar to that of most CM2 chondrites [7,8]. The larger ^{13}C depletion of amorphous organic matter relative to bulk carbon has been observed in the Sayama, Murchison and Y-791198, probably because of more abundant isotopically heavy carbonate and/or bituminous organic compounds in these meteorites.

Conclusions

The H/C and N/C atomic ratios of solvent-insoluble amorphous organic matter purified from the Sayama meteorite are 0.68 and 0.035, respectively, which are similar to those of the Murchison, Y-791198 and A-881458. The Sayama has not been thermally altered nor metamorphosed. The $\delta^{13}C$ value of the amorphous organic matter is –15.3‰, which is also similar to that of the Murchison, Y-791198 and A-881458. The chemical and isotopic signatures of the Sayama suggest the existence of indigenous bituminous organic matter in this chondrite.

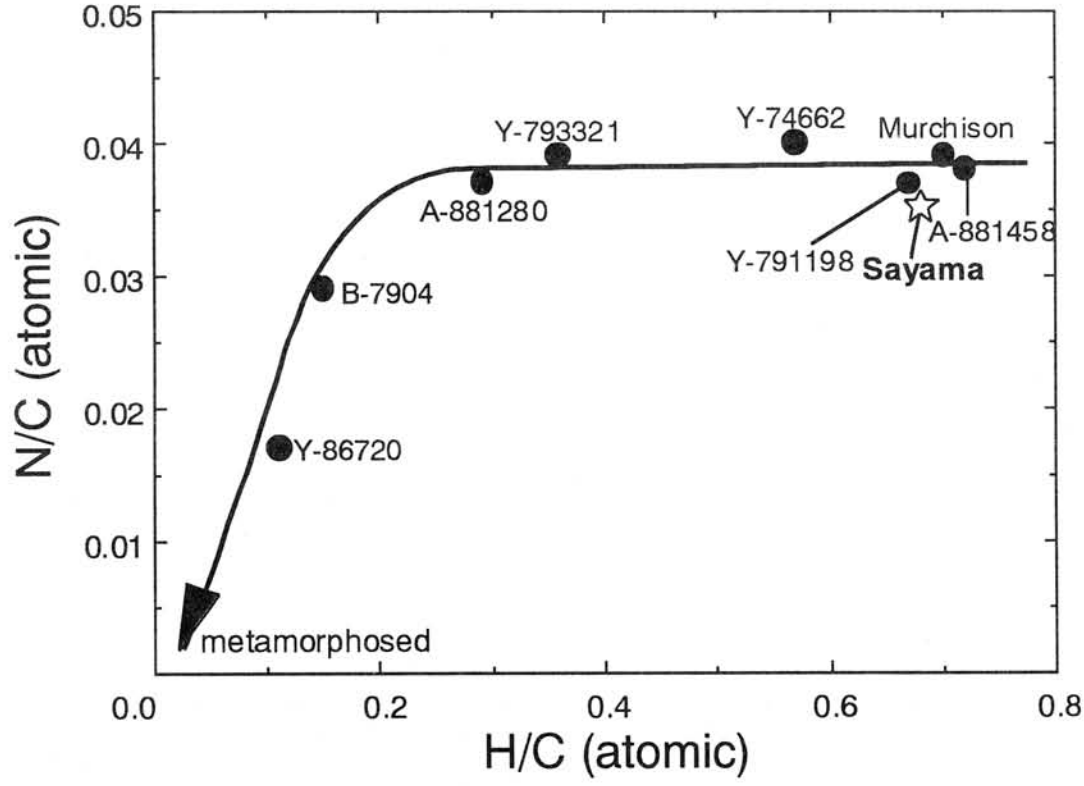

Fig. 1 Atomic H/C-N/C plot of amorphous organic matter purified from various CM2 chondrites including the Sayama

References

[1] Yoneda S. et al. (2001) Antarctic Meteorites XXVI, 172-174. [2] Nakamura T. et al. (2001) Antarctic Meteorites XXVI, 96-97. [3] Grady M. M. et al. (1986) *Proc. 11th Symp. Antarc. Meteor.*, 162-178. [4] Naraoka H. et al. submitted. [5] Hayatsu R. et al. (1977) *GCA*, **41**, 1325-1339. [6] Gardinier A. et al. (2000) *EPSL*, **184**, 9-21. [7] Kerridge J. F. et al. (1987) *GCA*, **51**, 2527-2540. [8] Naraoka H. et al. (1997) *Geochem. J.* **31**, 155-168.

THE LONAR IMPACT CRATER, INDIA- A TERRESTRIAL ANALOGUE WITH CRATERS ON MARS

V.K. NAYAK

Department of Applied Geology, University of Saugar, Saugar (M.P.), India

Abstract:- The Indian Lonar Impact Crater is unique in being the only terrestrial crater in basaltic rocks. It has it's own peculiarities and provides scientific data of immense value. Lonar is considered to be a terrestrial analogue not only with the lunar craters but also with the craters on the Mars. Reviews of evidences from the Lonar crater supporting such an analogy with the craters on the Mars are furnished. It is believed that future studies of the Lonar crater in a planetary context will be extremely rewarding.

The significance of terrestrial impact craters has greatly increased owing to planetary exploration efforts since the man first landed on the Moon in 1969. Empirical information and data from more than 150 terrestrial impact craters have now established that impact cratering was a ubiquitous geological process in the history of the solar system and planetary evolution (Grieve, 1998).

The young, 1.8 Km. diameter, impact crater at Lonar, India (19° 58' N : 76° 31'E), is unique in being the only terrestrial crater in basaltic terrain. (Nayak, 1972; Fredriksson et al.1973). An appraisal of significant features of the Lonar crater and their comparison with those of the lunar craters were furnished in a planetary context (Nayak, 2001). In fact, Lonar has provided important breakthrough in understanding the planetary geology (Fredriksson et al. 1978; Kieffer et al. 1976; Schall,1976). Scientific data of value found in the Lonar material will be very useful in comprehending the processes on the planets, particularly the Moon and the Mars. Some of the features of the Lonar crater provide opportunities to compare and correlate with craters of the Mars (Fudali et al.1980; Hagerty and Newsom, 2001 ; Newsom et al.2002). This contribution reviews the characteristic features which support an analogy between the terrestrial Lonar crater and the Mars.

The original morphology of the Lonar crater was reconstructed and mechanism of its excavation suggested by Fudali et al. 1980. Accordingly, the low rim height/diameter ratio of Lonar is not the result of post-cratering erosion but is considered due to the nature of its target basaltic rocks. This situation is not restricted to the Earth only but can be extended to some lunar and mercurian craters which are expected to be low-rimmed because of the target rocks like basalts as at Lonar.

The excellent preservation of continuous ejecta blanket and substrate around Lonar strongly indicates that the dominant mechanism of debris transportation and deposition was a ground–hugging fluidized surge owing to strong gravity field and an atmosphere (Fudali et al. 1980). Consideration of these aspects led Fudali et al. (1980) to suggest that Lonar should be considered as an analogue to the fluidized craters of the Mars.

Recently, Hagerty and Newsom (2001) found new evidence for impact-induced hydrothermal alteration in basalts at the Lonar crater and considered its implications for effects of small craters on the mineralogy and chemistry of the Martian regolith. The identification of saponite and celadonite, geochemical modelling of alteration process, replacement textures, isotopic data of carbonates at Lonar demonstrates post-impact hydrothermal alteration. Further, Newsom et al. (2002) studied the mass balance model with new SIMS and EMP data for mobile elements (e.g. S, Cl, K, Br, Li, B, Be, Ba)in altered material of the Indian Lonar crater; Mistastin Crater ,Canada and small crateras on Mars and found remarkably similar behaviour, This similarity strongly supports the use of terrestrial analogues to comprehend the geochemical processes on the Mars.

It should be mentioned that there is an on-going project on, 'Impact Crater Hydrothermal Systems, under the supervision of Prof. H.E.Newsom and his group at the Institute of Meteoritics, Department of Earth and Planetary Sciences, University of New Mexico, Albuquerque, U.S.A. This project involves the study of processes with regards to water and impact craters on the Mars, using terrestrial analogues and remote sensing data. It is believed that the Indian Lonar crater in basaltic

rocks will provide significant clues and constraints to understand the processes on the Mars. Also, the data from the Lonar crater will be compared with the Martian data obtained by Mars Global Surveyor (MGS) and Viking Spacecraft to better understand about the aqueous processes in impact craters on the Mars.

All these studies are stimulating and are likely to shed new light on the significance of water and cratering processes on planetary bodies. The Lonar crater in basalts can serve as a case study to answer several unresolved questions in understanding the geochmical processes on the Mars and other planets in the solar system. Eventually, the results of these researches will help to plan a long term mission for habitation on the celestial bodies.

References :-

Fredriksson, K.,Dube, A., Milton, D.J. and Balasundaram, M.S. (1973) . Science, 180,862-864.

Fredriksson, K., Brenner, P., Dube, A. , Milton, D.J., Mooring, C. and Nelen, J.A. (1978). Smithsonian Contribution Earth – Science , 22, 1-13.

Fudali,R.F., Milton, D.J.,Fredriksson, K. and Dube, A. (1980) Moon and planets, 23, 493515

Grieve ,R.A.F. (1998) . In Meteorite-Flux with Time and Impact Effects (Eds. Grady, Hutchison, McCall and Rothery) , Geol. Soc., London , Special Publication , 140, 105-131.

Hagerty, J.J. and Newsom, H.E.(2001). 32nd Lunar and Planetary Science Conference (LPSC), No. 1131.

Kieffer, S.W., Schaal, R.B., Gibbons, R., Horz, F., Milton, D.J. and Dube , A. (1976). Proc. 7th Lun. Sci..Conf.,1391-1412.

Nayak, V.K. (1972). Earth and Planet. Sci. Letts., 14 (1), 1-6.

Nayak , V.K. (2001). 26th Symposium on Antarctic Meteorites, Nat. Inst. Polar Research, Tokyo, Japan, 104 - 106

Newsom, H.E.,Hagerty, J.J. and Shearer, C.W. (2002). 33rd Lunar and Planetary Science Conference (LPSC).

Schaal, R.B. and Horz, F. (1976). Proc. 8th Lun. Sci. Conf., 1697-1729.

Thermoluminescence Study of Japanese Antarctic Meteorites VI

K. Ninagawa[1], M.Ohta[1], Y.Mieda[1], N. Imae [2], H. Kojima[2], and K. Yanai[3]

[1] Department of Applied Physics, Okayama Univ. of Science, 1-1, Ridai-cho, Okayama 700, Japan
[2] National Institute of Polar Research, 9-10, Kaga 1-chome, Itabashi-ku, Tokyo 173, Japan
[3] Department of Civil and Environ., Iwate Univ., Ueda 4-3-5, Morioka 020, Japan

Natural TL (thermoluminescence), the luminescence of a sample that has received no irradiation in the laboratory, reflects the thermal history of the meteorite in space and on Earth. Natural TL data thus provide insights into such topics as the orbits of meteoroids, the effects of shock heating, and the terrestrial history of meteorites. Induced TL, the response of a luminescent phosphor to a laboratory dose of radiation, reflects the mineralogy and structure of the phosphor, and provides valuable information on the metamorphic and thermal history of meteorites. The sensitivity of the induced TL is used to determine petrologic type of type 3 ordinary chondrites.

As reliable pairing approach, TL properties within large chondrites were analyzed, taking advantage of the fact that serial samples from these meteorites is known to be paired [1]. Then a set of TL pairing criteria: 1) the natural TL peak height ratios, LT/HT, should be within 20%; 2) that ratios of raw natural TL signal to induced TL signal should be within 50%; 3) the TL peak temperatures should be within 20℃ and peak widths within 10℃ was proposed. This set of TL pairing criteria is less restrictive than previously used [1].

We have measured TL of 121 Japanese Antarctic unequilibrated chondrites so far [1,2,3]. This time we measured TL of more 30 Asuka chondrites. The TL data of them are listed in Table. The petrologic subtype was determined from their TL sensitivity. Eight chondrites, A-881236, A-881083, A-881026, A-881088, A-881125, A-881090, A-881244, and A-881096 were found to be primitive below subtype 3.2. However, we found no chondrites in the lower cluster. An unusual TL glow curve was measured in A-881026 (H3). It would contain unknown phosphorescent mineral. Two-dimensional TL observation of its thin sections is necessary to identify the mineral. Above pairing criteria were also applied to the Asuka unequilibrated chondrites. A-880941 and A-880956 were paired in H3 chondrites. A-880966, A-881242, and A-881249 were also paired in H3 chondrites.

References: [1] Ninagawa *et al.* (1998): *Antarctic Meteorite Res.*, **11**, 1-17. [2] Ninagawa *et al.* (2000): *Antarctic Meteorite Res.*, **13**, 112-120. [3] Ninagawa *et al.* (2002): *Antarctic Meteorite Res.*, in press.

Table Thermoluminescence data of Okayama for thirty unequilibrated Japanese ordinary chondrites

		Natural TL						Induced TL												LT			
Meteorite	Clas	LT/HT			LT			TL Sensitivity			Peak Temp.			Width			TL	/TL Sens.			Pairing
					(10^3 counts)			(Dhajala=1)			(℃)			(℃)			Subtype	($x10^3$)			
A-880930	H3	0.14	±	0.01	2.3	±	0.2	0.47	±	0.03	153	±	5	133	±	1	3.6-3.7	4.8	±	0.5	
A-880973	H3	0.29	±	0.01	1.88	±	0.05	0.36	±	0.01	163	±	3	131	±	1	3.6	5.2	±	0.1	
A-880941	H3	0.47	±	0.02	0.21	±	0.02	0.025	±	0.001	151	±	2	136	±	1	3.3	8.3	±	0.8	A-880956
A-880956	H3	0.52	±	0.02	8.60	±	0.03	0.77	±	0.01	165	±	1	135	±	3	3.7	11.2	±	0.2	
A-881069	H3	0.55	±	0.03	6.8	±	1.2	0.66	±	0.04	179	±	4	146	±	1	3.7	10.2	±	2.0	
A-881240	H3	0.90	±	0.01	11.4	±	0.4	0.51	±	0.01	154	±	1	122	±	2	3.7	22.6	±	0.8	
A-881216	H3	1.14	±	0.01	21.3	±	1.6	0.73	±	0.03	154	±	1	133	±	1	3.7	28.9	±	2.5	
A-881093	H3	1.58	±	0.01	11.88	±	0.01	0.56	±	0.01	168	±	6	128	±	1	3.7	21.3	±	0.2	
A-880966	H3	1.62	±	0.02	20.8	±	2.8	0.56	±	0.10	166	±	7	133	±	1	3.6-3.7	37.4	±	8.4	A-881242,1249
A-881242	H3	1.64	±	0.07	20.4	±	0.3	0.54	±	0.03	163	±	5	123	±	2	3.7	38.0	±	2.1	
A-881249	H3	1.72	±	0.12	21.1	±	1.1	0.60	±	0.05	172	±	4	137	±	2	3.7	34.9	±	3.5	
A-880951	H3	2.04	±	0.08	98.3	±	4.4	1.07	±	0.01	164	±	5	142	±	6	3.8	92.1	±	4.2	
A-880925	H3	3.26	±	0.48	78.6	±	11.8	0.73	±	0.10	165	±	2	157	±	5	3.7	107	±	22	
A-881212	H3	4.49	±	0.01	24.6	±	0.6	0.21	±	0.01	161	±	4	152	±	1	3.5-3.6	119	±	4	
A-881080	H3	5.48	±	0.31	87.7	±	1.3	0.63	±	0.04	161	±	1	135	±	1	3.7	140	±	9	
A-881236	H3				0.18	±	0.02	0.010	±	0.005	166	±	19	170	±	35	3.0-3.2	18.8	±	9.6	
A-881083	H3							0.006	±	0.005	152	±	16	107	±	52	3.0-3.2				
A-881026	H3							0.003	±	0.001	161	±	1				3.0				
A-880938	L3	0.79	±	0.02	8.8	±	3.1	0.09	±	0.01	182	±	9	149	±	4	3.4-3.5	98	±	38	
A-881079	L3	1.15	±	0.01	39.8	±	3.4	0.96	±	0.08	157	±	2	134	±	2	3.7-3.8	41	±	5	
A-881124	L3	2.07	±	0.08	13.0	±	0.1	0.09	±	0.01	173	±	2	147	±	2	3.4-3.5	144	±	9	
A-881088	L3							0.018	±	0.001	139	±	14	164	±	19	3.2				
A-881125	L3							0.006	±	0.001	157	±	1	138	±	9	3.1				
A-881090	L3							0.008	±	0.001	144	±	4	137	±	22	3.1				
A-881244	L3							0.001	±	0.001	147	±	1	120	±	5	3.0				
A-881096	L3							0.007	±	0.001	160	±	7	122	±	13	3.1				
A-881199	LL3	1.02	±	0.28	1.6	±	0.1	0.046	±	0.002	128	±	2	119	±	7	3.3-3.4	34	±	2	
A-881146	LL3	1.39	±	0.05	90	±	1	1.88	±	0.14	145	±	3	134	±	7	3.8-3.9	48	±	4	
A-881105	LL3	2.20	±	0.06	183	±	16	2.07	±	0.07	156	±	1	129	±	1	3.8-3.9	88	±	8	
A-881077	LL3	7.77	±	0.25	102	±	20	0.35	±	0.0089	181	±	1	166	±	2	3.6	291	±	58	

Mineralogical variation of phyllosilicate-rich micrometeorites: comparison with hydrated carbonaceous chondrites.

Takaaki Noguchi[1], Tomoki Nakamura[2], and Wataru Nozaki[2]
[1]: Materials and Biological Sci., Ibaraki University, Bunkyo, Mito 310-8512, Japan
[2]: Earth Planet. Sci., Kyushu University, Hakozaki, Fukuoka 812-8581, Japan.

Introduction Micrometeorites (MMs) that contain abundant phyllosilicates experienced slight to weak heating during atmospheric entry. MMs represent more unbiased samples of asteroids than meteorites because of the different evolution of orbits between MMs and meteorites [e. g. 1]. Chemical composition of unmelted MMs suggests that they are related to the hydrated carbonaceous chondrites such as CI and CM chondrites [e. g. 1]. Therefore, the population of phyllosilicate-rich MMs having different mineralogical features probably reflects the population of hydrated asteroids more correctly than that of hydrated carbonaceous chondrites do. We have been investigating mineralogy of Antarctic MMs by combination of synchrotron radiation X-ray diffraction (SR-XRD) and transmission electron microscopy (TEM) [e. g. 2, 3, 4]. Until recently, we had found 5 phyllosilicate-rich MMs among about 1000 unmelted ones. Detailed TEM observation of the MMs revealed that four among five MMs contain only saponite as phyllosilicates [4]. Two among the saponite-rich MMs contain fine-grained magnesiowüstite ((Mg, Fe)O) aggregates that are probably decomposition products of Mg- and Fe-carbonate. The other two saponite-rich MMs contains abundant framboidal aggregates of magnetite and do not contain magnesiowüstite. Only one MM contains only serpentine as phyllosilicate. We pointed out that the mineralogical similarities between the magnesiowüstite-bearing saponite-rich MMs and the matrix of Tagish Lake (hereafter TL) carbonate-rich lithology and between the saponite-rich MMs including abundant framboidal magnetite and TL carbonate-poor lithology [4].

Sample and Methods Recently, the authors' group thoroughly collected about 700 unmelted Antarctic MMs with 20 to 300 μm across. Based on the surface features observed by low-vacuum scanning electron microscope (LV-SEM), we selected 44 MMs that seem to have experienced slight to weak heating during atmospheric entry. These MMs were investigated separately by SR-XRD. We found 25 phyllosilicate-rich MMs among them. Difference in the population of phyllosilicate-rich MMs in this study and our previous study [4] resulted from the fact that phyllosilicate-rich MMs were more abundant among smaller MMs, especially in the size range between 20 to 40 μm across. Here, we report mineralogical features of these 30 phyllosilicate-rich MMs and compare the MMs with hydrated carbonaceous chondrites. SR-XRD analysis was performed at high entry accelerator research organization, Tsukuba, Japan.

Results and discussion Phyllosilicate-rich MMs were classified based on mineral species of phyllosilicates and mineral assemblages. We also used the degree of atmospheric entry heating deduced by the (001) spacing of saponite for saponite-bearing MMs and by the sharpness of the (001) peak of serpentine for serpentine-rich MMs. Seven types of phyllosilicate-rich MMs were recognized based on mineral assemblages (see Table). The most abundant types of phyllosilicate-rich MMs are Tagish Lake carbonate-poor lithology-like (TL Cp-like) and CI-like MMs. Nine TL Cp-like MMs are composed of saponite, magnetite, pyrrhotite, and small amounts of carbonates (calcite, siderite, and magnesite). The mineral assemblage is very similar to that of TL carbonate-poor lithology. Nine CI-like MMs are composed of saponite, serpentine, magnetite, pyrrhotite, and small amounts of carbonates (calcite, magnesite, and siderite). Saponite is more abundant than serpentine. Their mineralogy is almost identical to that of CI chondrites. In a previous study [5], a CI-like MM was reported. However, in the MM, saponite-like material was amorphous in spite of the presence of serpentine. In this study, saponite was identified by SR-XRD. It is interesting that most of the MMs in these two types were slightly heated during atmospheric entry based on

the degree of dehydration of saponite in them. This means that the TL Cp-like MMs are not heated CI-like MMs in which serpentine was decomposed preferentially.

Next abundant phyllosilicate-rich MMs are CM-like MMs. Although four MMs have similar mineralogy to that of CM chondrites, tochilinite was not found. However, the absence of tochilinite was due to the preferential breakdown of tochilinite during atmospheric entry heating [4].

In the case of weakly heated saponite-rich MMs, it was sometimes difficult to distinguish heated CI-like from heated TL Cp-like MMs because of preferential breakdown of serpentine [6, 7]. Two saponite-rich MMs could not estimate their mineralogy before entering the earth's atmosphere. Three saponite-rich MMs contain magnesiowüstite. Because their estimated mineral assemblage before entering the earth are very similar to that of TL carbonate-rich lithology, the MMs were classified as Tagish Lake carbonate-rich lithology-like (TL Cr-like) MMs. Two among them were described in detail in our previous study [4].

As shown above, mineralogies of 25 phyllosilicate-rich MMs are very similar to those of known hydrated carbonaceous chondrites, Tagish Lake, CI, and CM chondrites. Abundant TL (Cp or Cr)-like and CI-like MMs and much less abundant CM-like MMs suggest that that TL- and CI-like asteroids may be much more abundant than CM-like asteroids.

There are three phyllosilicate-rich MMs, whose mineralogies do not coincide with that of known meteorites. Two MMs contain abundant saponite but are poor in Fe oxides. Because sub-μm-sized magnetite are ubiquitously distributed in the TL-like and CI-like MMs, the low abundance of magnetite in these two MMs may indicate fundamental difference in the conditions of aqueous alteration among the TL-like and CI-like MMs and these MMs. Another MM contains saponite and serpentine as well as magnetite, pyrrhotite, and ferrihydrite. However, serpentine is more abundant than saponite. It is contrary to the case of CI chondrites. These MMs show that there are extraterrestrial materials that we have not found as meteorites yet.

References [1] Jessberger, E. K. et al. (2001) In: Interplanetary dust, pp 253-294. [2] Nakamura, T. et al. (2001) *GCA, 65,* 4385–4398. [3] Noguchi, T. (2001) *LPSC XXXII,* #1541. [4] Noguchi, T. et al. (in press) *EPSL.* [5] Genge, M. J. et al. (2001) *LPSC XXXII,* #1546. [6] Nozaki, W. et al. (2001) *MAPS, 36,* A151. [7] Nozaki, W. et al. (2002) in this volume.

Table Population of phyllosilicate-rich MMs investigated in this study.

Mineralogical features of MMs	slightly heated	weakly heated	total
CI-like	7	2	9
Tagish Lake carbonate-poor lithology-like (TL Cp-like)	8	1	9
Tagish Lake carbonate-rich lithology-like (TL Cr-like)	0	3	3
CI- or Tagish Lake carbonate-poor lithology-like (heated sap-rich)	-	2	2
Saponite-rich, very poor in magnetite (sap-rich and mt-poor)	2	0	2
Serpentine is more abundant than saponite (serp-rich and sap-poor)	1	0	1
CM-like, without tochilinite (CM-like)	3	1	4
			30

Abbreviations of each type of phyllosilicate-rich MMs are shown in parentheses.

Experimental reproduction of micrometeorites by pulse-heating of carbonaceous chondrites.

Wataru NOZAKI[1], Tomoki NAKAMURA[1], and Takaaki NOGUCHI[2]

[1]: Earth Planet. Sci., Kyushu University, Hakozaki, Fukuoka 812-8581, Japan.
[2]: Materials and Biological Sci., Ibaraki University, Bunkyo, Mito 310-8512, Japan

Introduction Micrometeorites are small (<1mm) extraterrestrial material, which constitute the major fraction of extraterrestrial material fall onto the Earth (Grün et al., 1985; Love and Brownlee, 1993). To identify their parent body is one of the major objective of micrometeorite researches. Although bulk mineralogy provides an important clue to the origins of micrometeorites, primary mineralogy of micrometeorites has been altered by various degrees of heating during atmospheric entry. Thus, it is important to clarify the mineralogical changes in micrometeorites during atmospheric entry heating.

Experiment We performed pulse-heating experiments of a small piece of Orgueil (CI1) carbonaceous chondrite from 200°C to 1000°C with 100°C interval under ambient atmospheric pressure of 1.5×10^{-2} torr. In each step, the sample was heated for 120 sec and bulk mineralogy was analyzed by Synchrotron radiation X-ray diffraction (SR-XRD). SR-XRD was performed at high energy accelerator research organization, Tsukuba, Japan.

Results Before heating, the Orgueil sample consisted of saponite, serpentine, magnetite, ferrihydrite, carbonate (dolomite), Ca-sulfate, and minor amount of Fe-Sulfide. By heating at 200 and 300°C, the bulk mineralogy did not change. At 400°C, diffraction peaks of Ca-sulfate disappeared and those of newly formed anhydrite appeared. Relative intensity of diffraction peaks of serpentine decreased at 500°C and disappeared at 600°C. Intensities of diffraction peaks of saponite decreased and the basal spacing (001) of saponite shrunk to ~12Å at 600°C. Diffraction peaks of saponite were hardly identified at 700°C. TEM observation of another Orgueil sample heated at this temperature revealed both of saponite and serpentine have only remnant layer structure and the majority of them are almost completely decomposed into amorphous material. Dolomite and ferrihydrite also decomposed at 700°C. At 800°C, newly formed olivine and Fe-oxide (magnesiowüstite) appeared. At 900 to 1000°C, the abundance and crystallinity of olivine increased progressively.

Discussion Phyllosilicate-bearing micrometeorites are thought to be the least heated samples, because saponite and serpentine are decomposed below ~700°C (Nozaki et al., 2001). Most of phyllosilicate-bearing micrometeorites can be classfied

into three major mineralogical types based on the major minerals in them; type A: mainly consist of saponite, serpentine, and magnetite, type B: saponite and magnetite, and type C: serpentine (Noguchi et al., 2002). We also found micrometeorites that consist of amorphous material and magnetite (hereafter type D).

It is likely that type A and B micrometeorites were formed by weak heating of CI chondrite-like material, which is composed mainly of saponite, serpentine, and magnetite. Because serpentine is decomposed at lower temperature than saponite, it is plausible that serpentine was preferentially decomposed into amorphous material by weak atmospheric entry heating. Therefore, there is a possibility that type B micrometeorites were made from CI chondrite-like material.

The heating experiments show that the mineralogy of the Orgueil sample heated below 500°C matches well with that of type A phyllosilicate-rich micrometeorites. The Orgueil sample heated at 600°C, where serpentine has decomposed while saponite and magnetite still remains, show similar bulk mineralogy to type B micrometeorites. However, there is a great difference in mineralogy between the heated Orgueil sample and type B micrometeorites. In the heated Orgueil sample, basal spacing of saponite has shrunk down to ~12Å by weak heating, while that in the majority of the type B micrometeorites show no shrinkage (13 ~ 14Å), suggesting that type B micrometeorites have not been heated above 600°C and originally not contained serpentine. Thus, precursor material of type B micrometeorites may contain abundant saponite and magnetite, such mineralogy can be found in 'Carbonate-poor lithology' of Tagish Lake CI2 chondrite (Gounelle et al., 2001; Mikouchi et al., 2001).

When the Orgueil sample was heated 700°C, phyllosilicates have almost completely decomposed and only magnetite can be seen in the diffraction pattern. This mineralogical feature is similar to that of type D micrometeorites. It is possible that type D micrometeorites could be formed from micrometeoroids with mineralogy similar to 'Carbonate-poor lithology' of Tagish Lake. Therefore, it is plausible that there are type D micrometeorites originated from moderately heated CI-like and 'Carbonate-poor lithology' of Tagish Lake-like micrometeoroids. There may be micrometeorites contain primary amorphous materials and magnetite. Therefore, further investigation is needed to distinguish these possibilities.

References

Gounelle M. et al (2001) LPSC XXXII, #1616 CD-ROM.
Grün E. et al (1985) Icarus 62, 244-272.
Love S. G. and Brownlee D. E. (1993) Science 262, 550-553.
Mikouchi T. et al (2001) LPSC XXXII, #1371 CD-ROM.
Noguchi T. et al (2002) in this volume.
Nozaki W. et al (2001) MAPS, 36, A151.

Noble gases in Antarctic nakhlites, Yamato 000593 and Yamato 000749

R. Okazaki[1)], K. Nagao[1)], N. Imae[2)], and H. Kojima[2)]
1) Laboratory for Earthquake Chemistry, Graduate School of Science, University of Tokyo, 3-1, Hongo 7-chome, Bunkyo-ku, Tokyo 113-0033, Japan
2) Antarctic Meteorite Research Center, National Institute of Polar Research, 9-10, Kaga 1-chome, Itabashi-ku, Tokyo 173-8515, Japan

Introduction and analytical methods

Japanese Antarctic Research Expeditions in 2001 (JARE-41) have found a number of meteorites over 3500 pieces. The JARE-41 recovered a heavy achondrite (Yamato 000593) up to 13.7 kg around the Yamato Mountains together with a probably paired piece (Yamato 000749) of 1.3 kg [1]. Petrographical and mineralogical features of Y000593 and Y000749 are similar to those of nakhlites [2, 3]. We have reported in [3] a result of noble gas analysis for Y000749 and pointed out several features characteristic of nakhlites.

In addition to Y000749, we recently measured noble gases in Y000593 in order to confirm the pairing. An ^{81}Kr-Kr age was also determined for Y000593. The ^{81}Kr-Kr age can give the most reliable cosmic-ray exposure (CRE) age because the ^{81}Kr-Kr age calculation needs only Kr isotope composition. Here we present results of noble gas analyses for Y000593 and Y000749, and discuss their noble gas signatures and K-Ar and CRE ages.

Samples of Y000593 (0.1622 g) and Y000749 (0.2048 g) were investigated through a step-heating method in order to separate noble gas components, such as radiogenic, cosmogenic, and trapped ones. These samples were heated at 400, 600, 800, 1000, 1300, and 1750°C in a Mo crucible. Another sample of Y000593 (0.2963 g) was completely melted (heated at 1750 °C) to determine the ^{81}Kr-Kr age. Noble gases evolved from each sample were purified to eliminate active gases and were measured separately as four fractions (He-Ne, Ar, Kr, and Xe) with a modified VG-5400 mass spectrometer (MS-II) at the Laboratory for Earthquake Chemistry, University of Tokyo [4].

Results and discussion

The most important feature of nakhlites is a presence of iddingsite that is inferred to have been produced via reactions with water on Mars. In a system of trapped ^{129}Xe/^{132}Xe against ^{84}Kr/^{132}Xe, noble gas in iddingsite is distinguishable from those in shergottites and Chassigny [5]. Noble gases released at 1000-1750 °C from Y000593 and Y000749 plot along a mixing line between Chassigny and iddingsite (Fig. 1). This strongly supports the petrologic and mineralogical judgment [2, 3] that these meteorites are Nakhla-type Martian meteorites.

Both isotopic ratios and concentrations of He, Ne and Ar of Y000593 are essentially identical to those of Y000749 (Table 1), although there are differences in Kr and Xe (discussed below). The light noble gases confirm the pairing between Y000593 and Y000749, which is consistent with their field recognition and petrographical similarities [2, 3].

Light noble gases in both meteorites are dominated by cosmogenic gases and radiogenic components. Table 2 is a summary of K-Ar and CRE ages for Y000593 and Y000749. The K-Ar age of 1.33 ± 0.18 Ga for Y00593 and Y000749 is concordant with radiometric ages, such as ^{39}Ar-^{40}Ar, Rb-Sr, and Sm-Nd ages, of other nakhlites [6]. Thus, it is inferred that nakhlites have been crystallized at the same time around 1.3 Ga.

There are differences among mean CRE ages T_{3He}, T_{21Ne}, and T_{38Ar} although each of a mean CRE age shows good consistency between Y000593 and Y000749 (Table 2). Because no diffusive loss of cosmogenic gases was observed, the discrepancies in CRE ages obtained from different cosmogenic gases are probably due to uncertainties in corrections of their production rates for variations in chemical compositions and in shielding conditions. Recent studies by [7] estimated the production rate for cosmogenic ^{21}Ne in a basaltic shergottite Dhofar 019 based on radionuclides ^{10}Be, ^{26}Al, and ^{36}Cl. The estimated P_{21Ne} is 2.4-2.7 $\times 10^{-9}$ cm^3 STP/g/Ma, which is in good agreement with 2.46 calculated for Dhofar 019 in the same way applied for Y000593 and Y000749. Therefore, we assume that T_{21Ne} of 12.16 ± 0.18 Ma is a preferred exposure age for these meteorites.

An ^{81}Kr-Kr age for Y000593 was calculated to be 11.8 ± 0.18 Ma. This ^{81}Kr-Kr age agrees with T_{21Ne}, suggesting a very short resistance in Antarctica for Y000593 and Y000749. The T_{21Ne} and ^{81}Kr-Kr ages give the most reliable CRE age of 11.98 ± 0.25 for these meteorites, and this age corresponds to timing of ejection from Mars. The ejection age of 11.98 Ma is consistent with those for Nakhlites (10.0-11.9 Ma; see [6] and references therein).

Contrary to the consistencies in light noble gases between Y000593 and Y000749, there are some gaps in concentrations and isotopic ratios of heavy noble gases Kr and Xe between these meteorites. Differences in concentrations of Kr and Xe between these meteorites are prominent at 400, 600, 1300, and 1750 °C. As shown in Fig. 1, the 1300 and 1750 °C fractions of Y000593 are shifted toward Chassigny relative to those of Y000749. This suggests that iddingsite-containing gases in Y000593 are not as much as Y000749. Microscopic observation revealed that iddingsite shows lower occurrence in Y000593 than in Y000749, which is consistent with the noble gas signature.

On the other hand, Y000593 shows high ^{84}Kr/^{132}Xe and low ^{129}Xe/^{132}Xe ratios at 400 and 600 °C (Fig. 1), indicative of contributions from adsorbed terrestrial atmosphere. Hence, the excessive Kr and Xe in the 400 and 600 fractions of Y000593 are suspected to be due to larger contributions of adsorbed terrestrial gases than those in Y000749.

References: [1] Imae N. et al. (2002) *Antarct. Meteorite Res. 15* (in press). [2] Kojima H. (2001) *Meteorite Newsletter 10*, No. 2. [3] Imae N. et al. (2002), *Lunar Planet. Sci. 33*, CD-ROM (#1483). [4] Nagao K. et al. (1999) *Antarct. Meteorite Res. 12*, 81-93. [5] Drake M. J. et al. (1994) *Meteoritics 29*, 854-859. [6] Nyquist L. E. et al. (2001) *Space Sci. Revs. 96*, 105-164. [7] Nishiizumi K. et al. (2002) *Lunar Planet. Sci. 33*, CD-ROM (#1366). [8] Eugster O. & Michel T. (1995) *GCA 59*, 177-199.

Table 1: Concnetrations and isotopic ratios in bulk Y000593 and Y000749 samples

Sample	Weight (g)	Analytical method	^{4}He	^{3}He/^{4}He	^{22}Ne	^{20}Ne/^{22}Ne	^{21}Ne/^{22}Ne	^{36}Ar	^{38}Ar/^{36}Ar	^{40}Ar/^{36}Ar	^{84}Kr	^{129}Xe	^{132}Xe
Y000593 (I)	0.1622	step heat	10825	0.0197	24.4	0.836	0.8239	13.3	1.308	1002	111	31.2	28.5
Y000593 (II)	0.2963	total melt	8917	0.0240	25.3	0.830	0.8258	11.5	1.443	791	155	41.9	38.6
Y000749	0.2048	step heat	9010	0.0232	25.7	0.823	0.8352	12.1	1.431	984	46	17.0	14.5

He, Ne, and Ar: in 10^{-9} cm^3 STP/g. Kr and Xe: in 10^{-12} cm^3 STP/g.

Table 2: K-Ar and cosmic-ray exposure (CRE) ages for Y000593 and Y000749

Sample	$^{40}Ar_m$ [1]	K [2] (ppm)	K-Ar age (Ga)	Cosmogenic gases [3] ^3He_m [1]	$^{21}Ne_c$	$^{38}Ar_c$	$^{81}Kr_c$	$^{83}Kr_c$	$(^{22}Ne/^{21}Ne)_c$	$(^{78}Kr/^{83}Kr)_c$	$(^{81}Kr/^{83}Kr)_c$	Production rates [4] P_{3He}	P_{21Ne}	P_{38Ar}	P_{81Kr}/P_{83Kr}	CRE ages (Ma) T_{3He}	T_{21Ne}	T_{38Ar}	T_{81Kr}
Y000593 (I)	13294	1494	1.48 ±0.14	213	20.1	16.9	-	-	1.206	-	-	16.0	1.70	2.15	-	13.3	11.9	7.88	-
Y000593 (II)	9093	1494	1.13 ±0.12	214	20.9	16.4	0.102	6.41	1.206	0.183 ±0.051	0.0159 ±0.0025	16.0	1.70	2.15	0.612	13.4	12.3	7.64	**11.8 ±1.8**
Y000749	11888	1494	1.37 ±0.14	209	21.5	17.1	-	-	1.191	-	-	16.1	1.74	2.15	-	13.0	12.3	7.96	-
Mean K-Ar age (Ga)			**1.33 ±0.18**												**Mean CRE ages (Ma)**	**13.23 ±0.20**	**12.16 ±0.26**	**7.83 ±0.16**	

He, Ne, and Ar: in 10^{-9} cm^3 STP/g. Kr: in 10^{-12} cm^3 STP/g.
1) Bulk concentrations of measured $^{40}Ar_m$ and ^3He_m (the subscript "m" denotes "measured"). Contributions of trapped ones are not considered. 2) Bulk K content of Y000593 analyzed by H. Haramura. 3) Corrected for contributions of trapped ones (the subscript "c" means "cosmogenic"), except for ^{3}He. 4) Production rates for ^{3}He, ^{21}Ne, and ^{38}Ar (shown in 10^{-9} cm^3 STP/g/Ma) are corrected for chemical compositions and shielding conditions using equations in [8]. Applied bulk composition is determined for Y000593 by H. Haramura.

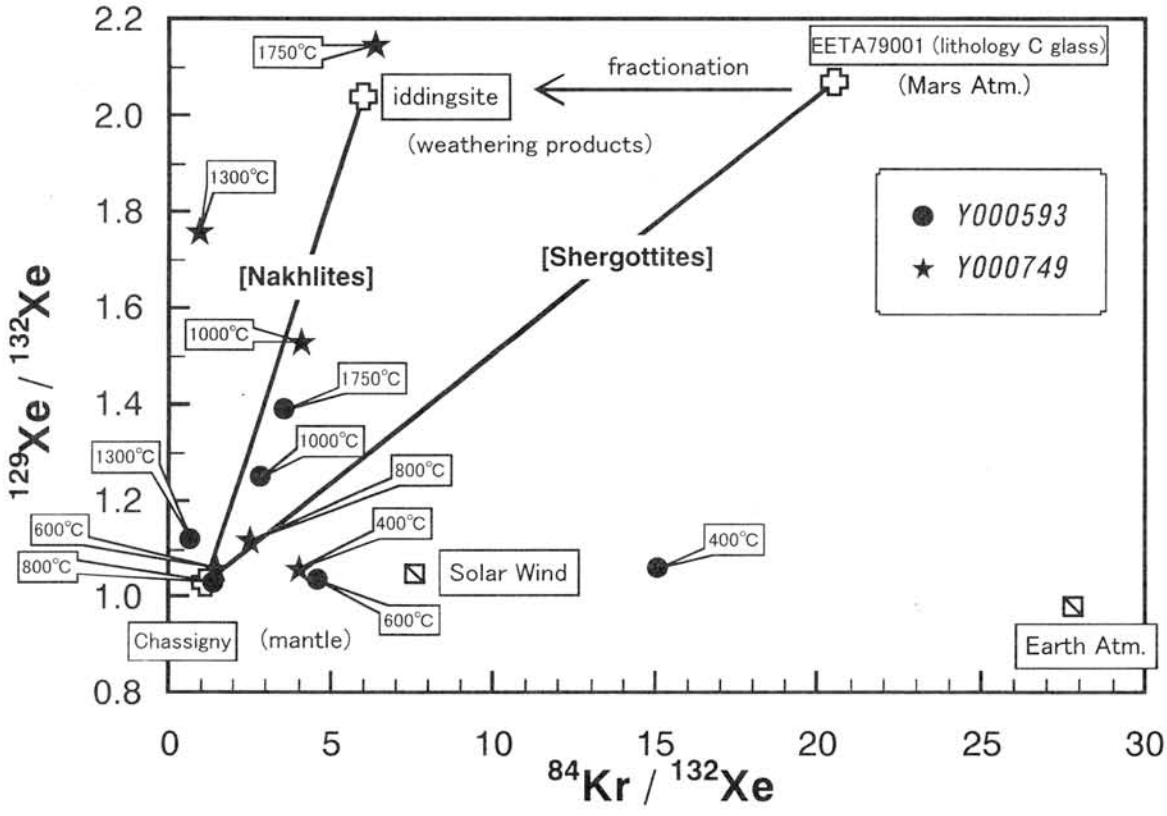

Fig. 1: Trapped $^{129}Xe/^{132}Xe$ and $^{84}Kr/^{132}Xe$ ratios of Y000593 and Y000749. Cosmogenic ^{84}Kr and ^{132}Xe are subtracted from measured ones, respectively. Noble gases released at 1000-1750 °C from Y000593 and Y000749 plot along a Chassigny-iddingsite line.

Measurement of densities of Antarctic micrometeorites using X-ray microtomography

Takahiro Okazawa[(1)*], Akira Tsuchiyama[(1)], Hajime Yano[(2)], Takaaki Noguchi[(3)], Takahito Osawa[(4)], Tsukasa Nakano[(5)], and Kentaro Uesugi[(6)]

(1) Department of Earth and Space Science, Graduate School of Science, Osaka University, 1-1 Mchikaneyama-cho, 560-0043, Japan, *okazawa@ess.sci.osaka-u.ac.jp, (2) Planetary Science Division, Institute of Space and Astronautical Science, 3-1-1 Yoshinodai, Sagamihara, Kanagawa, 229-8510, Japan, (3) Department of Materials and Biological Sciences, Ibaraki University, Bunkyo, 2-1-1, Mito, 310-8512, Ibaraki, Japan, (4) Laboratory for Earthquake Chemistry, Graduate School of Science, The University of Tokyo, Hongo, Tokyo 113-0033, Japan, (5) National Institute of Advanced Industrial Science and Technology, Tsukuba, 305-8567, Japan, (6)Japan Synchrotron Radiation Research Institute, Mikaduki, 679-5198, Japan

Introduction

Density, which is determined by the chemical composition and the structure of a material, is one of the most important physical properties. The densities of micrometeorites are important for discussion about the formation of planetesimals as well as for classification of micrometeorites because the planetesimals were formed by aggregation of dust grains. However, the densities have not been measured precisely because of their small sizes. The purpose of the present study is to obtain the densities of Antarctic micrometeorites (AMMs) precisely. We used X-ray computed tomography (CT) for measuring the volumes and microbalances for the masses.

Experiments

X-ray CT is a non-destructive method to obtain two-dimentional distribution of X-ray linear attention coefficient (LAC) of samples by using X-ray attenuation. We can obtain three-dimentional structures by piling up successive cross-sectional CT images.

In this study, we used three AMMs (Y98M03PR003, Y98M02KS068 and Y98M02KS074), which were collected from MinamiYamato in Antarctica by 39th JARE [1]. They were imaged with a micro X-ray CT system at SPring-8 of SR facility in Japan [2-4]. Each sample was attached to the tip of a fine glass fiber with glycol phthalate. Monochromatic X-ray beams of 10 kev were used for the imaging. Cross-sectional CT images were reconstructed from 360-720 projections with a convolution back projection method. Three-dimentional structures were obtained from successive CT images with the voxel size of $0.50 \times 0.50 \times 0.50 \times \mu$m, which gives the spatial resolution of about $1 \sim 2$ μm.

AMMs are brighter than a background (air and glycol phthalate) in the CT images because AMMs have larger LACs than the air and glycol phthalate. We removed each AMM from the background by image analysis using a LAC threshold. Two different values of the threshold for the AMM surfaces and the boundaries between the AMMs and void inclusions were used. The boundaries between the AMMs and air are slightly diffused probably due to a minor artifact by moving samples during imaging . To minimize such artifacts, we applied erosion-dilation operation, where the surface of the sample (AMM) was eroded by a certain number of voxels and then dilated by the same number of voxels. The volumes of AMMs were calculated from

the number of voxels that belongs to the AMMs as the voxel size is known. Finally, we obtained the bulk volumes including void inclusions and the solid volumes without the inclusions.

The masses of two AMMs (Y98M03KS068 and Y98M02PR003) were measured with a microbalance equipped at Tokyo University or NIPR. The precision of these microbalances was 0.1 μg. We measured the mass of each AMM for several times and the mean value was adopted.

Results

Examples of the CT images of the samples are shown in Figure 1. The threshold values and the number of voxels for the erosion-dilation operation were determined appropreately from the CT images. The results are shown in Table 1. Y98M02PR003 and Y98M03KS068 are vesicular and have the porosities of about 10%. In contrast, we can not recognize any voids in Y98M03KS074 within the present spatial resolution. The bulk and solid densities are 2.0, 2.3 g/cm^3 for Y98M02PR003, and 2.0, 2.3 g/cm^3 for Y98M03KS068, respectively.

Table 1: Results of the present measurments

sample	size (μm $\times$ μm $\times$ μm)	mass (μg)	bulk volume (cm^3)	solid volume (cm^3)
Y98M02PR003	120 $\times$ 140 $\times$ 200	3.4($\pm$ 0.0)	1.69×10^{-6} ($1.66 \sim 1.72$)	1.51×10^{-6} ($1.48 \sim 1.54$)
Y98M03KS068	140 $\times$ 105 $\times$ 100	1.2($\pm$ 0.2)	6.00×10^{-7} ($5.94 \sim 6.06$)	5.28×10^{-7} ($5.12 \sim 5.44$)
Y98M03KS074	120 $\times$ 95 $\times$ 100	n.d.	3.64×10^{-7} ($3.57 \sim 3.71$)	3.64×10^{-7} ($3.57 \sim 3.71$)

n.d. : not determined

sample	porosity (%)	bulk density (g/cm^3)	solid density (g/cm^3)
Y98M02PR003	10.7 ($7.0 \sim 14.2$)	2.0 ($2.0 \sim 2.1$)	2.3 ($2.2 \sim 2.3$)
Y98M03KS068	12.0 ($8.4 \sim 15.5$)	2.0 ($1.7 \sim 2.5$)	2.3 ($1.8 \sim 2.7$)

Discussion

It propsed that many AMMs resemble to CM chondrites [5]. Void inclusions in AMMs were formed by heating and dehydration of hydrous minerals of AMM during entering into the atomosphere. If serpentine (density 2.6 g/cm^3), which is a typical hydrous mineral in CM chondrites, was lost its crystalline water without changing its volume, the density becomes 2.3 g/cm^3. This value is consistent with the solid densities of the two AMMs.

In the present study, we successfully obtained the precise volumes of AMMs using X-ray CT and an microbalance. However, this method is possible only for relatively large AMMs (larger than 50 μm $\sim$ 100 μm in diameter) because of the limitation of measurable mass by the microbalance. Therefore, it is hard to obtain the densities of small AMMs and IDPs precisely.

Density of a material (ρ) is related to LAC (μ) and mass attenuation coeficient (τ) as follows:

$$\rho = \frac{\mu}{\tau}. \qquad (1)$$

LAC can be estimated from CT images if we use monochromatic X-ray beams as in the present study. The τ values can be obtained from the chemical compositions of a material. Therefore, we may estimate the density from the CT images without measuring the mass if we know or estimate the chemical compositions of samples. The availability of this method should be examined for a father study.

Acknowledgement

The AMM samples were supplied by the National Institute of Polar Research through the open research proposal scheme for the Yamato 98 AMM sample allocation.

References

[1]Yada and Kojima (2000) *Antarctic Meteor Res*, **13**, 9-18.
[2]Uesugi et al. (2001) *Proc. Nucl. Instr. Methods. Ser.A*, **467-468**, 853-856.
[3]Uesugi et al. (2002) *Proc. SPIE*, **4503**, 291-298.
[4]Tsuchiyama et al. (2001) *Antarctic Meteorites*, **XXVI**, 151-153.
[5]Noguchi et al. (2002) *Earth Planet. Sci. Lett*, in press

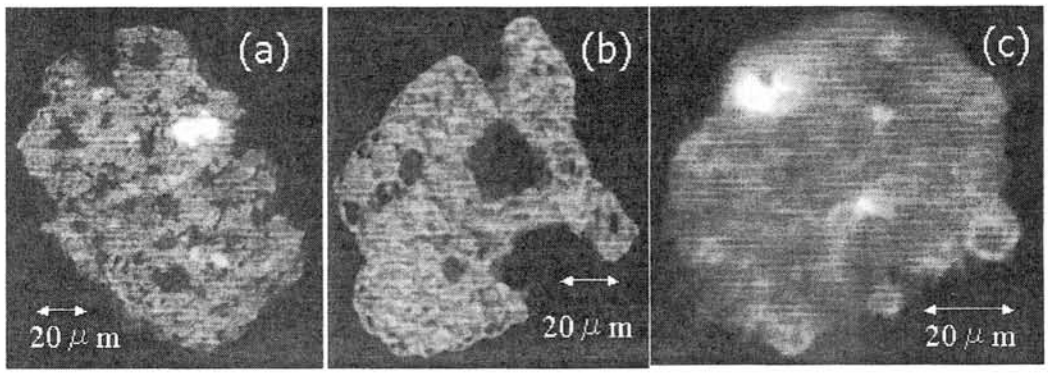

Figure 1: CT images of AMMs. (a) Y98M02PR003. (b) Y98M03KS068. (c) Y98M03KS074. Objects with bright contrasts have high LAC values and vice versa.

Noble Gases in Antarctic Cosmic Spherules

Takahito OSAWA & Keisuke NAGAO

Laboratory for Earthquake Chemistry, Graduate School of Science,
The University of Tokyo, Hongo, Tokyo 113-0033, Japan
(osawa@eqchem.s.u-tokyo.ac.jp)

Introduction

Cosmic spherules are spheroidal particles with sizes <1 mm. Details of cosmic spherules were first described by Murray (1876), in a report of the results of the H.M.S. Challenger Expedition of 1873-1876. Although it was thought that cosmic spherules are extraterrestrial particles for a long time, reliable evidence was not obtained until 1980's. In order to identify the spherules as extraterrestrial, cosmic-ray-produced nuclides, *i.e.* ^{53}Mn, ^{59}Ni, ^{10}Be, and ^{26}Al, have been measured [*e.g.*, 1]. Noble gas analyses were done for unmelted cosmic dust particles to clarify their extraterrestrial origin, since the noble gas isotopic compositions in the extraterrestrial materials are quite differ from those of the terrestrial materials [*e.g.*, 2]. However, there is no comprehensive noble gas measurement for individual cosmic spherules, because cosmic spherules generally have considerably low noble gas concentrations due to the severe heating, therefore the noble gas analysis for single spherule is difficult [3,4]. Highly sensitive mass spectrometer with low blank level is required determining all noble gas isotopic compositions in the cosmic spherules. In the present work, we determined the noble gas compositions for individual cosmic spherules using laser gas extraction.

Samples

The spherules measured in this work were collected from a bare ice region near the Tottuki Point of Soya Coast at northeastern part of the Lüzow-Holm Bay [5]. The large-scale micrometeorite collection was carried out by 41st Japanese Antarctic Research Expedition (JARE). Micrometeorites were collected by filtration of melted ice. Antarctic ice was melted by a heated radiator in which warmed non-freezing liquid was circulating. AMMs in the melted ice were riddled by four different filters (opening of 10, 40, 100, and 238 μm). These collections were done in sixteen points for twenty-one days [5].

All spherules were picked up from the 100 μm-opening filter of the Tottuki #4. The majority of the particles attached on the filter were removed by washing in clear water and residual particles were removed by ultrasonic washing. Of all samples, eights are from water-washing particles and eights are from ultrasonic-washing particles. The ultrasonic-washing samples are smaller than the water-washing samples. The cosmic

spherules are roughly classified to three groups: Stony (S), Glassy (G), and Iron (I) type, the classification follows the method of [6]. Eleven spherules were classified to S-type and two and three spherules were to I- and G-type, respectively, based on their textures and chemical compositions determined by EDS (energy dispersive spectrometer) analysis. Transparencies and colors of the spheres were determined by the optical microscopy. follows the method of [6]. Eleven spherules were classified to S-type and two and three spherules were to I- and G-type, respectively, based on their textures and chemical compositions determined by EDS (energy dispersive spectrometer) analysis.

Results

Noble gas concentrations of the spherules were considerably lower than those of unmelted micrometeorites, indicating severe heating during atmospheric entry. Although ^{3}He in most of the spherules were not detectable, Ne and Ar isotopic compositions were determined for more than the half of the samples. Four samples have high ^{21}Ne/^{22}Ne ratios, which may reflect cosmogenic ^{21}Ne, although blank corrections could not be done for them due to low concentrations of Ne. Two particles, T004uTC003 and T004uTC013, preserved SEP (solar energetic particles)-like Ne, they have relatively high Ne concentrations. They also preserved extraterrestrial Ar and their ^{40}Ar/^{36}Ar ratios were clearly lower than the atmospheric value of 296, proving their extraterrestrial origins. A stony spherule, T004TC006, has the lowest ^{40}Ar/^{36}Ar ratio of 19.5±2.0 among the spherules measured in this study, instead of deficit of solar-Ne. The low Ar isotopic ratios for these particles reflect the chondritic Ar composition rather than solar-Ar, since they have ^{36}Ar/^{84}Kr ratios close to the Q-component. Backscattered electron images of them are shown in Figure 1. Only T004uTC013 is a non-spherical particle. The particles presumably preserve the extraterrestrial noble gases in their interiors instead of severe heating. On the other hand, extraterrestrial Ne and Ar were not identified in other particles.

However, the relative noble gas abundances of them were similar to those of

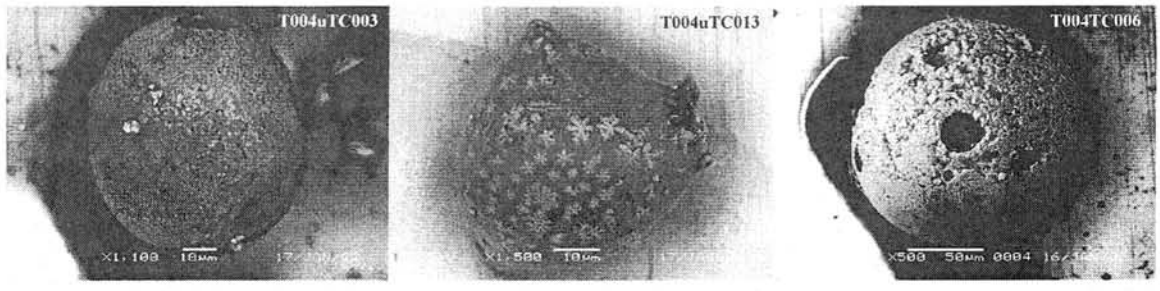

Figure 1: Cosmic spherules with extraterrestrial Ar. T004uTC003 and T004uTC013 also have SEP-like Ne. T004TC006 and T004uTC003 with spherical shapes will be classified to porphyritic or relic-grain-bearing spherule. T004uTC013 has non-spherical shape and dendritic magnetite appears on its surface. Extraterrestrial Ne and Ar may be preserved in unmelted portions in the particles.

unmelted micrometeorites and were clearly distinguishable from those of terrestrial materials, such as basalts, air, and waters, reflecting their extraterrestrial origins (Figure 2). Since the noble gas abundances are explained by a mixing of the solar and Q-components and the contribution of adsorption air is negligible, the majority of the Antarctic spherules are presumably extraterrestrial and not volcanic products.

References

[1] Nishiizumi K. (1983) *Earth Planet. Sci. Lett.* **63**, 223-228. [2] Osawa and Nagao (2002) *Meteoritics Planet. Sci.* (in press) [3] Stuart *et al.* (1999) *Geochim. Cosmochim. Acta* **63**, 2653-2665. [4] Osawa *et al.* (2000) *Antarct. Meteorite Res.* **13**, 322-341. [5] Iwata and Imae, (2001) *Antarctic Meteorites* **XXVI**, 50-51. [6] Blanchard *et al.* (1980) *Earth Planet. Sci. Lett.* **46**, 178-190.

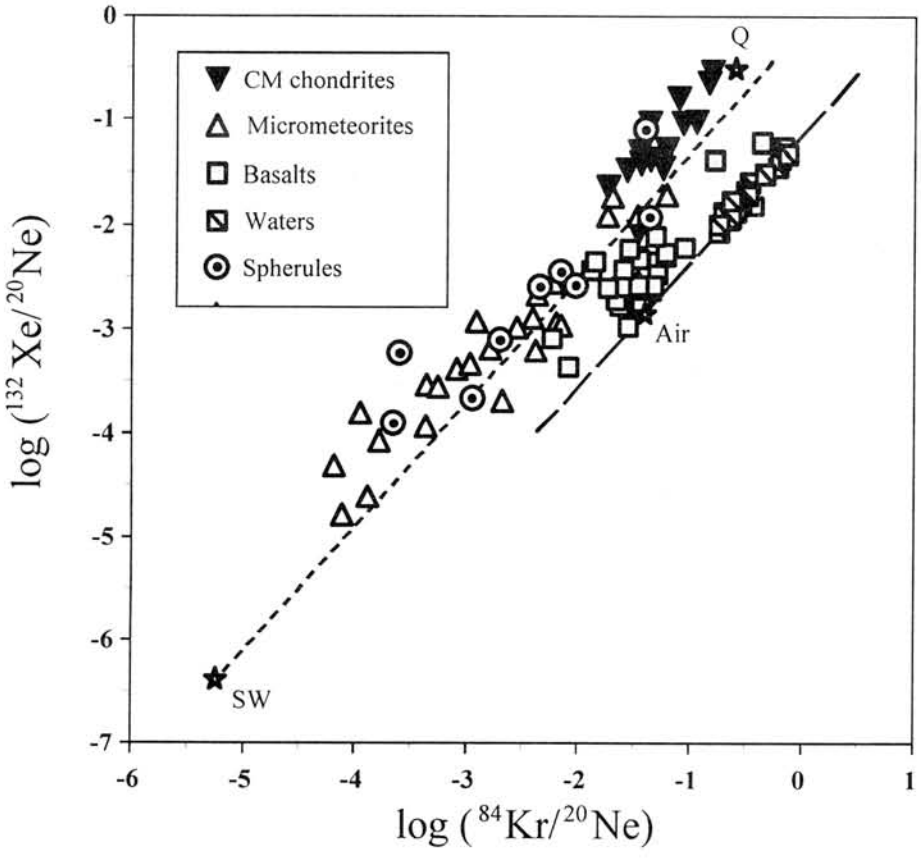

Figure 2: Noble gas abundances of the cosmic spherules and other extraterrestrial and terrestrial materials. Dotted line and broken line show theoretical fractionation lines established by mass-dependent Rayleigh distillation. Spherules have noble gas compositions similar to those of unmelted micrometeorites, indicating extraterrestrial origins.

Chemical Composition of Y000593 and Y000749

Y. Oura, N. Shirai, and M. Ebihara.

Graduate School of Science, Tokyo Metropolitan University, Hachioji, Tokyo 192-0397, Japan

Y000593 and a possibly paired meteorite Y000749 are grouped into nakhlites, a group of SNC meteorites, by their noble gas compositions (Imae et al. 2002). They are the first nakhlite recovered on Antarctica. So far about 30 SNC meteorites (shergottite, nakhlite and chassignite) have been identified, most of which are classified into shergottites. Nakhlites are rare, to which 6 meteorites including Y000593 and Y000749 belong. In this study, we analyzed Y000593, Y000749 and Nakhla for their bulk chemical compositions by nuclear analytical methods. In this symposium we will report preliminary results because of not completing our all analytical procedures.

Lump samples of Y000593,66 (1.2 g), Y000749,46 (3.6 g) and Nakhla (0.88 g) were analyzed by neutron induced prompt gamma-ray analysis (PGA) using cold neutron beam at JRR-3M, Japan Atomic Energy Research Institute. The specimens of Y000593 and Y000749 were loaned from NIPR and were subjected to PGA without any additional treatment at our side. Because the size of the Y000749 specimen is larger than the neutron beam size used in PGA, only content ratios normalized to Si content were determined for Y000749 and the other samples by the internal monostandard method developed by our group. Absolute contents were also obtained for Y000593 and Nakhla by comparison method using JB-1 (a basaltic geological reference sample issued by GSJ) and chemicals of analytical grade as reference standards for quantifiction.

Since Si-normalized contents for major elements obtained by the internal monostandard method are almost the same for three nakhlites analyzed, it is inferred that their absolute elemental abundances are also similar. Our absolute content values for Y000593 and Nakhla are shown in Table 1 with contents in Nakhla compiled by Lodders (1998). All major elements and several trace elements were able to be determined by PGA. It is seen in Table 1 that there is no apparent difference in contents of analyzed elements between Y000593 and Nakhla except for H and Cl and that our determinations in Nakhla are also consistent with compilation data by Lodders (1998). There appear clear boundaries in Mg/Si, Al/Si, Ca/Si, and/or Ti/Si weight ratios among SNC groups; for example, Mg/Si - Ca/Si diagram is shown in Fig.1. These ratios for Y000593 and Y000749 are different from those for Shergotty and Chassigny but consistent with those for Nakhla. Therefore it is suggested based on chemical composition that Y000593 is a nakhlite. Our determination of Cl in Nahkla is about 16 times higher than the compilation data. As our sample of Nakhla was sampled from the

interior of a large mass at the lunar sample processing room at JSC, NASA and no additional treatment was given for PGA, a high content of Cl cannot be attributed to experimental contamination. It must be highly probable that Cl is heterogeneously distributed in nakhlite, just like the case for chondrites (Zorenski et al., 1999). As only one value has been reported for Cl content in Nakhla, additional analyses are desired for Cl (and other halogens) in future.

In order to determine additional elements including trace elements, we are now performing additional nuclear analytical methods, instrumental neutron activation analysis and instrumental photon activation analysis, for powder samples prepared from different parts of the meteorites.

References

N. Imae et al., *Lunar Planet. Sci.* **XXXIII**, #1483 (2002).

K. Lodders, *Meteoritics Planet. Sci.* **33**, A183-A190 (1998).

M. E. Zolensky, et al., *Science* **285**, 1377-1379 (1999).

Table 1. Preliminary results of chemical compositions determined by PGA.

	Y000593	Nakhla	*Nakhla**
H, %	0.0541±0.0014	0.0252±0.0010	
B, ppm	3.47±0.06	3.02±0.07	*4.6*
Na, %	0.432±0.03	0.447±0.025	*0.34±0.05*
Mg, %	6.26±0.26	6.93±0.29	*7.3±0.2*
Al, %	0.999±0.030	0.974±0.033	*0.89±0.11*
Si, %	22.2±0.4	23.5±0.4	*22.7±0.8*
Cl, ppm	52.9±6.1	872±13	*80*
K, %	0.119±0.007	0.117±0.007	*0.107±0.019*
Ca, %	10.2±0.3	10.8±0.5	*10.5±0.5*
Ti, %	0.218±0.004	0.208±0.004	*0.202±0.025*
Cr, %	0.179±0.006	0.208±0.007	*0.177±0.028*
Mn, %	0.398±0.027	0.388±0.03	*0.382±0.31*
Fe, %	15.3±0.5	14.5±0.4	*16.0±1.2*
Co, ppm	91±11	79±12	*48±5*
Ni, %	0.0179±0.0048	0.0191±0.0055	*0.0090*
Sm, ppm	1.46±0.09	1.01±0.07	*0.77±0.08*
Gd, ppm	1.17±0.09	1.08±0.07	*0.86±0.08*

*Compilation by Lodders (1998).

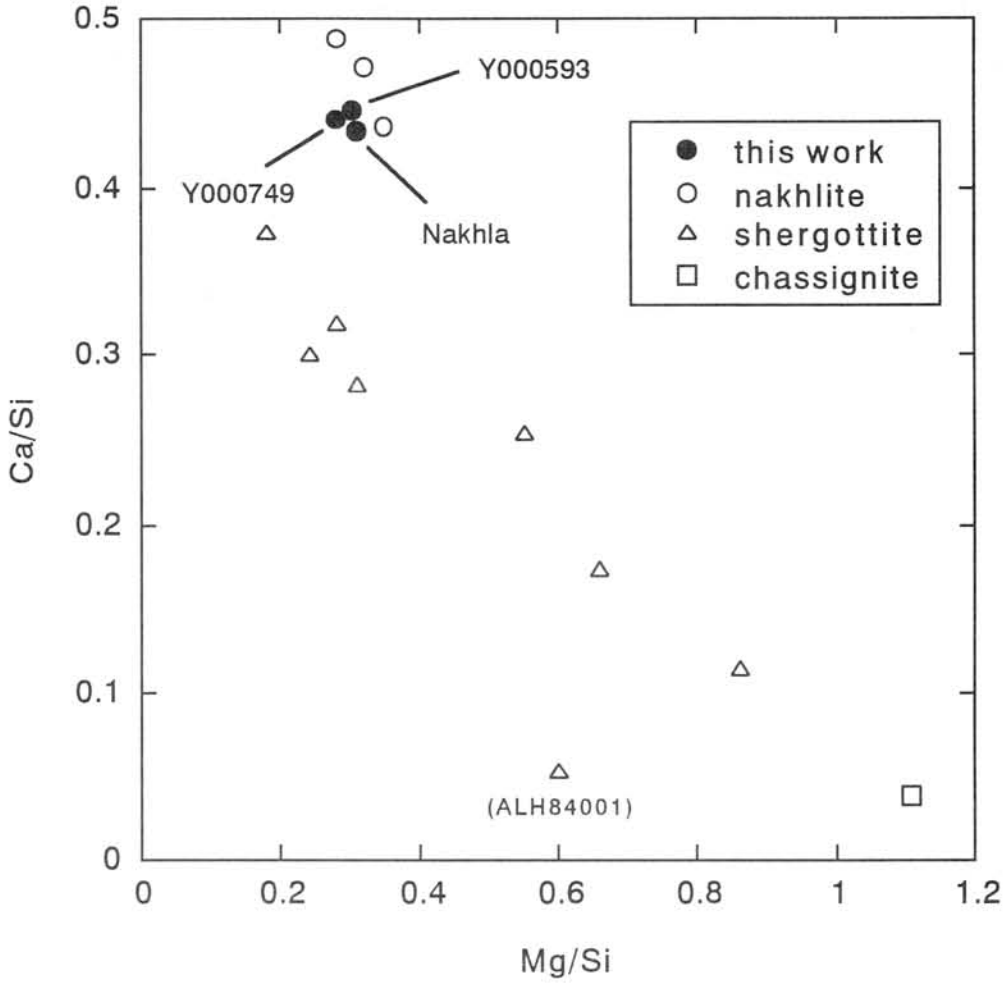

Fig1. Mg/Si – Ca/Si weight ratios diagram for SNC meteorites. Closed circles and open symbols show our results and compiled dara by Lodders (1998), respectively.

Elemental fractionation in primitive solar nebula and early solar chronology

M. Ozima[1], Yayoi Miura[2], and F.A. Podosek[3]

[1] Department of Earth and Planetary Science, University of Tokyo, Tokyo 113-0033, Japan (EZZ03651@nifty.ne.jp)

[2] Earthquake Research Institute, University of Tokyo, Tokyo 113-0032, Japan

[3] Department of Earth and Planetary Sciences, Washington University, St. Louis, MO 63130-4899, USA

Radioactive decay systems of short-lived nuclides such as ^{129}I - ^{129}Xe, ^{53}Mn - ^{53}Cr or ^{26}Al - ^{26}Mg give unparalleled information on early solar chronology. However, in order for these isotope systematics to serve as a useful chronological tool, a basic premise must in the first place be ascertained, that is, an assumption on a common primordial isotopic composition for radioactive parent nuclides. Unfortunately, there is at present no definitive way to prove this very important assumption, although observations generally appears to favor the assumption. In this report, we propose a new approach based on a correlation plot for initial isotopic ratios of parent and daughter elements (hereafter, we call it a I-R (Initial Ratio) plot), and show that this approach is useful in resolving this issue. We applied this method to ^{129}I - ^{129}Xe and ^{53}Mn - ^{53}Cr systematics, that are at present only two cases for which we have analytical data to construct an I-R plot.

Several workers have noted that there exists a negative correlation between the initial $^{129}I/^{127}I$ ratio and the $^{129}Xe/^{132}Xe$ ratio in a trapped Xe component in chondrules (e.g.,1, 2). Swindle et al.(2) interpreted that initial $^{129}I/^{127}I$ ratios (R_i) in the samples had evolved in pre-chondrule environment from a common primordial iodine with a same primordial ratio (R_0), and hence the negative trend gave a support for a chronological interpretation of ^{129}I - ^{129}Xe systematics. Swindle (3) further pointed out that if the pre-chondritic environment were of a closed system, the negative trend should be a straight line with a slope corresponding to I/Xe ratio in the pre-chondrule environment. Although the negative trend is apparent in Chainpur chondrules (2) and also supported by new Xe isotopic data on dark inclusions in Allende meteorite (4), the observed slope matches neither the solar I/Xe ratio nor values commonly observed in meteorites. We show that the characteristic features of Xe isotopic data seen in an I - R plot are consistently explained by assuming that Xe has been fractionated from I in the solar nebula that was dissipating exponentially with time.

We assumed exponential dissipation of solar nebula, and that Xe as well as I was captured by chondrules in the dissipating nebula. We show that the observed negative trend in an I - R plot is well simulated by a Xe isotope evolution equation which was derived for dissipating solar nebula. From fitting the data in an I - R plot to the Xe isotope evolution equation with free parameters (nebula dissipation time constant, primordial I and Xe isotopic ratios at the beginning of the solar system), we infer that the time constant for the nebula dissipation is about 25 Ma. This time constant is consistent with a generally assumed life of proto-solar nebula. From the model, we also infer that the primordial $^{129}I/^{127}I$ and $^{129}Xe/^{132}Xe$ ratios are considerably smaller than the values hitherto assumed from meteorite data, although the estimation of the primordial ratios involves large uncertainties. We note that some chondrules have the $^{129}Xe/^{132}Xe$ ratio of a trapped Xe as low as 0.9, well below the solar Xe ratio and even the least radiogenic $^{129}Xe/^{132}Xe$ ratio (Novo Urei meteorite). The new data on Allende dark inclusions (4) also support this smaller primordial $^{129}Xe/^{132}Xe$ ratio. If the primordial $^{129}Xe/^{132}Xe$ ratio were indeed as small as 0.9, this bears far reaching implications on early solar chronology. For example, the currently estimated value of the initial $^{129}I/^{127}I$ isotopic ratio of about 10^{-6} in the Earth (5) would become larger, and reduce the puzzling gap in an initial $^{129}I/^{127}I$ ratio (about 10^{-4} in meteorites) or in a formation age interval between the Earth and meteorites.

Although analytical data are still scanty and a definite conclusion cannot be deduced, a I-R plot for currently available ^{53}Mn - ^{53}Cr data show a rough negative correlation. This suggests that meteorite samples inherited initial Mn isotopes which had evolved from a same primordial Mn in a pre-meteorite reservoir. Therefore, like I-Xe systematics, Mn-Cr systematics seems to reflect a chronological effect. The implication of this conclusion is that short-lived nuclide ^{53}Mn was fairly uniformly distributed at least in the formation region of these meteorites.

Acknowledgements We thank C.M.Hohenberg and O.Pravdivtseva for allowing us to use their unpublished Xe isotopic data on Allende dark inclusions.

References

(1) Podosek F.A. (1970) *Geochimica et Cosmochimica Acta* **34**, 341-365.

(2) Swindle T.D. et al. (1991) *Geochimica et Cosmochimica Acta* **55**, 861-880.

(3) Swindle T.D. (1998) *Meteoritics and Planetary Sciences* **33**, 1147-1155.

(4) Hohenberg C.M and Pravdivtseva O. (2002) *Written communication.*

(5) Ozima M. and Podosek F.A. (1999) *Journal Geophysical Research* **104**, 25,493-9.

Graphitization process of carbon grain produced in methane gas atmosphere

Takeshi Sato[1], Yoshio Saito[2] and Chihiro Kaito[1]

[1]*Department of Nanophysics in Frontier Projects, Ritsumeikan University, Shiga 525-8577, Japan*

[2]*Department of Electron and Information Science, Kyoto Institute of Technology, Kyoto 606-8585, Japan*

Many types of carbon and carbonaceous materials have been proposed to explain the 217nm feature. One of the most plausible interstellar dust is so called "dark QCC", which formed from an ejecta of methane plasma [1]. Studies on the point of view of the growth on these carbonaceous grains have hardly done.

In the present studies, dynamic behavior of the QCC like carbon grains were examined by high resolution electron microscopy (HREM) at high temperature equipped with real-time video recording system. The carbon grains were produced by conventional carbon arc-discharge method in the methane gas atmosphere at 80Torr [2]. The produced carbon grains showed the amorphous halo diffraction ring. But the HREM image showed clearly the QCC like structure as indicated in Fig.1. The fundamental structure of the QCC had the hole at the central of carbon grain [3]. In the present grains, there is no hole. Curved fringes corresponding to the (002) graphite lattice image are seen as well as the QCC. These samples were set directly in a special heating stage in electron microscope [4] and structural change of the grains were photographed on video film by HREM mode. As is shown in the video images of the grains in Fig.2, these samples drastically changed their structure by heating temperatures. The structures of the curved graphite structure were distorted by the heating at 100℃ for 30 minutes as shown in Fig.2(a). This distortion is thought due to the elimination of the functional group such as -OH into vacuum. By the increase of heating temperature at about 260℃, well developed the graphitic or QCC like structures appeared as seen in Fig.2(b). The curved graphite layer of each grain became clear from the surface of each grain. The central parts of each grain became transparence on electron beam. This suggests that the developing of the graphitic structure introduced the voids in the central part of the grains. Therefor the structure of the QCC may be grown with the same process as indicated in Fig.2(b). By further heating at 550℃, each grains combined with graphite lattice relation in the form of the sheet as shown in Fig.2(c). The nano-diyamond grown from the QCC at 100℃ [4] was hardly grown in the present specimen. This may be due to the difference of the grain formation method and the sp^3-C terminated with

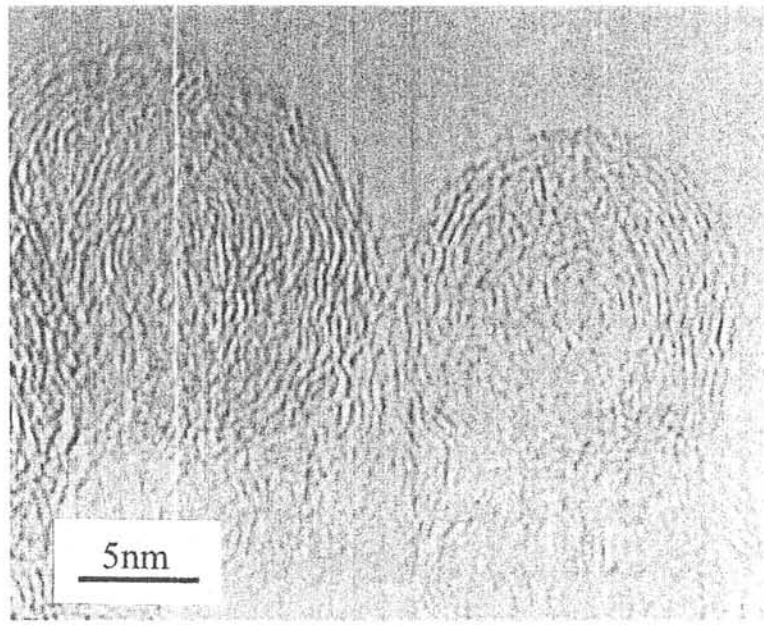

Fig. 1. HREM image of the carbon grains produced in the CH_4 gas atmosphere. The structure has QCC like grains.

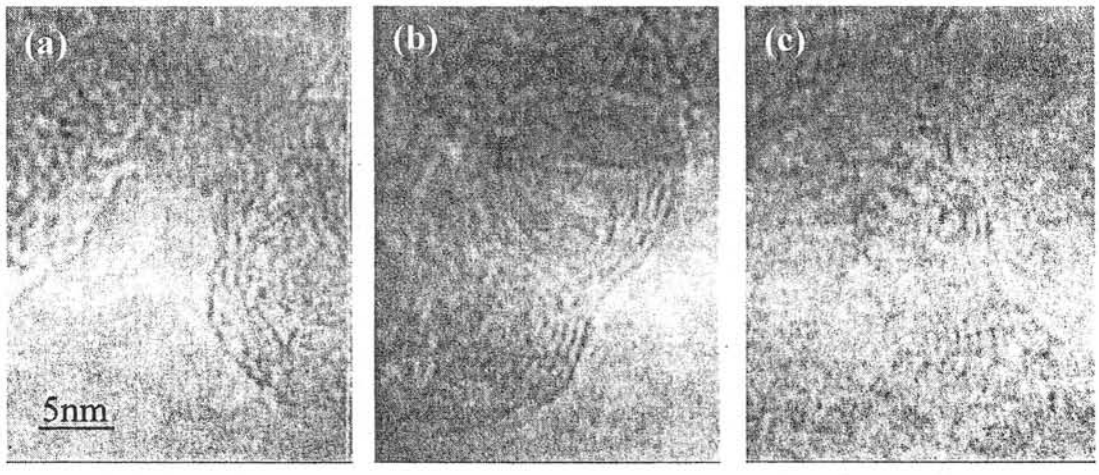

Fig. 2. Structural changes of the QCC like grains by heating in vacuum. (a) the grains heated at 100 degrees centigrade, (b) heated at 260 degrees centigrade and (C) heated at 550 degrees centigrade.

hydrogen atoms is hardly produced [4]. Typical amorphous carbon grains have been produced by the arc-discharge in He and Ar gases [5]. By heating of these grains produced inert gases, grains are hardly changed at the present temperature. If the atmosphere was in CH_4 gas, the grain of the QCC like structure were predominately produced. These results indicate that the various fundamental structures of the carbon grains can be produced by the selection of gas atmosphere.

References

[1] A. Sakata, et al. Nature 301 (1983) 493

[2] C. Kaito, et al. Planet. Space Sci. 43 (1995) 1271

[3] S. Wada, et al. Astron. Astrophys. 345 (1999) 259

[4] S. Kimura, et al. Antarct. Meteorite Res. 13 (2000) 145

[5] C.Kaito, et al. Mem. Inst. Sci. and Eng. Rits. Univ. 58 (1999) 11

CRYSTALLIZATION AGE OF ANTARCTIC NAKHLITE Y000593: FURTHER EVIDENCE OF NAKHLITE LAUNCH PAIRING. C.-Y. Shih[1], H. Wiesmann[1], L. E. Nyquist[2] and K. Misawa[3]. [1]Mail Code C23, Lockheed-Martin Space Operations, 2400 NASA Road 1, Houston, TX 77058, (chi-yu.shih1@jsc.nasa.gov), [2]Mail Code SR, NASA Johnson Space Center, Houston, TX 77058, (l.nyquist@jsc.nasa.gov), [3]Antarctic Meteorite Research Center, National Institute of Polar Research, 1-9-10 Kaga, Itabashi, Tokyo 173-8515.

Introduction: Nakhlites are clinopyroxene-rich meteorites that probably came from Mars [*e.g.* 1]. A total of six nakhlites have been identified so far including three recent finds, one small sample (~100 g) from the hot desert of Morocco (NWA 817) [2] and two large kilogram-sized samples from the Yamato Mountains of Antarctica (Y000593 and Y000749) [3]. Unlike other martian meteorites (*e.g.* shergottites), nakhlites have not been subjected to severe shock metamorphism and their original igneous textures are still well-preserved. Also, these meteorites have much older crystallization ages of ~1.3 Ga compared to ages of shergottites of ~0.18-0.47 Ga [*e.g.* 4]. In this report, we present preliminary Rb-Sr and Sm-Nd isochron data for the Y000593 Antarctic nahklite and discuss the age correlation with other nakhlites and the nature of their source crater on Mars. Results of further experiments and a full report will be presented elsewhere by K. M. when he visits Johnson Space Center later this year as a guest scientist.

Samples and Analytical Procedures: A sample of Y000593, weighing ~2.3 g, was kindly allocated by the National Institute of Polar Research (NIPR) of Japan. The sample is a coarse-grained rock and is extremely friable. One medium-sized fragment, plus fines, weighing ~0.5 g, was processed for this study by gently crushing it to grain size <149 μm. The sample was coned and about half of the crushed sample was taken as the whole rock sample. The rest of the crushed sample was sieved into two size fractions, 149-74 μm and <74 μm. Mineral separations were made from the coarser fraction using a Frantz magnetic separator. At 0.2 ampere, we obtained a green clinopyroxene (Cpx) sample of >95% purity. Two whole rock samples (WR1 and WR) and one Cpx sample weighing ~25 mg each were taken for this preliminary study. The WR and Cpx samples were washed with 2N HCl in an ultrasonic bath for 10 minutes to eliminate possible terrestrial contaminations or martian alteration products. Both the residues (r) and leachates (l) of these samples, plus unleached sample WR1, were analyzed for Rb, Sr, Sm, and Nd following the chemical procedures of [5]. The isotopic measurements were made on a Finnigan-MAT 261 multi-collector mass spectrometer following the procedures of [6]. The average values of $^{87}Sr/^{86}Sr$ for NBS 987 during the course of the study were 0.710237±0.000014 ($2\sigma_p$, 6 analyses), normalized to $^{88}Sr/^{86}Sr$=8.37521. The $^{87}Sr/^{86}Sr$ results reported here were renormalized to the NBS 987 $^{87}Sr/^{86}Sr$ =0.710250 of [7]. Because of the low Sm and Nd contents of the samples, Sm and Nd isotopic data were measured as SmO^+ and NdO^+. The $^{143}Nd/^{144}Nd$ results for samples reported here were renormalized to $^{143}Nd/^{144}Nd$ =0.511138 for the Caltech Nd standard n(Nd)β [8].

Rb-Sr Systematics: The Rb and Sr concentrations for four nakhlites are summarized in Fig. 1. Nakhla and Governador Valadares have similarly higher Rb and Sr contents than Lafayette, probably due to a higher olivine content in Lafayette. The Antarctic nakhlite Y000593 has similar Sr abundance as Nakhla and Governador Valadares, but among the nakhlites has an intermediate Rb abundance. The Rb and Sr distributions do not seem to correlate with the amounts of mesostasis in nakhlites as summarized by [3].

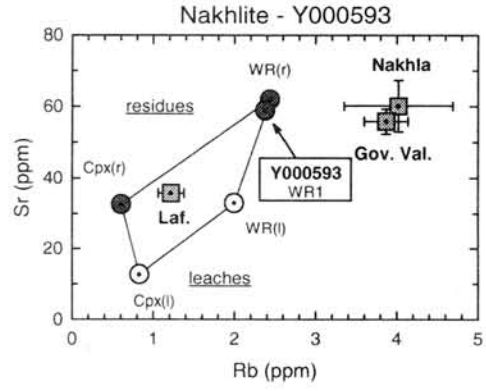

Figure 1. Rb and Sr concentrations in Y000593 and other nakhlites. Squares are bulk nakhlites. Circles are samples from Y000593. Solid circles are unleached WR and residues (r) from WR and Cpx. Open circles are WR and Cpx leachates (l).

The Rb and Sr concentrations for whole rocks and Cpx for Y000593 are also shown in Fig. 1. The near constancy of Rb and Sr in acid-leached and unleached WR samples, WR1 and WR(r), strongly suggests the terrestrial weathering effect on Rb and Sr is less significant for this Antarctic meteorite than for hot desert meteorites. The Sr abundances in the leachates from the WR and Cpx samples are 1/2 and 1/3 of those in their respective residues. However, the Rb contents of the leachates and residues are similar, resulting in significantly higher Rb/Sr in

leachates relative to residues. This probably is related to the dissolution of minor aqueous alteration products (e.g. iddingsites, halites, carbonates, and sulfates) in the samples by the acids.

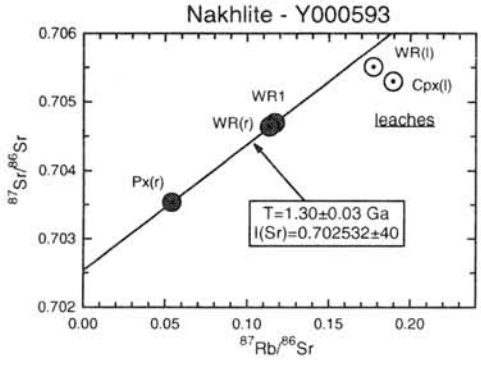

Figure 2. Rb-Sr isochron of nakhlite Y000593.

The $^{87}Rb/^{86}Sr$ and $^{87}Sr/^{86}Sr$ data for one unleached WR1, two residues and two leachates from WR and Cpx are shown in Fig 2. These samples do not define a single linear array. However, samples of WR1, WR(r) and Cpx(r) do form a line in the $^{87}Rb/^{86}Sr$ and $^{87}Sr/^{86}Sr$ correlation diagram. These three data yield an Rb-Sr age of 1.30±0.03 Ga for $\lambda(^{87}Rb)$ = 0.01402 Ga^{-1} and an initial $^{87}Sr/^{86}Sr$ of 0.702532±0.000040, using the Williamson (1968) regression program [9]. If the unleached WR1 datum were ignored, the tie-line defined by residues of WR and Cpx yields an identical age with a slightly higher error of ±0.04 Ga. This preliminary Rb-Sr isochron age for Y000593 is in excellent agreement with radiometric ages determined previously by various methods for three other nakhlites and Chassigny [e.g. 4-5]. Data for the two leachates, WR(l) and Cpx(l), plot to the right of the line, probably due to the presence of secondary aqueous alteration products (e.g. iddingsites) in the meteorites. This secondary alteration effect has been previously reported for other nakhlites, i.e., for Governador Valadares and Lafayette [5,10]. The initial $^{87}Sr/^{86}Sr$ for Y000593 nakhlite is within error limits of that of Lafayette [10] and Chassigny [11] but slightly different from that of other nakhlites. The slight discrepancy in the initial $^{87}Sr/^{86}Sr$ in nakhlites may be attributed to sampling of different flows of the same clinopyroxenite-dunite lithology on Mars.

Sm-Nd Systematics: The Sm and Nd concentrations of whole rock and Cpx samples of Y000593 and other bulk nakhlite samples are shown in Fig. 3. Like the Sr abundances in bulk nakhlites, Y000593, Nakhla and Governador Valadares have similarly higher Sm and Nd than Lafayette. This is also consistent with high abundances of olivine, in which REE occur in low abundance, in Lafayette. The very high Sm and Nd abundances in acid leachates of Y000593 whole rock and Cpx clearly suggest the presence of some chlorapatite, a REE-carrier phase commonly found in nakhlites [12], in Y000593.

The preliminary Sm-Nd isochron of nakhlite Y000593 is presented in Fig. 4. All five data analyzed so far, including two leachates, WR(l) and Cpx(l), define a good linear array corresponding to a Sm-Nd age of 1.31±0.03 Ga for $\lambda(^{147}Sm)$ = 0.00654 Ga^{-1} using the Williamson regression program [9]. This age is in excellent agreement with the Rb-Sr age obtained from the same samples. The concordancy of Sm-Nd and Rb-Sr ages strongly suggests that Y000593 crystallized 1.31 Ga ago. The age datum for this new Antarctic nakhlite provides additional evidence that nakhlites, and probably Chassigny as well, crystallized within a short period of time ~1.3 Ga ago. The initial ε_{Nd} value corresponding to the age for Y000593 is +15.7±0.2 ε, which is close to, but not within error limits of, those reported for other nakhlites and Chassigny. In a similar manner to the initial $^{87}Sr/^{86}Sr$ of nakhlites and Chassigny, the initial ε_{Nd} values of these rocks suggest they came from different flows of the same ultramafic lithology derived from melting of depleted mantle sources on Mars.

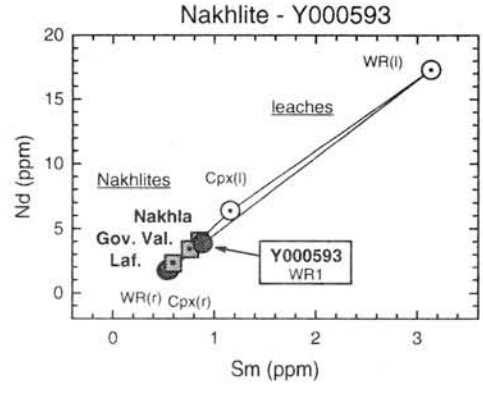

Figure 3. Sm and Nd abundances in Y000593 and other nakhlites. Symbols are the same in Fig. 1.

Discussion: The mineralogical-petrological and rare gas features of Y000749 are not exactly the same as those of Y000593 [13,14]. The modal abundance of olivine in Y000749 is higher than in Y000593, and in addition, the olivine composition in Y000749 is slightly richer in Mg compared with Y000593 olivine [13]. Additionally, the $^{129}Xe/^{132}Xe$ ratio in Y000749 is higher than in Y000593 [14], consistent with the petrological observation that iddingsite is more abundant in Y000749, and with the assumption that iddingsite is one of the carrier phases of ^{129}Xe. Nevertheless, assuming that Y000593 and Y000749 are indeed paired, the cosmic ray exposure

(CRE) age of Y000749/Y000593, 11±2.2 Ma, is consistent within error limits with the CRE ages of the nakhlites Nakhla, Governador Valadaras, and Lafayette (Summarized in [4] and Fig. 5). The CRE age of the third recently recovered nakhlite, NWA817, is 9.7±1.1 Ma [15]. Thus, there is a strong suggestion that all the nakhlites were ejected from Mars in the same event. Including the dunite Chassigny, which shares the same cosmic ray and crystallization ages as the nakhlites [4] the recovered mass from this event is ~60 kg. This is ~2/3 of the total recovered mass (~93 kg) of Martian meteorites. Even if the largest mass (Nakhla, ~40 kg [16]) is subtracted from the total, the nakhlites would still account for ~29% of the total mass of Martian meteorites. Additionally, the second-largest nakhlite, Y000593, is the largest achondrite to be recovered from the Antarctic. Thus, the nakhlite ejection event must have been large.

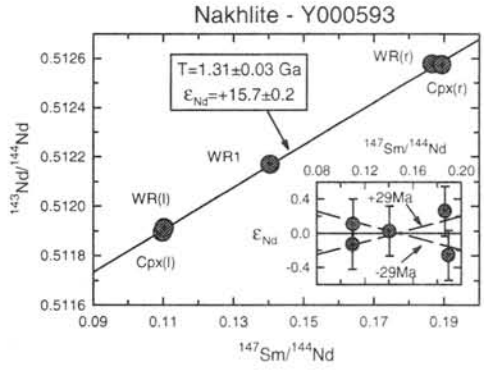

Figure 4. Sm-Nd isochron of nakhlite Y000593.

Conclusions: Warren [17] estimated a residual crater diameter of ~15 km for the nakhlite source crater prior to recovery of the Antarctic and Saharan nakhlites. One might expect some variation in crystallization ages for the rocks ejected by this event. Indeed, the data summarized by [4] suggests an age of 1.27±0.01 Ga for Nakhla, and slightly older ages of 1.32±0.02 Ga and 1.33±0.01 Ga for Lafayette, and Governador Valadares, respectively. The age of the dunite, Chassigny, could be older still, since the "preferred age" is 1.34±0.05 Ga [4]. Finding exactly where Y000593 belongs within this putative age sequence will require additional analyses. Finally, if the nakhlites and Chassigny are derived from a single crater, a careful characterization of impact-related phenomena, such as the degree of shock metamorphism, among the individual nakhlites and Chassigny may yield important constraints on the mechanism of their impact ejection from Mars. Peak shock pressures for Nakhla, Governador Valadares, and Lafayette are summarized in [4] as 20±5 GPa, whereas that for Chassigny is given as ~35 GPa. If peak shock pressures for the the newly recovered nakhlites continue to lie within a narrow range, it would suggest the nakhlites were excavated from a single stratum, or closely associated strata, of Martian rock.

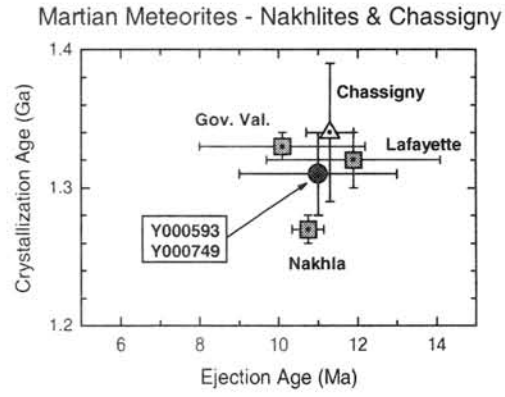

Figure 5. Crystallization and ejection ages of Y000593 (circle), other nakhlites (squares), and Chassigny (triangle).

REFERENCES: [1] McSween H.Y., Jr. (1994) *Met. Planet. Sci.* **29**, 757-779. [2] Gillet Ph. *et al.* (2001) *Met. Planet. Sci.* **36**, (Suppl.) A66. [3] Imae N. *et al.* (2002) *Lunar Planet. Sci.* **XXXIII**, CD-ROM #1483. [4] Nyquist L.E. *et al.* (2001) *Chronology and Evolution of Mars*, R. Kallenbach, J. Geiss, W.K. Hartmann, Eds. 96, 105-164. Kluwer Academic Publ. Dordrecht/ Boston/London. [5] Shih C.-Y. *et al.* (1999) *Met. Planet. Sci.* **34**, 647-655. [6] Nyquist *et al.* (1994) *Met. Planet. Sci.* **29**, 872-885. [7] Nyquist *et al.* (1990) *GCA*, **54**, 2195-2206. [8] Wasserburg *et al.* (1981) *GCA*, **45**, 2311-2323. [9] Williamson J.H. (1968) *Canadian J. Phys.* **46**, 1845-1847. [10] Shih C.-Y. et al. (1998) *Lunar Planet. Sci.* **XXIX**, CD-ROM #1145. [11] Nakamura N. *et al.* (1982) *Meteoritics*, **17**, 257-258. [12] Wadhwa M. and Crozaz G. (1995) *GCA*, **59**, 3629-3645. [13] Imae N. *et al.* (2002) this volume. [14] Okazaki R. *et al.* (2002) this volume. [15] Marty B., *et al.* (2001) *Met. Planet. Sci.* **36**, (Suppl.) A122-A123. [16] Graham A.L. *et al.* (1985) Catalogue of Meteorites, 4th Ed., Univ. Ariz. Press, Tucson. [17] Warren P.H. (1994) *Icarus*, **111**, 338-363.

Petrology and Reflectance Spectroscopy of a Lunar Meteorite Y981031

T. Sugihara[1], M. Ohtake[1], H. Takeda[2], A. Owada[3], T. Ishii[4], and M. Otsuki[4].

[1]Lunar Mission Research Center, Office of Satellite Technology, Research and Applications, National Space Development Agency of Japan, 2-1-1 Sengen, Tsukuba City, Ibaragi 305-0084, Japan (sugi-t@hope.tksc.nasda.go.jp).

[2]Research Inst., Chiba Inst. of Technology, 2-17-1 Tsudanuma, Narashino City, Chiba 275-0016, Japan.

[3]Advanced Engineering Service Co., 2-1-1 Sengen, Tsukuba City, Ibaragi 305-0084, Japan.

[4]Ocean Res. Inst., Univ. of Tokyo, 1-15-1 Minamidai, Nakano-ku, Tokyo 164-0014, Japan.

Introduction

In order to understand global distribution of surface materials on the moon, regional remote sensing data such as Clementine visible to near infra red (VIS-NIR) multi band spectral image have been employed as a powerful tool. However the "ground truth" information which is directly collected from the moon, is required to carry out calibrations and analysis of the spectral data precisely [e.g. 1]. Although returned samples from the Apollo missions are important for remote sensing ground truth, their information represents only those of very restricted area, and some assumptions can not be excluded on geological and petrological study of the moon. Yamato (Y) 981031 is a lunar mare meteorite[2, 3], and is considered to be good example of "ground truth" of the surface rocks which have not been obtained by Apollo. Hence, petrological and reflectance spectroscopic characteristics of Y981031 were investigated to gain better understanding of origin of the lunar meteorites and to establish relationship between the lunar surface rocks as ground truth and spectral data derived from regional remote sensing.

Methods

Analyses of mineral compositions of PTS Y981031-53-6 were carried out by a JEOL 733 electron probe micro analyzer at the Ocean Research Institute, University of Tokyo. Reflectance spectra of Y981031 were measured by a JASCO diffuse reflectance spectrometer at National Space Development Agency of Japan. Powder samples for the reflectance measurement were prepared from a fragment of Y981031-68 by crushing in an agate mortar. The powders were sieved out and collected only particles less than 75 μm. Measurement of the reflectance spectrum was performed on the particles. Incident and emission angles of the spectrometer are 30° and 0° , respectively.

Results

Y981031 is a polymict regolith breccia, and contains a number of mineral fragments in a dark comminuted matrix, which are composed of pyroxene, plagioclase, olivine and some iron oxide. Various lithic clasts including a few lithic fragments with granulitic texture, are also observed. Chemical compositions of plagioclase fragments show two FeO and MgO variation trends against anorthite content. Plagioclase grains in mare basalts have higher FeO and MgO contents than those of highland rocks with identical An content. The presence of two trends implies involvement of highland components having different petrological characteristics from mare materials. Based on these discussions, it is proposed that Y981031 is a mixture of major mare and minor highland components. A large apatite crystal and high-potassium plagioclase are also observed. Trace KREEPy materials would be involved in Y981031. There is dark yellow fusion crust on one side of the thin section. The glass is well vesiculated and no altered minerals such as clay minerals have been found under the microscope. Chemical compositions of the fusion glass are very similar to bulk chemical composition of Y981031 [2] although a range of chemical heterogeneity is also observed on the Al_2O_3-TiO_2 diagram (Fig. 1). Therefore, chemical composition of the fusion glass represents well mixed bulk rock chemistry and chemical modification by the alteration is not so prominent. The observed chemical heterogeneity would indicate difference of mixing ratio between the constituents in the meteorite. Fig.1 also show compositional relationship of

Y981031 bulk rock and fusion crust glass with mare basalts and lunar surface regolith returned by the Apollo and Luna missions. In Fig. 1 the chemical compositions of the regolith from each landing site fall on mixing lines between those of subsurface bedrock of a landing site and highland component having high-Al_2O_3 and low-TiO_2 compositions [4]. Then the bulk rock and fusion glass of Y981031 are on mixing line between very low-Ti (VLT) basalts and highland component, suggesting Y981031 was formed by mixing of the VLT basalts with some minor highland materials.

Bi-directional reflectance spectrum of Y981031 <75um fraction is shown in Fig. 2. Continum-divided spectrum is also shown. Pyroxene chemical compositions are plotted in the pyroxene quadrilateral in Fig. 3 with contours of 1 and 2 μm absorption wavelength of pyroxene [5]. The continum-divided spectrum shows clear absorption bands around 1 and 2 μm in wavelength, and positions of these absorption minima are well correspond to pyroxene chemical composition of the mineral fragments. Olivine absorption band around 1.2 μm is also observed. Although some absorption bands of orthopyroxene which was probably derived from highland rocks, can be identified around 2 μm, the most dominant feature is of high-Ca pyroxene, which is observed as large mineral fragment or in mare basalt clasts. Based on the mineralogical data, it is suggested that reflectance spectroscopic characteristics show mainly those of the source VLT basalts, though absolute value of the reflectance seems to be influenced by highland-materials. Pyroxene chemical compositions of Y981031 resemble to those of Y793274, which has been proposed to be derived from VLT basalt materials [6]. The data is consistent with a proposal that Y981031 is paired with Y793274.

Discussion

According to data of Clementine lunar exploration, VLT mare basalts are located only in northern part of near side maria, mainly in Mare Frigoris [7]. As mentioned above, the source basalt component of Y981031 is considered to be VLT basalts. Therefore Y981031 might be formed by an impact event in or near Mare Frigoris. Pyroxene compositional variation in Y981031 is not so complex except for contamination of some minor highland components. These observations imply source units of Y981031 were chemically similar to VLT basalt units, and another basalt units (e.g. low to high-Ti basalts) were not dominant. This interpretation is supported by Fig. 1 and TiO_2 trend in pyroxene crystals of Y981031 [3]. In Mare Frigoris, only VLT basalt units are observed. Mixing of highland materials would be easily taken place, since Mare Frigoris basalt units are proposed to be very thin and highland materials are excavated by 1 to 2 km crater. As compared with multi band spectrum from Clementine VIS-NIR image, the reflectance spectrum of Y981031 is similar to those of materials in a small crater (about 2km) or ejecta from the crater. Mare materials not overlaid cratering ejecta have spectroscopic characteristics having low reflectance and less obvious 1μm absorption, that is "mature" spectrum. These imply that Y981031 was a mixture of "fresh" major VLT mare components and minor highland materials, and it was ejected from a crater in or near Mare Frigoris. Comparison of regional remote sensing data with laboratory spectral data indicates that fresh mare basalt characteristics can be obtained from a small crater, even if highland materials are excavated in site or transported from a distant site. Such interpretation is important for geological study of the moon using the remote sensing multi spectral image.

In Conclusions, (1) The source unit(s) of Y981031 are VLT mare basalts, and a minor degree of mixing with highland materials, (2) The reflectance spectra of Y981031 is similar to those of materials in a small crater or ejecta from a crater in the VLT mare basalt region (e.g. Mare Frigoris), (3) Although highland materials were mixed, the reflectance characteristics of Y981031 represent those of VLT mare basalt components as the most dominant one

References

[1] Lucey P.G., Blewett D.T. and Hawke B.R. (1998) Jour. Geophys. Res. **103**, 3679-3699. [2] Kojima H., Kaiden H. and Yada T. (2000) Antarct. Meteorite Res., **13**, 1-8. [3] Arai T., Ishi T. and Otsuki M. (2002) LPSC **33**, abstr. #2064. [4] Papike J.J. and Simon S.B. (1982) Rev. Geophys. Spacephys. **20**, 761-826. [5] Arai T., Takeda H. and Warren P.H. (1996) Meteoritics Planet. Sci. **31**, 877-892. [6] Cloutis, E.A. and Gaffey M.J. (1991) Jour. Geophys. Res. **96**, 22809-22826. [7] Giguere T.M., Taylor G.J., Hawke B.R. and Lucey P.G. (2000) Meteoritics Planet. Sci. **35**, 209-212.

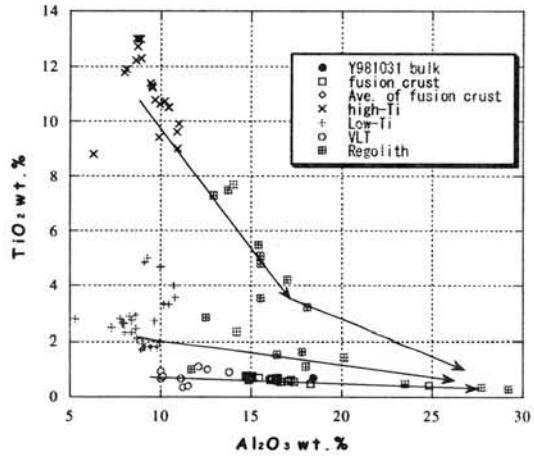

Fig. 1 TiO_2-Al_2O_3 variation diagram.

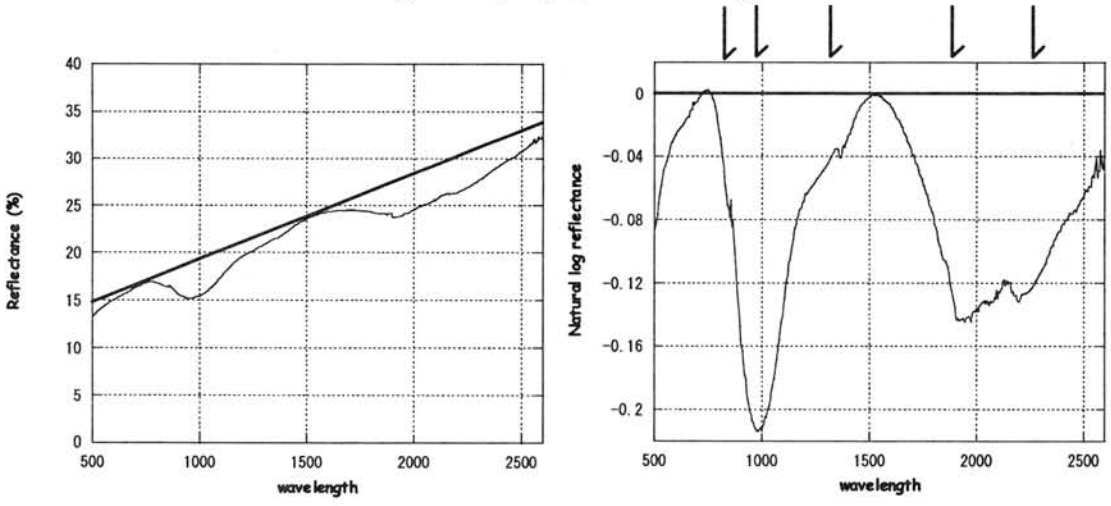

Fig. 2 Bi-directional reflectance and continuum-divided spectrum of Y981031.

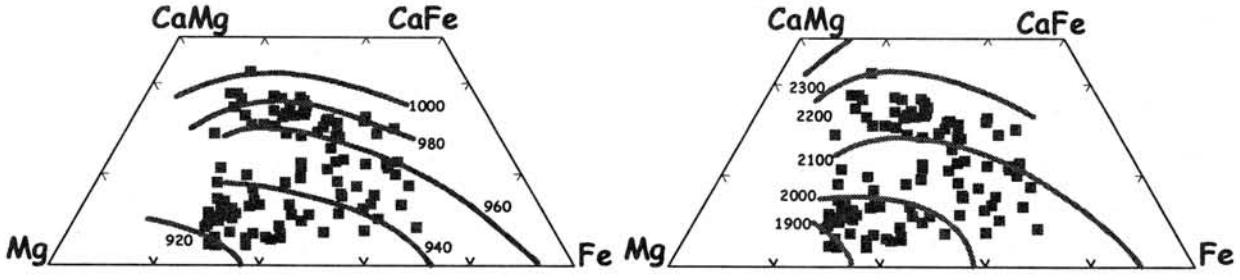

Fig. 3 Pyroxene composition of the mineral fragments in Y981031

Mineralogy and Trace Element Chemistry of Plagioclase and Ca Phosphate in Some Antarctic Lodranites.

Hiroshi Takeda[1], Weibiao Hsu[2,3] and Hiromi Ogata[1].

[1]*Research Inst., Chiba Inst. of Technology, 2-17-1 Tsudanuma, Narashino City, Chiba 275-0016,*

[2]*Purple Mountain Observatory, Chinese Academy of Sciences, Nanjing, China,*

[3]*Division of Geological and Planetary Science, Calif. Inst. of Tech., Pasadena, CA91125, U.S.A.*

Introduction

In spite of extensive petrologic studies of the primitive achondrites [1-3], basalts representing their complementary partial melts such as andesitic materials in the IAB irons [4], are almost unknown in lodranites-acapulcoite group. A plagioclase-enriched region was found in the EET84302 acapulcoite [2]. An evaluation of the trace element distributions in the individual minerals of a variety of acapulcoites and lodranites by Floss [5], has provided useful constraints on the partial melting processes that took place on the acapulcoite-lodranite parent body. The depletion of the rare earth elements (REEs) and other incompatible trace elements from lodranites, relative to acapulcoite pyroxenes, are consistent with the formation and removal of silicate partial melts from the lodranites. However, some rare lodranites still contain plagioclase, Ca-phosphates and diopside, which are considered as components of partial melts. We found that Y791493 and Y74357 contain such minerals. Because these lodranites have not been analyzed by Floss, we studied REE abundance of individual minerals of these lodranites. The textures and mineralogy suggest that the andesitic materials in the IAB and IIE irons were formed by inhomogeneous segregation of partial melts from chondritic source materials [4]. The segregation is one of the oldest differentiation events in the earliest solar system (4.516 Ga to 4.523 Ga) [4]. We made in situ ion probe analyses of individual minerals in the two lodranites, IAB and IIE irons at Caltech. In this study, we calculated the whole rock REE concentrations of the bulk meteorites based on their modal abundances. Torigoye *et al.* [6] performed model calculation of partial melting to match the analyzed alkali and REEs of some lodranites. Nagahara [7] also discussed the REE problems on Y8002. Based on the measured REE concentrations of individual minerals, we also computed bulk REE concentrations of Y8002. Our data are compared with other lodranite data by Floss [5] and with Caddo County [8] and Colomera by Hsu *et al.* [9].

Samples and Experimental Techniques

PTSs Y791493,91-3 and Y74357,62-1 were supplied from the NIPR. PTS Y791493,91-3 is a thin section of a small elongated chip 1.8×5.2 mm in size and contains plagioclase. PTS Y74357,62-1 was studied previously by us [3] and contains diopside (Di) and a small grain of merrillite (whitlokite). The presence of Ca phosphates was searched for nearly the entire areas of the PTS Y74357,62-1, using the Chemical Map Analysis (CMA) technique of the JEOL 8900 electron probe microanalyzer (EPMA) at the Geol. Inst. of Univ. of Tokyo. Chemical compositions of minerals were obtained by the JEOL 733 EPMA at Ocean Research Inst. of Univ. of Tokyo.

REE data for albite, diopside, orthopyroxene, Ca-phosphates and olivine were obtained with a Cameca IMS 3f ion probe at Caltech [9]. The method is the same as those used for the Colomera IIE irons by Hsu [8,9]. Samples were bombarded with primary O+ ions, using a current of 1-5 nA and an impact energy of 17 kV. The primary beam diameter on the samples was ~5-15 micrometer. The secondary ion mass spectrometer was operated at low mass resolving power and a 32V energy window. Secondary ions were energy filtered using a sample offset of 100V to suppress signals from complex molecular interferences and measured signals were deconvolved into REE and REE-oxide components following standard techniques [10, 11]. Absolute concentrations of each element we determined based on empirical relationships between measured peak/^{30}Si+ ratios, normalized to the SiO_2 content determined by prior EMP analysis. Standards were a synthetic Ti-pyroxene glass, NBS-612 glass, plagioclase glass, and Durango apatite.

Results

A mineralogical description of PTS Y74357,62-1 has been given by Takeda *et al.* [3]. Y74357 is a coarse-grained rocks and contains remarkable amounts of olivine (83 vol. %). Orthopyroxene (Opx 6 %) and diopside (Di 3 %) fill interstices of olivine grains. A Ca-phosphate (merrillite) grain was found to be adjacent to olivine. PTS Y791493,91-3 is smaller than that studied previously and consists of coarse-grained Opx and olivine grains. One twinned grain of plagioclase 0.11×0.39 mm in size was found in a junction of Opx, olivine, and opaque minerals.

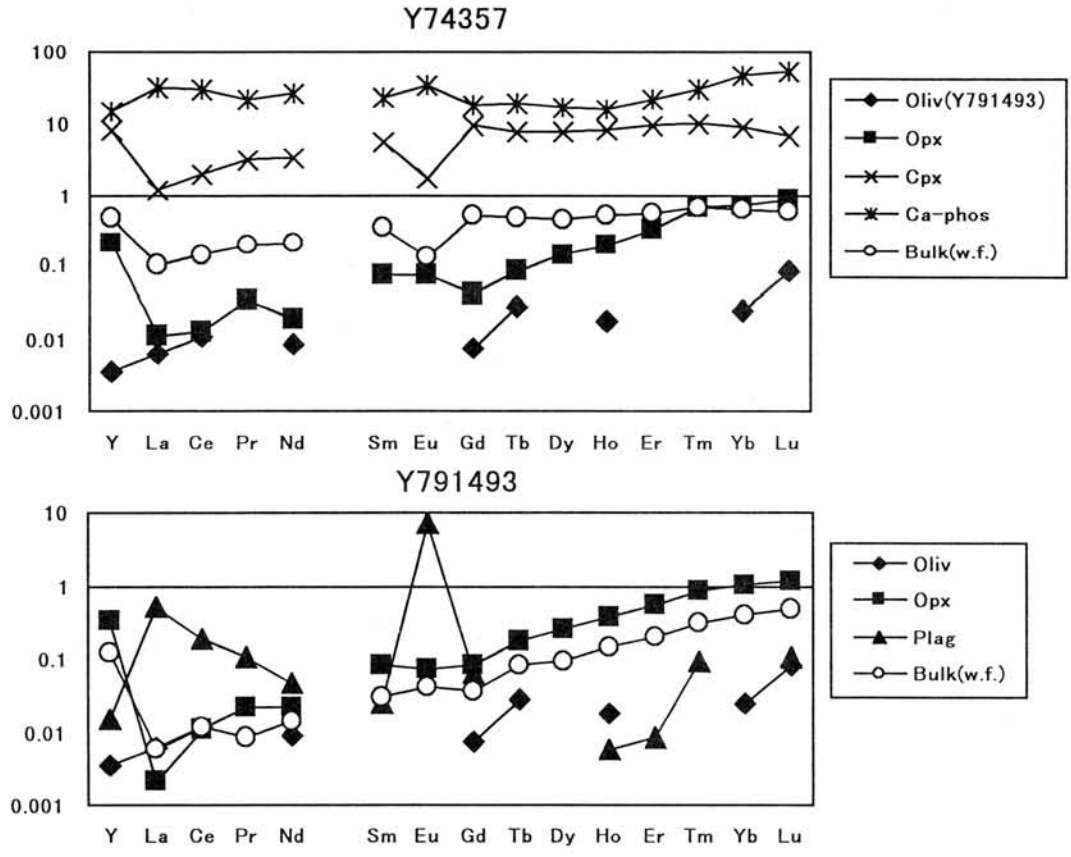

Fig. 1. CI-normalized REE data for the Y74357 and Y791493 lodranites (Cpx: diopside).

Table 1. REE Concentrations (ppm) of Minerals in Lodranites, Caddo Co. IAB iron and Colomera IIE iron.

	Diopsides		Plagioclase		Orthopyroxene		Ca-phosp		Bulk	Glass
	Y74357	Colomera	Y791493	Colomera	Y791493	Colomera	Y74357	Colomera	Caddo Co.	Colomera
Y	12.886	16.116	0.023	0.056	0.514	7.085	22.676	253.965	7.779	3.235
La	0.273	0.540	0.118	0.038	0.001	0.006	7.532	74.673	1.294	0.131
Ce	1.172	2.312	0.113	0.037	0.007	0.025	17.413	181.156	3.068	0.253
Pr	0.274	0.440	0.009	0.006	0.002	0.008	1.891	27.555	0.512	0.033
Nd	1.483	2.750	0.021	0.022	0.010	0.067	12.073	119.155	2.476	0.184
Sm	0.840	1.088	0.004	0.016	0.013	0.021	3.279	37.072	0.912	0.032
Eu	0.096	0.165	0.419	0.757	0.004	0.004	1.936	3.669	0.292	0.165
Gd	1.803	1.971	0.012	0.010	0.017	0.417	3.408	38.729	1.541	0.126
Tb	0.283	0.342		0.003	0.007	0.103	0.695	7.295	0.169	0.027
Dy	1.843	2.274		0.014	0.063	0.866	4.126	43.036	1.052	0.218
Ho	0.460	0.550	----	0.010	0.021	0.229	0.866	8.078	0.197	0.060
Er	1.460	1.820	----	0.023	0.087	0.956	3.415	23.508	0.747	0.244
Tm	0.247	0.260	----	0.005	0.021	0.152	0.691	2.964	0.110	0.040
Yb	1.404	1.879		0.011	0.170	0.362	7.432	24.653	0.719	0.117
Lu	0.167	0.270	----	0.002	0.028	0.157	1.256	2.833	0.091	0.057

----: below detection limits.

Fig. 1 shows CI-normalized REE abundances for the Y74357 and Y791493 lodranites. They are compared to those of other lodranites analyzed by Floss [5] and those of Caddo County [4,8] and Colomera [9] in Table 1. The bulk REE concentrations were calculated from the REE data of minerals measured by SIMS and modal abundance of the minerals. The mineral REE data reported by Floss [5] are broadly similar to those of minerals analyzed by Hsu for two lodranites. Calculated REE concentrations of the bulk meteorites, based on their modal abundance of minerals and the individual mineral data (Table 1), are also plotted in Fig. 1.

Discussion

The REE distribution patterns in the various phases of two lodranites are broadly similar to those in acapulcoite-lodranite by Floss [5]. The REE abundances (~10 to 50xCI) of the Y74357 merrillite are significantly lower than those in Caddo Co. and Colomera (> 100xCI). Phosphate of Y74357 has a relatively HREE-enriched pattern with a positive Eu anomaly whereas phosphate in Colomera has a relatively LREE-enriched pattern with a negative Eu anomaly. The REE of plagioclase in the Y791493 lodranite are not significantly lower than those of Caddo Co. and Colomera. Plag of Y791493 has similar REEs as that of Colomera, and the Eu anomaly is as high as those of Caddo Co. and Colomera. The lower REE concentrations of plagioclase and Ca-phosphate in two lodranites, may be explained by their formation process that they were not crystallized directly from the partial melts, but the mechanism is not clear. In Y74357, phosphate has a relatively HREE-enriched REE pattern, and in Colomera, phosphate has a relatively LREE-enriched REE pattern. We may have to consider the possibility of phosphate formation in lodranites by secondary metamorphism, such as redox reaction between P and CaO of pyroxene.

The REE concentrations of olivine in two lodranites has significantly lower REEs than that of Colomera. The REE concentrations of Opx in two lodranites show a similar trend. A little lower REE concentrations of the Y74357 Opx than Y791493 are within the analytical uncertainty. The REE trends of Opx and Di are more light REE depleted than those of Caddo Co. and Colomera. The Opx REE patterns of two lodranites have steeper slope towards the heavy REE, but they are not significantly different from those of Colomera and Caddo Co.

The calculated bulk REE compositions of the Y791493 lodranite are lower than those of IAB (Fig. 1) and show similar trends to those of the Y791493 Opx. The trend of Y74357 approaches to more flat trend, but mostly reflects the trend of the Y74357 Di. Torigoye *et al.* [6] and Nagahra [7] discussed the calculated REE abundance for Y8002 and the V-shaped pattern. We tried to reproduce the V-shaped REE pattern of Y8002 from the REE data of individual minerals in EET84302 of Floss [5], but the V-shaped pattern is not as pronounced as those of the above one. The bulk REE pattern is more flat with more positive Eu anomaly than those of Y74357. The Y74357 REEs are intermediate between Y791493 and Y8002.

In conclusions, the trends of REE concentrations obtained in this study for the Y74357 and Y791493 lodranites agree with those obtained previously for other members [5], and are broadly consistent with residues of partial melting with some liquids, in accord with the petrologic model. The level and slope of the REE distributions of Y74357 is intermediate between those of Y791493 and Y8002.

Acknowledgments: We acknowledge NIPR for supplying us with the samples of lodranites. This work was supported in part by funds from the cooperative program (No. 84134), 2000 provided by Ocean Research Inst., Univ. of Tokyo, and by a Grant-in-Aid for Sci. Res. from the Japanese Ministry of Education, Sci. and Culture and is carried out as a part of "Ground Research Announcement for Space Utilization" promoted by Japan Space Forum. Additional support came from NASA grants to G. J. Wasserburg and to G. R. Huss. We acknowledge Mrs. M. Otsuki, M. Hatano and M. Okamoto, for their technical assistance and Drs. T. Ishii, K. Yugami for their help in microanalysis. We are indebted to Profs. G. J. Wasserburg, G. Huss, Y. Ikeda, M. Miyamoto, Yuzo Kato, and to Drs. L. E. Nyquist, D. D. Bogard, N. Torigoye and H. Kojima for discussion and supports.

References: [1] McCOY T. J., KEIL K., MUENOW D. W. and WILSON L. (1997) *Geochim. Cosmochim. Acta* **61**, 639-650. [2] BENEDIX G. K., McCOY T. J., KEIL K., BOGARD D. D. AND GARRISON D. H. (1998) *Geochim. Cosmochim. Acta* **62**, 2535-2553. [3] TAKEDA H., MORI H., HIROI T. and SAITO J. (1994) *Meteoritics* **29**, 830-842. [4] TAKEDA H., BOGARD D. D., MITTLEFEHLDT D. W., GARRISON D. H. (2000) *Geochim. Cosmochim. Acta* **64**, 1311-1327. [5] FLOSS C. (2000) *Geochim. Cosmochim. Acta* **35**, 1073-1085. [6] TORIGOYE N., YAMAMOTO K., MISAWA K. AND NAKAMURA N. (1993) *Proc. NIPR Symp. Antarct. Meteoriies* **6**, 100-119. [7] NAGAHARA H. (1992) *Proc. NIPR Symp. Antarct. Meteoriies* **5**, 191-223. [8] TAKEDA H., HSU W. AND OGATA H. (2001) *Antarct. Meteorites* **XXVI**, 135-137. [9] HSU W., TAKEDA H., HUSS G. R. and WASSERBURG G. J. (1997) *Meteoritics and Planet. Sci.* **32**, A61-62. [10] ZINNER E. AND CROZAZ G. (1986) *Int. J. Mass Spectrom. Ion Processes* **69**, 17-38. [11] FAHEY A. J., GOSWAMI J. N., MCKEEGAN K. D. and ZINNER E. (1987) *Geochim. Cosmochim. Acta* **51**, 329-350.

Impact-induced comminution and dispersal of hydrated asteroids: Implications from shock experiments on carbonaceous chondrites

K. Tomeoka, K. Kiriyama, K. Nakamura, Y. Yamahana and T. Sekine*

Department of Earth and Planetary Sciences, Faculty of Science, Kobe University, Nada, Kobe 657-8501, Japan. *National Institute for Materials Science, Tsukuba 305-0044, Japan.

Introduction

Dust particles dominate the amount of interplanetary materials in the solar system [1]. Those collected on the Earth surface, termed micrometeorites, are generally 50-500 μm in size, whereas those collected in the stratosphere, termed interplanetary dust particles (IDPs), are <50 μm [2]. Mineralogical and chemical studies indicate that most of micrometeorites and hydrated IDPs are related to CI and CM carbonaceous chondrite matrix [2-6] that is composed mainly of hydrous phyllosilicates. This contrasts with the fact that CI and CM chondrites comprise only 2.8% of meteorite falls [7]. Considering that most of both dust particles and meteorites probably come from asteroids [e.g. 4, 8], the great difference in abundance of those objects is problematic.

Apart from this, there is a major unresolved problem regarding the shock metamorphic history of CI and CM chondrites. These chondrites are regarded as having once been part of the early planetesimals, and it is widely believed that the planetesimals accumulated through mutual collisions and grew to form larger planetary bodies. If this hypothesis is correct, CI and CM parent bodies must have been involved in extensive shock events in the early solar system. However, among CI and CM chondrites, those having been shocked to high pressures (>10 GPa) are absent [9], while all other groups of chondrites exhibit evidence of shock at much higher pressures. This fact is contradictory to the above mentioned model for planetesimal evolution.

We have performed a series of shock-recovery experiments on the Murchison CM and Allende CV carbonaceous chondrites. Both meteorites contain major fractions of porous matrix, but the matrix of Murchison is hydrated (~12 wt% H_2O in bulk meteorite), while the matrix of Allende is anhydrous (<0.1 wt% H_2O) . In the process of our experiments, we found that the Murchison matrix shows unusual textural changes in response to shock at a certain pressure range. This discovery gives insights into the above raised problems. We here present new implications for the problems based on the results of our shock experimental studies.

Materials and Methods

Shock-recovery experiments were performed by using a single stage 30-mm bore propellant gun. Murchison samples were shocked at 7, 11, 21, 26, 28, 30, 34, 36 and 49 GPa, whereas Allende samples were shocked at 27, 31, 37, 41 and 49 GPa. Details of the shock experimental procedures are described in [10]. Recovered samples were studied by using an optical microscope, a scanning electron microscope equipped with EDS and an electron microprobe analyzer equipped with WDS. Some samples were studied by using a transmission electron microscope (TEM) equipped with EDS.

Results

Matrix in Murchison (CM)

At < 25 GPa, randomly oriented fractures (1-5 μm wide) form in the matrix. Minor amounts of local melts occur as veins and pockets at 21 GPa. Otherwise no marked changes in texture are observed. However, at 25-30 GPa, matrix exhibits dramatic changes in texture. Narrow (1-5 μm) subparallel fractures form at high density, at intervals of 5 to 10 μm in directions roughly perpendicular to the compression axis. The high density fractures occur locally at 25 GPa, and extend throughout the matrix at 30 GPa. At 30 GPa, in addition to the narrow fractures, wider (20-50 μm) fractures occur in a mesh-like network throughout the meteorite, thus dividing the whole meteorite sample into small domains that range in size from 50 to 500 μm. At 25-30 GPa, local melts also occur in the matrix. At >30 GPa, local melts extend pervasively throughout the matrix and form intermixtures with fine grains of matrix, olivines and pyroxenes, and the original chondrite texture is increasingly disrupted. At 49 GPa, the matrix is totally melted.

We made ultra-thin sections, using an ultra-microtome, from small particles plucked from the Murchison sample shocked at 30 GPa, and observed them using a TEM. The particles consist of abundant fine grains (0.2-1.0 μm) of Fe-rich olivine embedded in an amorphous to microcrystalline material. The latter contains numerous small grains (5-20 nm) of Fe-(Ni) sulfide and Fe-rich phases, probably oxides. In places, phyllosilicate grains having an interlayer spacing of ~0.7 nm occur, which are probably Fe-rich serpentine. Tochilinite has not been observed. The overall texture and

constituent minerals are similar to those of fine-grained unmelted micrometeorites and some hydrated IDPs.

Matrix in Allende (CV)

At < 40 GPa, randomly oriented fractures form, but high density fractures such as formed in the Murchison samples are not observed. Minor amounts of local melts are present in the samples shocked at 27 and 37 GPa. These characteristics resemble those of the matrix of Murchison shocked at <25 GPa. At 41 GPa, narrow fractures form at high density, although locally, in directions roughly perpendicular to the compression axis. At 49 GPa, the matrix is totally melted.

Discussion

Our study reveals that dense, narrow fractures form in the matrix of Murchison by shock at ~25 GPa and extend throughout the matrix at ~30 GPa. Those fractures have never been known from natural chondritic meteorites. They were probably produced during volume expansion on release of shock pressure. At 21-30 GPa, local melting also occurs, which indicates that shock heating increases dramatically, simultaneously with the comminution. The heating must cause dehydration of hydrous minerals and evaporation of volatiles (mostly H_2O), and as a result, contribute to a generation of great expansive force on pressure release. In our experiments, the meteorite samples were encapsulated within stainless steel containers, so they could be recovered. Otherwise the comminuted samples must have been dispersed explosively.

Our study also reveals that Allende responds to shock compression differently from Murchison. High density fractures also form in the matrix of Allende, but they start to form at pressures much higher than those for Murchison (~40 GPa vs. ~25 GPa). In Allende, the matrix becomes totally melted at ~49 GPa that is almost the same as that for Murchison; so the range of pressures in which matrix is totally comminuted but not totally melted is much narrower in Allende (perhaps 43-47 GPa) than in Murchison (30-47 GPa). It appears that the difference in shock response between these two meteorites is mainly caused by the difference in mineral constituents in matrix. The formation of dense fractures in matrix is probably characteristic of hydrated chondrites such as CI and CM chondrites.

Scott et al. [9] showed, based on petrographic observations, that almost all CM chondrites are shock stage S1 (virtually unshocked). This contrasts with the fact that ordinary chondrites and enstatite chondrites (both comprise 81% of meteorite falls) include major fractions of meteorites shocked to shock stage S4-S6. To explain this, Scott et al. [9] hypothesized that CM chondrites shocked above 20-30 GPa escaped from the parent asteroids due to explosive expansion of shocked material on pressure release and formed particles that are too small to survive as meteorites. The results of our experiments support their hypothesis.

From these results, we suggest that if hydrated porous asteroids are shocked on the surface at pressures 25-45 GPa, the shocked materials would be densely comminuted, and on pressure release, the comminuted particles would be explosively dispersed into interplanetary space. A substantial fraction of CI- and CM-like micrometeorites and IDPs existing in interplanetary medium were probably produced by this process from CI- and CM-like asteroids. It is rather surprising that the size of particles (50-500 μm) formed in Murchison shocked at 30 GPa is comparable to the size of micrometeorites recovered on the Earth. Those particles of Murchison appear to be partially altered by shock heating, but most still contain undecomposed serpentine; these mineralogical characteristics are also consistent with those of most unmelted micrometeorites and hydrated IDPs.

References

[1] Love S.G. and Brownlee D.E. (1993) Science 262, 550-553.

[2] Engrand C. and Maurette M. (1998) Meteor. Planet. Sci. 33, 565-580.

[3] Kurat et al. (1994) Geochim. Cosmochim. Acta 58, 3879-3904.

[4] Genge M.J., Grady M.M. and Hutchison R. (1997) Geochim. Cosmochim. Acta 61, 5149-5162.

[5] Nakamura T. et al. (2001) Geochim. Cosmochim. Acta 65, 4385-4397.

[6] Schramm L.S., Brownlee D.E. and Wheelock M.M. (1988) Meteoritics 24, 99-112.

[7] Sears D.W. and Dodd R.T. (1988) Meteorites and the Early Solar Solar System, pp. 3-34.

[8] Flynn G.J., Sutton S.R. and Klock W. (1993) Proc. NIPR Symp. Antarct. Meteorites 6, 304-324.

[9] Scott E.R.D., Keil K. and Stoffler D. (1992) Geochim. Cosmochim. Acta 56, 4281-4293.

[10] Tomeoka K., Yamahana Y. and Sekine T. (1999) Geochim. Cosmochim. Acta 63, 3683-3703.

The first discovery of diopside $CaMgSi_2O_6$ breakdown under high pressure in a shocked H chondrite

Naotaka Tomioka[1], Makoto Kimura[2]

[1]Department of Earth and Planetary Sciences, Faculty of Science, Kobe University, 657-8501, Japan

[2]Faculty of Science, Ibaraki University, Mito 310-8512, Japan

Introduction: Olivine, pyroxene and plagioclase are the major constituent minerals of chondritic meteorites. Previously, most of ultrahigh-pressure polymorphs of olivine, low-Ca pyroxene, and plagioclase have been discovered in shock-induced melt veins in ordinary chondrites by analytical transmission electron microscopy (ATEM), X-ray diffraction and Raman spectroscopy [1]. Ultrahigh-pressure minerals not only record shock histories of chondrites but also provide clues to understand the structure and dynamics of the deep Earth. However, only high-pressure phase transition of Ca-rich pyroxene has not been found probably due to relatively low abundance among major silicates in ordinary chondrites. Here we report the first evidence for dissociation of $CaMgSi_2O_6$ pyroxene under high pressure in shocked Yamato-75100 chondrite.

Results: Y-75100 is classified as an H6 chondrite and consists of olivine, low-Ca pyroxene, Ca-rich pyroxene, plagioclase, kamacite, and troilite. It has shock-induced melt veins of less than 1 mm in thickness. In these veins, rounded to irregular fragments (~10-100 μm) of host minerals are enclosed in fine-grained (< 5 μm) mineral aggregates. Laser Raman spectroscopy clarified that shock veins contain polycrystalline fragments of high-pressure minerals such as ringwoodite, wadsleyite (olivine polymorphs), akimotoite (pyroxene polymorph) and hollandite-phase and jadeite (plagioclase polymorphs) [2]. The fine-grained matrix of veins is dominated by majorite or low-Ca pyroxene. In examined area by ATEM, low-Ca majorite occurs as relatively large crystals (~1-3 μm) and their interstices are filled with kamacite and troilite. Fe-rich inclusions are often enclosed as tiny blebs inside majorite crystals. This lithology suggests low-Ca-majorite has been crystallized from shock-induced melt, which is supported by incorporation of Na and Al in these majorites [2]. Very fine-grained assemblages were also found in a shock vein (Fig. 1). They are adjacent to the polycrystalline fragment of $NaAlSi_3O_8$-hollandite or majorite+FeS+FeNi assemblages. Individual grains are 100-400 nanometer in size. These aggregates consist of two kinds of grains. Selected area electron diffraction patterns taken from one phase are consistent with a body-centered cubic cell of garnet structure (majorite) with a space group *Ia-3d*. Quantitative chemical analyses by ATEM revealed that it has pyroxene stoichiometry. Its averaged composition is $En_{65}Fs_9Wo_{26}$. This majorite is enriched in Ca and poor in Al compared with majorite that was crystallized melt in the matrix of shock veins. Another phase coexisting with Ca-rich-majorite does not show any diffraction spots, therefore it is amorphous. It also has pyroxene chemistry of $En_{23}Fs_5Wo_{72}$. We also tried ATEM analyses of these Ca-rich–majorite + Ca-rich-glass

aggregates using broader electron beam (~1-2 μm). The averaged composition of these aggregates is $En_{49}Fs_8Wo_{43}$. It is similar to the chemistry of Ca-rich clinopyroxene ($En_{47}Fs_6Wo_{47}$) in the host rock, although there is little difference between their compositions, probably due to relatively large grain to the size of electron beam.

Discussion: Both Ca-rich-majorite and –glass in Y-75100 have different chemistry especially in Ca in host diopside, but the bulk composition of their aggregates is nearly the same. In addition, Fe-rich interstitial phases or inclusions are not contained in the aggregates. This suggests that Ca-rich-majorite and -glass are dissociation products of diopside in a solid-state reaction rather than by crystallization from shock-induced melt. Ca-rich glass is especially rich in $CaSiO_3$ component. According to high-pressure experiments in $CaSiO_3$, perovskite-structure phase is stable above ~12 GPa at ~1000 °C, but it retrogressively transforms into glass on release of pressure [3-4]. Therefore, Ca-rich glass in Y-75100 would have initially formed as $CaSiO_3$-perovskite and subsequently vitrified during decompression process. As for chemistry of majorite solid solution, the solubility of $CaSiO_3$ component into $MgSiO_3$ majorite is at most ~14 mol % at the pressure range of 16-22 GPa [5]. In this study, however, $CaSiO_3$ in Ca-rich-majorite is ~26 mol %. Other components such as Fe or Al may significantly increase the solubility of $CaSiO_3$ components in majorite. Majorite and $CaSiO_3$-perovskite are abundant minerals in subducting basaltic clast at the upper most of the Earth's lower mantle [6]. Therefore, systematic experiments on the element partitioning between majorite and $CaSiO_3$-perovskite are necessary to understand the fate of subducting slabs. The assemblage of Ca-bearing-majorite and -glass (assumed as $CaSiO_3$-perovskite) suggests that the dissociation of diopside in Y-75100 occurred at ~18-24 GPa based on the phase diagram of $CaMgSi_2O_6$ [7]. This is consistent with the formations of ringwoodite, akimotoite and $NaAlSi_3O_8$-hollandite found in shock veins in Y-75100.

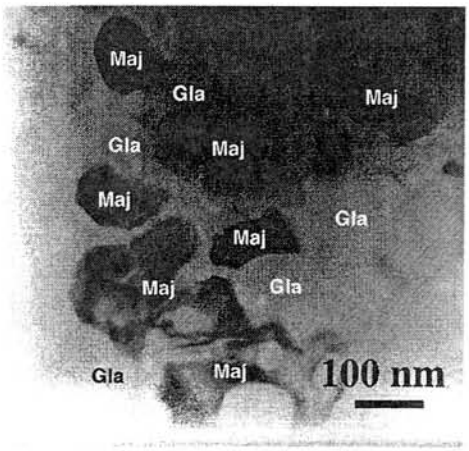

Figure 1. Transmission electron micrograph of the assemblage of Ca-rich majorite (Maj) and Ca-rich glass (Gla).

References: [1] e.g. Sharp T. et al. (1997) *Science* **277**, 352-355; Tomioka N. and Fujino K. (1997) *Science* **277**, 1084-1086; Gillet P. et al. (2000) *Science* **287**, 1633-1636; Tomioka et al. (2000) *Geophys. Res. Lett.* **27**, 3997-4000. Xie Z. et al. (2001) *Meteorite. Planet. Sci.* **36**, A226-A227. [2] Kimura M. et al. (2000) *Meteorite. Planet. Sci.* **35**, A87-A88. [3] Liu L. and Ringwood A.E. (1975) *Earth Planet. Sci. Lett.* **28**, 209-211. [4] Liu L. (1987) *Geophys. Res. Lett.* **14**, 1079-1082. [5] Gasparik T. (1996) *Contrib. Mineral. Petrol.*, **124**, 139-153. [6] Irifune T. & Ringwood A.E. (1993) *Earth Planet. Sci. Lett.*, **117**, 101-110. [7] Oguri K. et al. (1997) *Phys. Earth Planet. Inter.*, **104**, 363-370.

Redistribution of Mn and Cr during thermal metamorphism of L chondrites.

T. Tomiyama[1] and K. Misawa[1,2]

[1]Department of Polar Science, School of Mathematical and Physical Science, Graduate University for Advanced Studies, 1-9-10 Kaga, Itabashi, Tokyo 173-8515, Japan. [2]Antarctic Meteorite Research Center, National Institute of Polar Research, 1-9-10 Kaga, Itabashi, Tokyo 173-8515, Japan.

Introduction: The degrees of metamorphism of ordinary chondrites (OCs) are variable, reflecting individual thermal histories on their parent bodies. Based on chemical and petrologic characteristics, OCs have generally been classified into petrologic types 3 to 6 [1]. OCs with higher petrologic types have suffered more intense or prolonged thermal metamorphism than those with lower petrologic types..

If the OC parent body was heated by internal heat sources such as the decay of ^{26}Al [2], it would result in a concentric gradation of metamorphic degrees which has been called the onion-shell structure [3, 4]. This onion-shell model predicts the positive correlation between petrologic type and duration of thermal metamorphism as well as peak metamorphic temperature. Evidence supporting the onion-shell model was reported for H chondrites, based on the U-Pb chronology of phosphates [5] and on the fission-track density of phosphates and pyroxenes [6]. On the other hand, there is no clear relationship between petrologic types and cooling rates estimated from Fe-Ni zoning in kamacite [7,8] or from pyroxene structure [9]. The rubble-pile model as the result of breakup and reassembly of the parent body was proposed to describe the lack of correlation between cooling rates and petrologic types of OCs [7,8]. The discrepancy between these two models could be caused by the ambiguity in the thermodynamic data of the diffusion-controlled processes along with the insufficient time resolution of the clocks using long-lived radionuclides.

If the ^{53}Mn-^{53}Cr ($t_{1/2}$= 3.7 Myr) system is applicable to OCs, it may provide better constraints on the time scale of the thermal metamorphism. For the precise determination of Mn-Cr ages, the isotopic analysis should be done for phases with high Mn/Cr ratios. Thus we studied the behavior of Mn and Cr in olivine, because one of the Mn-rich, Cr-poor phases in OCs.

Experiments: Polished thin-sections of 12 unbrecciated L chondrites (type 3 to 6) were examined in this study. Electron probe analysis was carried out at an accelerating voltage of 15 kV with a beam current of 30 nA. Counting

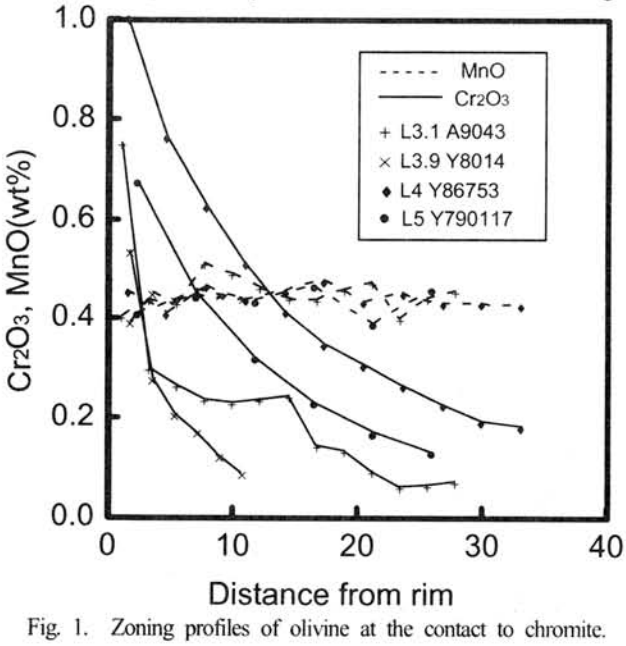

Fig. 1. Zoning profiles of olivine at the contact to chromite. Althouvh The MnO abundances of olvines range widely in L3 chondrites, presented gains show only weak zonings.

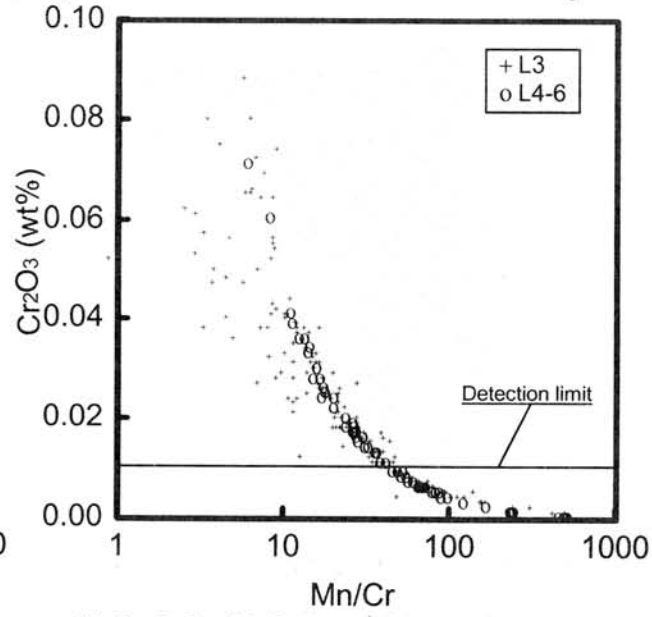

Fig. 2. Cr_2O_3 to Mn/Cr diagram of olivine in L chondrites.

time was 30 sec for Mn and 90 sec for Cr. Typical detection limits for MnO and Cr_2O_3 were 0.02 wt% and 0.01 wt%, respectively.

Results and Discussion: The MnO abundances of olivine in equilibrated L chondrites are within the range 0.4-0.5 wt%, whereas those in unequilibrated chondrites have a wider range from below detection limits to 0.8 wt%. Although the ranges of Cr_2O_3 abundances of olivines in unequilibrated L chondrites and in equilibrated L chondrites overlap, olivines in equilibrated L chondrites are generally depleted in Cr_2O_3 in comparison with those in unequilibrated L chondrites. The Cr_2O_3 abundances of olivines are commonly below detection limit in equilibrated L chondrites. However, in those chondrites, olivines adjacent to chromites are enriched in Cr_2O_3 and their Cr_2O_3 abundances become richer near the grain boundaries (Fig. 1).

These results are consistent with the redistribution of Mn and Cr among olivines and other phases during thermal metamorphism. It is known that olivine, pyroxene and Fe-Ni metal in equilibrated ordinary chondrites are depleted in Cr in comparison with those in unequilibrated ordinary chondrites [10-12]. Chromium may have redistributed from these minerals to chromite during thermal metamorphism. However, chemical zoning of Cr-rich olivines near chromites in equilibrated L chondrites is inconsistent with the diffusional redistribution of Cr from olivine to chromites. If Cr was redistributed from olivine to chromite during thermal metamorphism, olivines should be depleted in Cr in their rim. This could have resulted from resetting of the chemical zoning at high temperature by the redistribution of Cr from chromite to Cr-poor olivine during cooling.

We can expect an Mn/Cr ratio of at least several tens when Cr-poor portions of olivine are selected for analysis (FIG. 2). If the parent body with asteroidal size was heated by the decay ^{26}Al ($t_{1/2}$ = 0.73 Myr), the estimated time scale of thermal metamorphism would be 10 Myr for type 3-5 chondrites and 100 Myr for type 6 chondrites [3,4]. If this was the case, we could apply the ^{53}Mn-^{53}Cr system only when the thermal metamorphism occurred at a very early stage in the Solar System. However, chondrite parent bodies may have experienced disruptive collision during thermal metamorphism and some materials may have been excavated from the interior and cooled rapidly [7,8]. Among the examined samples, the olivine-spinel geothermometry [13] gives higher equilibration temperatures for Y-86753 (Fig.3). Y-86753 may have rapidly cooled after thermal metamorphism. The ^{53}Mn-^{53}Cr system could be applicable for this type of samples.

References: [1] Van Schmus, W. R. and Wood, J. A. (1967) *GCA 31*, 747. [2] Lee, T. et al. (1976) *GRL 3*, 109. [3] Miyamoto, M. et al. (1981) *PLPSC 12B*, 1145. [4] Bennet, M. E. III and McSween, H. R. Jr. (1996) *MAPS 31*, 783. [5] Göppel, C. et al. (1994) *EPSL 121*, 153. [6] Pellas, P. and Storzer, D. (1981) *Proc. R. Soc. London, A374*, 253. [7] Scott, E. R. D. and Rajan, R. S. (1981) *GCA 45*, 53. [8] Taylor, G. J. et al., (1987) *Icarus 69*, 1. [9] Folco, L. et al., (1997) *MAPS 32*, 567. [10] Kong, P. and Ebihara, M. (1995) *GCA 60*, 2667. [11] Kong, P. and Ebihara, M. (1997) *GCA 61*, 2317. [12] McCoy T. J. et al. (1991) *GCA 55*, 601. [13] Fabriés, J. (1979) *CMP 69*, 329.

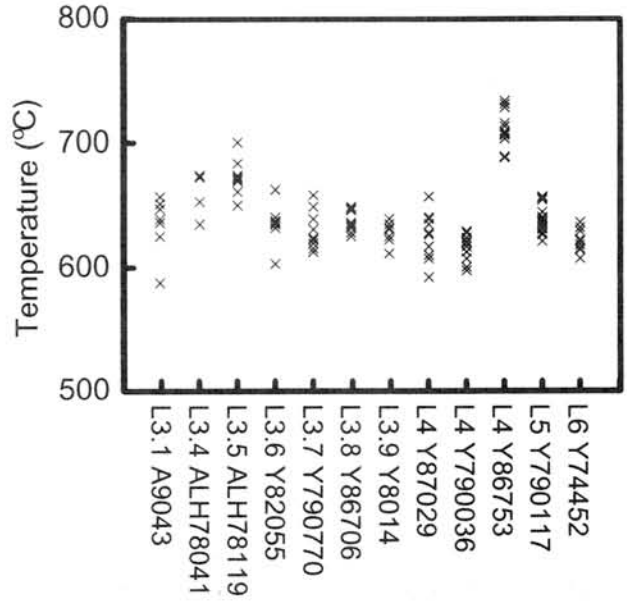

Fig. 3. Olivine-spinel equilibration temperatures of L chondrites. Equilibration temperatures are calculated using the calibration system of Fabriés (1979).

Pre-Terrestrial Aqueous Alteration of the Y-000749 Nakhlite Meteorite

Allan H. Treiman[1] and Cyrena A. Goodrich[2]

[1]Lunar and Planetary Institute, 3600 Bay Area Boulevard, Houston Texas 77058 U.S.A. [2]University of Hawai'i at Manoa, Hawaii Institute of Geophysics and Planetology, 2525 Correa Rd., Honolulu, Hawaii 96822 U.S.A.

The Y-000593 and Y-000749 Antarctic meteorites are paired nakhlites – Martian cumulate rocks composed principally of augite and olivine [1]. Other nakhlite meteorites contain magmatic inclusions in their olivines [2,3], and we examined a thin section of each new nakhlite for these magmatic inclusions. Our sections contained a single magmatic inclusion like those in Nakhla olivine [2]: a rounded inclusion containing radiating elongate crystals of Al-Ti augite distinct from the cumulus augite (Table 1), and a halo of Cr-magnetite grains near its boundary with the host olivine (Fig. 1c,d of [2]). Unlike magmatic inclusions in Nakhla, our single example was extensively altered to "iddingsite." Our attention then focused on the "iddingsite" alteration material.

Alteration Material

Thin sections of Y-000593 and Y-000749 show extensive alteration of olivine and mesostasis glass to yellow, orange and red material, which is comparable to the pre-terrestrial "iddingsite" in other nakhlites [4-7]. Y-000749 has abundant alteration material; we recognized three types of alteration that are, or may be, pre-terrestrial.

Type 1 is yellow to orange in thin section. It occurs as veinlets replacing olivine and as massive replacement of mesostasis glass. Type 1 material is pre-terrestrial; veinlets of Type 1 material are cut by, and melted at, the meteorite's fusion crust (Fig. 1).

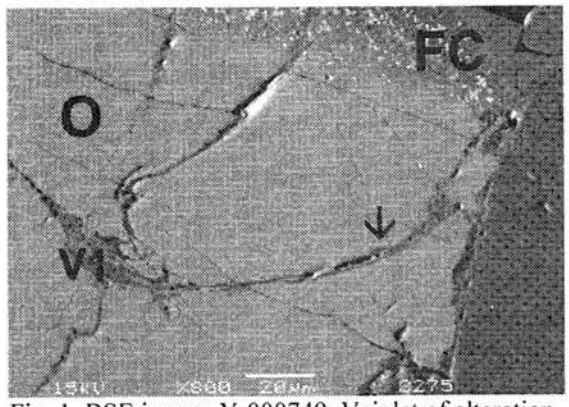

Fig. 1. BSE image, Y-000749. Veinlet of alteration material Type 1 (V1) crosses olivine (O) and is melted (arrow) as it approaches fusion crust (FC). Thus, V1 is pre-terrestrial.

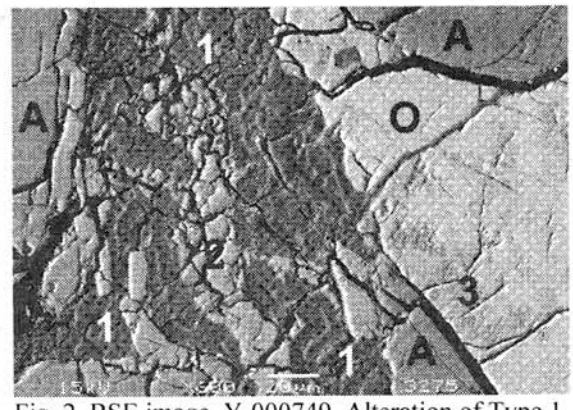

Fig. 2. BSE image, Y-000749. Alteration of Type 1 (1) and Type 2 (2) replacing mesostasis among olivine (O) and augite (A). Varying Mg* in Type 1 appears as brighter and darker layers. Type 2 follows the layering of Type 1 and fills its core. Type 3 alteration (3) appears as darker, rougher areas in olivine.

Type 1 material is chemically zoned by variation in Mg* (Table 1), which is visible optically as color bands and in SEM/BSE images as bands of differing brightness (Fig. 2). In veinlets, the zoning is parallel to the veinlet walls; in masses, the zoning is parallel to the walls of the mass (Fig. 2). The chemical formula of Type 1 material is near

$(Mg,Fe)_2(Si,Al)_3O_8 \cdot nH_2O \cdot E^+_{0.05}$, fits either sepiolite or stevensite (saponite) clay. Extensive cracking (Fig. 2), suggestive of dehydration, is consistent with stevensite.

Table 1. Mineral Compositions in Y-000749.

	Igneous Minerals			Alteration Material				
wt %	Inclusion Augite	Cumulus Augite	Cumulus Olivine	Type 1 Mg-rich	Type 1-Fe-rich	Type 2	Type 2	Type 3
SiO_2	44.03	49.67	31.21	49.08	52.24	14.38	8.89	31.27
TiO_2	1.99	0.14	0.01	0.02	0.03	0.00	0.00	0.04
Al_2O_3	4.89	0.42	0.02	3.49	3.12	1.63	2.95	0.49
Cr_2O_3	0.10	0.02	0.02	0.03	0.00	0.08	0.25	0.01
FeO	20.14	21.03	55.53	28.75	30.03	64.39	65.88	52.72
MnO	0.40	0.52	1.00	0.15	0.31	0.22	0.14	0.92
MgO	4.32	8.68	9.54	7.49	3.99	0.50	0.13	7.96
CaO	21.44	17.56	0.44	0.45	0.46	0.27	0.15	0.42
Na_2O	0.30	0.19	0.00	0.13	0.11	0.07	0.05	0.01
K_2O	0.01	0.01	0.00	0.55	0.29	0.04	0.00	0.01
P_2O_5	0.60	0.14	0.00	0.15	0.26	2.07	0.00	0.04
SO_3	0.02	0.01	0.00	0.09	0.35	1.91	2.49	0.14
Sum	98.23	98.39	97.77	90.38	91.18	88.55	80.93	93.58
Mg*	27.6	42.4	30.6	31.7	19.2	1.4	0.4	21.2

EMP WDS analyses at Johnson Space Center, USA. Anhydrous phases (olivine, augite) show perfect stoichiometry, so their low totals probably reflect different carbon coats on standards and the Y000749 thin section.

Type 2 alteration material is red-orange to dark red in thin section and is bright in BSE imagery (Fig. 2). Chemically, it is an iron compound with very low analytical totals and variable proportions of Si, P, and S (Table 1). It is probably ferrihydrite, a ferric oxide-hydroxide gel-like mineral that contains abundant water and strongly adsorbs silicate and other anions. Type 2 material commonly forms the cores of layered masses of Type 1 alteration (Fig. 2); in this texture, it appears to be pre-terrestrial like Type 1. Type 2 material also occurs as veinlets which can cross-cut veinlets of Type 1 material.

Alteration Type 3 appears as greenish-brown patches in olivine (Fig. 2). It grows from the fractures in the olivine into triangular shapes. In high-resolution BSE imagery, Type 3 material is seen as micron-scale interlayers of brighter and darker material. Its chemical composition is nearly that of the host olivine (Table 1), but with low analytical total, decreased Mg abundance, and small proportions of Al and S. This suggests that Type 3 may be slight alteration of olivine to ferrihydrite (see Table 1). Type 3 alteration is not observed in the thin section of Y-000539. It appears to have formed after alteration Types 1 and 2, but its textures do not indicate whether it is terrestrial or pre-terrestrial.

Y-000749 also contains alteration material that is clearly terrestrial. Some bubbles in the fusion crust contain dark-red material (like Type 2). Some small cracks that cross the fusion crust contain similar material. Rare larger cracks that cross the fusion crust are filled with clear, nearly isotropic material.

Acknowledgments. We thank the NIPR for loan of thin sections. C. Schwandt assisted with SEM imagery and EMP analyses.

References. [1] Imae N. (2002) *Lunar Planet. Sci.* **XXXII**, Abstract #1483. [2] Treiman A.H. (1993) *Geochim. Cosmochim. Acta* **57**, 4753. [3] Harvey R.P. and McSween H.Y.Jr. (1992) *Earth Planet. Sci. Lett.* **111**, 467. [4] Bunch T.E. and Reid A.M. (1975) *Meteoritics* **10**, 303. [5] Gooding J.L. et al. (1991) *Meteoritics* 26, 135. [6] Treiman A.H. et al. (1993) *Meteoritics* 28, 86. [7] Gillet Ph. et al. (2002?) *Earth Planet. Sci. Lett.*, in press.

Three-dimensional shapes and internal structures of chondrules from the Allende meteorite by X-ray CT: high-speed rotation.

TSUCHIYAMA, Akira[1]*, SHIGEYOSHI, Ryoichi[2], NAKANO, Tsikasa[3], UESUGI, Kentaro[4] and SHIRONO, Shin-ichi[5]

*1) Department of Earth and Space Science, Osaka University, 1-1 Machikaneyama-cho, Toyonaka 560-0043, JAPAN, *akira@ess.sci.osaka-u.ac.jp, 2) Graduate School of Science and Engineering, Kagoshima University, Kagoshima 890-0065, JAPAN, 3) Institute of Geoscience, National Institute of Advanced Industrial Science and Technology, Tshukuba, 305-8567 JAPAN, 4) Japan Synchrotron Radiation Research Institute, Mikazuki, 679-5198 JAPAN, 5) Graduate School of Environmental Studies, Nagoya University, Nagoya 464-0814, JAPAN*

Introduction

Chondrules have been studied by many researchers to understand their formation process and discuss the evolution of the primordial solar nebula. Recent development of analytical apparatus has brought about intensive studies about the elemental and isotopic compositions of chondrules and important information, such as about their high-temperature processes and formation ages, were obtained. On the other hand, progress in physical aspects has not been made much.

It has been accepted from their spherical shapes that chondrules were once molten in a free space under micro-gravity, probably in the primordial solar nebula, and cooled rapidly. However, they are not strictly spheres. Recent research on three-dimensional structures of chondrules using high-resolution X-ray CT (computed tomography) found an oblate chondrule [1,2]. Three-dimensional distribution of voids in the chondrule indicates that it was spinning during melting. However, such conclusion should be confirmed by a statistical study.

Experiments

In the present study, we imaged forty-seven chondrules removed from the Allende meteorite (CV3) with a high-resolution X-ray CT system equipped at synchrotron radiation facility, SPring-8 [3]. The chondrules were mounted into cylinders of epoxy (about 3mm in diameter) to reduce artifacts of CT images and to reserve the slice directions. They were imaged at beamline BL20B2 with monochromatic beams at 18-30 keV depending on the sample size and composition. Cross-sectional images were reconstructed from 300-360 projections with a convolution back projection method. Each CT image has a contrast, which corresponds to the X-ray LACs (linear attenuation coefficients) of materials. Three-dimensional structures were reconstructed from successive CT images with the voxel size of 5.83 $\times$5.83$\times$5.83 μ m, which gives the spatial resolution of about 13 μ m [3].

Twenty chondrules with perfect shapes and smooth surfaces were selected for the present analysis. The data for one chondrule imaged by an industrial micro-focus X-ray CT scanner [1] was also used. The external shapes and distribution of metal/sulfide grains and voids inside of the chondrules were examined. Some chondrules were thin-sectioned as parallel as possible to the sliced direction of the CT images. The thin sections were observed under a polarized optical microscope and a scanning electron microscope (SEM) to confirm the presence of metal/sulfide grains and voids in the chondrules. A three-dimensional plaster figure of one prolate chondrule was formed by rapid prototyping method.

Results

Some chondrules have fine–grained rim or matrix on the surfaces. They were removed by image analysis using appropriate thresholds of LACs. We approximated the external shapes of these naked chondrules as three-axial ellipsoids with a-, b- and c-axes (axial radii are A, B and C ($A \geq B \geq C$), respectively) using the moments of inertia of the chondrules. The rotation axes with the minimum and maximum moments correspond to the a- and c-axes, respectively.

The plots of C/B vs. B/A are shown in Fig.1, where the aspect ratio, p=C/A, and the degree of

oblate or prolate shape, log n (n is defined as $C/B=(B/A)^n$: $\log(n)\rightarrow\infty$ for oblate shapes and $\log(n)\rightarrow-\infty$ for prolate shapes) are also shown. We found that the shapes are diverse from oblate (A~B>C: log(n)>>0), general three-axial ellipsoid (A>B>C) to prolate chondrules (A>B~C: log(n)<<-0). However, if we concern the aspect ratio, two groups can be recognized: oblate to prolate chondrules with small p of 0.85-0.98 (group-A) and prolate chondrules with large p of 0.74 to0.78 (group-B). The relation between the size and p for the oblate chondrules are shown in Fig.2.

Chondrules contain metal and/or sulfide grains (up to 6.8 vol.%) and voids (up to 2.9 vol.%). If oblate chondrules were formed by rotation during melting, heavy metal/sulfide grains and light voids should be moved away from and toward the short axis (c-axis), respectively, due to centrifugal force. To check this possibility, the moments of inertia of metal/sulfide grains or voids around the c-axis of the oblate chondrules, M, were calculated. The comparison with those of random distribution, Mr, shows that M/Mr>1 for metal/sulfide (Fig.3a) and M/Mr<1 for voids (Fig.3b) if the degree of oblate, log(n), is sufficiently large. M/Mr>1 indicates concentration of metal/sulfide grains toward the surface from the c-axis while M/Mr<1 indicates concentration of voids toward the c-axis.

Discussion

We can estimate rotation rates for the oblate chondrules by assuming that these flat shapes were equilibrium shapes, where centrifugal force was balanced with surface tension of chondrule melts [4]. In this case, the shape including the aspect ratio, p, is determined uniquely by the parameter, Σ:

$$\Sigma=\rho A^3\Omega^2/8\gamma, \qquad (1)$$

where ρ is the density of a chondrule melt, Ω is the angular velocity and γ is the surface tension. The rotation rates calculated from Eq.(1) are also shown in Fig.2. They were estimated to be about 50 to 350 rps for the oblate chondrules. As the aspect rations in Fig.2 should be the values at the time of chondrule solidification, the rotation rates might be larger during melting (approximately 100-500 rps). If Σ exceeds the critical value of 0.844 ($p\geq0.490$), the rotated melts become unstable [4] and should split into small pieces. The lower limit of the aspect ratio of about 0.85 in Fig.2 might correspond to this critical aspect ratio (0.490) during melting.

It is not easy to explain the prolate chondrules as stable shapes. If molten chondrules were moving in an ambient gas, the chondrules should be flattened by a gas drag from analogy of the shapes of rain droplets. If the prolate chondrules were rotated, the stable axis for the rotation is the short axis (c-axis). A possible explanation for the prolate shapes with large aspect ratios (group-B in Fig.1) is that they were formed from unstable droplets, where Σ exceeds the critical value. If this is the case, the upper limit of chondrule size can be explained by the high-speed rotation. The general three-axial ellipsoids and prolate chondrules with small aspect ratios in group-A (Fig.1) should be formed by some modification during solidification or precession during rotation.

High-speed rotation of molten chondrules largely constrains their formation process. This is possible by the shock wave model [5] or impact model. The shock wave model may be favorable because the impact model has a problem about energies to make molten droplets by collision of planetesimals [6].

Most of the chondrules imaged in this study have voids. This shows that voids are important constituents of chondrules as well as silicates and metal/sulfides although their amounts are small (less than 3 vol.%). Three-dimensional distribution of voids in an oblate barred olivine chondrule suggests that the voids were formed by bubbling due to increase of the concentration of volatile components in a melt by olivine crystallization.

[1] Kawabata et al. (1999) *Antarctic Meteor.* **XXIV**, 64-66. [2] Tsuchiyama et al. (2000) *LPSC*, **XXXI**,1566. [3] Uesugi et al. (1999) *Proc. SPIE*, **3772**, 214. [4] Chandrasekhar (1965) *Proc. Roy. Soc. London, A*, **286**, 1-26. [5] Susa and Nakamoto (2002) *Astrophys. J.* **564**, L57-L60. [6] Levy (1988) In *Meteorites and the Early Solar System* (eds. Kerridge and Matthews) 697-711.

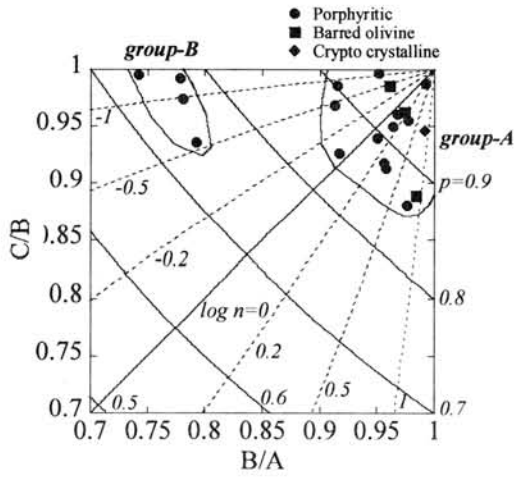

Figure 1. Chondrule shapes approximated as three-axial ellipsoids. Relation between the ratios of the axial radii (A≥ B≥ C) are shown for chondrule textures. The aspect ratio, p=C/A, and the degree of oblate or prolate shape, log n (log(n) $\rightarrow \infty$ and $-\infty$ for oblate and prolate shapes, respectively), are also shown.

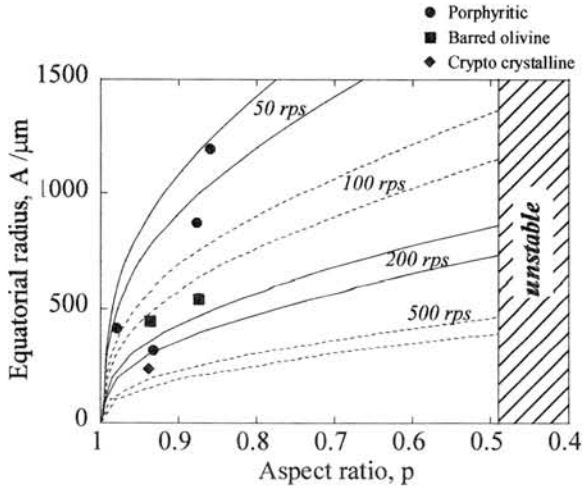

Figure 2. The equatorial radius of oblate chondrules, A, plotted against the aspect ratio, p. The rotation rates were calculated from Eq.(1). The upper and lower limits of the surface tension, γ, for basalts at 1000-1500°C (250-420 dyn/cm) were used for the calculation.

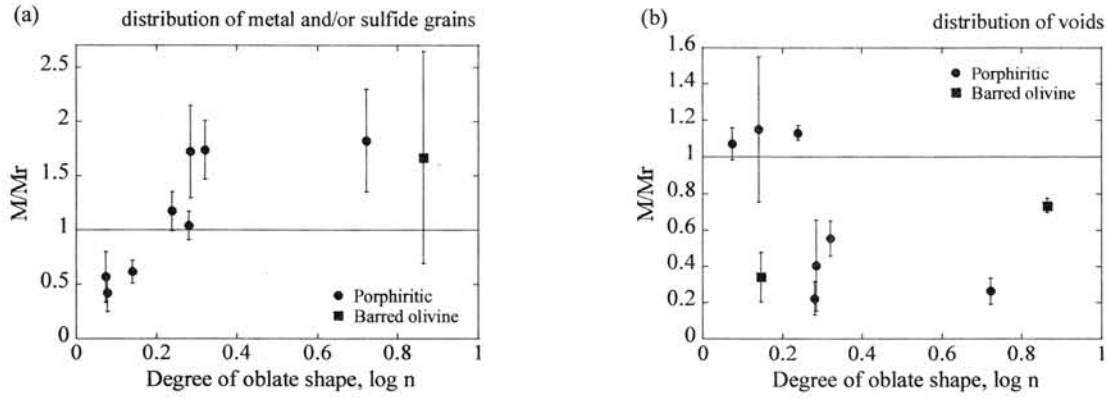

Figure 3. The ratio of the moments of inertia between the real and random distribution of objects around the short axis (c-axis) of oblate chondrules, M/Mr, plotted against the degree of oblate shape, log n. (a) Metal/sulfide grains. (b) Voids. M/Mr>1 indicates concentration of the objects away from the axis and vise versa.

FIRST ANALYSIS OF THE REFLECTANCE SPECTRUM OF YAMATO-000593: THE SPECTROSCOPIC SIMILARITY BETWEEN YAMATO-000593 AND NAKHLA

[1]Ueda Y., [1]Mikouchi T., [1]Miyamoto M. and [2]Hiroi T.
[1]Department of Earth and Planetary Science, the University of Tokyo,
7-3-1 Hongo, Bunkyo-ku, Tokyo 113-0033, Japan.
[2]Department of Geological Sciences, Brown University,
Providence, Rhode Island 02912, USA
E-mail: yueda@space.eps.s.u-tokyo.ac.jp

Introduction

Yamato-000593 is a nakhlite first found in the Antarctic meteorite collection [1]. The nakhlite is one of the SNC meteorite groups that are believed to derive from the Martian igneous rock, and belong to an olivine-bearing clinopyroxenite. The most abundant mineral is augite (~85%), and olivine (~5%) is present as the second major mineral [2, 3]. It is reported that Yamato-000593 is compositionally quite similar to Nakhla [3]. Although the reflectance spectra of shergottites such as Zagami and EETA79001 were measured several times in previous works [e.g., 4-6], the reflectance spectrum of nakhlite except for Nakhla has not been measured almost at all, and the analytical comparison between the reflectance spectra of nakhlites has not been performed. In this abstract, we will report the spectroscopic comparison between Yamato-000593 and Nakhla.

Samples and Instruments

Yamato-000593 was supplied by National Institute of Polar Research, and Nakhla was by University Museum, Univ. of Tokyo. Both samples were hand-grounded with a corundum mortar and pestle. After grounded, they were sieved under 100 μm in size. The bidirectional reflectance spectra were measured by a UV-Visible-NIR spectrometer. All spectra were measured at incidence and emergence angles of 30°. Halon was used as a standard. In addition to the powder samples, the reflectance spectra of chip of Yamato-000593 were measured at the same condition, although its spectra were not used in this report because of the ambiguity of the effect of surface roughness. The dry air was pumped into the spectrometer chamber for preventing samples from water absorption in the air.

Method

To analyze the reflectance spectra, the modified Gaussian model (MGM) [7, 8] was used in this study. The MGM is one of the most powerful tools for deconvolving a reflectance spectrum of mineral mixture such as olivine and pyroxene. The natural logarithm of a reflectance spectrum is deconvolved into absorption bands and a background continuum, where each absorption band is expressed as a Gaussian in wavelength, and the continuum as a linear function of wavenumber.

Original MGM formula is expressed as:

$$\ln R(\lambda) \cong f(\lambda) = C(\lambda) + \sum_i s_i \cdot \exp\left[-\frac{1}{2}\{(\lambda-\mu_i)/\sigma_i\}^2\right], \quad (1)$$

where $R(\lambda)$ is the measured reflectance and band parameters s, μ and σ mean the band strength, center

and width, respectively. Since the reflectance spectrum is converted to the natural logarithm, the band strength is always negative. The background continuum component is expressed as:

$$C(\lambda) = c_0 + c_1/\lambda, \quad (2)$$

where c_0 and c_1 are constants.

The full width at half maximum (FWHM) is calculated by

$$\mathrm{FWHM} = 2\sqrt{2\ln 2}\cdot\sigma \cong 2.35482\sigma. \quad (3)$$

Results and Discussion

The reflectance spectrum of augite (Ca-rich pyroxene) has two major absorption bands around 1 μm and 2.3 μm in wavelength, which is different from that of Ca-poor pyroxene and olivine [e.g., 9, 10]. The reflectance spectrum of Ca-poor pyroxene has two characteristic absorption bands around 0.9 μm and 1.9 μm, and that of olivine has three major absorption bands around 1 μm in wavelength and shows the complex absorption feature.

Shown in Fig. 1 are the reflectance spectra of Yamato-000593 and Nakhla. The characteristic absorption bands of Ca-rich pyroxene are observed around 1 μm and 2.3 μm. Both spectra remarkably resemble each other, except for the slope around 0.6-0.85 μm.

The MGM deconvolution of Yamato-000593 is shown in Fig. 2. Listed in Table 1 are the band 1-3 parameters of Yamato-000593 and Nakhla. The band 1 and 3 parameters of the MGM deconvolution of both nakhlites are well coincident with each other. Three absorption bands of olivine around 1 μm could not be separated, probably because of the complex overlapping with the absorption band of augite. The small absorption bands around 0.9 μm and 2 μm would be the absorption of pigeonite [3].

Mikouchi *et al.* [3] reported that the augite cores in both meteorites have almost the same composition ($En_{39}Fs_{22}Wo_{39}$), and our spectral analysis is consistent with them.

Conclusion

As mentioned above, the reflectance spectra of two nakhlites that were measured in this study show quite similar spectra to each other, although some spectral differences around 0.6-0.85 μm in wavelength are observed. Since the reflectance spectrum of other nakhlites has not been measured, spectroscopic measurement of other nakhlites will be required to further discuss spectroscopic characteristics of nakhlites in general.

References

[1] Imae N. *et al.* (2002) *LPSC* **33**, CD-ROM #1483 [2] Harvey R. P. and McSween H. Y. Jr. (1992) *GCA* **56**, 1655-1663 [3] Mikouchi, T. *et al.* (2002) *NIPR Symp.*, **27,** this volume. [4] Schade U. and Wasch R. (1999) *MAPS* **34**, 417-427. [5] Pieters C. M. and McFadden L. A. (1994) *Annu. Rev. Earth Planet. Sci.* **22**, 457-497. [6] McFadden L. A. (1988) *BAAS* **20**, 849. [7] Sunshine J. M. *et al.* (1990) *JGR* **95**, 6955-6966. [8] Sunshine J. M. and Pieters C. M. (1993) *JGR* **98**, 9075-9087. [9] Cloutis E. A. and Gaffey M. J. (1991) *JGR* **96**, 22809-22826. [10] Sunshine J. M. and Pieters C. M. (1998) *JGR* **103**, 13675-13688.

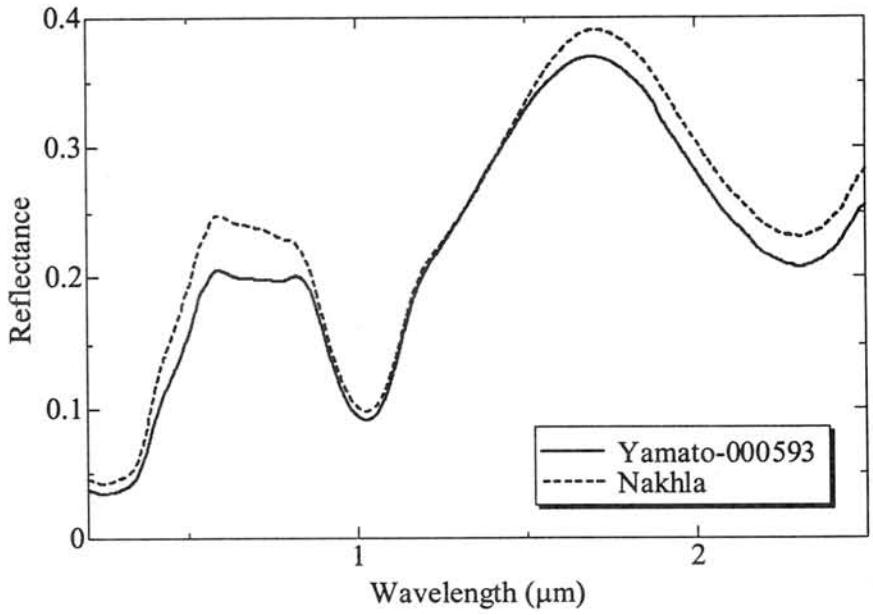

Fig. 1. The reflectance spectra of Yamato-000593 and Nakhla.

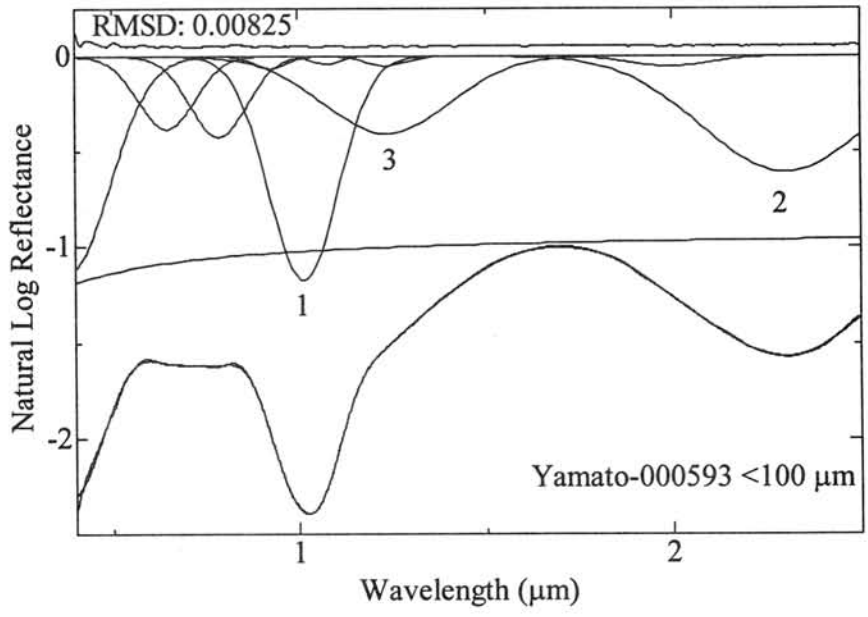

Fig. 2. MGM deconvolution of Yamato-000593. RMS error is offset about 0.05.

Table 1. Band parameters of major band 1-3 in Yamato-000593 and Nakhla.

	Yamato-000593			Nakhla		
	Band 1	Band 3	Band 2	Band 1	Band 3	Band 2
Center (μm)	1.014	1.237	2.302	1.020	1.280	2.300
FWHM (μm)	0.092	0.169	0.221	0.094	0.169	0.229
Strength	-1.18	-0.404	-0.609	-1.20	-0.442	-0.579

Oxygen isotopic compositions of pyroxenes and olivines in Antarctic micrometeorites.

[1,2]Toru Yada, [2]Tomoki Nakamura, [3]Takehiko Setoyanagi, [2]Nobuo Takaoka, and [4]Hideyasu Kojima.

[1]Dept. Earth and Planet. Science, University of Tokyo, Tokyo 113-0033, Japan (yada@space.eps.s.u-tokyo.ac.jp), [2]. Dept. Earth and Planet. Science, Kyushu University, Fukuoka 812-8581, Japan, [3] Dept. Chemistry, Tokyo Metropolitan University, Hachioji 192-0397, Japan, [4] National Institute of Polar Research, Tokyo 173-8515, Japan.

Introduction: Micrometeorites are extraterrestrial dust collected on the Earth's surface. They are closely related to carbonaceous chondrites (e.g. [1]), however, identification of their parent bodies is difficult because of their small size and heating effect during atmospheric entry. Most of micrometeorites consist of fine-grained portion which is supposed to be decomposed from phyllosilicates due to atmospheric entry heating [2]. On the other hand, relict pyroxene and olivine grains are found generally among fine-grained portion or as a single grain [3]. These mineral grains must retain original information in elemental and isotopic compositions before their entry to the Earth. Oxygen isotopic ratio is distinct in each type of meteorite in bulk isotopic analysis [4] and may be helpful for identification of parent bodies in micrometeorites. We analyzed oxygen isotopic composition of olivines and pyroxenes in micrometeorites by secondary ion mass spectrometer (SIMS) to obtain information about their parent bodies.

Samples and Methods: Micrometeorites studied in this work were collected from blue ice around Yamato Mts. in Antarctica, here after they are called as Antarctic micrometeorite (AMM) [5]. Chondritic particles are selected based on the surface qualitative analysis data by scanning electron microscope equipped with energy dispersive spectroscopy, JEOL JSM5800LV in National Institute of Polar Research (NIPR). They are mounted in epoxy resin and polished to expose their cross sections, to which we performed quantitative elemental analyses by electron microprobe, JXA8800 in NIPR. Among the 170 of AMMs, nineteen of those contain or consist of olivine and/or pyroxene are analyzed their oxygen isotopic ratios by SIMS, CAMECA IMS6F, installed in Kyushu University. Analytical condition is as follows. Primary

Cs^+ beam of 0.9nA is accelerated at 19.5kV to spatter the mineral's surface. Size of the primary beam spot is about 20μm. Secondary ions are accelerated at -9.5kV to go through electrostatic field and magnet sector (mass resolution power: 5000) and detected by a Faraday cup (^{16}O) and an electron multiplier (^{17}O and ^{18}O). In order to correct instrumental mass fractionation, either San Carlos olivine (Fo_{89}, $\delta^{18}O$ = +5.68‰) or Norway enstatite ($En_{86}Wo_1$, $\delta^{18}O$ = +9.68‰) is set together with samples in a same folder and analyzed repeatedly before and after the analyses of olivines or pyroxenes, respectively. Standard deviation of the repeated analyses of standard minerals is contained within an error of the sample's data reported here. Oxygen isotopic ratio is expressed as delta value, which stand for deviation of an oxygen isotopic ratio from that of standard mean ocean water, represented in permillage.

Results and Discussion: Fourteen pyroxenes and five olivines were analyzed their oxygen isotopic compositions by SIMS. Fig. 1 shows an oxygen three isotope plot of pyroxenes and olivines in AMMs. Most of data are plotted between the terrestrial fractionation (TF) line and the carbonaceous chondrite anhydrous minerals (CCAM) line. This tendency is similar to previous work on oxygen isotopic compositions of AMM's minerals [6], indicating that most of them have character of anhydrous minerals of carbonaceous chondrite rather than those of ordinary chondrite. However, several data are plotted on and above the TF line, and the one which has the highest $\delta^{17}O$ value is plotted on the region of ordinary chondrite in fayalite to CaO content diagram (Fig. 2). Therefore, the olivine grain is supposed to originate from a parent body of ordinary chondrite. Pyroxenes are generally more ^{16}O-rich composition than olivines even though only five olivine data exist. This inclination was not reported in the previous work, thus additional data of olivines in AMMs are necessary for farther discussion.

References

[1] Engrand C. and Maurette M. (1998), Meteoritics Planet. Sci., 33, 565-580. [2] Nozaki, W et al. (2001), Meteoritics Planet. Sci., 36, A150. [3] Beckerling, W. and Bischoff, A. (1995), Planet. Space Sci., 43, 435-449. [4] Crayton, R. N. (1993), Ann. Rev. Earth Planet. Sci., 21, 115-149. [5] Yada, T. and Kojima, H. (2000), Antarct. Meteorite Res., 13, 9-18. [6] Engrand, C. et al. (1999), Geochim. Cosmochim. Acta, 63, 2623-2636.

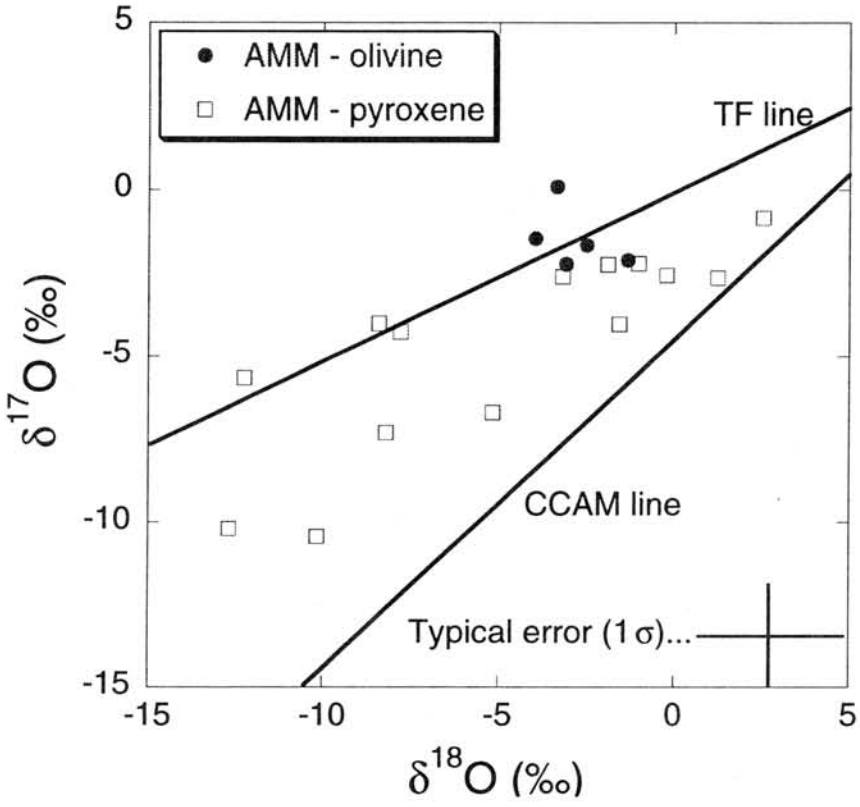

Fig. 1. Oxygen three isotope plot of olivines and pyroxenes in AMMs.

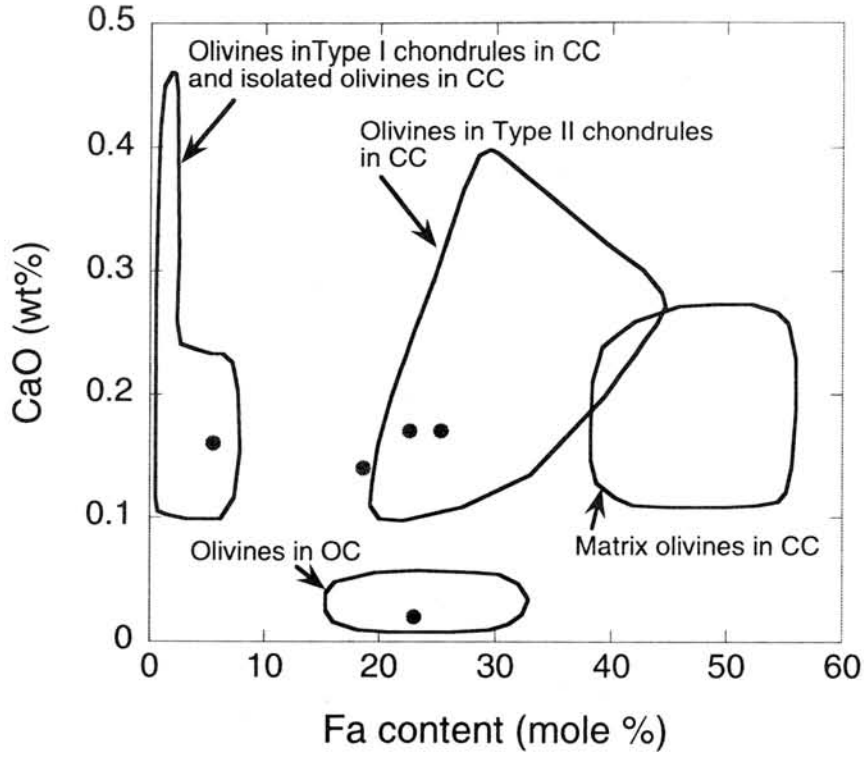

Fig. 2. Fayalite content to CaO content plot of olivines in AMMs whose oxygen isotopic ratios were analyzed.

Origin of a recrystallized magnesian eucrite, Dhofar 007

Akira Yamaguchi[1,2], Takehiko Setoyanagi[3], and Mitsuru Ebihara[3]
[1]Antarctic Meteorite Research Center, National Institute of Polar Research, Tokyo 173-8515, [2]The Graduate University for Advanced Studies, Tokyo 173-8515, [3]Department of Chemistry, Tokyo Metropolitan University, Hachioji, Tokyo 192-0397.

A eucrite, Dhofar 007 was found in the Oman desert and was initially classified as a cumulate eucrite [1]. One of our samples of Dhofar 007 is a breccia that contains glassy clasts, indicating that this meteorite may be a polymict breccia. Both the clasts and clastic matrix of Dhofar 007 are cut by thin impact melt veins (<10-30 μm thick) suggesting that Dhofar 007 experienced at least two-stages of shock metamorphism. In this work, we focus on the origin of a coarse-grained clast (CG), and compared with other basaltic and Mg-rich eucrites. We studied a large chip (14.0 g), which is entirely a coarse-grained clast. PTSs were examined by optical and scanning electron microscopy and with an electron microprobe (EPMA). A portion of the meteorite adjacent to the PTSs (0.882 g) was powdered for INAA and PGA [2].

The PTSs of the CG clast show a granular texture composed of fine pyroxene (0.2-0.3 mm in size) (~51 vol%) and plagioclase (50-100 μm in size) (~47 vol%) (Fig. 1). Relatively large grains of pyroxene (<1.2 mm in size) and aggregates (~2 mm in size) of plagioclase occur in some cases, implying the texture was originally igneous. There are several elongated crystals of plagioclase that have dusty inclusions such as FeS in the cores. These plagioclase crystals could be relicts of precursor rock. The minor minerals (<2 vol%) include chromite, silica minerals, troilite, metallic phases (kamacite and taenite), and Ca-phosphates. Chromite (50-250 μm in size) typically shows a poikiloblastic texture that partly or totally encloses pyroxene and plagioclase. These textures could have been formed by metamorphism followed by impact brecciation.

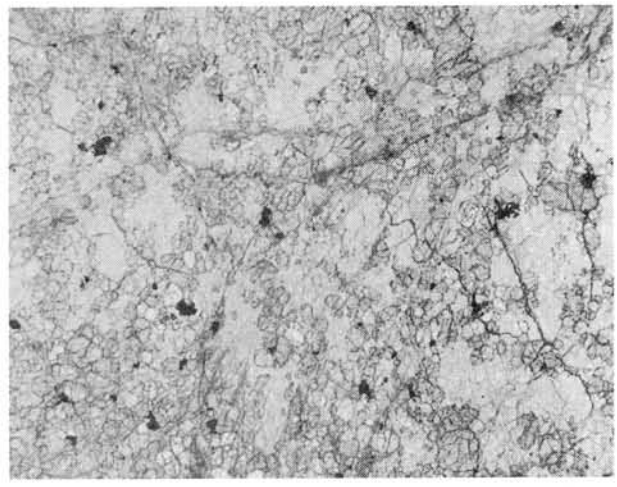

Fig. 1. Photomicrograph of C1 clast in Dhofar 007. Width is 6.9 mm. Plane light.

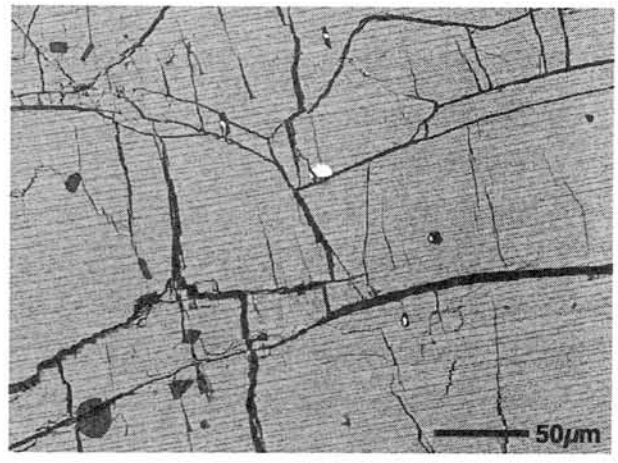

Fig. 2. Backscattered electron image (BEI) of pyroxene in CG clast. Pigeonite (light gray) has very thin augite lamellae (medium gray). Black: epoxy.

Pyroxenes are pigeonites that have closely spaced (<2-3 μm wide), very fine augite exsolution lamellae (<<1 μm thick) (Fig. 2). This is in contrast to the fact that pigeonites in most Mg-rich eucrites (cumulate eucrites) are partly or totally inverted to orthopyroxene [3]. Chemical compositions of pyroxenes are plotted on a single tie line from $Wo_{2.89}En_{53.29}$ to $Wo_{16.67}En_{48.23}$ (Fig. 3). The bulk composition of pyroxene determined by

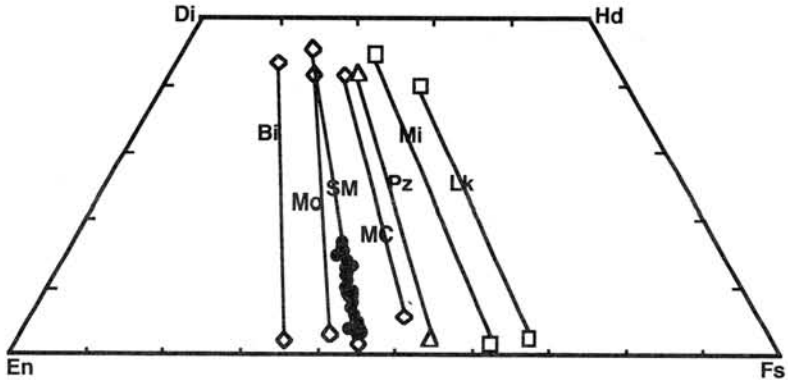

Fig. 3. Pyroxene compositions of C1 clast in Dhofar 007 (solid circles) and of typical cumulate eucrites (Bi: Binda; Mo: Moama; SM: Serra de Mage) and basaltic eucrites (Pz: Pmozdino; Mi: Millbillillie; Lk: Lakangaon). Mg/Fe in pyroxenes in C1 clast is simiar to those in Serra de Mage.

broad electron beam (~30 μm in diameter) is $Wo_{8.76}En_{51.19}$. The composition of augite lamellae is not resolvable by EPMA. The FeO/MnO ratio of pyroxenes is 32, comparable to those of eucrites [e.g., 4]. Plagioclase has slight chemical variation ($An_{94.50}Or_{0.27}$ to $An_{90.81}Or_{0.27}$). There is no chemical difference between the granular plagioclases and remnant crystals. Chromite shows slight chemical variation ($Ulv_{24.01}Chm_{61.09}$-$Ulv_{10.43}Chm_{70.92}$). We find two metallic phases, kamacite (0.02 vol%) and taenite (0.04 vol%), closely associated with troilite (Fig. 4). These two metallic phases are not in contact in the PTSs. The Ni contents of kamacite and taenite vary significantly (kamacite: 3.67-7.14 wt%; taenite: 39.49-48.10 wt%). The Ni/Co ratios of kamacite are 3.30-4.65. We could not detect P in these two phases by EPMA.

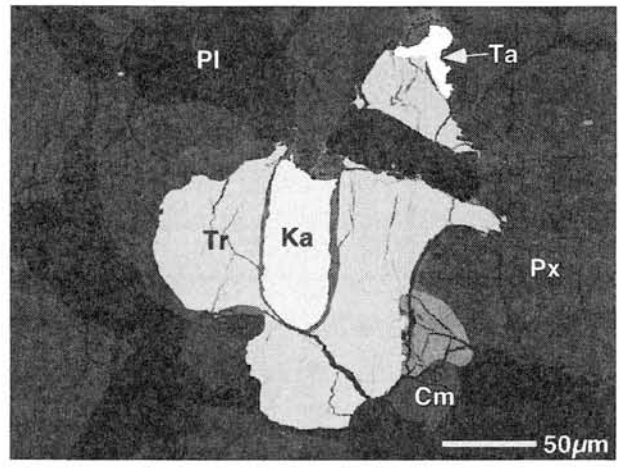

Fig. 4. BEI of the assemblage composed of troilite (Tr), kamacite (Ka), taenite (Ta), and chromite (Cm). The metal phases are in many cases rimmed by weathering products. Px: pyroxene; Pl: plagioclase.

The INAA and PGA are preliminary. The bulk composition (wt%) of the CG clast is CaO = 11.0, Al_2O_3 = 13.0, MgO = 9.4, Ni = 0.087, and Co < 0.038. The analysis of other trace elements such as REEs is in progress.

Although the CG clast in Dhofar 007 has been texturally disturbed by later impact and thermal events, several petrologic features imply the nature of the precursor rock. The CG clast is slightly enriched in plagioclase (~47 vol%) compared to compositions of basaltic eucrites (~42 vol%, [5]) although the contents of CaO and Al_2O_3 are marginally within the range of basaltic eucrites. The pyroxene is Mg-rich (Fig. 2) and plagioclase has Ca-rich composition with limited chemical variation. The presence of large pyroxenes and aggregates of plagioclase imply the relict texture of coarse-grained rocks. These facts indicate that the precursor rock could be a cumulate eucrite that cooled slowly under plutonic conditions. However, we found several unusual features in the CG clast in Dhofar 007 uncommon in the known Mg-rich eucrites (cumulate eucrites) [3]. First, pigeonite in the CG clast is not inverted orthopyroxene, and has very fine augite lamellae. Second, this clast contains a significant amount of metallic phases. Taenite has been rarely found in unbrecciated eucritic clasts [6,7].

In general, pigeonites in cumulate eucrites are orthopyroxenes inverted from

pigeonite and have thick augite lamellae because of the very slow cooling rates in plutonic conditions [3]. Pyroxenes in other Mg-rich eucrites such as Moore County exhibit finer exsolution lamellae, often partial inversion to orthopyroxene [3]. Miyamoto and Takeda [8] suggested that Moore County was excavated from the deep interior at the asteroid during slow cooling. The presence of inverted pigeonite in these cumulate eucrites indicates that they originally cooled very slowly deep in the eucritic crust [3]. However, this view is not consistent with the pyroxene textures observed in the CG clast in Dhofar 007. Pyroxenes in the CG clast have very thin augite lamellae and are not inverted to orthopyroxene. It seems unlikely that the CG clast was cooled very rapidly during initial crystallization. After the slow initial cooling from the melt, the CG clast was cooled very rapidly from high temperature above the pyroxene solvus (~1000 °C) during slow subsolidus cooling. The cooling rate was too rapid to invert from pigeonite to orthopyroxene and to produce thick augite lamellae.

The presence of taenite (~0.04 vol%) in the CG clast is enigmatic. Combined with the EPMA data and mode of metallic phases, we estimate the bulk Ni content to be ~200-300 ppm, lower than the value (870 ppm) obtained by PGA. These values are significantly higher than those of typical "monomict eucrites" (generally <13 ppm) [9]. At the low value, the taenite would not be found in PTSs. This is consistent with the fact that taenite is rarely found in eucrites. It is unlikely that FeNi-metal was incorporated by the recent shock events that produced melt veins and breccia texture because most of the FeNi-metal is not associated with these textures. Thus, metallic phases were formed or incorporated into the CG clast before or during recrystallization. There are several possible origins of the metallic phases. Metallic phases in eucrites can be formed by reduction of silicate and oxide minerals or are pristine phases that crystallized from basaltic melt [6,7,10]. However, the metallic phases formed by these processes are generally Ni-poor [6,7,10]. It may be possible that the CG clast is a fragment of basaltic inclusion in mesosiderite; metallic phases were incorporated during metal-silicate mixing. However, the FeO/MnO ratios of pyroxenes are comparable to eucrites: pyroxenes in mesosiderite basalts may have slightly higher FeO/MnO ratios [11]. This possibility cannot be ruled out based on the evidence from pyroxene chemistry. It is more likely that the high Ni content is resulted from contamination of projectile materials during impact events. This is consistent with the textural evidence that the CG clast was brecciated before recrystallization.

It seems that Dhofar 007 experienced a complicated shock and thermal history; (1) initial crystallization from melt under plutonic conditions, (2) some brecciation and contamination from projectiles, (3) thermal metamorphism (slow cooling) to recrystallized the breccia, (4) rapid cooling not allowing the inversion of pigeonite, (5) impact brecciation to produce clast-matrix texture, and (6) final shock event to produce thin impact melt veins. It is possible that the early impact event (event 2) occurred during initial crystallization (event 1). The event (4) is likely to have caused impact excavation during slow cooling. This is a very similar geologic history to that suggested for Moore County [8] and several highly metamorphosed basaltic eucrites such as Ibitira and EET90020 [12]. This is additional evidence for large-scale impact event during global metamorphism. Further study is required to understand the petrogenesis of the CG clast and the origin of metallic phases.

Acknowledgement. We thank H. Takeda, P.C. Buchanan, and K. Misawa for discussion.

References: [1] Afanasiev S.V. et al. (2000) MAPS 35, A19. [2] Yamaguchi A. et al. (2002) Science 296, 334-336. [3] Takeda H. (1997) MAPS 32, 841-854. [4] Ikeda Y. and Takeda H. (1985) PLPSC 15 (JGR 90), C649-C663. [5] Delaney J.S. et al. (1984) PLPSC 15 (JGR 89) C251-C288. [6] Hewins R.H. (1979) GCA 43, 1663-1673. [7] Palme H. et al. (1988) Meteoritics 23, 49-57. [8] Miyamoto M. and Takeda H. (1994) EPSL 122, 343-349. [9] Barrat J.A. et al. (2000) MAPS 35, 1087-1100. [10] Duke M.B. (1965) JGR 70, 1523-1527. [11] Mittlefehldt D.W. (1990) GCA 54, 1165-1173. [12] Yamaguchi A. et al. (2001) GCA 65, 3577-3599.

Pb isotopic signature of Martian meteorite Yamato 000593 (A preliminary report).

K. Yamashita[1] and N. Nakamura[1], N. Imae[2], K. Misawa[2] and Hideyasu Kojima[2]

[1]Dept. of Earth and Planetary Sciences, Kobe University, 1-1 Rokkou-dai, Nada, Kobe 657-8501, Japan. [2]Antarctic Meteorite Research Center, NIPR, 9-10, Kaga 1-chome, Itabashi, Tokyo 173-8515.

Introduction

As part of the consortium study on the new nakhlites from Antarctica (Y000593 and Y000749, Imae *et al.* 2002), we are currently undertaking a detailed Pb isotopic study of whole rock and mineral separates from Y000593. As an initial step, we have undertaken a two-step leaching experiment on a coarsely ground whole rock powder using dilute HCl and HNO_3. We hope that further work will help shed light on the nature of Martian mantle.

Analytical procedure

A brief summary of our initial leaching experiment is outlined in Table 1. All reagents used for this experiment were purified using a two-teflon still modified from Mattinson (1972). Pb blanks for the reagents were 0.35 ppt for 6N HCl, 1.0 ppt for 1N HBr and <3 ppt for 13N HNO_3. H_2O was taken directly from a commercial purification system (blank = 0.4 ppt). Sample handling was conducted under a clean air condition, and the total procedural blanks were in the order of ~6pg for leachates and 19pg for residue. Pb was extracted from the leachate/residue using HBr-HNO_3 media chemistry modified from Lugmair and Galer (1992). The isotopic ratios were measured on a MAT 262 thermal ionization mass spectrometer in a static mode. All ratios were corrected for mass discrimination of 0.125 +/- 0.025 (2σ) %/a.m.u.

Results and discussion

The results for the three fractions analyzed so far (L1, L2 and R) are shown in Figure 1. Also shown in this figure are the results for the A3 fraction (a fraction taken from the interior of the meteorite) of Nakhla (Nakamura et al. 1982). The reference line is a best-fit line through the data of Nakhla, excluding the ethanol leachate (*cf.* Nakamura et al. 1982).

Interestingly, the data for the two fractions L1 and R plot on this line within the analytical uncertainty. Only the less precise data of L2 has a somewhat elevated $^{207}Pb/^{204}Pb$ ratio. The reason for this high $^{207}Pb/^{204}Pb$ may be (a) accidental contamination during the chemical procedure or (b) preferential leaching of phase(s) (or part(s) of meteorite?) that was more susceptible to terrestrial weathering. Regarding the former possibility, it will require a contamination of ~180pg in order to shift the data from the reference line to the point measured. Such a contamination, however, is ~30 times the blank measured during the course of this study and thus we find this possibility unlikely. Should this be a result of terrestrial contamination, we must be careful when handling Pb isotopic data of samples that were not severely leached using, for example, HNO_3. In any case, this issue needs to be clarified by undertaking a similar leaching experiment(s) on a separate powder aliquot and/or mineral separates.

The fact that the data for the L1 and R fractions plot on the regression line defined by Nakhla hints toward the possibility that these isotopic signatures are true (*i.e.*, terrestrially uncontaminated) signature of Nakhla and Y000593. Whether the age calculated from this slope (~2.1 Ga) has any geological meaning or not is not clear at this stage. However, this issue deserves further investigation through the analyses of mineral separates (hopefully including the U-Pb concentration data).

Assuming that the elevated $^{207}Pb/^{204}Pb$ ratio of the L2 is a result of terrestrial contamination, we can correct for this by subtracting the terrestrial Pb to fit the data onto the regression line. We can then add up the Pb from L1, R and corrected L2 to obtain an estimate of the "bulk" Y000593. The isotopic ratios of the bulk Y000593 are 11.98, 11.57 and 32.21 for $^{206}Pb/^{204}Pb$, $^{207}Pb/^{204}Pb$ and $^{208}Pb/^{204}Pb$, respectively. These numbers are, of course, based on the assumptions that (a) L1 and R are not contaminated by terrestrial Pb and (b) the acetone wash contains no Pb of meteorite origin. For these reasons, they must be taken only as a crude estimate based on the data available so far. We can, however, use these values and the Cañon Diablo troilite Pb (T~4.56 Ga) to construct a two-stage Pb evolution model and obtain a μ_1 of about 1.9 (t_1: 1.28~2.10 Ga). This result is generally consistent with the earlier work that argues for a low-μ nature of the nakhlite source (*e.g.*, Dreibus and Jagoutz 2002).

Table 1. Leaching procedure and the amount of Pb extracted during each process.

	Procedure	Pb extracted (ng)	Blank (pg)
Acetone wash (AW)	3 mL distilled acetone (untrasonicate for 30 sec) x 5	nm	nm
Leach 1 (L1)	1 mL 0.1 N HCl (untrasonicate for 30 sec) x 8	14.8	6.0
Leach 2 (L2)	1 mL 1.0 N HNO3 (untrasonicate for 10 min) x 3	7.4	5.5
Residue (R)	HF/HNO3 dissolution after L2	22.2	19.1

nm: Not measured

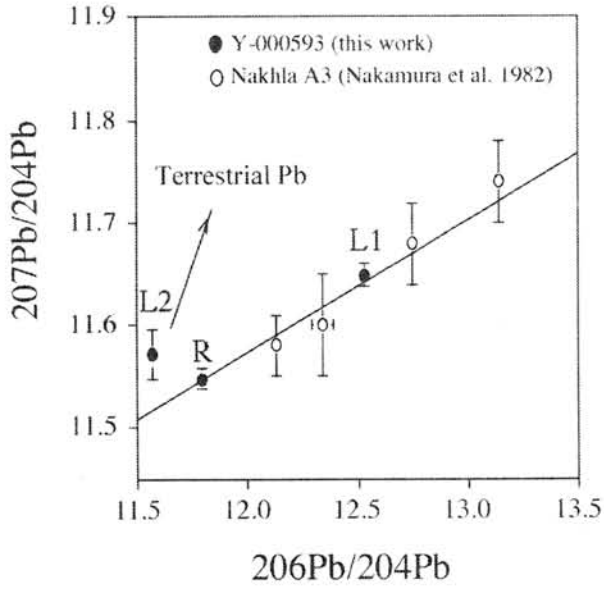

Figure 1. Pb isotopic ratios of Y000593. The reference line is a best-fit line through the data of Nakhla A3 (Nakamura *et al.* 1982) excluding the data of ethanol leachate.

References:

Dreibus and Jagoutz (2002) LPSC, XXXIII, #1040.

Imae *et al.* (2002) LPSC, XXXIII, #1483.

Lugmair and Galer (1992) GCA, 56, 1673-1694

Mattinson (1972) Anal. Chem., 44 2247-2264.

Nakamura *et al.* (1982) GCA, 46, 1555-1573.

Minerals of Ordinary Chondrites Providing Evidence for Significant Pressures within Their Parent Bodies

Nina G. Zinovieva, Olga B. Mitreikina, and Lev B. Granovsky

Department of Petrology, Faculty of Geology, Moscow State University, Lenin Gory, Moscow 119992, Russia
Correspondence author's e-mail address: zinov@geol.msu.ru

Introduction: The principal sources of information on the evolution of the solar system are meteorites, first of all, chondrites, which represent the most primitive iron-stony matter. The burning character of chondrite studies is determined by the fact that there is still no consistent theory of their genesis. This stems, in our opinion, from the impossibility of explaining some petrological features of chondrites within the guidelines of traditional concepts, in which chondrites are treated as condensates or partial-melting products of the originally solid material in the protosolar nebula. This puts forth the necessity of considering the accumulation of material on the basis of an alternative magmatic hypothesis for the genesis of chondrites early in the evolutionary course of their parent planetary bodies.

Results and Discussion: A fact of crucial importance is that ordinary chondrites contain mineral phases whose composition provides information on the high pressures of their crystallization when in parent bodies. In this context, particularly interesting are solid-solution exsolution textures in equilibrated chondrites and the early chondrules of unequilibrated chondrites, which were not affected by shock metamorphism. Exsolution textures are also known in terrestrial rocks: magmatic (in which these textures are mostly caused by cooling of these rocks) and high-pressure metamorphic (their exsolution textures result from nearly isothermal decompression). Decompression-related exsolution textures in terrestrial rocks [10] include quartz needles in clinopyroxene, magnetite needles and platelets in olivine, and several other types. Each mineral with abound lamellae of another phase carries information about its homogeneous precursor and makes it possible to assay the physicochemical conditions of its crystallization. Because of this, it is interesting to discuss the following examples of exsolution textures occurring in ordinary chondrites:

(1) Elongated tabular aggregates of Cr-spinel and plagioclase grains from porphyritic pyroxene-olivine chondrules of the Raguli H3.8, Elenovka L5, and Berdyansk L6 chondrites [7, 13, 21, 22], which are pseudomorphs after a complex jadeite- and ureyite-bearing pyroxene, whose composition is 36 mol % *Ur*, 15 mol % *Jd*, 10 mol % *Di*, 7 mol % Ca-*Tsch*, and 32 mol % Fe,Mg-*Tsch* in the Raguli H3.8 ordinary chondrite and 46 mol % *Ur*, 9 mol % *Jd*, 2 mol % *Di*, 15 mol % Ca-*Tsch*, and 28 mol % Fe,Mg-*Tsch* in the Berdyansk L6 chondrite. In an *Ur-Jd* join, this corresponds to 71 mol % *Ur*, 29 mol % *Jd* for Raguli H3.8 and 83 mol % *Ur*, 17 mol % *Jd* for Berdyansk L6. As is known, an enrichment of the jadeite end member in pyroxenes of various isomorphic series is suggestive of its high crystallization pressures [1, 9, 14,]. Na-Cr-Al clinopyroxene (44 mol % *Ur*, 20 mol % *Jd*, 25 mol % *Di* with minor contents of enstatite and acmite) of composition similar to that in the Raguli and Berdyansk chondrites was found in diamondiferous kimberlites from Yakutia [16], a fact illustrating the possibility of high-pressure conditions during the origin of such a compositionally complex pyroxene. It is hardly probable that the pressures were as high as those of the eclogite facies, but, judging from the composition and structure of the chondritic pyroxenes, they crystallized within chondrules under pressures above 1 kbar [1].

(2) We were the first to detect that chondrules in the Yamato-82133 H3 unequilibrated ordinary chondrite bear crystals of pyroxene regularly oriented relative to the chondrule structure and containing parallel elongated lamellae of silica [21]. Their textures and composition are comparable with those typical of terrestrial high-pressure exsolution textures in clinopyroxene with excess silica (Figs 1a, 1b), which develop with a decrease in the temperature and, first and foremost, pressure [10, 17]. The original silica-oversaturated terrestrial clinopyroxene is often nonstoichiometric [15]: (Si + Ti - 2Na) > (Mg + Ca + Fe^{2+} + Ni + Mn). Silica-oversaturated clinopyroxenes of various compositions were reproduced experimentally [2, 8, 20]. It was established that (1) under high pressure, clinopyroxene is characterized by an elevated isomorphic capacity and can dissolve significant amounts of silica, which are excessive relative to the normal pyroxene stoichiometry of Si : (A + B) = 1 : 1 (where A and B are Na, Ca, Mg, Fe, and sixfold-coordinated Al); and (2) silica-oversaturated clinopyroxenes of various compositions are stable under pressures above 35 kbar.

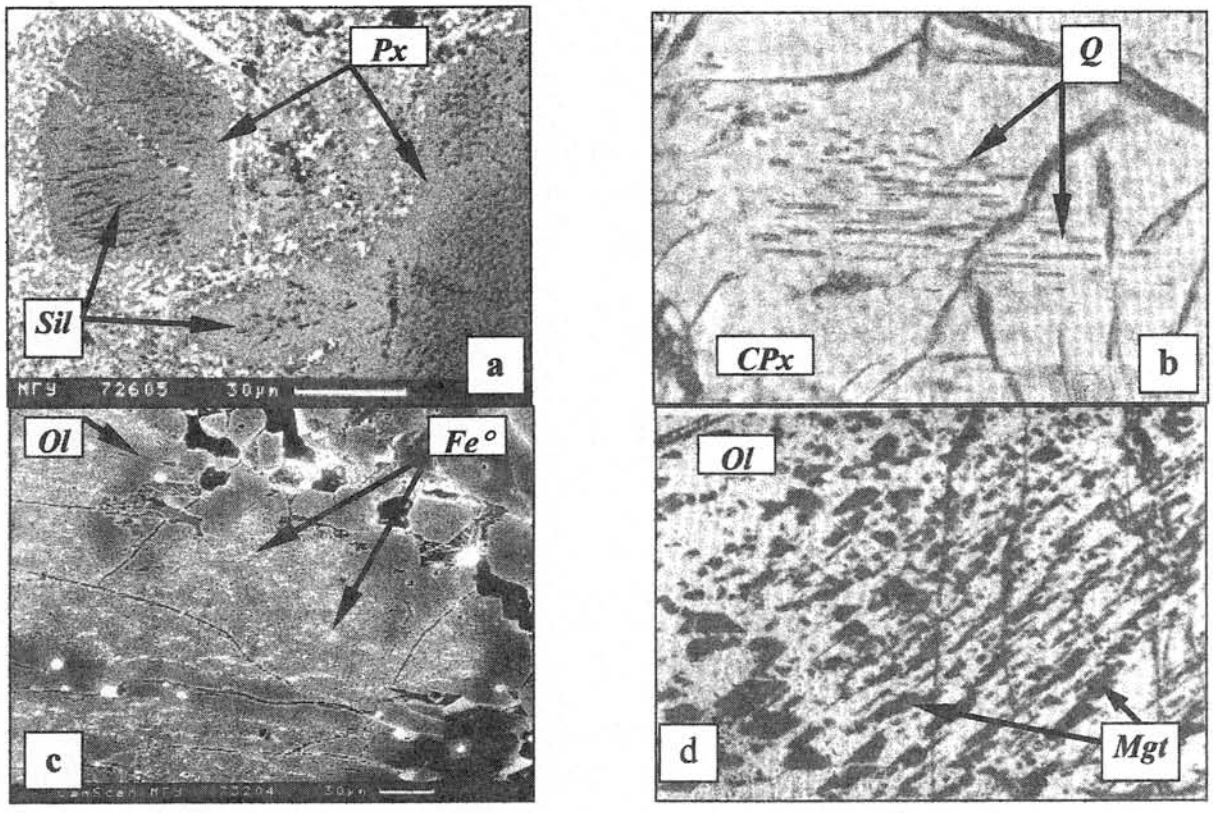

Fig. 1. Microphotograph of (a) acicular silica segregations (*Sil*) in pyroxene (*Px*) of a silica-pyroxene chondrule 22 and (c) subparallel trails of Ni-free Fe (Fe^o) in a relict olivine grain of magnesian chondrule 15 of the Yamato-82133 H3 ordinary chondrite. Exsolution lamellae in high-pressure minerals: (b) quartz needles in the cores of clinopyroxene grains in eclogite from the Northern Dabie Mountains, China, [17] and (d) magnetite lamellae (black) in olivine (light gray) from harzburgite from the Dabie Mountains [19].
Microphotographs (a) and (c) are back-scattered electron images taken on a SEM CamScan-4DV, (b) and (d) are photographs in polarized light, field of vision equals 0.32 mm.

(3) The early magnesian chondrules of the same chondrite may bear relict olivine cores. The cores of grains abound in tiny inclusions of Ni-free native Fe, which occur as subparallel trails (Fig. 1c). Petrological [21] and experimental [3, 4] study of the replacement

of Fe-rich olivine by Mg-rich olivine and native Fe have demonstrated that the decomposition of ferrous olivine is facilitated by a reduced fluid, with the main role played by the oxygen chemical potential but not the bulk fluid composition (hydrogen, argon, or H_2/CO_2 and CO/CO_2 mixtures).

(4) The kamacite of the Okhansk H4 chondrite, which were not affected by shock metamorphism, contains segregations of native silicon. As is known [5], micron-sized segregations of native silicon in native iron, which exsolved from the silicate melt as a result of liquid immiscibility onset, crystallize under significant pressures even prior the full release of the shock pressure load that has caused the melting and immiscible layering of the melt.

(5) Fine-crystalline diamond found in chondrites is prone to occur mainly in their fine-grained iron-silicate matrix [6, 12, 18]. The experimental inspection of the Fe-C system [11] made it possible to establish that the C-bearing Fe solid solution decomposes, and diamond or graphite exsolve within the native Fe, in response to a temperature and pressure decrease. Hence, C incorporation in the kamacite solid solution early in the chondrite evolution and the subsequent exsolution of the solid solution at a temperature and pressure decrease may have produced fine-crystalline diamond.

Summary: It follows that fine grains with exsolution textures in chondrites are comparable with the exsolution textures of the solid solutions of the same minerals in terrestrial rocks that crystallized under high pressures. Also, the presence of native Si, along with kamacite, and diamond in chondrites testify that the crystallization of immiscible chondritic melts was preceded by the evolution of these melts under reduced conditions and significant pressures in the interiors of their parent planets.

Acknowledgments: This work was supported by Russian Foundation for Basic Research, grant 00-05-64607 and Program "Universities of Russia - Basic Researches".

References: [1] Abs-Wurmbach & Neuhaus A. (1976) *Neues Jahrb. Mineral. Abh.* **127**, 213-241; [2] Angel R.J. et al. (1988) *Nature* **335**, 156-158; [3] Boland J.N. & Duba A. (1981) *Nature* **294**, 142-144; [4] Danielson L.R. & Jones R.H. (1995) *LPSC XXVI*, 309-310; [5] Feldman V.I. et al. (1999) *Doklady AN* **365**, N2, 253-256; [6] Huss G.R. (1990) *Nature* **347**, 159-162; [7] Ivanova M.A. et al. (1992) *LPSC XXIII*, 587-588; [8] Khanukhova L.T. et al. (1976) *Doklady AN* **229**, N1, 182-184; [9] Kushiro I. (1965) *Carnegy Inst. Wash. Year Book* **64**, 109-112; [10] Liou J.G. et al. (1998) *Reviews in mineralogy* **37**, 33-96; [11] Lipschutz M.E. & Anders E. (1964) *GCA* **28** N 5, 699-711; [12] Makjanic J. et al. (1993) *Meteoritics* **28**, 63-70; [13] Mitreikina O.B. et al. (1994) *Petrology* **2**, N3, 311-324; [14] Perchuk A.L. (1992) *Doklady Russian akad. of Science* **324**, N6, 1286-1289; [15] Smith D.C. & Cheeney R.F. (1980) *26th Geol. Congress. France* **1**, 145; [16] Sobolev V.S. et al. (1975) *Neues Jahrb. Mineral. Abh.* **123**, 213-241; [17] Tsai C.H. (1998) Ph.D. Thesis. Stanford; [18] Valter A.A. et al. (1992) *Udarno-metamorphogennye mineraly ugleroda*, Kiev, Naukova Dumka-press, p. 170; [19] N.G. Zhang R.Y. et al. (1999) *Amer. Mineral.* **84**, 564-569; [20] Zharikov V.A. et al. (1984) *Sov. Geol. and Geophys.* **25**, 53-61; [21] Zinovieva N.G. (2001) *Petrologiya obyknovennykch kchondritov*, Moscow, p. 262; [22] Zinovieva N.G. et al. (2000) *LPSC* **31** #1064.

Searching for Samples of Asteroid Ponded Deposits in Meteorites

Michael Zolensky, ST, NASA Johnson Space Center, Houston, TX 77058 USA

One of the many unexpected observations of asteroid 433 Eros by the Near Earth Asteroid Rendezvous (NEAR) mission was the many ponds of fine-grained (<1cm) materials [1&2]. These ponds are characteristically smooth and are found mainly within craters (figure 1). Though level to a first approximation (and corresponding well to the gravitational equipotential field [3], they can exhibit small, steep-walled, fault-like features (figure 1), which suggests that the pond deposits can be indurated to some degree [2]. The ponds are distributed preferentially in low latitudes, near the ends of the elongated asteroid. These latitudes coincide with surfaces that spend the most time near Eros' terminator, as well as being the regions with the lowest surface gravity [1].

There have been two principal, somewhat complementary, theories advanced to explain the ponds. Robinson et al. [4] proposed that electrostatic levitation of small grains played a major role in their formation. Electrostatic levitation and movement of fine-grained dust has been observed on the moon, and is hypothesized to operate on other atmosphereless bodies [5&6]. Others propose the segregation and migration of fines by seismic shaking [1,2,7].

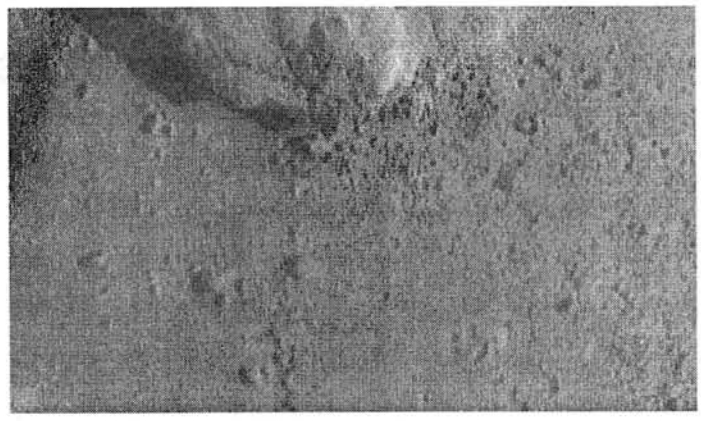

Figure 1. Closeup of a pond on Eros. A sinuous slump feature at the lower center shows that the pond in indurated to some degree. View is a couple of meters across.

We seek to provide the resolution of an observational delemma posed by the NEAR mission at Eros. The results of this comparison will permit us to understand the true nature of asteroid Eros for the first time, and then provide us with a tool to correctly interpret spectroscopic observations and regolith samples collected by future asteroid missions. Thus, our work provides an important lever to greatly increase the value of even earth-based asteroid studies. This work is critical to the successful interpretation of the mineralogic and compositional data collected at asteroid Eros by the recently completed NEAR Mission. In addition, this research will be similarly critical to the successful completion of the Muses-C asteroid sample return mission as it will permit us to determine the true nature of an asteroid from its fine-grained regolith.

There are now abundant observations of ponds on asteroid Eros, especially as the NEAR spacecraft fortuitously landed on the edge on one. The ponds have smooth surfaces, and define equipotential surfaces up to 10's of meters in diameter. The ponds have a uniformly sub-cm grain size. The ponds appear to be cohesive or indurated to some degree, as revealed by slumping evident in some images (see figure 1). The ponds appear to be concentrated within 30 degrees of the equator of Eros. This geographical bias in pond location is consistent with an origin involving electrostatic grain levitation and transportation as well as impact shaking. This is an important point. It is impossible to determine from the available NEAR data which of these two quite different processes is responsible for the ponds.

In addition to the observations of pond physical properties, there is some insight into the mineralogy and composition of the ponds' surfaces from NEAR spectroscopy [1,2,8,9]. Compared to the bulk asteroid, ponds: (1) Are distinctly bluer (high 550/760 nm ratio), possibly

due to loss of metal or a grain-size difference?; (2) Have a deeper 1um mafic band, which could be due to higher olivine and pyroxene content; (3) Have reflectance elevated by 5%.

The pertinent physical and mineralogic characteristics of the surface of Eros have been characterized by the NEAR spacecraft [1,2,8,9]. These are the critical results: (1) Eros' surface is depleted in S/Si relative to the chondritic value. This is possibly due to preferential volatilization of sulfide minerals during micrometeorite impacts; (2) Eros' surface Fe/Si ratio is apparently lower than the chondritic value; (3) Eros pond surface Fe/Si ratios are possibly lower than that for the average Eros surface. It has been hypothesized that this could be due to removal of Fe-Ni metal grains by size-sorting or settling.

Unfortunately, despite detailed data returned from the very capable NEAR spacecraft, and even an actual landing on Eros' surface, considerable uncertainty regarding the nature of the asteroid remains. The data are equally well matched by both very primitive material (ordinary chondrite-like) as well as by a geologically evolved body (achondrite-like) [10]. A first step in understanding how the mineralogy of asteroid regoliths relate to that of a bulk asteroid must involved a detailed mineralogic study of a pond deposit.

Do we have any meteoritic evidence of ponds on asteroids, and if so which of the proposed formation mechanisms does it support (if any)? There has been considerable work on the petrography and diversity of "dark clasts" present within chondrites and HED meteorites [11-14]. Some of the clasts found in CV chondrites, called "Type C" by Krot et al. [12], consist of uniformly fine-grained olivine (Figure 2). These clasts could have originated in fine-grained ponds, but a general lack of detailed studies does not permit us to say much about the formation mechanism. Of greater immediate interest is a cm-sized clast located years ago in the Vigarano CV chondrite [11-14].

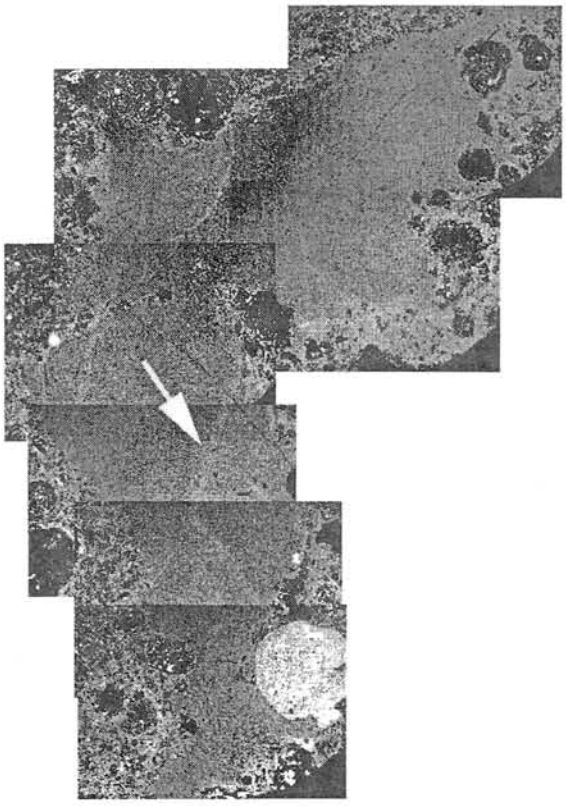

Figure 2. Backscattered electron (BSE) image of crossbeds (arrowed) in the Vigarano clast. "Up" is to the upper left. View ~1 cm across.

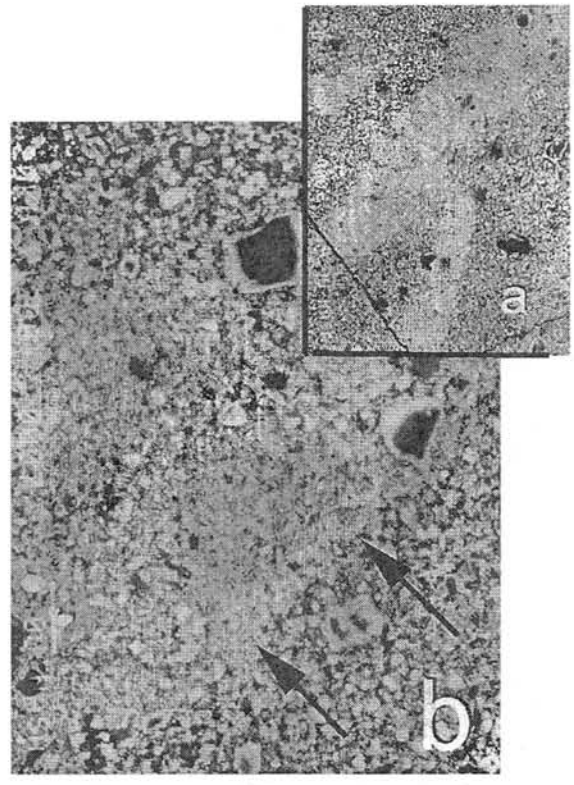

Figure 3 a: Higher mag. BSE electron image of crossbeds in the Vigarano clast. "Up" is to the upper left. View measures ~0.5mm across. **b**: Highest mag. BSE image of the bottom of one bed from the inset image. Iron-rich band stands out as bright; its lower boundary (arrowed) is sharp, while the upper boundary is gradational

We have recently found two other examples of this type of clast. As revealed by SEM, microprobe and TEM analyses performed at JSC, these Vigarano clasts consist nearly entirely of 5 micron- to submicron-sized grains of olivine: Fo43-78, with a pronounced peak at Fo50. This is essentially the distribution of olivine compositions in Vigarano itself [12], and since most

CVs have distinctive olivine distributions this fact suggests that the clasts are indigenous to the Vigarano host asteroid. Larger olivine grains up to a few 10s of μm are present in the clasts, and most of these have normal compositional zoning (iron-rich edges, iron-poor cores). The smallest olivine grains in the clasts are among the most iron-rich, having compositions to Fo43. Pyroxene, spinel, pentlandite and other accessory phases are present, and are well described by Tomeoka and Kojima [14]. The most distinctive feature of these clasts are numerous, closely-spaced, cross-bedded, arcuate bands. These bands are apparent in both reflected light and BSE images, because they contain a high proportion of the finest-grained, iron-rich olivine. We define each layer as a "bed", each of which contains within it a "band" with a high concentration of iron-rich olivine. Figure 2 shows a BSE image of the first-discovered Vigarano clast, with obvious arcuate, crossbedding. Figure 3 shows a closeup BSE image of a band in this clast. The entire clast consists of a porous aggregate of olivine grains; the pores in the arcuate bands are almost entirely filled with very fine-grained, iron-rich olivine. From the sense of the crossbedding we can tell which way "up" was (a rare feature in meteorites!), and inspection of figure 3 indicates that the relatively fine-grained bands are located at the bottom of each bed: the top of each iron-rich band is a transitional boundary, but the bottoms are very sharp. Impact-induced seismic shaking can result in grain-size separation with fine-grained materials "percolating" through a coarse matrix to the bottom [15], which is exactly what we observe in the Vigarano clasts.

Based upon our initial asessment, we propose the following scenario for the Vigarano clasts. (1) Some process separates fines from the bulk regolith material; this could well have involved electrostatic levitation, which could have separated the finest material from coarse accumulations; much work is neceassary on this point. (2) An impact generates seismic shaking, forming one bed, with the finest grains percolating to the bottom of the bed. This presumably would be most effective at elongated portions of the asteroid, which is where ponds are observed on Eros. (3) Since each shaking episode should erase the layering from previous episodes, some process must periodically lithify the beds to some degree to preserve them. Maybe heating from an impact? Later impacts can then cause degradation, but not total destruction of previously deposited beds. (4) Slumping, or impact-triggered motions, causes older beds to rotate, and subsequent beds can be deposited on an eroded, flat surface at an angle, creating the crossbeds.

We hypothesize that the Vigarano clasts formed in ponds that experienced seismic shaking. The Eros ponds may have formed the same way. There is a suggestion that the Eros pond surfaces are depleted in iron, based upon the gamma ray spectrum measured at the NEAR landing site [16]. This would be explained by percolation downward of iron-rich olivine and/or dense Fe-Ni sulfides. The latter phases are shown to be preferentially comminuted by multiple lab impacts into chondritic targets, being performed by Mark Cintala. Further, we do observe such a downward percolation of metal grains in the Vigarano clasts.

We believe that we have shown in this preliminary assessment of the Vigarano clasts that materials that likely originated in asteroid ponded deposits have survived and traveled to earth within meteorites. The questions we now propose to answer are (1) whether other pond samples have similarly survived travel to terrestrial laboratories, (2) what these samples can tell us about asteroidal regolith processes (for other classes of asteroids), and (3) how these results will permit us to better understand the actual nature of bulk asteroids from observations of asteroidal surfaces, and returned samples from the uppermost regolith layers, all of which we now know to be biased in rather unknown ways.

References: [1] Cheng et al. *MAPS*, submitted; [2] Veverka et al. (2001) *Science* **292**, 484-488; [3] Cheng et al. (2001) *Science* **292**, 488-491; [4] Robinson et al. (2001) *Nature* **413**, 396-400; [5] Criswell (1972) *Proc. 3rd LSC*, 2671-2680; [6] Lee (1996) *Icarus* **124**, 181-194; [7] Asphaug et al. (2001) *LPSC XXXII*, 1708.pdf; [8] Nittler et al. (2001) *MAPS* **36**, 1673; [9] Trombka et al. (2001) *MAPS* **36**, 1605-1616; [10] McCoy et al. (2001) *MAPS* **36**, 1661-1672; [11] Johnson et al. (1990) *GCA* **54**, 819-831; [12] Krot et al. (1995) *MAPS* **30**, 748-775; [13] Kojima and Tomeoka (1996) *GCA* **60**, 2651-2666; [14] Tomeoka and Kojima (1998) *MAPS* **33**, 519-525; [15] Horz and Schaal (1981) *Icarus* **46**, 337-353; [16] Evans et al. (2001) *MAPS* **36**, 1639-1660.

AUTHOR INDEX